AD_____

Award Number: DAMD17-98-1-8627

TITLE: Mitochondrial Mechanisms of Neuronal Injury

PRINCIPAL INVESTIGATOR: Ian J. Reynolds, Ph.D.
Teresa G. Hastings, Ph.D.

CONTRACTING ORGANIZATION: University of Pittsburgh
Pittsburgh, Pennsylvania 15261

REPORT DATE: September 2001

TYPE OF REPORT: Annual

PREPARED FOR: U.S. Army Medical Research and Materiel Command
Fort Detrick, Maryland 21702-5012

REPORT DOCUMENTATION PAGE

Form Approved
OMB No. 074-0188

1. AGENCY USE ONLY (Leave blank)	2. REPORT DATE	3. REPORT TYPE AND DATES COVERED
	September 2001	Annual (1 Sep 00 - 31 Aug 01)

4. TITLE AND SUBTITLE
Mitochondrial Mechanisms of Neuronal Injury

5. FUNDING NUMBERS
DAMD17-98-1-8627

6. AUTHOR(S)
Ian J. Reynolds, Ph.D.
Teresa G. Hastings, Ph.D.

7. PERFORMING ORGANIZATION NAME(S) AND ADDRESS(ES)
University of Pittsburgh
Pittsburgh, Pennsylvania 15261

E-Mail: iannmda@pitt.edu

8. PERFORMING ORGANIZATION REPORT NUMBER

9. SPONSORING / MONITORING AGENCY NAME(S) AND ADDRESS(ES)
U.S. Army Medical Research and Materiel Command
Fort Detrick, Maryland 21702-5012

10. SPONSORING / MONITORING AGENCY REPORT NUMBER

11. SUPPLEMENTARY NOTES
Report contains color

12a. DISTRIBUTION / AVAILABILITY STATEMENT
Approved for Public Release; Distribution Unlimited

12b. DISTRIBUTION CODE

13. ABSTRACT ***(Maximum 200 Words)***

This project is investigating the contribution of mitochondria to neuronal injury. Our previous studies have shown that glutamate mediated injury to neurons requires mitochondrial calcium accumulation. However, we know little about the magnitude of the mitochondrial calcium load that causes injury, or the mechanisms that link calcium to neuronal death. We have now characterized the properties of calcium transport, the mechanisms of mitochondrial oxidant generation, and a novel interaction between these two parameters that may be of particular relevance to Parkinson's disease.We have also identified a new property of mitochondria in the form of spontaneous mitochondrial depolarizations, and have found that this property is expressed in many different cell types. We are also investigating the properties of cytochrome c release in relation to apoptosis, which may be an important regulator of mitochondrial function. Finally, we have begun to establish a cell culture model of Parkinsons disease so that we can apply some of our studies to specific, vulnerable cell populations. These studies are providing important new information related to the control of neuronal injury by mitochondrial function.

14. SUBJECT TERMS
Neurotoxin, mitochondria, neurodegeneration, excitotoxicity, apoptosis, stroke, Parkinson's disease

15. NUMBER OF PAGES
98

16. PRICE CODE

17. SECURITY CLASSIFICATION OF REPORT	18. SECURITY CLASSIFICATION OF THIS PAGE	19. SECURITY CLASSIFICATION OF ABSTRACT	20. LIMITATION OF ABSTRACT
Unclassified	Unclassified	Unclassified	Unlimited

Table of Contents

Mitochondrial Mechanisms of Neurotoxicity
DAMD17-98-1-8627
Ian J. Reynolds, Ph.D., Principal Investigator
Teresa G. Hastings, Ph.D., Co-P.I.

Introduction

This project is designed to investigate intracellular signaling mechanisms associated with neuronal cell injury. In the acute form, this injury accounts for neural injury following stroke and head trauma, while in the chronic phenotype, it may account for degenerative diseases such as Parkinson's disease. Our preliminary studies have suggested that mitochondria play a pivotal role in the signaling processes that result in neuronal death. Accordingly, we have designed a series of experiments that are intended to elucidate the mechanisms by which mitochondria contribute to neuronal death, with the ultimate goal of identifying strategies for neuroprotection that can be applied to both acute and chronic disease states. These studies are performed on cultured neurons and on tissue derived from mature rodents.

Progress Report.

The progress reported here relates to the revised statement of work dated 7/20/98. This SOW is now focused on the first two technical objectives of the original proposal, based on the recommendations provided by the review process. The project was recently awarded a supplement to develop the techniques necessary to translate some of the observations made in dissociated cell culture into an organotypic slice model of Parkinson's Disease (PD), and some preliminary data is provided that addresses the topic of the supplement.

Objective 1. Glutamate Injury Model. The first technical objective is concerned with the mechanisms underlying the injurious effects of glutamate in neuronal cultures. We have made a number of important advances in meeting the proposed technical objectives.
Intramitochondrial Ca^{2+} determination. As reported last year, we have made substantial progress in developing a novel technique to assess intramitochondrial calcium accumulation. The paper describing this work has now been published in the *Journal of Physiology* (Brocard et al, 2001) and is included with this report. This report establishes that mitochondria accumulate millimolar amounts of calcium during exposure to excitotoxins. Surprisingly, however, our attempts to modify calcium release from mitochondria did not result in enhancement of glutamate mediated injury. These findings are now published in *Cell Calcium* (Scanlon et al, 2000). This reflects our ignorance of the basic mitochondrial calcium transport pathways in neurons, as well as the poor understanding of the pharmacology of these pathways in intact cells. We have started to characterize calcium transport in isolated mitochondria to provide a basis for further studies of these processes in intact cells. Preliminary findings from this study were published in abstract form (Votyakova et al, 2001), and we expect to complete this study for publication in the near future.

Characterization of MitoTracker dyes. Mitotrackers have been proposed to be potential-sensitive

fixable mitochondrial markers that are gaining in popularity. Our detailed study on the properties of these dyes has now been published in the *Journal of Neuroscience Methods* (Buckman et al, 2000) and is included in the appendix.

Measurements of $\Delta\psi m$. Prior progress reports mentioned our original finding of spontaneous changes in the signal of $\Delta\psi_m$-sensitive dyes in neurons. We have now published the first report of this phenomenon in the *Journal of Neuroscience* (Buckman et al, 2001). Our follow up studies have taken similar experimental approaches in astrocytes. Interestingly, we have been able to observe two kinds of spontaneous events in astrocytes. The first is a small transient increase in dye signal which appears to be a similar phenomenon to that observed in neurons, while the second is manifested as a substantial but transient decrease in dye signal. These phenomena are illustrated in Figure 1. We have had some difficulty in the quantitative analysis of these phenomena because the fluorescent objects move substantially and also change shape in addition to changing in intensity. Additional examples of these phenomena are shown in figure 2. We are very interested in determining the mechanistic basis for these phenomena, and are currently developing new methods to facilitate the study of the spontaneous events. Note, however, that this series of experiments extends beyond the original set of technical objectives proposed in this project.

Mechanisms of ROS generation. We have now completed our first study of the mechanisms of ROS generation by brain mitochondria, and these findings were recently published in the *Journal of Neurochemistry* (Votyakova and Reynolds, 2001). The issue of the mechanism by which ROS generation is stimulated by conditions associated with injury is still open. However, we have been able to define one set of circumstances under which ROS production by brain mitochondria is actually inhibited by calcium. This occurs when mitochondria respiring on succinate are challenged with calcium, and the inhibition of ROS generation is presumably the result of the decrease in $\Delta\psi_m$ associated with calcium transport (Figure 3). Interestingly, however, we have found that calcium very effectively stimulates ROS generation when mitochondria are respiring on glutamate and malate and complex I is subjected to a low level (~40%) of inhibition by rotenone (Figure 4). This exciting finding raises the possibility that a calcium stimulated, complex I mediated mechanism might underlie excessive ROS production in PD, where complex I impairment is a frequent pathological finding. We expect to submit our first communication describing this finding in the near future.

Objective 2. Mechanism of "Death Factor" Release. We continued experiments this year directed at understanding the characteristics of the release of factors that cause neuronal injury. We previously reported findings related to the characterization of PTP in brain mitochondria and to the impact of tamoxifen on glutamate induced mitochondrial depolarization, and these findings were documented in the progress report last year.

Cytochrome c release. We previously reported an immunocytochemical approach for investigating cytochrome c release. We have continued these experiments using Western blotting to provide a quantitative assessment of cytochrome c release (Figure 5). Interestingly, agents such as methamphetamine and dopamine in the presence of tyrosinase promote cytochrome c release from brain mitochondria. This clearly establishes the principle that

dopaminergic neurotoxins, or circumstances that may prevail within dopaminergic neurons, may result in circumstances under which apoptogenic factors are liberated by mitochondria. We feel that such findings emphasize the need to study these mechanisms in a relevant population of neurons, and it is for this reason that we are enthusiastic about developing the organotypic slice culture model.

New objective supported by the supplement. Development of organotypic slice cultures and methods of investigation in these cultures. Our objective in this one year supplement is to establish the organotypic slice model in which slices of substantia nigra, striatum and pre-frontal cortex are grown together in vitro, to establish effective toxicity paradigms so that we can selectively kill dopaminergic neurons, and to develop fluorescence imaging techniques to make live recordings from the slice. We have been able to generate the cultures reliably, and have embarked on the toxicity studies at this point. In our estimation, 6-hydroxydopamine (6-OHDA) may be the most straightforward toxin to use, and our initial experiments have used this agent. Figures 6 and 7 show tyrosine hydroxylase staining (of dopaminergic neurons in fixed tissue), while figures 8 and 9 show 5,7-dihydroxytryptamine (5,7-DHT) staining (of dopaminergic neurons in *live* slices) and propidium iodide (PI) staining, also in live slices, which is a simple marker of cells that have lost their plasma membrane integrity. 6-OHDA was applied at a relatively high concentration (5mM) for a short exposure time (15min) and the injury assessed 24hr later. Compared to controls (figure 6), 6-OHDA treatment produces a clear, relatively acute injury manifested as a disruption of the fine network of processes and the appearance of blebs in the processes (Figure 7). Figure 8 demonstrates that we are able to identify the dopaminergic neurons with 5,7-DHT, and that buffer exchange produces little PI staining. Interestingly, 6-OHDA treatment results in a large increase in PI staining (Figure 9), even though the PI does not co-localize with the 5,6-DHT. This suggests that this treatment protocol is not selective for dopaminergic neurons, so we are continuing to develop the toxin exposure protocol to gain selectivity. It seems likely that we will use lower concentrations but for longer periods of time to gain selectivity.

Figure 1. Spontaneous events in astrocytes. The top panel illustrates a transient increase in fluorescence signal in TMRM-loaded astrocyte mitochodria. The object labeled 1 shows a spontaneous transient increas in signal, while the adjacent objects do not change. Note the change in shape of object 3 over the course of this 30s series of images. The lower panel shows a mitochondrion that illustrates a sharp drop in fluorescence signal that also recovers. Note the difference in scale on the two fluorescence traces to the right of the figures.

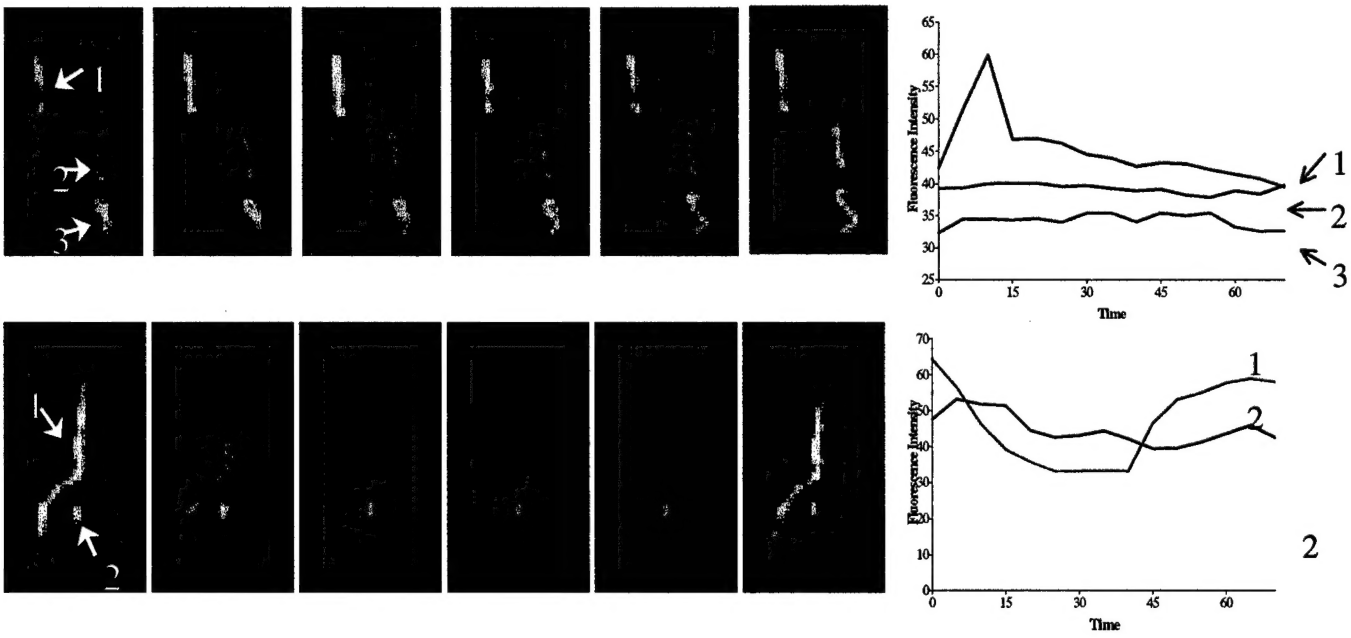

Figure 2. Spontaneous increases in signal in astrocyte mitochondria loaded with TMRM. In this 25s sequence the long mitochondrion on the left of the astrocyte transiently increases first, while the mitochondrion on the right increases some 15 sec later. In both cases the increase is transient, and is quite distinct from the profound loss of signal shown in figure 1.

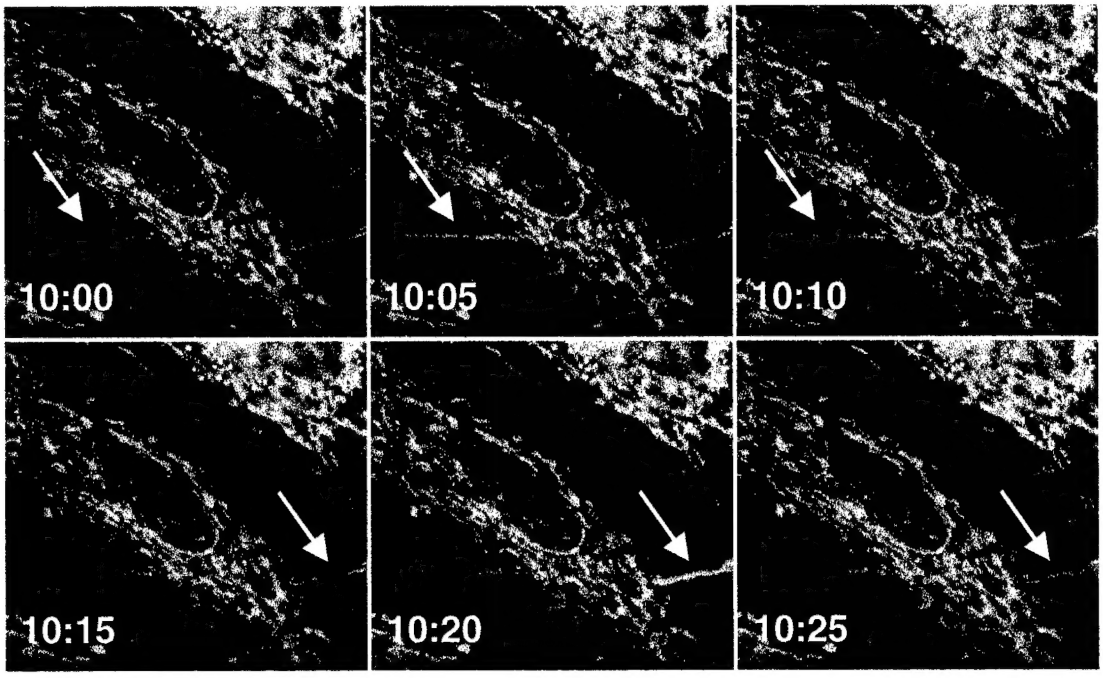

Figure 3. Inhibition of succinate-driven ROS generation by calcium.. ROS generation was detected with scopoletin (red), while parallel measurements of membrane potential (blue) and extramitochondrial calcium (green) were made with safranine O and calcium green 5N respectively. Note that the calcium load completely prevents scopoletin oxidation.

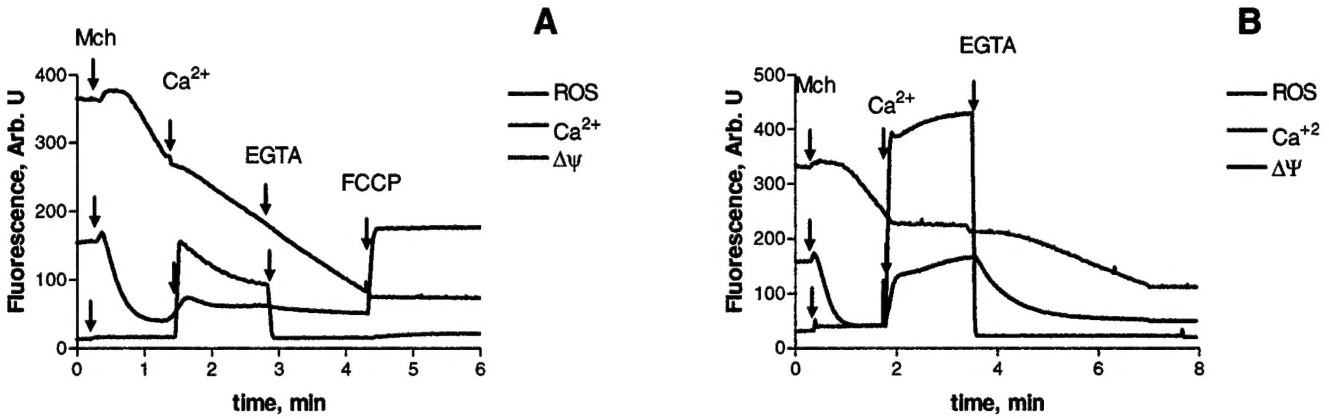

Figure 4. Calcium stimulates ROS generation when glutamate and malate are the substrates. In theleft panel, the numbers refer to the rotenone concentration in nM. The Amplex red signal was measured in the absence (dashed) or presence (solid) of 50nMoles of calcium. A parallel experiment showing calcium transport and membrane potential is shown in the right panel, indicating that calcium transport effectively occurs with this modest level or rotenone inhibtion.

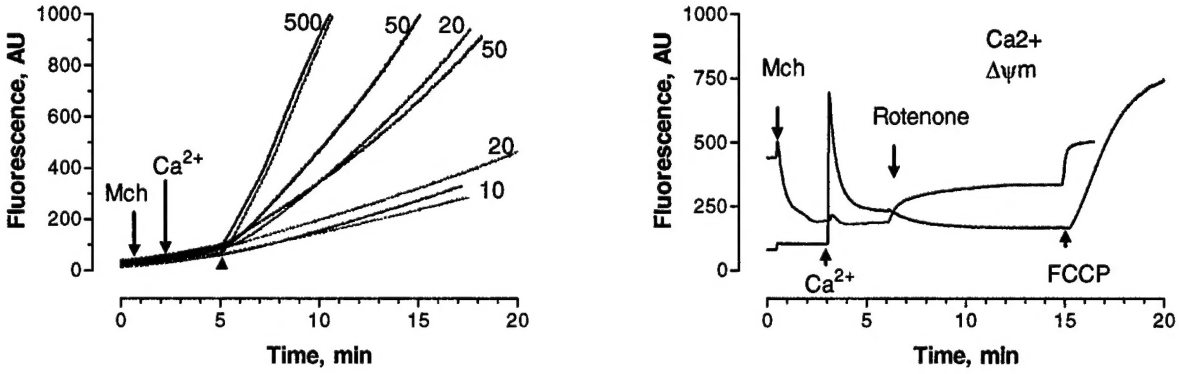

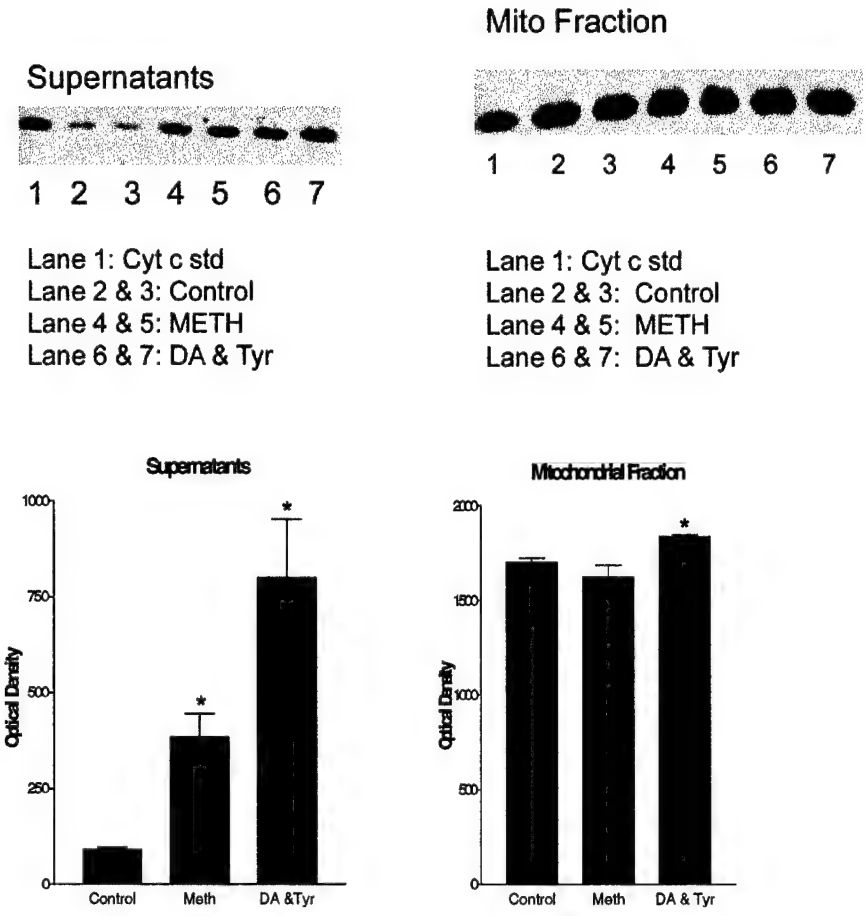

Figure 5. Brain mitochondria were isolated according to the procedure of Rosenthal (1987). Only mitochondria displaying coupled state 3:state 4 ratios above 6 were used for subsequent experiments. To examine cytochrome c release following various treatment conditions, mitochondria (360 µg protein) were incubated in standard respiration buffer containing substrates glutamate and malate (control) plus either methamphetamine (10 mM) or dopamine quinone (100 µM DA/1 U tyrosinase) for 15 min at 25°C. Following the incubation, the mitochondria were pelleted by centrifugation and separated from released cytochrome c in the supernatant. Equivalent volumes of the supernatant fraction and equivalent protein amounts of the mitochondrial fractions were run on 15% SDS-PAGE, transferred to nitrocellulose, and analyzed for cytochrome c levels by Western blot. Results showed that both methamphetamine and dopamine quinone treatment caused a release of cytochrome c into the supernatant that was several fold higher than controls.

Figure 6. TH staining in control slice cultures. The top panels were taken with a low-power objective that reveals essentially all of the dopaminergic cell bodies. The lower panel was taken using a 60x lens to illustrate processes more effectively.

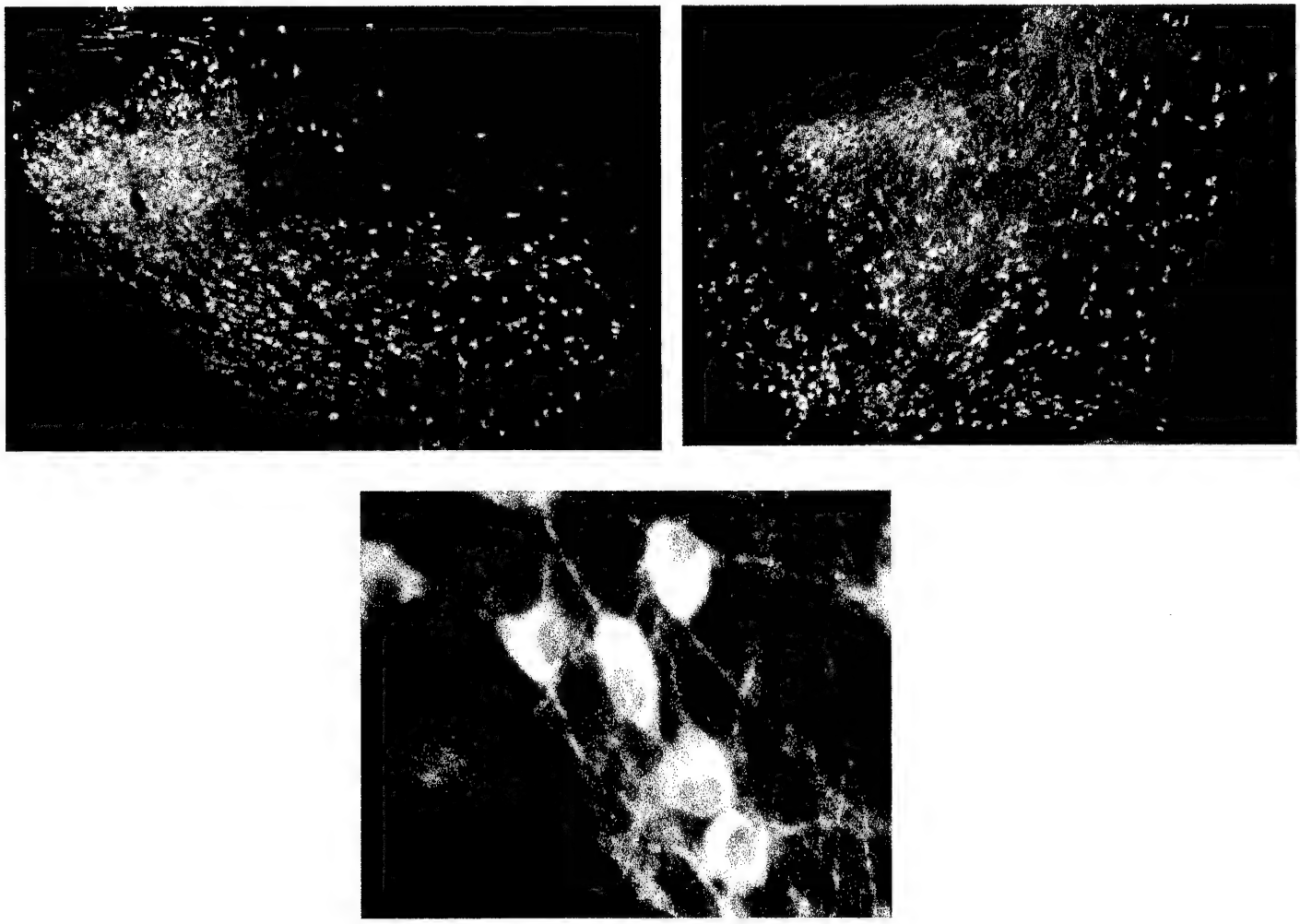

Figure 7. TH staining in slice cultures 24hr after a brief exposure to 5mM 6-OHDA. The top panels were taken with a low-power objective that reveals essentially all of the dopaminergic cell bodies. The lower panel was taken using a 60x lens to illustrate processes more effectively.

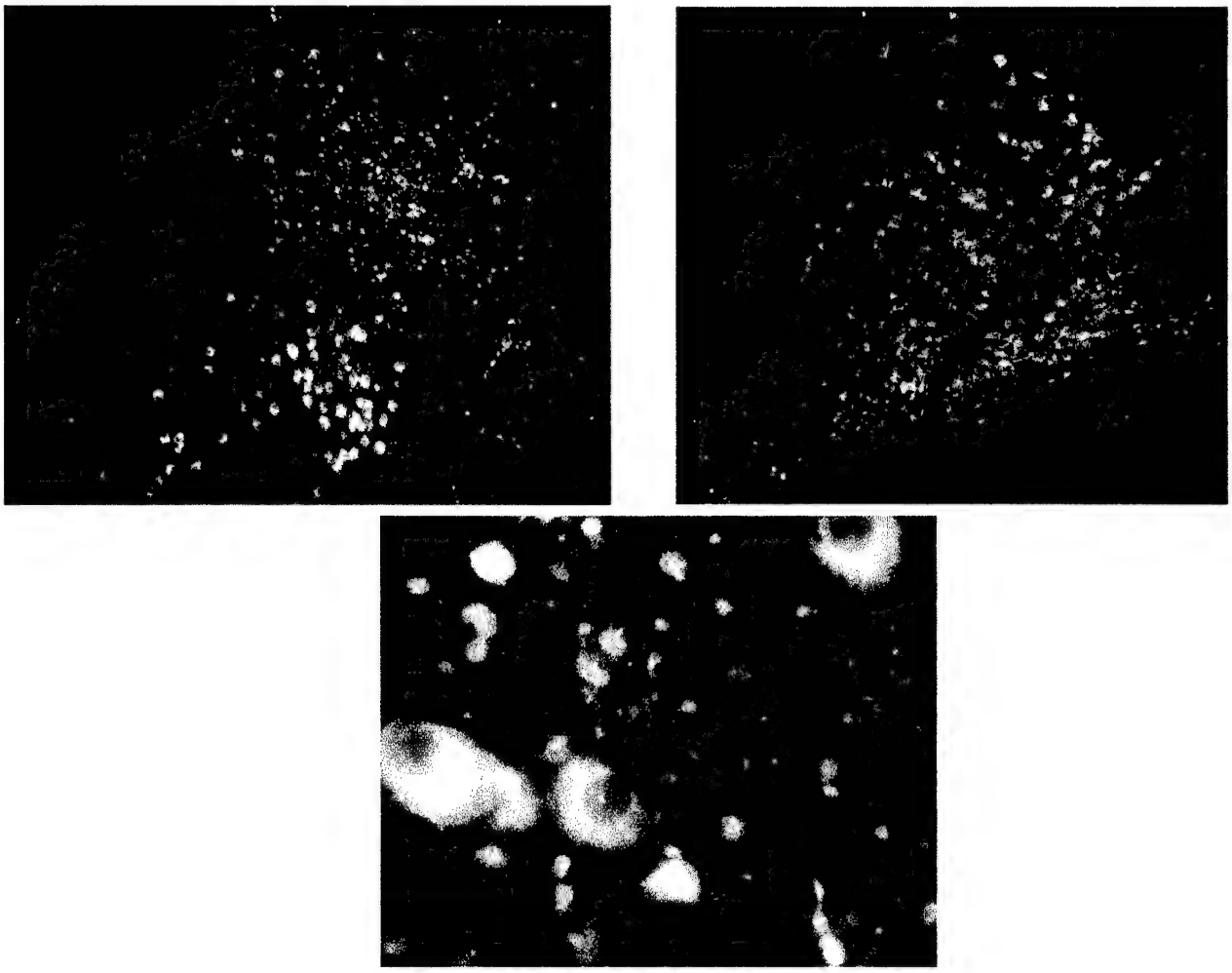

Figure 8. This panel illustrates 5,7-DHT staining (A1, B1) and PI staining (A2, B2) in a culture exposed to buffer changes alone. There is a small increase in PI staining as the result of the manipulation.

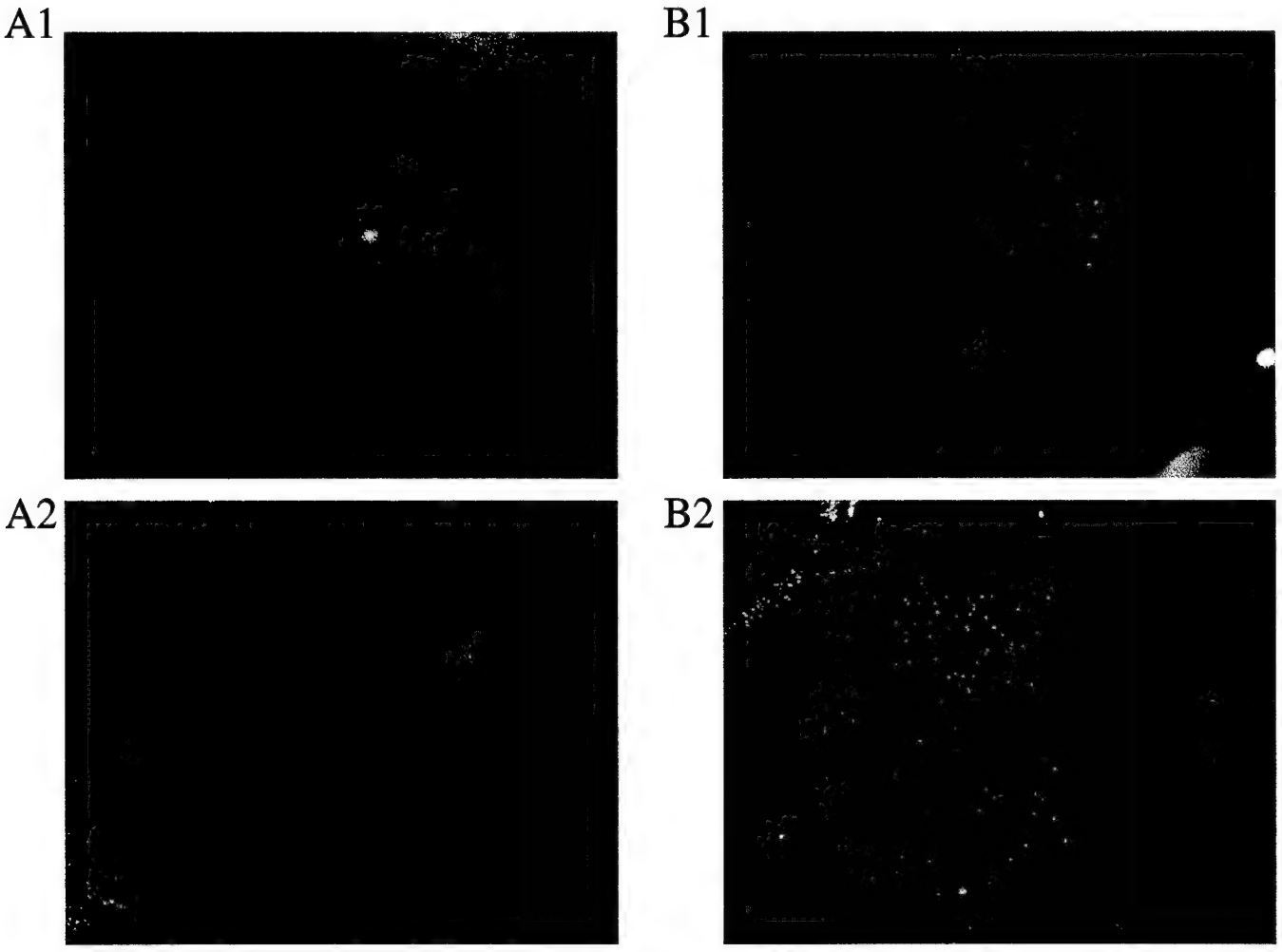

Figure 9. This panel illustrates 5,7-DHT staining (A1, B1) and PI staining (A2, B2). Note that the P.I.-defined injury does not coincide with the 5,7-DHT staining, suggesting that the injury is not selective.

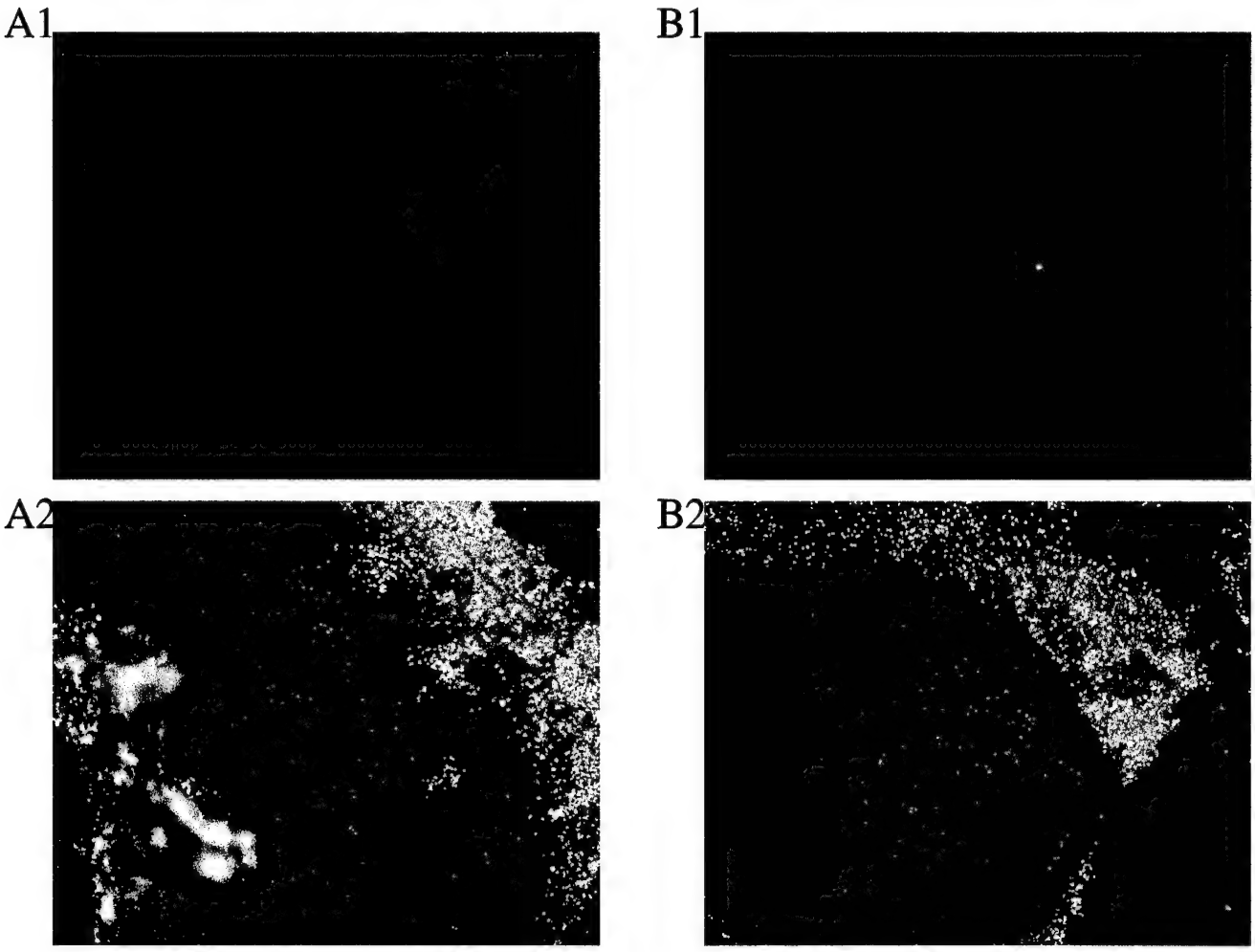

Key Research Accomplishments.

- Published the first study of spontaneous mitochondrial depolarization in neurons
- Discovered calcium-sensitive mechanisms of ROS generation by brain mitochondria.
- Established organotypic slice cultures of nigrostriatal dopaminergic pathway.

Reportable Outcomes.

The papers indicated by * are included in the appendix.

The following papers have been published:

Berman, S.B., Watkins, S.C. and Hastings, T.G. Quantitative biochemical and ultrastructural comparison of mitochondrial permeability transition in isolated brain and liver mitochondria: evidence for reduced sensitivity of brain mitochondria. Exp. Neurol. 164:415-425 (2000).

Hoyt, K.R., McLaughlin, B.A., Higgins, D.S. and Reynolds, I.J. Inhibition of glutamate-induced mitochondrial depolarization by tamoxifen in cultured neurons. J. Pharmacol. Exp.Ther. 293 480-486 (2000).

*Reynolds, I.J and Hastings, T.G. The role of the permeability transition in glutamate-mediated neuronal injury. In: Mitochondria and pathogenesis, Lemasters, J.J. and Nieminen, A.-L. (Eds), Plenum Press, New York. (2001).

*Brocard, J.B., Tassetto, M. and Reynolds, I.J. Quantitative evaluation of mitochondrial calcium content following an NMDA receptor stimulation in rat cortical neurones. J. Physiol. **531**:793-805 (2001).

*Scanlon, J.M., Brocard, J.B., Stout, A.K. and Reynolds, I.J. Pharmacological investigation of mitochondrial Ca^{2+} transport in central neurons: studies with CGP-37157, an inhibitor of the mitochondrial Na^{+}/Ca^{2+} exchanger. Cell Calcium. **28**:317-327 (2000).

*Buckman, J.F. and Reynolds, I.J. Spontaneous changes in mitochondrial membrane potential in cultured neurons. J. Neurosci. **21**: 5054-5065 (2001).

*Votyakova, T.V. and Reynolds, I.J. $\Delta\Psi_m$ - Dependent and independent production of reactive oxygen species by rat brain mitochondria. J. Neurochem. **79**:266-277 (2001).

The following abstracts have been published.

Brocard, J.B., Tassetto, M. and Reynolds, I.J. Quantitative evaluation of mitochondrial calcium content following NMDA receptor stimulation. Society for Neuroscience, 26: 1013, (2000).

Buckman, J.F., Han, Y. and Reynolds, I.J. Spontaneous mitochondrial depolarizations and motility in neurons. Society for Neuroscience, 26: 1016, (2000).

Votyakova, T.V. and Reynolds, I.J. $\Delta\psi$m-dependent and -independent ROS production by rat brain mitochondria. Society for Neuroscience, 26: 1016, (2000).

Kress, G.K., Dineley, K.E. and Reynolds, I.J. Intracellular Fe^{2+} fluorescence measurements and intracellular Fe^{2+} induced neurotoxicity. Society for Neuroscience, 26: 930, 2071(2000).

*Votyakova, T.V., Brocard, J.B., Santos, M.S. and Reynolds, I.J. An investigation of the properties of calcium uniporter inhibitors in neuronal mitochondria. Experimental Biology (2001).

*Buckman, J.F. and Reynolds, I.J. Spontaneous mitochondrial activities in astrocytes. Society for Neuroscience (2001).

*Vergun, O.V., Fuhr, J. and Reynolds, I.J. Hypoxia and hypoglycemia produce a stable increase in susceptibility to glutamate in cultured rat cortical neurons. Society for Neuroscience (2001).

*Brocard, J.B., Santos, M.S., Votyakova, T.V. and Reynolds, I.J. Effects of mitochondrial depolarization on calcium release from neuronal mitochondria. Society for Neuroscience (2001).

Conclusions.

In the three years originally supported by this project we have made good progress towards achieving the stated technical objectives. Our studies on calcium transport and ROS production have helped to characterize processes that are critical for the expression of neuronal injury following glutamate receptor activation, and may have illuminated the long-sought mechanism of calcium-stimulated ROS production. As a result of the work in this project we have identified a novel phenomenon of spontaneous changes in mitochondrial function that is exhibited by many different types of cell, including neurons and astrocytes. We have not yet been able to establish the precise significance of the phenomenon, but the indications are that this may be a sensitive marker of mitochondrial function in intact cells that might ultimately prove valuable for detecting early injury-induced events. Studies in this project have also illuminated important differences between brain mitochondria and mitochondria from other tissues with respect to the properties of permeability transition. Along with other workers in this field, we have found the study of the mechanisms of cytochrome c release to be challenging, and this has proven to be the most difficult of the technical objectives to accomplish.

We feel that the important next step in the study of mitochondrial function in relation to neuronal injury is to investigate some of these issues in specific populations of neurons that are known to be selectively vulnerable to injury, so that we can begin to understand which of the mitochondrial parameters are most closely associated with the injury to neurons. To approach this goal we have started to characterize an organotypic cell culture preparation that will allow the identification of vulnerable neurons prior to the execution of imaging studies. Because these neurons are the target of selective degeneration in Parkinson's disease, and because this disorder appears to be closely tied to alterations in mitochondrial function, we are optimistic that the model will provide a fascinating opportunity to specifically link critical changes in mitochondrial function to neuronal death, and to start to devise specific neuroprotective strategies that target mitochondrial function.

Chapter 15

Role of the Permeability Transition in Glutamate-Mediated Neuronal Injury

Ian J. Reynolds and Teresa G. Hastings

1. INTRODUCTION

Glutamate is the principal excitatory neurotransmitter in the brain. In addition to its critical role in fast excitatory neurotransmission, however, glutamate has a more sinister role as a potent and effective neurotoxin, a process termed *excitotoxicity* (Rothman and Olney, 1987). Glutamate is acutely toxic to central neurons in primary culture, and it is widely believed that similar mechanisms contribute to the neuron loss encountered in both acute and chronic neurodegenerative disease. In the former category, there is good evidence that neuronal injury encountered in stroke, cerebral ischemia, traumatic brain injury, and some forms of *status epilepticus* is mediated by excessive glutamate receptor activation. The links to chronic neurodegeneration are perhaps more tenuous. Glutamate may, however, mediate some part of the neurodegenerative process in amyotrophic lateral sclerosis, Huntington's disease, Parkinson's disease, dementia associated with acquired immunodeficiency syndrome, and possibly Alzheimer's disease (reviewed in Olney, 1990).

The wide range of diseases associated with aberrant activation of glutamate receptors suggests that drugs which interrupt excitotoxicity could be of great therapeutic significance. Glutamate receptor antagonists have been intensively investigated in this regard, and show some promising results in acute disease models (Doble, 1999; Koroshetz and Moskowitz, 1996). This approach has been associated with significant behavioral side effects, however, reflecting glutamate's important role in normal brain

Ian J. Reynolds Department of Pharmacology, University of Pittsburgh, Pittsburgh Pennsylvania 15261. **Teresa G. Hastings** Department of Neurology and Neuroscience, University of Pittsburgh, Pittsburgh, Pennsylvania 15261.

Mitochondria in Pathogenesis, edited by Lemasters and Nieminen.
Kluwer Academic/Plenum Publishers, New York, 2001.

function (Tricklebank *et al.*, 1987). An alternative approach to preventing excitotoxic injury could involve blocking some of the downstream processes activated by glutamate, and this would ideally focus on a target activated exclusively during injury so that drugs directed toward this target should have much greater functional selectivity than glutamate receptor antagonists.

Recent studies on the mechanisms underlying excitotoxicity have identified a central role for mitochondria in the injury process. Moreover, it has been suggested that the permeability transition pore (PTP) is activated in neuronal mitochondria specifically during pathophysiological states, and that its activation contributes to neurons demise. If this is true, then the pore should be considered a primary target for drug development in neurodegenerative disease. This review seeks to evaluate the validity of the conclusion that the PTP has a central role in neurodegeneration.

2. ROLE OF MITOCHONDRIA IN GLUTAMATE TOXICITY

There is considerable evidence of a role for glutamate in acute brain injury. Glutamate is stored at high concentrations inside both neurons and astrocytes and is released into the extracellular space as a result of injury (Benveniste *et al.*, 1984; Rothman, 1984; Strijbos *et al.*, 1996). Selective glutamate receptor antagonists can ameliorate ischemic and traumatic injury *in vivo* (Boast *et al.*, 1988; Gill *et al.*, 1987). Glutamate is also effective enough as a neurotoxin to kill neurons *in vitro* without the need for any other injurious agent (Choi *et al.*, 1987; Rothman, 1984). Thus studying glutamate's mechanism of action should provide insights into some aspects of the neuronal injury process, even though this approach undoubtedly takes an oversimplified view of the processes that causes *in vivo* neurons death. Glutamate-induced injury can take several forms depending on the type of receptor activated (Koh *et al.*, 1990; Mayer and Westbrook, 1987). The studies described here focus on the most acute form of glutamate-triggered neuronal injury, namely injury induced by the activation of *N*-methyl-D-aspartate (NMDA) receptors. Excessive activation of the other ionotropic glutamate receptors, the AMPA and kainate receptors, is also a highly effective way to kill neurons, but the cellular mechanisms responsible for injury are less well established.

2.1. Mitochondria in Neuronal Ca^{2+} Homeostasis

Some of the earliest *in vitro* studies on glutamate toxicity showed that extracellular Ca^{2+} is required for expression of NMDA-receptor-mediated injury (Choi, 1987), an observation consistent with the Ca^{2+} permeability of the NMDA-receptor-associated ion channel (MacDermott *et al.*, 1986). Moreover, the observation that extracellular Ca^{2+} decreases considerably during ischemia suggests that a robust Ca^{2+} entry into neurons occurs *in vivo* as well (Erecinska and Silver, 1996; Kristián *et al.*, 1994). The relationship between Ca^{2+} entry and neuronal death is still not entirely clear. Only recently was it established that toxic stimulation of NMDA receptors actually results in larger intracellular free Ca^{2+} changes than does benign activation of other, nontoxic Ca^{2+}-elevating mechanisms (Hyrc *et al.*, 1997; Stout and Reynolds, 1999). It has also been suggested that the route of Ca^{2+} entry is at least as important as the magnitude of influx, so the

precise location of a substantial Ca^{2+} influx may be the key to triggering injury (Sattler *et al.*, 1998; Tymianski *et al.*, 1993).

Studies of Ca^{2+} homeostasis mechanisms in neurons reveal an important role for mitochondrial Ca^{2+} transport following glutamate receptor activation (Khodorov *et al.*, 1996; Wang and Thayer, 1996; White and Reynolds, 1995). We demonstrated that both mitochondria and the plasma membrane Na^+/Ca^{2+} exchange (NCEp) clear the cytoplasm of Ca^{2+} following glutamate stimulus, and that mitochondria account for a progressively larger proportion of the buffering ability as glutamate stimulus intensity approaches toxicity (White and Reynolds, 1995, 1997). A second method of illustrating mitochondrial Ca^{2+} accumulation was via the use of the mitochondrial NCE (NCEm) inhibitor CGP-37157 (Cox and Matlib, 1993). The NCEm is the predominant efflux pathway in functional neuronal mitochondria, so blocking it and monitoring the change in the recovery characteristics of cytoplasmic Ca^{2+} concentrations allows inference of a mitochondrial Ca^{2+} load (Baron and Thayer, 1997; White and Reynolds, 1996, 1997). Several studies report the use of Ca^{2+} indicator Rhod-2 to illustrate mitochondrial Ca^{2+} loading in real time (Minta *et al.*, 1989; Peng and Greenamyre, 1998; Peng *et al.*, 1998), and these real-time methods complement other approaches that have found glutamate- or injury-induced mitochondrial Ca^{2+} loading in isolated mitochondria (Sciamanna *et al.*, 1992) or in brain slices using electron probe microanalysis (Taylor *et al.*, 1999).

Without inferring a mechanism by which Ca^{2+} alters mitochondrial function, the importance of mitochondrial Ca^{2+} accumulation to neuronal injury has been illustrated by two studies that blocked Ca^{2+} uptake during glutamate exposure and thereby prevented injury. Budd and Nicholls (1996a, 1996b) accomplished this in cerebellar granule cells using rotenone and oligomycin to depolarize mitochondria while maintaining intracellular ATP concentrations. We later accomplished the same neuroprotection in forebrain neurons using the protonophore FCCP; its reversibility provided a better window of opportunity for observing the neuroprotection (Stout *et al.*, 1998). These studies helped to establish that mitochondrial Ca^{2+} uptake is essential for excitotoxicity expression, although the precise target of Ca^{2+} within mitochondria is still unknown.

2.2. Reactive Oxygen Species and Glutamate Toxicity

Markers of oxidative stress are increased in association with ischemia and trauma, and in particular during the reperfusion phase following ischemia (Hall and Braughler, 1989; Phillis, 1994). There is also abundant evidence that chronic neurodegenerative states are associated with an increased oxidant burden (Götz *et al.*, 1994). In most of these cases, however, there are many potential sources of ROS (Halliwell, 1992), and the mechanisms responsible for glutamate-specific alteration of the oxidant/antioxidant balance remain poorly defined.

A series of reports have detailed processes that could link glutamate receptor activation to ROS generation by mitochondria. Lafon-Cazal and colleagues (1993) found that glutamate-stimulated cerebellar granule cells generated ROS that could be detected by electron spin resonance. Dykens showed in 1994 that isolated brain mitochondria increased superoxide generation when presented with Ca^{2+} and Na^+, the circumstance presented to mitochondria in neurons activated by glutamate. Subsequently, we (Reynolds and Hastings, 1995) and others (Bindokas *et al.*, 1996; Dugan *et al.*, 1995)

showed that glutamate-stimulated neurons in primary culture triggered ROS generation detectable with a range of oxidation-sensitive fluorescent dyes. Various arguments have been made to support a mitochondrial source for these effects. For example, one can infer from the location of the dye signal that oxidation occurs in the vicinity of mitochondria. This is not necessarily a compelling argument, given the limited resolution with which these measurements must be made, and given also the tendency of some of these dyes to distribute in cells to organelles that have no relation to their oxidation site. Interrupting the ROS-generating mechanism provides more persuasive insights into the source of ROS. We reported that glutamate-stimulated effects on dichlorofluorescin oxidation were Ca^{2+} dependent, and that FCCP prevented glutamate-induced ROS generation (Reynolds and Hastings, 1995). Although FCCP has numerous effects on neurons (Tretter *et al.*, 1998), the most straightforward basis for this inhibitory effect is the prevention of Ca^{2+} loading into mitochondria. Rotenone also blocks ROS generation by dihydroethidium (Bindokas *et al.*, 1996), presumably the result of inhibiting electron transport in Ca^{2+}-stimulated mitochondria. Together with the observation that oxygen-deprived neurons are resistant to glutamate-induced injury (Dubinsky *et al.*, 1995), these findings suggest that mitochondrially generated ROS may play a central role in excitotoxicity.

In addition to glutamate's ability to directly induce ROS generation, there may be an interaction between oxidative stress and glutamate toxicity in that an extrinsic oxidative stress may potentiate the toxicity of glutamate. Thus in neurons subjected to an oxidant burden, the threshold for glutamate toxicity may be decreased (*e.g.*, Hoyt *et al.*, 1997a), and following oxidant inhibition of the glutamate transporter, glutamate's potency may be increased (Berman and Hastings, 1997; Piani *et al.*, 1993; Volterra *et al.*, 1994), perhaps resulting in the increased vulnerability of selected neuron populations. Moreover, a possible critical ROS target is in fact the mitochondrion. Essentially, all complexes in the electron transport chain are vulnerable to inhibition by oxidants (Berman and Hastings, 1999; Dykens, 1994; Zhang *et al.*, 1990), and the activities of several enzymes in the tricarboxylic acid cycle are impaired by oxidation (Chinopoulos *et al.*, 1999). By further enhancing ROS generation, or by limiting ATP generation under circumstances that would normally place a great demand on ATP supply (Chinopoulos *et al.*, 1999), the impact of an oxidant burden together with glutamate exposure is potentially devastating.

One important example of this is the degeneration of dopaminergic neurons in the substantia nigra in Parkinson's disease. These neurons contain a high concentration of dopamine. Dopamine generates an oxidant burden either by its metabolism by monoamine oxidase (MAO), which generates hydrogen peroxide, or by the formation of highly reactive dopamine quinones (Graham, 1978; Hastings, 1995; Maker *et al.*, 1981). It is toxic to neurons in culture (Hoyt *et al.*, 1997b; Rosenberg, 1988), and it is also toxic when injected directly into the brain (Hastings *et al.*, 1996). Though dopamine's toxicity mechanism is not fully understood, a mitochondrial target is one important potential mechanism being evaluated. Thus we have demonstrated that MAO-catalyzed dopamine oxidation inhibits state 3 respiration in brain mitochondria (Berman and Hastings, 1999). Interestingly, dopamine quinone increased state 4 respiration, consistent with an uncoupling effect perhaps attributable to increased membrane permeability associated with PTP activation (Berman and Hastings, 1999). The oxidative burden associated with a high dopamine content and the concomitant bioenergetic impairment may render substantia nigra neurons especially vulnerable to excitotoxic stimuli (Greene and Greenamyre, 1996).

3. THE PERMEABILITY TRANSITION IN NEURONAL MITOCHONDRIA

Identification of mitochondria as a critical target for Ca^{2+} in neuronal injury moved the field one step closer to identifying the complete sequence of events necessary to execute the process of cell death. It seems likely that there are multiple mechanisms by which neurons may die following NMDA receptor activation (Ankarcrona *et al.*, 1995), not all of which are associated with gross Ca^{2+} overload. Even when considering the acute, high Ca^{2+} load-associated injury, the precise target within mitochondria and the cellular consequences of altering this target have not been established. A simple view is that neuronal death is merely a consequence of ATP loss, failure of ion homeostasis, and cell lysis as a result of uncontrolled solute accumulation. Given that Ca^{2+} and ROS do not shut down respiration or metabolism —indeed, Ca^{2+} stimulates ATP synthesis (McCormack *et al.*, 1990)—what mechanisms are available to impair ATP synthesis under the circumstances generated by intense stimulation of NMDA receptors?

An attractive conceptual mechanism is provided by the PTP. As a mitochondrial target activated by Ca^{2+}, oxidation, and mitochondrial membrane depolarization, this target appears the ideal point at which neuronal injury's principal effectors can converge. We have already discussed the importance of mitochondrial Ca^{2+} accumulation and ROS generation. The third component, alteration of mitochondrial membrane potential, is then provided by the cycling of Ca^{2+} through mitochondria, which occurs at the expense of the proton gradient (Gunter and Pfeiffer, 1990; Nicholls and Akerman, 1982). Thus the key pore activators should be present during glutamate exposure.

What evidence exists to support pore activation in the injury cascade triggered by glutamate? The key consequences of pore activation should be loss of membrane potential, alteration of mitochondrial shape, increased mitochondrial permeability to small molecules, and presumably, neuronal death. Observations consistent with these events have now been reported by several laboratories. Using fluorescent dyes that report mitochondrial membrane potential, several studies found that mitochondria in intact neurons are depolarized during glutamate exposure (Nieminen *et al.*, 1996; Schinder *et al.*, 1996; White and Reynolds, 1996). The partial sensitivity of these changes in membrane permeability to cyclosporin A is consistent with a contribution of the PTP. Shape changes in mitochondria are difficult to resolve at the light microscopic level. Nevertheless, Ca^{2+}-stimulated, cyclosporin-sensitive changes in mitochondrial morphology were reported, such that the predominant change was from rod-shaped to round in both neurons and astrocytes (Dubinsky and Levi, 1998; Kristal and Dubinsky, 1997). Recently, Friberg and colleagues (1998) established that swelling of neuronal mitochondria in hypoglycemic brain injury can be prevented by cyclosporin A, thereby suggesting a link to the pore. No neuron studies have shown explicit alteration in the mitochondrial permeability of small molecules in intact neurons. Several studies have found, however, that neuronal death can be prevented by cyclosporin A, again consistent with an essential role for the pore in the death pathway (Dawson *et al.*, 1993; Schinder *et al.*, 1996; White and Reynolds, 1996). Though we discuss below a number of potential limitations in these conclusions, there is plenty of evidence for a hypothesis that places transition as a final common pathway in neuron death.

4. LIMITATIONS OF THE PERMEABILITY TRANSITION HYPOTHESIS

Many of the pore's features are conceptually ideal in building a model of the glutamate-induced injury cascade. Indeed, it could be claimed that excitotoxicity is the clearest example of PTP involvement in a cellular or intact-tissue injury paradigm. Nevertheless, it is still necessary to apply the same critical standards to evaluating this hypothesis as to evaluating any other, because there are still major issues that need to be more fully considered.

4.1. Transition Measurement in Intact Cells

The first major difficulty in evaluating the PTP's contribution to injury is measuring transition in intact cells. Transition has been studied mainly in isolated mitochondria, and the most common approach for assaying transition is measurement of mitochondrial swelling using light scattering. Other approaches have been used, including measuring the release of low-molecular-weight solutes such as glutathione and also the influx of radioisotopes normally excluded from mitochondria with restricted permeability, but the limited ability to measure these parameters in cultured cells (because of the relative insensitivity of the methods) has prevented their application in models of excitotoxicity.

As noted above, recent studies have explicitly investigated mitochondrial morphology in brains exposed to injury and have reportedly prevented the appearance of swollen mitochondria in response to hypoglycemia by cyclosporin A (Friberg *et al.*, 1998). This is an exciting development, but the approach does not lend itself well to mechanistic studies because it is hard to do quantitative electron microscopic studies under circumstances where mitochondrial parameters can effectively be manipulated. Additional morphological approaches have been taken in permeabilized neurons and astrocytes. This is an interesting intermediate approach that falls between isolated mitochondria and intact cells. Dubinsky and colleagues were able to demonstrate Ca^{2+}-mediated alterations in mitochondrial morphology, assayed in mitochondria loaded with fluorescent dyes, that could be partially prevented by concomitant application of CsA (Dubinsky and Levi, 1998; Kristal and Dubinsky, 1997). These studies are also consistent with activation of the PTP in neural cells, although it is hard to be sure of the extent to which the mitochondrial environment in permeabilized or to which ionophore-treated cells reflects the glutamate exposure conditions. Indeed, in astrocytes lacking the efficient Ca^{2+} accumulation pathways of neurons, the pathophysiological relevance of a Ca^{2+} overload-induced alteration in mitochondrial function remains to be established.

Applying morphological approaches to the study of mitochondrial shape in intact cells may also be limited by the dyes. Many mitochondrion-specific dyes accumulate in the organelle based on membrane potential, and so the change in potential that accompanies increased permeability should grossly alter the dye-staining properties (White and Reynolds, 1996), potentially an important confound when applying purely morphometric approaches. Other dyes, such as the series of Mito Tracker dyes provided by Molecular Probes, may accumulate in mitochondria based on membrane potential but then become irreversibly bound as a result of the dye's chloromethyl moiety interacting with free sulfhydryls in (presumably) the mitochondrial matrix (Poot *et al.*, 1996). Though this provides the advantage of having a fluorescent marker that can be fixed, it has the

disadvantage of altering an important parameter controlling PTP activation: the balance of reduced and oxidized sulfhydryls (Chernyak and Bernardi, 1996). The observation that Mito Tracker orange can inhibit complex I with considerable potency and can also activate transition in isolated hepatic mitochondria (Scorrano *et al.*, 1999) further underscores the difficulty of this approach.

Most other claims of pore activation in neurons have been made based on cyclosporin-sensitive alterations in mitochondrial membrane potential (Nieminen *et al.*, 1996; Schinder *et al.*, 1996; White and Reynolds, 1996). These studies have typically reported an NMDA-receptor-stimulated, Ca^{2+}-dependent depolarization of mitochondrial membrane potential using a range of potential-sensitive indicators. These depolarizations are generally observed during the time required to commit neurons to die as a result of the glutamate exposure, but they occur well before loss of viability can be detected, suggesting that the phenomenon is upstream in the injury cascade. At least some of the time, depolarization is also reversible upon glutamate removal (White and Reynolds, 1996), although this is variable. It is tempting to suggest that the loss of potential reflects transition, but is this reasonable? Based on pharmacological evidence discussed below, where several putative transition inhibitors are effective it appears so. It is difficult, however, to exclude other possible mechanisms with confidence, We know that Ca^{2+} is clearly essential in this process, but mitochondrial Ca^{2+} cycling occurs at the expense of the proton gradient (Nicholls and Akerman, 1982). Thus a large amount of Ca^{2+} passing through mitochondrial uptake and release presumably results in depolarization. It would also be difficult to distinguish between cycling-induced depolarization and a PTP-triggered change, because blocking Ca^{2+} uptake would block both phenomena concomitantly. Although Ca^{2+} cycling-induced mitochondrial depolarization has been observed in synaptosomes (Nicholls and Akerman, 1982), it has never been explicitly demonstrated in intact neurons. Nevertheless, its potential contribution is consistent with the observation of hyperpolarization of mitochondrial membrane potential induced by the Ca^{2+} efflux inhibitor CGP37157 (White and Reynolds, 1996). It is important to recognize that depolarization of mitochondrial membrane potential is also a normal response to increased ATP demand. Given that NMDA receptor activation results in a substantial change in intracellular Na^+ as well as Ca^{2+} (Kiedrowski *et al.*, 1994), and that the Na^+/K^+ ATPase is a major consumer of ATP in neurons, the greatly increased Na^+ burden should require an increase in ATP synthesis accompanied by a depolarization of mitochondrial membrane potential. Thus, several major mechanisms could produce an alteration in membrane potential that would be completely independent of the PTP, and in fact represent the function of normal, healthy mitochondria.

The intricate intertwining of PTP-inducing stimuli and non-PTP-related changes is further illustrated by the impact of oxidants in this system. In isolated mitochondria, oxidants promote pore activation by oxidizing vicinal sulfhydryls or by increasing the pool of the oxidized form of glutathione (Chernyak and Bernardi, 1996). Oxidants can inhibit electron transport, however, and they may also limit the tricarboxylic acid (TCA) cycle, which could alter the ability of mitochondria to pump protons and maintain a potential (Chinopoulos *et al.*, 1999; Zhang *et al.*, 1990). There is the additional confound of peroxide-induced changes in the properties of JC-1, which appear unrelated to membrane potential (Chinopoulos *et al.*, 1999; Scanlon and Reynolds, 1998), and which can look like depolarization but which probably are not.

The approaches used in intact neurons have not proved effective in unequivocally establishing the phenomenon of pore activation. One potentially interesting approach not yet applied to neurons is the cobalt-induced calcein quenching reported by Petronilli and colleagues (1999), although it may prove difficult to apply the method to glutamate excitotoxicity models due to cobalt/Ca^{2+} interaction in this system. Approaches that combine morphology with membrane-potential measurements so that swelling can be observed in conjunction with loss of membrane potential, together with a careful functional assessment to preclude ATP synthesis and Ca^{2+} cycling as a cause of membrane-potential changes, may be necessary to definitively establish the expression of PTP activation in neurons.

4.2. Limitations of Pharmacological Approaches

The difficulty in identifying the PTP solely by functional criteria in intact cells emphasizes the value of pharmacological intervention. Additionally, the putative contribution of the PTP to glutamate-induced neuronal death might be mitigated by transition antagonists, so there is considerable interest in pore-specific drugs. Unfortunately, such agents are difficult to come by.

The classic pore inhibitor is cyclosporin A (CsA). This agent binds to cylophilin D in the matrix and prevents the association of cylophilin with the pore complex, thus preventing the facilitative effect on pore activation (Connern and Halestrap, 1994). The CsA binds to cyclophilin with high affinity and with a specificity distinct from that associated with immunophilins (Bernardi *et al.*, 1994; Connern and Halestrap, 1994). Thus, potent immunosuppressent agents such as FK506 do not alter transition in isolated brain mitochondria (Friberg *et al.*, 1998). Conversely, analogs of CsA such as *N*-methylvaline cyclosporin show pore inhibition with less immunosuppressant activity (Griffiths and Halestrap, 1991), but they are not commercially available, unfortunately CsA is a less-than-ideal agent in intact neurons. The cyclic peptide structure may limit cell penetration, and intact-cells studies generally require higher concentrations than isolated-mitochondria studies. Some of the immunophilin-mediated effects, such as inhibition of the Ca^{2+}-dependent phosphatase calcineurin, occur at concentrations too low to inhibit the PTP (Dawson *et al.*, 1993). Indeed, it has been proposed that calcineurin inhibition is neuroprotective independently of the PTP, a suggestion supported by the neuroprotective effects of FK506 in some studies (Dawson *et al.*, 1993; Lu *et al.*, 1996), but not others (Friberg *et al.*, 1998). The binding of CsA is also modulated by Ca^{2+} and Mg^{2+}, with the effect that PTP-inducing conditions may decrease the effectiveness of CsA binding (Novgorodov *et al.*, 1994). This may explain the loss of effectiveness sometimes observed when CsA is used as an inhibitor of transition-associated events (Scanlon and Reynolds, 1998). There is no question that CsA is the most potent and probably the most useful pore inhibitor currently available. Other actions of CsA are, clearly important for neuronal viability, however, independent of cyclophilin D and the PTP; also, CsA may not be effective even if pore-mediated effects are under investigation, which, along with the difficulty in controlling intracellular CsA concentrations, shows a definite need for more effective inhibitors.

In fact, a wide variety of agents have been used to modulate PTP activity, both inhibitors and activators (see Zoratti and Szabò, 1995), including atractyloside and bongkrekic acid, which bind to the ATP/ADP translocase. The suggestion that the PTP reflects a different functional state of the translocase is reflected in the ability of these agents to inhibit or promote pore activation, respectively (Halestrap and Davidson, 1990). Unfortunately, atractyloside is cell impermeant. The recent commercial availability of bongkrekic acid should soon allow its evaluation in neurons, although promoting pore activation will not effectively test the hypothesis that glutamate kills neurons following transition.

Other agents that alter transition in isolated mitochondria have been evaluated for their ability to block glutamate-mediated mitochondrial depolarization. Some of the more potent ones reviewed by Zoratti and Szabò (1995) include trifluoperazine and dibucaine. The former phenothiazine has a number of cellular effects, the most prominent of which may be the inhibition of calmodulin and phospholipase activity. Dibucaine is more widely known as a local anesthetic, an effect accomplished by inhibition of voltage-dependent Na^+ currents. These agents both delay mitochondrial depolarization induced by glutamate, but could not entirely prevent it (Hoyt *et al.*, 1997c). In addition, both appear to hyperpolarize mitochondria, and trifluoperazine may also inhibit mitochondrial Na^+/Ca^{2+} exchange (Hoyt *et al.*, 1997c). We have previously observed a hyperpolarizing response to the NCEm inhibitor CGP37157 (White and Reynolds, 1996), but it is not clear whether this represents ongoing NCEm activity; the other possibility is tonic activity, or perhaps a low-conductance state, of the pore (Ichas and Mazat, 1998). Given the limitations of using membrane potential to unequivocally identify transition it is difficult to make the distinction between these possibilities. These drugs, however, have multiple effects on mitochondria, besides their nonmitochondrial effects, that can be expected to alter the function of excitable cells, which illustrates the potential pharmacological limitations of these agents.

Other drugs have recently been proposed as PTP antagonists. The anti-estrogenic drug tamoxifen has been used as a pro-apoptotic agent in neural mitochondria at high concentrations (Ellerby *et al.*, 1997). Much lower concentrations prevented transition in hepatocytes, however (Custodio *et al.*, 1998). We evaluated tamoxifen actions in neurons and found a biphasic effect on membrane-potential changes induced by glutamate, with maximum depolarization protection at 0.3 μM, much lower than concentrations required to injure the neurons, but the maximally effective concentration of tamoxifen did not protect against excitotoxic injury (Hoyt, *et al.*, 2000). Fontaine and colleagues recently reported (1998) the effects of a series of ubiquinone analogues on mitochondrial function in permeabilized skeletal-muscle mitochondria. Several agents increased mitochondria's ability to accumulate Ca^{2+} in a manner consistent with transition inhibition. We evaluated these compounds in neurons, with rather different results (Scanlon and Reynolds, unpublished). Thus, the most effective agent in muscle, Ub0, appeared to promote mitochondrial depolarization in neurons and was quite toxic, likely a result of ROS generation. The greatest inhibition of depolarization was produced by UB5, but it did not protect against injury at all. It would be immensely valuable to have selective, potent, cell-permeable PTP inhibitors in such studies, but no currently known drugs possess these properties.

4.3. Limitations of Cell Culture Methodology

For understanding intracellular events associated with neuronal injury, cultured neurons have a great benefit: They are readily amenable to single-cell study and to the kinds of manipulation often necessary to grasp the basic mechanisms. The value of the model system only holds, however, in conjunction with its fidelity to the situation *in vivo*. The excitotoxicity model's value has been clearly established by its predictive ability in identifying the neuroprotective actions of glutamate-receptor antagonists, which was subsequently verified *in vivo*, but this model may have limitations not yet fully explored. For example, cells in culture may show a greater dependence on glycolysis than on oxidative phosphorylation as a source of ATP, which could obviously have a profound impact on studies designed to link bioenergetic phenomena with glutamate stimulation. Neurons *in situ* have a close and important interaction with astrocytes, which may be critical in the passage of nutrients from cerebral circulation to neurons (Tsacopoulos and Magistretti, 1996). Because the details of this interaction are poorly understood, it is hard to create such an arrangement *in vitro*. Many imaging studies are performed at room temperature, and this may also impact the neuronal bioenergetic state.

There are additional considerations. Many chronic neurodegenerative states are associated with chronic, relatively modest inhibition of one or more electron transport chain complexes. Indeed, one can model Parkinson and Huntington diseases using specific inhibitors of complex I and complex II, respectively (see below). Acute disorders such as stroke are associated with complete or partial restriction of oxygen and glucose, but studies investigating mitochondrial function after glutamate exposure have usually done so in an environment where oxygen and glucose are not limiting and where electron transport is in good working order. Given that ROS generation, for instance, may increase under both hypoxic (Vanden Hoek *et al.*, 1997) and hyperoxic conditions, studying states that more closely resemble actual diseases may be very important. There are many potential influences on mitochondrial function, Ca^{2+} transport, and ATP generation that must be elucidated to make these model systems more valuable.

4.4. Acutely Isolated Mitochondria Preparations

Much of what is known about the properties of mitochondria in the brain comes from studies of acutely isolated mitochondria, either in the from of purified organelles or in the context of synaptosomes, where mitochondria's immediate environment is better preserved, but revisiting these findings is beyond the scope of this review. Purified brain-derived mitochondria do exhibit a phenomenon similar to transition, in that mitochondria can be loaded with Ca^{2+} and exposed to oxidants to induce swelling (Andreyev *et al.*, 1998; Berman *et al.*, 2000; Friberg *et al.*, 1999). There are some important differences, however, between the characteristics of PTP activation in brain as compared with liver. For example, exposure to levels of oxidants, Ca^{2+}, or both that would normally trigger swelling in liver mitochondria produces only small amplitude changes in brain mitochondria, and the swelling is not accompanied by glutathione release as would be anticipated with PTP activation (Berman *et al.*, 2000). This is not due to an inability of brain mitochondria to swell, because higher-amplitude swelling can be accomplished with mastoparan (Berman *et al.*, 2000) or by removing adenine nucleotides and Mg^{2+}

(Andreyev *et al.*, 1998; Friberg *et al.*, 1999), but the CsA-sensitivity swelling is consistent with a key role for the pore in the swelling process. Interpreting these differences is a challenge, because an adenine-nucleotide-free condition is normally found in neurons, and Mg^{2+} concentrations are near millimolar in these cells (Brocard *et al.*, 1993). It has also been suggested that the polymerization state of creatine kinase in brain could be a key difference from liver (O'Gorman *et al.*, 1997). Nevertheless, the key point here is this: It should not be assumed that the PTP properties in brain are the same as those in the more completely characterized liver and heart preparations.

4.5. Mitochondrial Heterogeneity

The concept of transition is based largely, though not entirely, on observations made in liver mitochondria and many assumptions concerning the PTP's contribution to glutamate-induced neuronal injury are based on the notion that the processes governing PTP activation are the same in neural as in liver mitochondria. Though little explicit information points to functional differences in mitochondria that would account for the different pore properties, it is not far-fetched to suggest that they may exist. We know, for example, that there are differences in the Ca^{2+} efflux pathway between liver mitochondria and mitochondria from excitable cells (Gunter and Pfeiffer, 1990). Also, the fundamental properties of Ca^{2+} and oxidant-induced swelling are distinct, as noted above (Berman *et al.*, 2000). We have also seen that oxidants such as *tert*-butylhydroperoxide—highly effective pore-inducers in liver—have little effect on mitochondrial membrane potential in cultured neurons or in isolated brain mitochondria (Berman *et al.*, 2000; Scanlon and Reynolds, 1998), hence the need for a cautious approach to expectations about neuronal PTP properties.

One intriguing possibility is an additional level of heterogeneity for neurons and non-neuronal cells in the brain, between different populations of neurons, or perhaps even between mitochondria in different regions of the same cell. Recent findings (Beal *et al.*, 1993) have demonstrated, for instance, that systemic administration of complex II inhibitors produces selective degeneration of striatal neurons in rats, which has proved a useful model for Huntington disease. Remarkably, a similar approach using rotenone targets instead the striatal dopamine terminals followed by cell bodies in substantia nigra, producing a Parkinsonlike syndrome in rats (MacKenzie and Greenamyre, 1998). This raises the possibility that mitochondria from different types of neurons in the same brain region have distinct properties, leaving them vulnerable to different toxins. Another interpretation is that the mitochondria are in fact the same, but their environment is different. For example, chronic exposure to high dopamine concentrations could make nigral neurons vulnerable to complex I inhibition, rather than this being a fundamental functional difference in the mitochondria. An argument in favor of this was recently provided by Friberg and colleagues (1998), who demonstrated differences in PTP properties between mitochondria from cortex, hippocampus, and cerebellum. These differences, however, were apparently attributable to different concentrations of adenine nucleotides in the preparations rather than to a fundamental difference in the mitochondria, because nucleotide removal resulted in the mitochondria exhibiting similar swelling characteristics.

The relevance of these findings to glutamate-induced neuronal injury has yet to be fully established. Many chronic disease states that can be modeled using electron transport inhibitors may also have an excitotoxic component, and the interaction between bioenergetics and vulnerability to excitotoxic injury is well established (Greene and Greenamyre, 1996). The extent to which this interaction depends on PTP activation, however, remains unknown.

5. CONCLUSIONS

Glutamate can injure neurons in a way that is likely relevant to a number of acute neurodegenerative states, including stroke and head trauma. It is also likely that glutamate contributes to neurons degeneration in chronic diseases as well. Many studies have established a relationship between the bioenergetic state of neurons and their vulnerability to injury, and more-recent investigations have placed mitochondria at the center of the event cascade linking glutamate receptor activation to neuronal death. The key question posed at the start of this review concerned the role of the PTP in this process, however, and this is much less clear. There are significant concerns in interpretating studies which suggest that transition occurs in intact neurons, because of the difficulty in attributing alterations in membrane potential to pore activation, so these studies remain suggestive but not conclusive. Morphological approaches also imply pore involvement but contain similar methodological concerns. It is evident that CsA is neuroprotective under certain circumstances, but there are multiple mechanisms by which this might be so, and FK506 sometimes has neuroprotective actions as well. No other drugs that alter membrane potential have shown neuroprotective effects. Thus, the body of evidence linking the PTP to excitotoxicity, though suggestive and intriguing, remains to be firmly established.

ACKNOWLEDGMENTS. Our work was supported by USAMRMC grant DAMD-17-98-1-8627 and USPHS grants DA 09601, NS 19068, and NS 34138. The author is an established investigator of the American Heart Association.

REFERENCES

Andreyev, A. Y., Fahy, B., and Fiskum, G., 1998, Cyctochrome *c* release from brain mitochondria is independent of the mitochondrial permeability transition, *FEBS Lett.* **439**:373–376.

Ankarcrona, M., Dypbukt, J. M., Bonfoco, E., Zhivotovsky, B., Orrenius, S., Lipton, S. A., and Nicotera, P., 1995, Glutamate-induced neuronal death: A succession of necrosis or apoptosis depending on mitochondrial function, *Neuron* **15**:961–973.

Baron, K. T., and Thayer, S. A., 1997, CGP 37157 modulates mitochondrial Ca^{2+} homeostasis in cultured rat dorsal root ganglion neurons, *Eur. J. Pharmacol.* **340**:295–300.

Beal, M. F., Hyman, B. T., and Koroshetz, W., 1993, Do defects in mitochondrial energy metabolism underlie the pathology of neurodegenerative diseases? *Trends Neurosci.* **16**:125–131.

Benveniste, H., Drejer, J., Schousboe, A., and Diemer, N. H., 1984, Elevation of the extracellular concentrations of glutamate and aspartate in rat hippocampus during transient cerebral ischemia monitored by intracerebral microdialysis, *J. Neurochem.* **43**:1369–1374.

Berman, S. B., and Hastings, T. G., 1997, Inhibition of glutamate transport in synaptosomes by dopamine oxidation and reactive oxygen species, *J. Neurochem.* **69**:1185–1195.

Berman, S. B., and Hastings, T. G., 1999, Dopamine oxidation alters mitochondrial respiration and induces permeability transition in brain mitochondria: Implications for Parkinson's disease, *J. Neurochem.*, **73**:1127–1137.

Berman, S. B., Watkins, S.C., and Hastings, T. G., 2000, Quantitative biochemical and ultrastructural comparison of mitochondrial permeability transition in isolated brain and liver mitochondria: evidence for relative insensitivity of brain mitochondria. *Exp. Neurol.* **166**:615–625.

Bernardi, P., Broekemeier, K. M., and Pfeiffer, D. R., 1994, Recent progress on regulation of the mitochondrial permeability transition pore: A cyclosporin sensitive pore in the inner mitochondrial membrane, *J. Bioenerg. Biomemb.* **26**:509–517.

Bindokas, V. P., Jordan, J., Lee, C. C., and Miller, R. J., 1996, Superoxide production in rat hippocampal neurons: Selective imaging with hydroethidine, *J. Neurosci.* **16**:1324–1336.

Boast, C. A., Gerhardt, S. C., Pastor, G., Lehmann, J., Etienne, P. E., and Liebman, J. M., 1988, The *N*-methyl-D-aspartate antagonists CGS 19755 and CPP reduce ischemic brain damage in gerbils, *Brain Res.* **442**:345–348.

Brocard, J. B., Rajdev, S., and Reynolds, I. J., 1993, Glutamate induced increases in intracellular free Mg^{2+} in cultured cortical neurons, *Neuron* **11**:751–757.

Budd, S. L., and Nicholls, D. G., 1996a, A reevaluation of the role of mitochondria in neuronal Ca^{2+} homeostasis, *J. Neurochem.* **66**:403–411.

Budd, S. L., and Nicholls, D. G., 1996b, Mitochondria, calcium regulation, and acute glutamate excitotoxicity in cultured cerebellar granule cells, *J Neurochem.* **67**:2282–2291.

Chernyak, B. V., and Bernardi, P. 1996, The mitochondrial permeability transition pore is modulated by oxidative agents through both pyridine nucleotides and glutathione at two separate sites, *Eur. J. Biochem.* **238**:623–630.

Chinopoulos, C., Tretter, L., and Adam-Vizi, V., 1999, Depolarization of *in situ* mitochondria due to hydrogen peroxide-induced oxidative stress in nerve terminals: Inhibition of α-ketoglutarate dehydrogenase, *J. Neurochem.* **73**:220–228.

Choi, D. W., 1987, Ionic dependence of glutamate neurotoxicity, *J. Neurosci.* **7**:369–379.

Choi, D. W., Maulucci-Gedde, M., and Kriegstein, A. R., 1987, Glutamate neurotoxicity in cortical cell culture, *J. Neurosci.* **7**:357–368.

Connern, C. P., and Halestrap, A. P., 1994, Recruitment of mitochondrial cyclophilin to the mitochondrial inner membrane under conditions of oxidative stress that enhance opening of a calcium sensitive non-specific channel, *Biochem. J.* **302**:321–324.

Cox, D. A., and Matlib, M. A., 1993, Modulation of intramitochondrial free Ca^{2+} concentration by antagonists of Na^{+}-Ca^{2+} exchange, *Trends Pharmacol. sci.* **14**:408–413.

Custodio, J. B., Moreno, A. J., and Wallace, K. B., 1998, Tamoxifen inhibits induction of the mitochondrial permeability transition by Ca^{2+} and inorganic phosphate, *Toxicol. Appl. Pharmacol.* **152**:10–17.

Dawson, T. M., Steiner, J. P., Dawson, V. L., Dinerman, J. L., Uhl, G. R., and Snyder, S. H., 1993, Immunosuppressant FK506 enhances phosphorylation of nitric oxide synthase and protects against glutamate neurotoxicity, *Proc. Natl. Acad. Sci. USA* **90**:9808–9812.

Doble, A., 1999, The role of excitotoxicity in neurodegenerative disease: Implications for therapy, *Pharmacol. Ther.* **81**:163–221.

Dubinsky, J. M., and Levi, Y., 1998, Calcium induced activation of the mitochondrial permeability transition in hippocampal neurons, *J. Neurosci. Res.* **53**:728–741.

Dubinsky, J. M., Kristal, B. S., and Elizondo-Fournier, M., 1995, An obligate role for oxygen in the early stages if glutamate-induced, delayed neuronal death, *J. Neurosci.* **15**:7071–7078.

Dugan, L. L., Sensi, S. L., Canzoniero, L. M. T., Handran, S. D., Rothman, S. M., Lin, T.-S., Goldberg, M. P., and Choi, D. W., 1995, Mitochondrial production of reactive oxygen species in cortical neurons following exposure to *N*-methyl-D-aspartate, *J. Neurosci.* **15**:6377–6388.

Dykens, J. A., 1994, Isolated cerebral and cerebellar mitochondria produce free radicals when exposed to elevated Ca^{2+} and Na^{+}: Implications for neurodegeneration, *J. Neurochem.* **63**:584–591.

Ellerby, H. M., Martin, S. J., Ellerby, L. M., Naiem, S. S., Rabizadeh, S., Salvesen, G. S., Casiano, C. A., Cashman, N. R., Green, D. R., and Bredesen, D. E., 1997, Establishment of a cell-free system of neuronal apoptosis: Comparison of premitochondrial, mitochondrial, and postmitochondrial phases, *J Neurosci.* **17**:6165–6178.

Erecinska, M., and Silver, I. A., 1996, Calcium handling by hippocampal neurons under physiologic and pathologic conditions, *Adv. Neurol.* **71**:119–136.

Fontaine, E., Ichas, F., and Bernardi, P., 1998, A ubiquinone binding site regulates the mitochondrial permeability transition pore, *J. Biol. Chem.* **273**:25734–25740.

Friberg, H., Ferrand-Drake, M., Bengtsson, F., Halestrap, A. P., and Wieloch, T., 1998, Cyclosporin A, but not FK 506, protects mitochondria and neurons against hypoglycemic damage and implicates the mitochondrial permeability transition in cell death, *J. Neurosci.* **18**:5151–5159.

Friberg, H., Connern, C. P., Halestrap, A. P., and Wieloch, T., 1999, Differences in the activation of the mitochondrial permeability transition among brain regions correlates with selective vulnerability, *J. Neurochem.* **72**:2488–2497.

Gill, R., Foster, A. C., and Woodruff, G. N., 1987, Systemic administration of MK-801 protects against ischemia-induced hippocampal neurodegeneration in the gerbil, *J Neurosci.* **7**:3343–3349.

Götz, M. E., Künig, G., Riederer, P., and Youdim, M. B. H., 1994, Oxidative stress: Free radical production in neural degeneration, *Pharmacol. Ther.* **63**:37–122.

Graham, D. G., 1978, Oxidative pathways for catecholamines in the genesis of neuromelanin and cytotoxic quinones, *Mol. Pharmacol.* **14**:633–643.

Greene, J. G., and Greenamyre, J. T., 1996, Bioenergetics and glutamate excitotoxicity, *Prog. Neurobiol.* **48**:613–621.

Griffiths, E. J., and Halestrap, A. P., 1991, Further evidence that cyclosporin A protects mitochondria from calcium overload by inhibiting a matrix peptidyl–prolyl *cis–trans* isomerase, *Biochem. J.* **274**:611–614.

Gunter, T. E., and Pfeiffer, D. R., 1990, Mechanisms by which mitochondria transport calcium, *Am. J. Physiol. Cell Physiol.* **258**:C755–C786.

Halestrap, A. P., and Davidson, A. M., 1990, Inhibition of Ca^{2+} induced high amplitude swelling of liver and heart mitochondria by cyclosporin is probably caused by the inhibitor binding to mitochondrial matrix peptidyl–prolyl *cis–trans* isomerase and preventing it interacting with the adenine nucleotide translocase, *Biochem. J.* **268**:153–160.

Hall, E. D., and Braughler, J. M., 1989, Central nervous system trauma and stroke: II. Physiological and pharmacological evidence for involvement of oxygen radicals and lipid peroxidation, *Free Radical Biol. Med.* **6**:303–313.

Halliwell, B., 1992, Reactive oxygen species in the central nervous system, *J. Neurochem.* **59**:1609–1623.

Hastings, T. G., 1995, Enzymatic oxidation of dopamine: The role of prostaglandin H synthase, *J Neurochem.* **64**:919–924.

Hastings, T. G., Lewis, D. A., and Zigmond, M. J., 1996, Role of oxidation in the neurotoxic effects of intrastriatal dopamine injections, *Proc. Natl. Acad. Sci. USA* **93**:1956–1961.

Hoyt, K. R., Gallagher, A. J., Hastings, T. G., and Reynolds, I. J., 1997a, Characterization of hydrogen peroxide toxicity in cultured rat forebrain neurons, *Neurochem. Res.* **22**:333–340.

Hoyt, K. R., Reynolds, I. J., and Hastings, T. G., 1997b, Mechanisms of dopamine-induced cell death in cultured rat forebrain neurons: Interactions with and differences from glutamate-induced cell death, *Exp Neurol.* **143**:269–281.

Hoyt, K. R., Sharma, T. A., and Reynolds, I. J. 1997c, Trifluoperazine and dibucaine inhibit glutamate-induced mitochondrial depolarization in cultured rat forebrain neurones, *Br. J. Pharmacol.* **122**:803–808.

Hoyt, K.R. McLaughlin, B.A., Higgins, D.S., and Reynolds, I.J. Inhibition of glutamate-induced mitochondrial depolarization by tamoxifen in cultured neurons. *J. Pharmacol. Exp. Ther.* **293**:480–486, 2000.

Hyrc, K., Handran, S. D., Rothman, S. M., and Goldberg, M. P., 1997, Ionized intracellular calcium concentration predicts excitotoxic neuronal death: Observations with low affinity fluorescent calcium indicators, *J. Neurosci.* **17**:6669–6677.

Ichas, F., and Mazat, J. P., 1998, From calcium signaling to cell death: Two conformations for the mitochondrial permeability transition pore: Switching from low- to high-conductance state, *Biochim. Biophys. Acta* **1366**:33–50.

Khodorov, B., Pinelis, V., Storozhevykh, T., Vergun, O., and Vinskaya, N., 1996, Dominant role of mitochondria in protection against a delayed neuronal Ca^{2+} overload induced by endogenous excitatory amino acids following a glutamate pulse, *FEBS Lett.* **393**:135–138.

Kiedrowski, L., Wroblewski, J. T., and Costa, E., 1994, Intracellular sodium concentration in cultured cerebellar granule cells challenged with glutamate, *Mol. Pharmacol.* **45**:1050–1054.

Koh, J. Y., Goldberg, M. P., Hartley, D. M., and Choi, D. W., 1990, Non-NMDA receptor mediated neurotoxicity in cortical culture, *J. Neurosci.* **10**:693–705.

Koroshetz, W. J., and Moskowitz, M. A. 1996, Emerging treatments for stroke in humans, *Trends Pharmacol. Sci.* **17**:227–233.

Kristal, B. S., and Dubinsky, J. M., 1997, Mitochondrial permeability transition in the central nervous system: Induction by calcium cycling-dependent and independent pathways, *J. Neurochem.* **69**:524–538.

Kristián, T., Katsura, K., Gidö G., and Siesjö, B. K., 1994, The influence of pH on cellular calcium influx during ischemia, *Brain Res.* **641**:295–302.

Lafon-Cazal, M., Pietri, S., Culcasi, M., and Bockaert, J., 1993, NMDA-dependent superoxide production and neurotoxicity, *Nature* **364**:535–537.

Lu, Y. F., Tomizawa, K., Moriwaki, A., Hayashi, Y., Tokuda, M., Itano, T., Hatase, O., and Matsui, H., 1996, Calcineurin inhibitors, FK506 and cyclosporin A, suppress the NMDA receptor-mediated potentials and LTP, but not depotentiation in the rat hippocampus, *Brain Res.* **729**:142–146.

MacDermott, A. B., Mayer, M. L., Westbrook, G. L., Smith, S. J., and Barker, J. L., 1986, NMDA-receptor activation increases cytoplasmic calcium concentration in cultured spinal cord neurones, *Nature* **321**:519–522.

MacKenzie, G. M., and Greenamyre, J. T., 1998, A novel model of slowly progressive Parkinson's disease, *Soc. Neurosci.* **24**:1721(abstract).

Maker, H. S., Weiss, C., Silides, D. J., and Cohen, G., 1981, Coupling of dopamine oxidation (monamine oxidase activity) to glutathione oxidation via the generation of hydrogen peroxide in the brain, *J. Neurochem.* **36**:589–593.

Mayer, M. L., and Westbrook, G. L., 1987, Cellular mechanisms underlying excitotoxicity, *Trends Neurosci.* **10**:59–61.

McCormack, J. G., Halestrap, A. P., and Denton, R. M., 1990, Role of calcium ions in regulation of mammalian intramitochondrial metabolism, *Physiol. Rev.* **70**:391–425.

Minta, A., Kao, J. P. Y., and Tsien, R. Y., 1989, Fluorescent indicators for cytosolic calcium based on rhodamine and fluorescein chromophores, *J. Biol. Chem.* **264**:8171–8178.

Nicholls, D. G., and Akerman, K. E. O., 1982, Mitochondrial calcium transport, *Biochim. Biophys. Acta* **683**:57–88.

Nieminen, A.-L., Petrie, T. G., Lemasters, J. J., and Selman, W. R., 1996, Cyclosporin A delays mitochondrial depolarization induced by *N*-methyl-D-aspartate in cortical neurons: Evidence of the mitochondrial permeability transition, *Neuroscience* **75**:993–997.

Novgorodov, S. A., Gudz, T. I., Brierley, G. P., and Pfeiffer, D. R., 1994, Magnesium ion modulates the sensitivity of the mitochondrial permeability transition pore to cyclosporin A and ADP, *Arch. Biochem. Biophys.* **311**:219–228.

O'Gorman, E., Beutner, G., Dolder, M., Koretsky, A. P., Brdiczka, D., and Walliman, T., 1997, The role of creatine kinase in inhibition of mitochondrial permeability transition, *FEBS Lett.* **414**:253–257.

Olney, J. W., 1990, Excitotoxic amino acids and neuropsychiatric disorders. *Ann. Rev. Pharmacol. Toxicol.* **30**:47–71.

Peng, T. I., and Greenamyre, J. T., 1998, Privileged access to mitochondria of calcium influx through *N*-methyl-D-aspartate receptors, *Mol. Pharmacol.* **53**:974–980.

Peng, T. I., Jou, M. J., Sheu, S.-S., and Greenamyre, J. T., 1998, Vizualization of NMDA receptor-induced mitochondrial calcium accumulation in striatal neurons, *Exp. Neurol.* **149**:1–12.

Petronilli, V., Miotto, G., Canton, M., Brini, M., Ionna, R., Bernardi P., and Di Lisa, F., 1999, Transient and long-lasting openings of the mitochondrial permeability transition pore can be monitored directly in intact cells by changes in mitochondrial calcein fluorescence, *Biophys. J.* **76**:725–734.

Phillis, J. W., 1994, A "radical" view of cerebral ischemic injury, *Prog. Neurobiol.* **42**:441–448.

Piani, D., Frei, K., Pfister, H.-W., and Fontana, A., 1993, Glutamate uptake by astrocytes is inhibited by reactive oxygen intermediates but not by other macrophage-derived molecules including cytokines, leukotrienes, or platelet-activating factor, *J. Neuroimmunol.* **48**:99–104.

Poot, M., Zhang, Y. Z., KrÄmer, J. A., Wells, K. S., Jones, L., Hanzel, D. K., Lugade, A. G., Singer, V. L., and Haughland, R. P., 1996, Analysis of mitochondrial morphology and function with novel fixable fluorescent stains, *J. Histochem. Cytochem.* **44**:1363–1372.

Reynolds, I. J., and Hastings, T. G., 1995, Glutamate induces the production of reactive oxygen species in cultured forebrain neurons following NMDA receptor activation, *J. Neurosci.* **15**:3318–3327.

Rosenberg, P. A., 1988, Catecholamine toxicity in cerebral cortex in dissociated cell culture, *J. Neurosci.* **8**:2887–2894.

Rothman, S. M., 1984, Synaptic release of excitatory amino acid neurotransmitter mediates anoxic neuronal death, *J. Neurosci.* **4**:1884–1891.

Rothman, S. M., and Olney, J. W., 1987, Excitotoxicity and the NMDA receptor, *Trends Neurosci.* **10**:299–302.

Sattler, R., Charlton, M. P., Hafner, M., and Tymianski, M., 1998, Distinct influx pathways, not calcium load, determine neuronal vulnerability to calcium neurotoxicity, *J. Neurochem.* **71**:2349–2364.

Scanlon, J. M., and Reynolds, I. J. 1998, Effects of oxidants and glutamate receptor activation on mitochondrial membrane potential in rat forebrain neurons, *J. Neurochem.* **71**:2392–2401.

Schinder, A. F., Olson, E. C., Spitzer, N. C., and Montal, M., 1996, Mitochondrial dysfunction is a primary event in glutamate neurotoxicity, *J. Neurosci.* **16**:6125–6133.

Sciamanna, M. A., Zinkel, J., Fabi, A. Y., and Lee, C. P., 1992, Ischemic injury to rat forebrain mitochondria and cellular calcium homeostasis, *Biochim. Biophys. Acta Mol. Cell Res.* **1134**:223–232.

Scorrano L. Petronilli V. Colonna R. Di Lisa F. Bernardi P. Chloromethyltetramethylrosamine (Mitotracker Orange) induces the mitochondrial permeability transition and inhibits respiratory complex I. Implications for the mechanism of cytochrome c release. *J. Biol. Chem.* **274**:24657–24663, 1999.

Stout, A. K., and, Reynolds, I. J., 1999, High-affinity calcium indicators underestimate increases in intracellular calcium concentrations associated with excitotoxic glutamate stimulations, *Neuroscience* **89**:91–100.

Stout, A. K., Raphael, H. M., Kanterewicz, B. I., Klann, E., and Reynolds, I. J., 1998, Glutamate-induced neuron death requires mitochondrial calcium uptake, *Nature Neurosci.* **1**:366–373.

Strijbos, P. J. L. M., Leach, M. J., and Garthwaite, J., 1996, Vicious cycle involving Na^+ channels, glutamate release, and NMDA receptors mediates delayed neurodegeneration through nitric oxide formation, *J. Neurosci.* **16**:5004–5013.

Taylor, C. P., Weber, M. L., Gaughan, C. L., Lehning, E. J., and Lopachin, R. M., 1999, Oxygen/glucose deprivation in hippocampal slices: Altered intraneuronal elemental composition predicts structural and functional damage, *J. Neurosci.* **19**:619–629.

Tretter, L., Chinopoulos, C., and Adam-Vizi, V., 1998, Plasma membrane depolarization and disturbed Na^+ homeostasis induced by the protonophore carbonyl cyanide-*P*-trifluoromethoxyphenyl-hydrazone in isolated nerve terminals, *Mol. Pharmacol.* **53**:734–741.

Tricklebank, M. D., Singh, L., Oles, R. J., Wong, E. H. F., and Iversen, S. D., 1987, A role for receptors of *N*-methyl-D-aspartic acid in the discriminative stimulus properties of phencyclidine, *Eur. J. Pharmacol.* **141**:497–501.

Tsacopoulos, M., and Magistretti, P. J., 1996, Metabolic coupling between glia and neurons, *J. Neurosci.* **16**:877–885.

Tymianski, M., Charlton, M. P., Carlen, P. L., and Tator, C. H., 1993, Source specificity of early calcium neurotoxicity in cultured embryonic spinal neurons, *J. Neurosci.* **13**:2085–2104.

Vanden Hoek, T. L., Li, C., Shao, Z., Schumacker, P. T., and Becker, L. B., 1997, Significant levels of oxidants are generated by isolated cardiomyocytes during ischemia prior to reperfusion, *J. Mol. Cell. Cardiol.* **29**:2571–2583.

Volterra, A., Trotti, D., Tromba, C., Floridi, S., Racagni, G., 1994, Glutamate uptake inhibition by oxygen free radicals in rat cortical astrocytes, *J. Neurosci.* **14**:2924–2932.

Wang, G. J., and Thayer, S. A., 1996, Sequestration of glutamate-induced Ca^{2+} loads by mitochondria in cultured rat hippocampal neurons, *J. Neurophysiol.* **76**:1611–1621.

White, R. J., and Reynolds, I. J., 1995, Mitochondria and Na^+/Ca^{2+} exchange buffer glutamate-induced calcium loads in cultured cortical neurons, *J. Neurosci.* **15**:1318–1328.

White, R. J., and Reynolds, I. J., 1996, Mitochondrial depolarization in glutamate-stimulated neurons: An early signal specific to excitotoxin exposure, *J. Neurosci.* **16**:5688–5697.

White, R. J., and Reynolds, I. J., 1997, Mitochondria accumulate Ca^{2+} following intense glutamate stimulation of cultured rat forebrain neurones, *J. Physiol.*(London) **498**:31–47.

Zhang, Y., Marcillat, O., Guilivi, C., Ernster, L., and Davies, K. J. A., 1990, The oxidative inactivation of mitochondrial electron transport chain components and ATPase, *J. Biol. Chem.* **265**:16330–16336.

Zoratti, M., and Szabò, I. 1995, The mitochondrial permeability transition, *Biochim. Biophys. Acta* **1241**:139–176.

Research

Cell Calcium (2000) 28(5/6), 317–327

doi: 10.1054/ceca.2000.0171, available online at http://www.idealibrary.com on IDEAL®

Pharmacological investigation of mitochondrial Ca^{2+} transport in central neurons: studies with CGP-37157, an inhibitor of the mitochondrial Na^{+}–Ca^{2+} exchanger

J. M. Scanlon, J. B. Brocard, A. K. Stout, I. J. Reynolds

University of Pittsburgh, School of Medicine, Department of Pharmacology, Pittsburgh, USA

Summary Mitochondria buffer large changes in $[Ca^{2+}]_i$ following an excitotoxic glutamate stimulus. Mitochondrial sequestration of $[Ca^{2+}]_i$ can beneficially stimulate oxidative metabolism and ATP production. However, Ca^{2+} overload may have deleterious effects on mitochondrial function and cell survival, particularly Ca^{2+}–dependent production of reactive oxygen species (ROS) by the mitochondria. We recently demonstrated that the mitochondrial Na^{+}–Ca^{2+} exchanger in neurons is selectively inhibited by CGP-37157, a benzothiazepine analogue of diltiazem. In the present series of experiments we investigated the effects of CGP-37157 on mitochondrial functions regulated by Ca^{2+}. Our data showed that 25 μM CGP-37157 quenches DCF fluorescence similar to 100 μM glutamate and this effect was enhanced when the two stimuli were applied together. CGP-37157 did not increase ROS generation and did not alter glutamate or 3 mM hydrogen-peroxide-induced increases in ROS as measured by DHE fluorescence. CGP-37157 induces a slight decrease in intracellular pH, much less than that of glutamate. In addition, CGP-37157 does not enhance intracellular acidification induced by glutamate. Although it is possible that CGP-37157 can enhance mitochondrial respiration both by blocking Ca^{2+} cycling and by elevating intramitochondrial Ca^{2+}, we did not observe any changes in ATP levels or toxicity either in the presence or absence of glutamate. Finally, mitochondrial Ca^{2+} uptake during an excitotoxic glutamate stimulus was only slightly enhanced by inhibition of mitochondrial Ca^{2+} efflux. Thus, although CGP-37157 alters mitochondrial Ca^{2+} efflux in neurons, the inhibition of Na^{+}–Ca^{2+} exchange does not profoundly alter glutamate-mediated changes in mitochondrial function or mitochondrial Ca^{2+} content. © 2000 Harcourt Publishers Ltd

INTRODUCTION

Of the many ways in which neurons can die perhaps the most extensively studied are the processes collectively referred to as 'excitotoxicity' [1,2]. This phenomenon is associated with the release of glutamate from neuronal and non-neuronal stores and subsequently the excessive activation of ionotropic glutamate receptors. Excitotoxic glutamate injury probably reflects a collection of neurotoxic mechanisms depending on the duration and intensity of the glutamate exposure and the type of receptors activated. This is most readily appreciated, and well studied, in primary cell culture. In cortical neurons, for example, a brief exposure (approximately 5 min) to a high concentration of glutamate results in activation of the N-methyl-D-aspartate (NMDA) subtype of glutamate receptor, allows massive Ca^{2+} entry and results in predominantly necrotic cell injury [3,4]. Lower concentrations of glutamate can also be toxic via the activation of NMDA receptors, but it has been suggested that this results in apoptotic injury [5]. If non-NMDA glutamate receptors are activated a form of injury is triggered that depends less on extracellular calcium, and requires

Received 27 September 2000
Accepted 10 October 2000

Correspondence to: Dr Ian J. Reynolds, Department of Pharmacology, W1351 Biomedical Science Tower, University of Pittsburgh, School of Medicine, Pittsburgh, PA 15261, USA. Tel.: +1 412 648 2134; fax: +1 412 624 0794; e-mail: iannmda@pitt.edu

several hours of stimulation to commit neurons to die, but is expressed as necrotic cell death [6]. Evidence for all of these forms of injury have been found in vivo [2,7,8]. Thus, excitotoxicity should not be considered as a single homogenous phenomenon.

In this laboratory we have focused on the acute, necrotic injury that results from NMDA receptor activation and depends on Ca^{2+} entry [4]. This form of injury is likely to be a consequence of the particular effectiveness with which NMDA receptors permit neuronal Ca^{2+} accumulation, because they form a Ca^{2+}-permeable channel that only partially inactivates during prolonged exposure to agonists (unlike, for example, voltage-gated Ca^{2+} channels). Thus, excitotoxic NMDA receptor activation results in very high cytoplasmic free Ca^{2+} concentrations [9,10] in addition to potentially allowing Ca^{2+} entry into specific sites in neurons poised to cause injury [11]. As has been reported in several types of excitable cells [12–14], neuronal mitochondria buffer these glutamate-induced large Ca^{2+} loads particularly well [15–24]. However, it appears that the consequence of this mitochondrial Ca^{2+} buffering is lethal. Thus, if mitochondrial Ca^{2+} accumulation is prevented by eliminating the mitochondrial membrane potential (and thus abrogating the driving force for mitochondrial Ca^{2+} uptake) neurons are protected from NMDA receptor-mediated injury [25,26].

It remains unclear what links mitochondrial Ca^{2+} accumulation to injury. Studies in isolated mitochondria and intact neurons have suggested that glutamate-stimulated mitochondrial Ca^{2+} accumulation results in the production of reactive oxygen species (ROS) that may originate from mitochondria [27–31]. The activation of the permeability transition pore has also been suggested [32–34], although evidence supporting this mechanism is incomplete.

The finding that excitotoxicity requires mitochondrial Ca^{2+} accumulation is an exciting development because it suggests novel targets at which to aim neuroprotective drug strategies. However, at this stage the pharmacology of mitochondrial transport is rather poorly developed. The major Ca^{2+} uptake pathway is likely to be the Ca^{2+} uniporter [12], which may be complemented by a rapid uptake mode of the kind described in liver mitochondria [35,36]. There are several inhibitors of the Ca^{2+} uniporter, including ruthenium red and the related Ru360 [37], as well as some cobaltammine agents [38]. However, most of these agents penetrate cells very poorly, as exemplified by the 10 000-fold decrease in potency of Ru360 in intact cardiac myocytes compared to cardiac mitochondria [37]. Indeed, even applying relatively high concentrations of Ru360 (~10 μM) for several tens of minutes to intact neurons has very little effect on glutamate-induced cytosolic Ca^{2+} transients (JBB and IJR, unpublished observations). It was also recently suggested that mitochondrial Ca^{2+} accumulation can occur if the mitochondrial Na^+–Ca^{2+} exchanger reverses [39], although it is not known if this occurs in neurons.

An alternative approach to modifying mitochondrial Ca^{2+} loading is to manipulate the primary efflux pathways. In excitable cells mitochondrial Ca^{2+} efflux may be mediated by several different pathways. Under normal circumstances the mitochondrial Na^+–Ca^{2+} exchanger may be the primary mechanism for efflux [40]. In principle, it is also possible that the uniporter could reverse if the mitochondrial membrane potential is lost [41], and activation of permeability transition should also result in massive Ca^{2+} release [42]. Both of these latter situations would be associated with catastrophic alterations in mitochondrial membrane potential that might occur in relation to pathophysiological states, and we have seen little evidence for either process in intact neurons even following prolonged exposure to glutamate. However, using pharmacological approaches we have been able to demonstrate the presence of the mitochondrial Na^+–Ca^{2+} exchanger and the impact of mitochondrial Ca^{2+} release on cytosolic Ca^{2+} concentrations [43,44]. For example, when mitochondria are loaded with Ca^{2+} following the exposure of neurons to a relatively high glutamate concentration the resulting recovery of $[Ca^{2+}]_i$ to baseline levels is rather slow. This slow recovery is evidently due to the persistent efflux of mitochondrial Ca^{2+} stores through the Na^+–Ca^{2+} exchanger, because inhibiting this process with the diltiazem analogue CGP-37157 rapidly restores $[Ca^{2+}]_i$ to basal values, while removing the inhibitor is associated with a resumption of mitochondrial Ca^{2+} release. Similar effects are also observed in peripheral neurons that show a particularly prominent mitochondrial Ca^{2+} release component following the activation of voltage-gated Ca^{2+} channels [45]. Although CGP-37157 does have other pharmacological effects, such as the inhibition of voltage-gated Ca^{2+} channels [45], it rapidly and reversibly inhibits mitochondrial Ca^{2+} efflux in intact neurons and, as such, appears to be one of the more useful agents currently available to manipulate mitochondrial Ca^{2+} signalling.

In the experiments reported here we investigated the notion that by blocking what may be the major mitochondrial Ca^{2+} efflux pathway we could potentiate glutamate-stimulated, Ca^{2+}-mediated alterations in mitochondrial function. We examined the effects of CGP-37157 on several different aspects of mitochondrial physiology, including ROS generation, intracellular acidification, and excitotoxic neuronal injury, anticipating that CGP-37157 would increase mitochondrial Ca^{2+} accumulation and thereby potentiate glutamate-induced neuronal death.

MATERIALS AND METHODS

Cell culture

Primary neuronal cultures were obtained from the forebrains of embryonic day 17 Sprague-Dawley rats and dissociated as previously described [46]. Animals were handled in accordance with the National Institutes of Health Guide for the Care and Use of Laboratory Animals and with the Institutional Animal Care and Use Committee of the University of Pittsburgh. Briefly, the cortical lobes were incubated in 0.005–0.01% trypsin in Ca^{2+}-free, Mg^{2+}-free media (in mM: 116 NaCl, 5.4 KCl, 26.2 $NaHCO_3$, 11.7 NaH_2PO_4, 5 glucose, 0.001% Phenol Red, and minimum essential media amino acids; pH adjusted to 7.4 with NaOH) for 30 min at 37°C. Viability determinations were made with the trypan blue (0.08%) exclusion method. The plating suspension was diluted to 300 000 cells/ml using plating medium (v/v solution of 90% Dulbecco's modified Eagle's medium, 10% heat-inactivated fetal bovine serum, 24 U/ml penicillin, 24 μg/ml streptomycin; final glutamine concentration 3.1 mM). Cells were plated onto poly-L-lysine-coated (40 μg/ml) 31 mm glass coverslips that were inverted 1 day later in a maintenance medium (horse serum substituted for fetal calf serum, all other constituents identical). Inversion of the coverslips prevents glial proliferation. Cells were maintained under 95% air, 5% CO_2 until use 2 weeks later. Only those coverslips containing healthy neurons (rounded-oval, smooth, and bright cell bodies when viewed using phase-contrast optics) were used. On the day of experimentation, culture medium was removed and replaced with HEPES-buffered salt solution (HBSS) of the following composition (mM): 137 NaCl, 5 KCl, 0.9 $MgSO_4$, 1.4 $CaCl_2$, 3 $NaHCO_3$, 0.6 Na_2HPO_4, 0.4 KH_2PO_4, 5.6 glucose, and 20 HEPES; adjusted to pH 7.4 with NaOH.

Intracellular ROS production

ROS production was measured by fluorescence microscopy using the oxidation sensitive dyes, 2,7-dichlorodihydrofluorescein ($DCFH_2$) or dihydroethidium (DHE) [29,31] as previously described [47]. Fluorescence was recorded using a Meridian ACAS 570c laser scanning confocal imaging system. A 488 nm excitation line from an argon laser was used in conjunction with a 510 nm dichroic mirror and focused through a 225 m pinhole and a 40× phase-contrast objective to yield an optical slice of about 2.5 m through the middle of the neurons (0.20 m in diameter).

Forebrain neurons that were 2 weeks in culture were loaded with 10 M $DCFH_2$ or 2 M DHE for 15 min at 37°C in HBSS supplemented with 5 mg/ml bovine serum albumin; 4 mM stocks of $DCFH_2$ or DHE were made in methanol or anhydrous DMSO respectively. $DCFH_2$ was removed just prior to imaging whereas DHE was maintained in solution throughout the experiment. Fluorescence was recorded at room temperature from a single field of cells (180 × 180 μm) per coverslip typically containing 5–15 neurons. Cells were imaged over a period of 15 min at 1 scan per min. After obtaining 2 min of basal fluorescence, cells were exposed to various treatments for a period of 10–15 min Fluorescence was normalized to the intensity measured in the first scan to account for problems in equal dye loading. Data were presented for each test condition as the change in normalized fluorescence (mean ± SEM) over time (min). All experiments were performed on at least two coverslips from no less than two different culture dates. Cells displaying localized increases in DCF fluorescence were determined visually by an observer blinded to the treatment.

Measurement of intracellular pH

Fluorescence imaging, as previously described [26], was performed on a Nikon Diaphot 300 microscope fitted with a 40× quartz objective, a Dage-MTI cooled-CCD camera with 640 × 480-pixel resolution in combination with a Dage-MTI Gen II Sys image intensifier and a 75 watt Xenon lamp-based monochromator light source. Attenuation of incident light was achieved with a 0.1% neutral density filter and passed through a 515 nm dichroic mirror. Emitted fluorescence was measured with a 535 ± 12.5 nm band-pass filter after alternate excitation at 498 nm and 450 nm. Data acquisition analysis was controlled using Simple PCI software (Compix, Cranberry, PA). Forebrain neurons (2 weeks in culture) were incubated for 15 min at 37°C with 2′,7′-bis-(2-carboxyethyl)-5(and 6)-carboxyfluorescein (BCECF) (5 μM) in HBSS supplemented with 5 mg/ml BSA. After loading, coverslips were rinsed with HBSS, mounted in a recording chamber and perfused with HBSS at a rate of 20 ml/min. Cells were exposed to various treatments for a period of 5 min. After approximately 10 min of recovery in normal HBSS, cells were exposed to 25 mM NH_4Cl for 1 min as a positive control. Fluorescence was recorded at room temperature and background fluorescence values (determined from cell-free regions of each coverslip) were subtracted from all signals.

Toxicity assay

Forebrain neurons (2 weeks in culture) were rinsed twice with HBSS, and coverslips were inverted to orient the cultured neurons face-up. Neurons were exposed to various treatments for a period of 5 min and then rinsed with HBSS. Cells were placed in Minimum Essential

Medium containing penicillin (24 U/ml) and streptomycin (24 μg/ml) and allowed to incubate for 20–24 h at 37°C. Neuronal viability was then assessed with a trypan blue (0.4%) exclusion method as previously described [26]. Data are presented as the mean number of live cells from three experiments in which three fields, from each of three coverslips, were counted by an observer blinded to the treatment condition.

Determination of intracellular ATP

Forebrain neurons (2 weeks in culture) were rinsed twice with HBSS and coverslips were inverted to orient the cultured neurons face-up. Neurons were exposed to various treatments for a period of 10 min and then rinsed with ice-cold PBS. Cellular ATP was extracted from three coverslips per condition in 400 μL of 0.5% TCA/125 M EDTA using a disposable cell scraper. Extracts were centrifuged at 13 800 g for 5 min at 37°C. For each condition, 300 μL of supernatant was added to 120 μL of 0.1 M Tris and kept on ice throughout the experiment. ATP content was measured using a Luciferin-Luciferase Assay (Molecular Probes, Eugene, Oregon) with a scintillation counter (Beckman LS 1801) to detect luminescence. Sample [ATP] was determined using nonlinear regression analysis of the ATP Standard Curve. Data are presented as the percent of controls (mean ± SEM) from three separate experiments using two different cell culture dates.

Measurement of $[Ca^{2+}]_i$

The acetoxy methyl ester form of MagFura-2 (Molecular Probes, Oregon, USA) was diluted to 1 mM in anhydrous DMSO. Coverslips were incubated in HBSS containing 5 μM of MagFura-2, 0.5% of DMSO and 5 mg/ml of bovine serum albumin for 20 min at 37°C. Cells were then rinsed with HBSS, mounted on a record chamber and perfused with HBSS at a rate of 20 ml/min. All recordings were made at room temperature.

The imaging system consisted of a Nikon Diaphot 300 inverted microscope fitted with a 40 × objective, a digital Orca camera (Hamamatsu Corporation, New Jersey) and a 75 Watt Xenon lamp-based monochromator light source as previously described [10]. Cells were alternately illuminated with 335 and 375 nm beams. Incident light was attenuated with neutral density filters (typically by about 90%; Omega Optical, Vermont) and emitted fluorescence passed through a 515 nm dichroic mirror and a 535 ± 12.5 nm band-pass filter (Omega Optical, Vermont). Background fluorescence, determined from three cell-free regions of the coverslips, was subtracted from all the signals prior to calculating the ratios as described.

Materials

CGP-37157 (7-chloro-3,5-dihydro-5-phenyl-1H-4,1-benzothiazepine-2-on) was a generous gift from Ciba-Geigy Pharmaceuticals (Basel, Switzerland) and was also purchased from Tocris Cookson Inc. (Missouri). Stock solutions of CGP-37157 were prepared using anhydrous dimethyl sulfoxide and further diluted in HBSS. All fluorescent indicators were purchased from Molecular Probes (Eugene, Oregon).

Statistical analysis

Statistical significance between groups of three or more experimental conditions was determined by one-way analysis of variance (ANOVA) followed with a Bonferroni post-hoc analysis using Prism v3.0 (GraphPad Software, San Diego, CA). Statistical significance between two groups was determined using a two-tailed, unpaired student's *t*-test.

RESULTS

Effects of CGP-37157 on production of ROS

Several studies have demonstrated a Ca^{2+}-dependent production of ROS via the mitochondria following a glutamate stimulus [29–31]. If one can speculate that blocking Ca^{2+} entry into the mitochondria may potentially inhibit glutamate-induced ROS production, then along the same line of reasoning blocking Ca^{2+} efflux may enhance mitochondrial ROS generation. Thus, we studied the impact of the Na^{+}–Ca^{2+} exchange inhibitor on the fluorescence of two oxidation sensitive indicators in the presence or absence of glutamate or an exogenous oxidant.

In this model system glutamate induced a three-fold increase in DHE fluorescence (Fig. 1A). Interestingly, hydrogen peroxide produced a somewhat smaller oxidation of DHE compared to glutamate (Fig. 1B). DHE fluorescence after exposure to CGP-37157 was similar to controls (Figs 1A & B). In addition, CGP-37157 did not alter glutamate or hydrogen-peroxide-induced increases in DHE fluorescence (Figs 1A & B).

Both CGP-37157 and glutamate decreased DCF fluorescence to a similar extent (Fig. 1C). This effect was enhanced when the two stimuli were applied together (Fig. 1C). Glutamate but not CGP-37157 produces localized increases in intracellular DCF fluorescence (Fig. 2). We used a cell counting method to assess DCF oxidation responses, as we have previously described [29]. The number of cells displaying glutamate-induced increases in localized fluorescence was reduced by 73% when CGP-37157 is applied with glutamate ($t = 5.23$; $P < 0.0008$; Fig. 2). In these experiments we used hydrogen peroxide

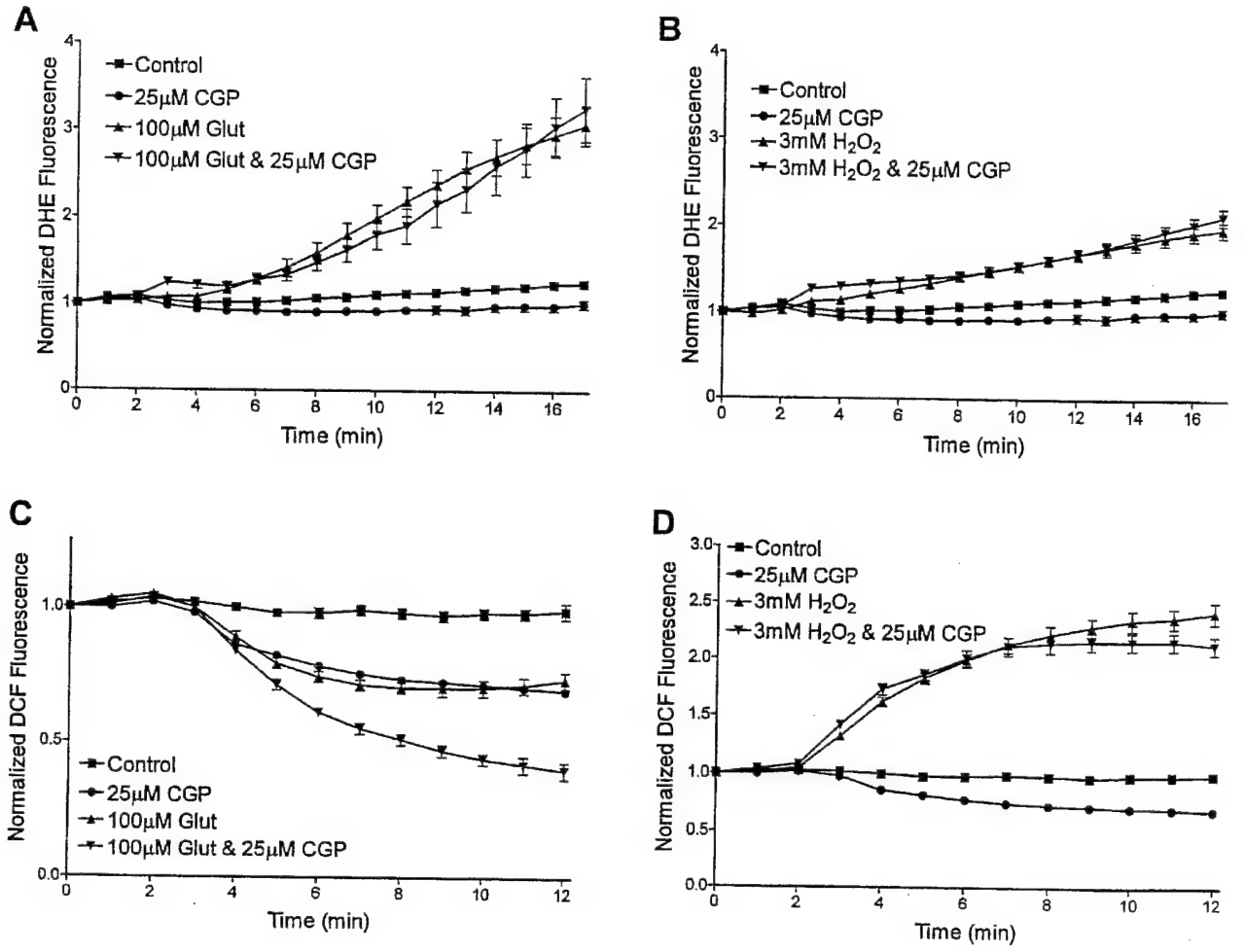

Fig. 1 CGP-37157 does not stimulate intracellular ROS generation. Neurons were loaded with 2 μM DHE (A, B) or 10 μM DCF (C, D) for 15 min at 37°C. After obtaining 2 min of basal fluorescence, neurons were exposed to various treatments for a period of 10–15 min (A, C). Data shows the effects of HBSS, 25 μM CGP-37157, 100 μM glutamate with 1 μM glycine, or both. (B, D) Data shows the effects of HBSS, 25 μM CGP-37157, 3 mM hydrogen peroxide, or both. Points represent the mean ± SEM from 20 to 100 neurons obtained from 2–6 coverslips from no less than 2 culture dates.

(3 mM) as a positive control, and this stimulus induced a 2–2.5-fold increase in DCF fluorescence which was not affected by the addition of CGP-37157 (Fig. 1D).

CGP-37157 produces decreases in intracellular pH

Glutamate will quench DCF fluorescence due to intracellular acidification [29]. Thus, we wanted to determine if CGP-37157 decreases DCF fluorescence due to a similar mechanism using the pH-sensitive indicator BCECF, which is not sensitive to ROS. CGP-37157 produces a slight and reversible decrease in intracellular pH (Fig. 3). The intracellular acidification induced by glutamate is much greater than the effect of CGP-37157. However, the intracellular acidification produced by glutamate is not altered by the addition of CGP-37157 (Fig. 3).

Blocking mitochondrial Na^+–Ca^{2+} exchange does not affect cellular ATP content

Ca^{2+} may act as a second messenger to stimulate ATP production. Mitochondrial Ca^{2+} can stimulate several key enzymes involved in cellular respiration [48]. Previous studies have shown that CGP-37157 will increase the P_m possibly as a result of enhanced mitochondrial activity [32]. Mitochondrial Ca^{2+} cycling following glutamate exposure uncouples oxidative respiration from ATP production. Thus, inhibition of mitochondrial Ca^{2+} cycling and enhancement of the mitochondrial Ca^{2+} load with CGP-37157 may enhance ATP production or inhibit decreases due to glutamate. A 5-min exposure to 100 μM glutamate and 1 μM glycine did not significantly decrease the ATP levels compared to controls (Fig. 4)

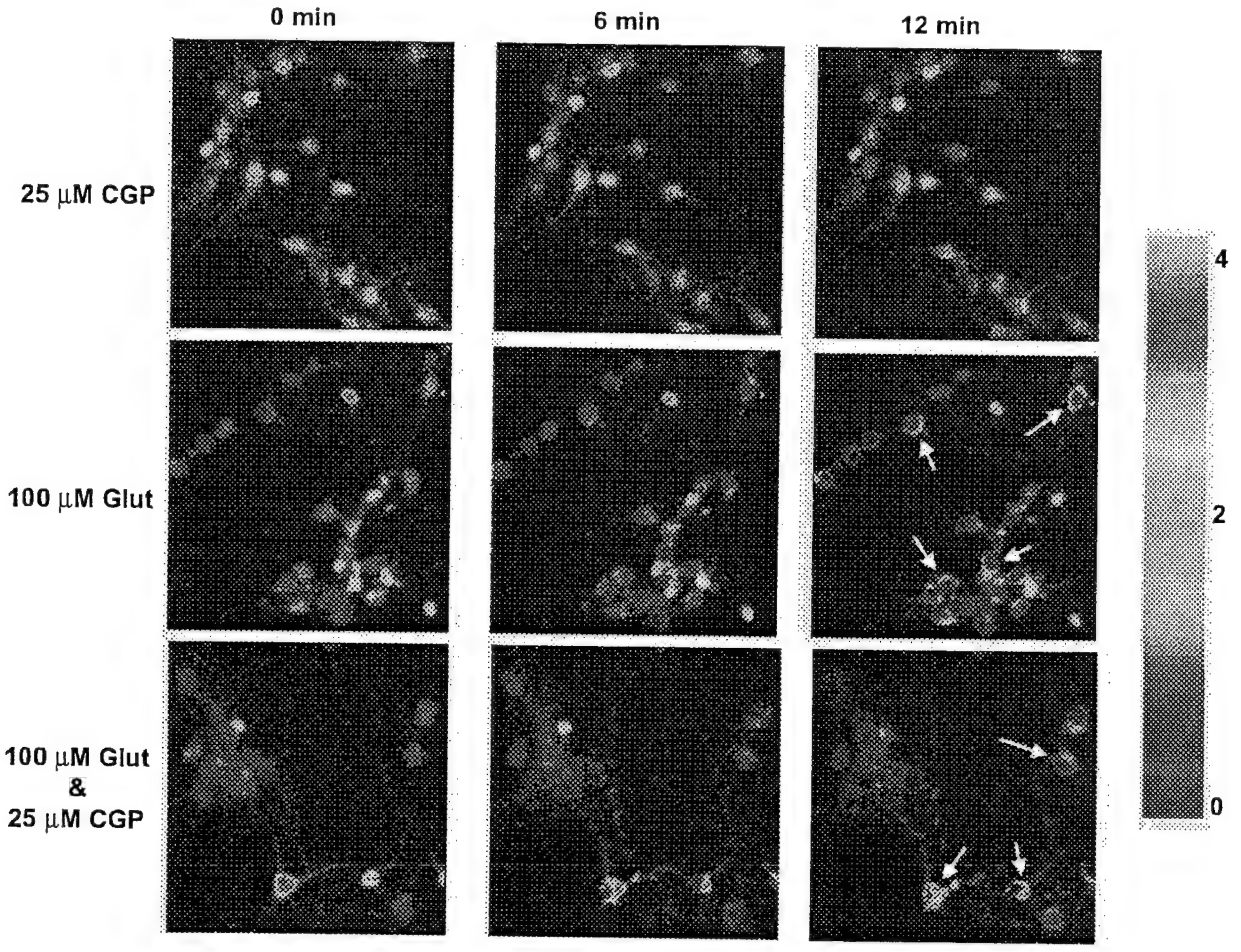

Fig. 2 CGP-37157 inhibits localized ROS production by glutamate. Representative images display the effects of 25 μM CGP-37157, 100 μM glutamate with 1 μM glycine, or both on intracellular DCF fluorescence. For each condition neurons are shown at the start of the experiment (3 min prior to exposure), 6 min (3 min after exposure), or 12 min (9 min after exposure). The colour scale represents arbitrary fluorescent units. Experiments were repeated on five different coverslips from four different culture dates typically yielding 50–100 cells ($n=5$). Glutamate produced localized increases in DCF fluorescence in 70.8% of the cells, whereas CGP-37157 plus glutamate only displayed localized increases in fluorescence in 18.8% of the cells. Examples of cells that would be scored as positive by the counting approach are identified by white arrows in the panels on the right. These effects were significantly different ($t=5.23$; $P<0.0008$, two-tailed, unpaired Student's *t*-test).

similar to a 5 min exposure to 750 nM FCCP (Fig. 4). CGP-37157 in the presence or absence of glutamate did not alter cellular ATP content (Fig. 4).

Effects of CGP-37157 on glutamate-induced neuronal viability

Excessive mitochondrial Ca^{2+} cycling following glutamate exposure can lead to mitochondrial depolarization and bioenergetic failure and may contribute to neuronal death. As a result of inhibiting Ca^{2+} cycling CGP-37157 may be neuroprotective following an excitotoxic glutamate stimulus. However, recent studies have demonstrated that inhibition of mitochondrial Ca^{2+} uptake is neuroprotective against glutamate excitotoxicity [25,26]. Also, mitochondrial Ca^{2+} can stimulate opening of the PTP. It is possible that enhancing mitochondrial Ca^{2+} loads with CGP-37157 could increase toxicity following a glutamate stimulus. Thus, we examined the effects of the Na^{+}–Ca^{2+} exchange inhibitor on glutamate-induced neurotoxicity. Our results show that a 5-min exposure to 100 μM glutamate/1 μM glycine typically produces a 40% loss in viable neurons as compared to cells exposed to buffer changes alone (Fig. 5). CGP-37157 does not alter neuronal viability. Glutamate and the combination of glutamate and CGP-37157 significantly decrease cell viability compared to controls ($P<0.01$). However, these two conditions are not significantly different from each other.

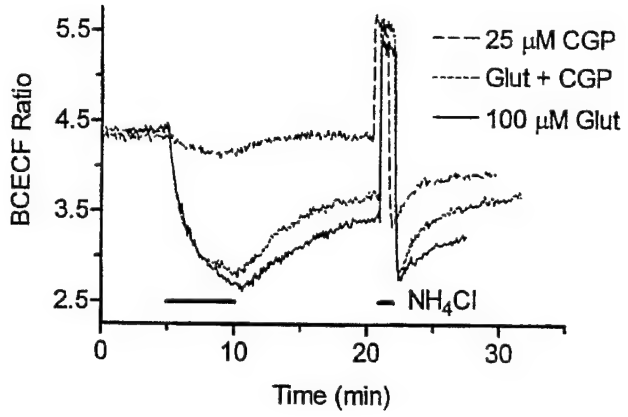

Fig. 3 Effects of CGP-37157 and glutamate on intracellular pH. Neurons were stimulated with 25 μM CGP-37157, 100 μM glutamate with 10 μM glycine, or both for 5 min (indicated by the bar). After approximately 10 min of recovery in normal HBSS, neurons were exposed to 25 mM NH_4Cl for 1 min as a positive control to display the dynamic range of dye response. A decrease in the BCECF ratio indicates a decrease in intracellular pH. Traces represent the mean data from separate coverslips containing 17–25 neurons. Similar results were obtained in cells from two additional culture dates.

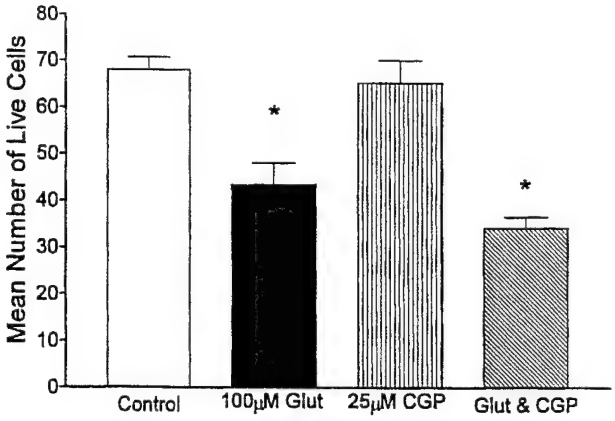

Fig. 5 CGP-37157 does not alter neuronal death. Bars represent the mean results from three experiments in which three fields from each of three coverslips were counted for each treatment condition in a blinded manner. On each experimental day coverslips were exposed (in triplicate) for 5 min to the following conditions: HBSS, 25 μM CGP-37157, 100 μM glutamate plus 1 μM glycine, or glutamate and CGP-37157. Cells excluding trypan blue were counted. Statistical significance was determined using a one-way ANOVA test followed by Bonferroni post-hoc analysis. *Significantly different ($P<0.01$) compared to control.

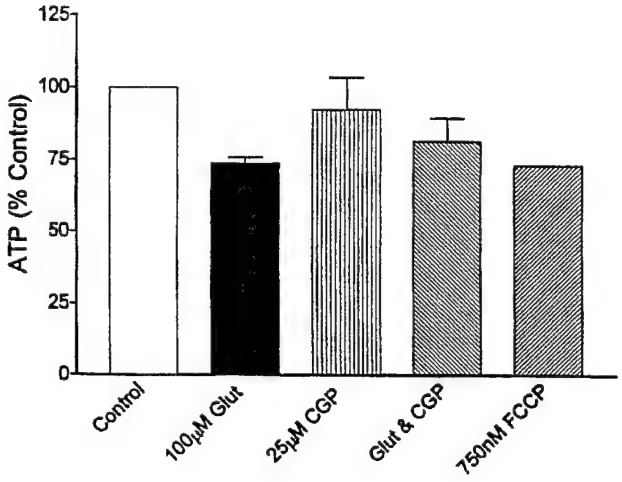

Fig. 4 Effects of CGP-37157 and glutamate on cellular ATP levels. Neuronal ATP levels are presented as the percent ATP of control values. Neurons were exposed to either HBSS, 750 nM FCCP, 25 μM CGP-37157, 100 μM glutamate with 1 μM glycine, or both CGP-37157 and glutamate for 10 min prior to extraction of cell lysate. Cell extracts were harvested from three coverslips per condition. ATP levels were determined by a luciferase assay system. Data are presented as the percent of control (mean ± SEM) of three separate experiments from two different culture dates. None of the conditions were significantly different from control as determined by ANOVA followed by a Bonferroni post-hoc analysis.

Effects of CGP-37157 on glutamate-induced changes in $[Ca^{2+}]_i$ and mitochondrial Ca^{2+}

The relative lack of effect of CGP-37157 on mitochondrial function and glutamate-induced changes in mitochondrial function led us to examine the effects of Na^+–Ca^{2+}-exchange inhibition on glutamate-induced changes in $[Ca^{2+}]_i$ and mitochondrial Ca^{2+} loads. We have recently demonstrated the feasibility of estimating matrix Ca^{2+} by using FCCP to release mitochondrial Ca^{2+} and MagFura-2 to measure the $[Ca^{2+}]_i$ after this procedure (Fig. 6A, [49]).

A 5-min exposure to 100 μM glutamate and 1 μM glycine increases $[Ca^{2+}]_i$ as measured with MagFura-2 (Fig. 6D grey bar; glutamate). However, this may not indicate the full extent of Ca^{2+} influx following glutamate-receptor activation as the mitochondria are simultaneously buffering $[Ca^{2+}]_i$ (Fig. 6A). Thus, we used 750 nM FCCP to release accumulated mitochondrial Ca^{2+} following glutamate stimulation (Fig. 6D grey bar; FCCP). FCCP is applied in Ca^{2+}-free HBSS to ensure that Ca^{2+} entry is not occurring via voltage-sensitive Ca^{2+} channels as a result of FCCP-induced depolarization of the plasma membrane. The application of CGP-37157 during the 5-min glutamate stimulus had no significant effect on measurable $[Ca^{2+}]_i$ levels (Fig. 6D black bar; glutamate). Surprisingly, inhibition of the Na^+–Ca^{2+} exchanger only produced a slight enhancement of accumulated mitochondrial Ca^{2+} (Fig. 6D black bar; FCCP). Although the use of the low-affinity Ca^{2+} indicator MagFura-2 in these experiments makes it unlikely that dye saturation occurred during these experiments, this is a possible explanation for the failure of CGP-37157 to enhance glutamate-induced mitochondrial Ca^{2+} accumulation. To exclude this possibility we also monitored the effects of CGP-37157 using the same paradigm but

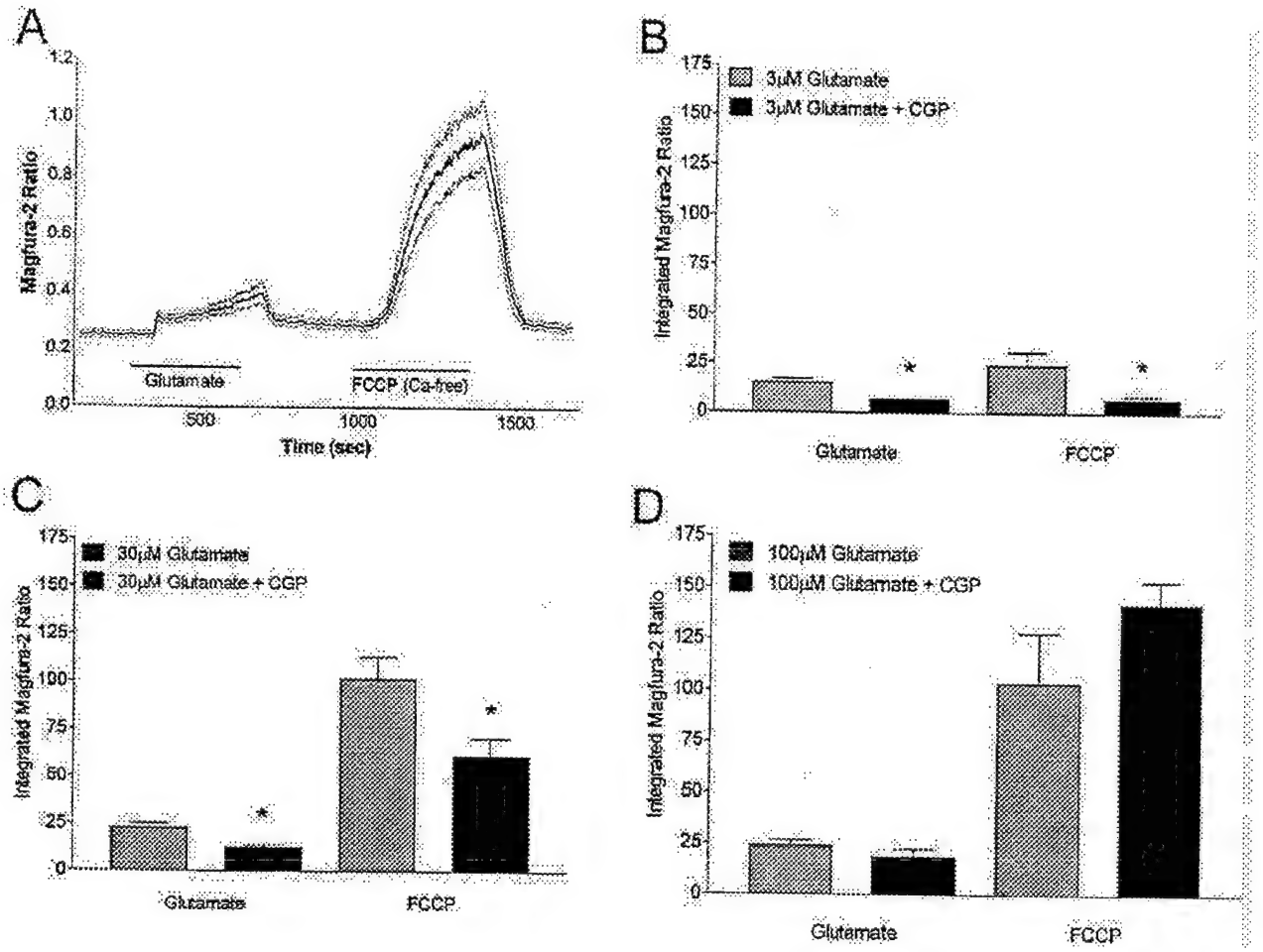

Fig. 6 Effects of CGP-37157 on glutamate-induced mitochondrial Ca^{2+} loading. (A) A representative trace is included to display the experimental paradigm. After 4 min of baseline monitoring of MagFura-2-loaded cells, glutamate (30 μM) and glycine (1 μM), were applied for 5 min. Cells were then rinsed with HBSS for 5 min and perfused with FCCP (750 nM) for a further 5 min. The baseline was taken as the ratio preceding the introduction of glutamate in the buffer. The solid line represents the mean of 15 neurons from a single cover slip, while the broken line shows the SEM for these cells. (B–D) Mean data obtained using this paradigm while varying the concentration of glutamate between three and 100 μM as indicated. Note that the experiments depicted in B and C were performed with 10 μM CGP-37157 while the experiment in D used 25 μM. Data represent the integrated area under the curve of baseline-subtracted values obtained during exposure to glutamate or to FCCP. Bars represent the mean results from 5–7 coverslips over two or more culture dates. CGP-37157 significantly *decreased* the glutamate-induced cytosolic and mitochondrial Ca^{2+} changes determined using ANOVA (*indicates significantly different from control, $P<0.05$).

with lower glutamate concentrations which result in reduced cytoplasmic and mitochondrial Ca^{2+} accumulation (Figs 6B & C). However, although an increase in mitochondrial Ca^{2+} might be expected in the presence of CGP-37157 we actually observed a decrease in cytosolic and mitochondrial Ca^{2+} under these conditions.

DISCUSSION

In this study we have explored the effect of the mitochondrial Na^+–Ca^{2+}-exchange inhibitor CGP-37157 on glutamate-stimulated, NMDA receptor-mediated changes in mitochondrial function in central neurons. Our anticipation in approaching these experiments was that CGP-37157 would increase matrix Ca^{2+} concentrations and thereby potentiate the glutamate stimulated changes in function. What is quite obvious from the present experiments is that this is not at all the case.

The oxidation sensitive dyes DCF and DHE are able to report several phenomena associated with glutamate receptor activation. DHE is preferentially oxidized by superoxide [31], but may also report alterations in mitochondrial membrane potential ($\Delta\Psi_m$) [50]. However, CGP-37157 did not potentiate the DHE signal. That it did not alter the effects of peroxide on DHE fluorescence argues that the apparent lack of effect is not due to some non-specific effect on the dye or that it has antioxidant properties (Fig. 1B). DCF is sensitive to the formation of

ROS and is also quenched by intracellular acidification [29]. The CGP-37157-induced decrease in DCF may be con-sistent with intracellular acidification, as is the potentiation of the effects of glutamate (although see below). Detecting an increase in oxidation of DCF can be somewhat problematic with the marked decrease in signal that occurs with acidification. However, counting the cells that show the characteristic localized increases in fluorescence circumvents this problem [29]. Once again, these results are not consistent with enhancement of the accumulation of matrix calcium.

Increases in matrix Ca^{2+} stimulates Ca^{2+}-sensitive, rate-limiting dehydrogenases involved in metabolism, and thus couples increased energy demand signalled by an elevation in $[Ca^{2+}]_i$ to the aerobic production of ATP [48]. This should have several consequences for the neurons stimulated by glutamate. Enhanced metabolic activation has been proposed to account for the well-documented intracellular acidification associated with NMDA receptor activation and Ca^{2+} influx [51–53], and this would be consistent with the increased quenching of DCF shown in Figure 1B. However, an authentic pH indicator, BCECF, showed relatively little effect either of CGP-37157 alone or in combination with glutamate (Fig. 3). In addition, mitochondrial Na^+–Ca^{2+} exchange occurs at the expense of ATP generation [40,53], so that inhibition of this process should at least prevent ATP loss. However, increases in the $\Delta\Psi_m$ can also result from ATP hydrolysis in an effort to maintain or restore $\Delta\Psi_m$ [19,54] and may alternatively explain the hyperpolarization induced by CGP-37157 over neuronal cultures. Surprisingly, CGP-37157 had no effect on cellular ATP levels, compared to controls, in the presence or absence of glutamate (Fig. 4). One could speculate that the lack of change in cellular ATP levels in our culture system is because of a greater dependence on glycolytic ATP production than on oxidative phosphorylation as seen in cultured cerebellar granule cells [19,25], but again it is difficult to relate these observations simply to enhanced matrix Ca^{2+} accumulation. The ultimate question with respect to glutamate-induced alterations in mitochondrial function is the impact of CGP-37157 on neuronal viability, and CGP-37157 evidently has no beneficial or detrimental effect on the viability of neurons in the absence or presence of glutamate (Fig. 5). Thus, although mitochondrial uptake of Ca^{2+} during excitotoxicity is clearly detrimental to cell viability [25,26], CGP-37157 clearly does not have a substantial impact on this process.

This raises the question of whether CGP-37157 has any effect on matrix Ca^{2+} content at all. This has been a difficult question to address experimentally for a variety of reasons. In the kinds of experimental approach used here, several laboratories have used the Ca^{2+} indicator rhod-2 to estimate matrix Ca^{2+} changes [55–60]. This is clearly an effective approach provided that the dye can be localized to the mitochondrial matrix rather than any other cellular compartment, and also provided that the matrix Ca^{2+} concentrations do not exceed the dynamic range of the dye. Indeed, some of the other reports in this volume elegantly demonstrate the use of this approach. However, under conditions of excitotoxicity it is likely that matrix Ca^{2+} greatly exceeds the limit of sensitivity of this dye (~5 μM, based on an affinity of about 500 nM). Thus, although it is possible to load the dye into mitochondria in neurons and to monitor changes in matrix Ca^{2+} [59–61] it is not clear that the dye faithfully reports the full extent of the Ca^{2+} change.

We recently developed an alternative approach to determining mitochondrial Ca^{2+} content following glutamate exposure [49]. This approach takes advantage of the reversibility of the Ca^{2+} uniporter [13]. Thus, following exposure of neurons to glutamate the cells are exposed to FCCP which collapses the mitochondrial membrane potential and releases Ca^{2+} into the matrix, presumably by the reversal of the uniporter. A low-affinity Ca^{2+} indicator (MagFura-2 in this case) can then be used to report the Ca^{2+} changes, and provide a semiquantitative insight into the Ca^{2+} contents of the mitochondria.

Using this approach we were thus able to monitor the Ca^{2+} loading of mitochondria following glutamate exposure in the absence or presence of CGP-37157 (Fig. 6). Rather surprisingly, CGP-37157 had little effect on the matrix Ca^{2+} content under the conditions employed for most of the studies reported here (i.e. 100 μM glutamate for 5 min). To ensure that the failure to observe an effect of CGP-37157 was not due to dye saturation, or to the possibility that mitochondria are overwhelmed with the Ca^{2+} load caused by this toxic stimulus, we also tried lower glutamate concentration, but also failed to see an effect of CGP-37157 beyond a small inhibition of the glutamate triggered Ca^{2+} entry, which may be a consequence of the Ca^{2+} channel inhibition produced by this drug.

It is not at all clear how to account for the lack of effect of a drug that, under some circumstances at least, has a substantial effect on the egress of Ca^{2+} from neuronal mitochondria [43,45,62]. Although the failure to increase matrix Ca^{2+} accounts for the lack of effect of CGP-37157 on ROS generation, ATP depletion or synthesis and neuronal viability, it is not obvious why Ca^{2+} was not increased. Perhaps the most obvious suggestion is that the major Ca^{2+} efflux pathway in effect during glutamate exposure is not, in fact, the Na^+–Ca^{2+} exchanger. Based on the observations of the effects of FCCP it is clear that a loss of $\Delta\Psi_m$ can result in release of Ca^{2+} from mitochondria, presumably via reversal of the uniporter. We know that at least some of the neurons will exhibit mitochondrial depolarization during glutamate exposure [32] which might result in Ca^{2+} release.

Activation of the permeability transition pore would also result in Ca^{2+} release that is insensitive to CGP-37157, although evidence for the activation of this process during glutamate stimulation is less than robust. Most tissues also have a Na^+-independent mitochondrial Ca^{2+} efflux pathway [40]. Although the Na^+–Ca^{2+} exchanger is considered to be the dominant mechanism in brain, it is perhaps possible that the Na^+-independent pathway is more active in our neurons under the circumstances of Na^+–Ca^{2+} exchanger inhibition. A more trivial explanation of such observations would be that CGP-37157 blocks NMDA receptors at the concentrations used. We have no evidence for such an effect at this point (and this would certainly not account for its ability to alter mitochondrial Ca^{2+} efflux previously reported) but this remains an issue with all pharmacological approaches to studying physiological function.

More broadly, the difficulties in interpreting what should be a straightforward set of results illustrate the problems encountered with the pharmacological manipulation of mitochondrial Ca^{2+} transport. The drugs that inhibit the main mitochondrial influx pathways do not penetrate cells well (Ru360), are not very specific for the uniporter (ruthenium red) and do not very clearly distinguish between the different modes of Ca^{2+} uptake [36]. Assuming that the Na^+–Ca^{2+} exchanger is the main efflux pathway, an apparently specific and effective inhibitor does not at all have the anticipated effect, as reported here. This leaves one with the option of manipulating these processes indirectly, such as by the use of FCCP or by inhibition of electron transport to manipulate membrane potential. However, these approaches cannot be considered specific either, and the other actions of FCCP, for example, are well recognized [63]. Thus, investigating mitochondrial Ca^{2+} transport in intact cells using pharmacological approaches remains quite problematic.

ACKNOWLEDGMENTS

These studies were supported by USAMRMC grant DAMD17-98-1-8627 and by NIH grant NS 34138 (IJR). JBB was supported by a Long-Term Fellowship from the Human Frontiers Science Program (LT0500/1999B).

REFERENCES

1. Mayer ML, Westbrook GL. Cellular mechanisms underlying excitotoxicity. *Trends Neurosci* 1987; **10**: 59–61.
2. Choi DW. Glutamate neurotoxicity and diseases of the nervous system. *Neuron* 1988; **1**: 623–634.
3. Choi DW, Maulucci-Gedde M, Kriegstein AR. Glutamate neurotoxicity in cortical cell culture. *J Neurosci* 1987; **7**: 357–368.
4. Choi DW. Ionic dependence of glutamate neurotoxicity. *J Neurosci* 1987; **7**: 369–379.
5. Ankarcrona M, Dypbukt JM, Bonfoco E et al. Glutamate-induced neuronal death: a succession of necrosis or apoptosis depending on mitochondrial function. *Neuron* 1995; **15**: 961–973.
6. Koh JY, Goldberg MP, Hartley DM, Choi DW. Non-NMDA receptor mediated neurotoxicity in cortical culture. *J Neurosci* 1990; **10**: 693–705.
7. Kristián T, Ouyang Y, Siesjö BK. Calcium-induced neuronal cell death in vivo and in vitro: are the pathophysiologic mechanisms different? *Adv Neurol* 1996; **71**: 107–118.
8. Doble A. The role of excitotoxicity in neurodegenerative disease: implications for therapy. *Pharmacol Ther* 1999; **81**: 163–221.
9. Hyrc K, Handran SD, Rothman SM, Goldberg MP. Ionized intracellular calcium concentration predicts excitotoxic neuronal death: observations with low affinity fluorescent calcium indicators. *J Neurosci* 1997; **17**: 6669–6677.
10. Stout AK, Reynolds IJ. High-affinity calcium indicators underestimate increases in intracellular calcium concentrations associated with excitotoxic glutamate stimulations. *Neuroscience* 1999; **89**: 91–100.
11. Sattler R, Xiong Z, Lu WY, Hafner M, MacDonald JF, Tymianski M. Specific coupling of NMDA receptor activation to nitric oxide neurotoxicity by PSD-95 protein. *Science* 1999; **284**: 1845–1848.
12. Nicholls DG, Akerman KEO. Mitochondrial calcium transport. *Biochim Biophys Acta* 1982; **683**: 57–88.
13. Gunter TE, Pfeiffer DR. Mechanisms by which mitochondria transport calcium. *Am J Physiol Cell Physiol* 1990; **258**: C755–C786.
14. Babcock DF, Hille B. Mitochondrial oversight of cellular Ca^{2+} signalling. *Curr Opin Neurobiol* 1998; **8**: 398–404.
15. Duchen MR. Ca^{2+}-dependent changes in the mitochondrial energetics in single dissociated mouse sensory neurons. *Biochem J* 1992; **283**: 41–50.
16. Friel DD, Tsien RW. An FCCP-sensitive Ca^{2+} store in bullfrog sympathetic neurons and its participation in stimulus-evoked changes in $[Ca^{2+}]_i$. *J Neurosci* 1994; **14**: 4007–4024.
17. Werth JL, Thayer SA. Mitochondria buffer physiological calcium loads in cultured rat dorsal root ganglion neurons. *J Neurosci* 1994; **14**: 348–356.
18. Kiedrowski L, Costa E. Glutamate-induced destabilization of intracellular calcium concentration homeostasis in cultured cerebellar granule cells: role of mitochondria in calcium buffering. *Mol Pharmacol* 1995; **47**: 140–147.
19. Budd SL, Nicholls DG. A reevaluation of the role of mitochondria in neuronal Ca^{2+} homeostasis. *J Neurochem* 1996; **66**: 403–411.
20. Khodorov B, Pinelis V, Storozhevykh T, Vergun O, Vinskaya N. Dominant role of mitochondria in protection against a delayed neuronal Ca^{2+} overload induced by endogenous excitatory amino acids following a glutamate pulse. *FEBS Lett* 1996; **393**: 135–138.
21. Wang GJ, Thayer SA. Sequestration of glutamate-induced Ca^{2+} loads by mitochondria in cultured rat hippocampal neurons. *J Neurophysiol* 1996; **76**: 1611–1621.
22. Brorson JR, Sulit RA, Zhang H. Nitric oxide disrupts Ca^{2+} homeostasis in hippocampal neurons. *J Neurochem* 1997; **68**: 95–105.
23. Murchison D, Griffith WH. Age-related alterations in caffeine-sensitive calcium stores and mitochondrial buffering in rat basal forebrain. *Cell Calcium* 1999; **25**: 439–452.
24. Pivovarova NB, Hongpaisan J, Andrews SB, Friel DD. Depolarization-induced mitochondrial Ca accumulation in sympathetic neurons: spatial and temporal characteristics. *J Neurosci* 1999; **19**: 6372–6384.

25. Budd SL, Nicholls DG. Mitochondria, calcium regulation and acute glutamate excitotoxicity in cultured cerebellar granule cells. *J Neurochem* 1996; **67**: 2282–2291.
26. Stout AK, Raphael HM, Kanterewicz BI, Klann E, Reynolds IJ. Glutamate-induced neuron death requires mitochondrial calcium uptake. *Nature Neurosci* 1998; **1**: 366–373.
27. Lafon-Cazal M, Pietri S, Culcasi M, Bockaert J. NMDA-dependent superoxide production and neurotoxicity. *Nature* 1993; **364**: 535–537.
28. Dykens JA. Isolated cerebral and cerebellar mitochondria produce free radicals when exposed to elevated Ca^{2+} and Na^{+}: implications for neurodegeneration. *J Neurochem* 1994; **63**: 584–591.
29. Reynolds IJ, Hastings TG. Glutamate induces the production of reactive oxygen species in cultured forebrain neurons following NMDA receptor activation. *J Neurosci* 1995; **15**: 3318–3327.
30. Dugan LL, Sensi SL, Canzoniero LMT et al. Mitochondrial production of reactive oxygen species in cortical neurons following exposure to N-methyl-D-aspartate. *J Neurosci* 1995; **15**: 6377–6388.
31. Bindokas VP, Jordan J, Lee CC, Miller RJ. Superoxide production in rat hippocampal neurons: selective imaging with hydroethidine. *J Neurosci* 1996; **16**: 1324–1336.
32. White RJ, Reynolds IJ. Mitochondrial depolarization in glutamate-stimulated neurons: An early signal specific to excitotoxin exposure. *J Neurosci* 1996; **16**: 5688–5697.
33. Schinder AF, Olson EC, Spitzer NC, Montal M. Mitochondrial dysfunction is a primary event in glutamate neurotoxicity. *J Neurosci* 1996; **16**: 6125–6133.
34. Nieminen A-L, Petrie TG, Lemasters JJ, Selman WR. Cyclosporin A delays mitochondrial depolarization induced by N-methyl-D-aspartate in cortical neurons: evidence of the mitochodrial permeability transition. *Neuroscience* 1996; **75**: 993–997.
35. Sparagna GC, Gunter KK, Sheu S-S, Gunter TE. Mitochondrial calcium uptake from physiological-type pulses of calcium. A description of the rapid uptake mode. *J Biol Chem* 1996; **270**: 27510–27515.
36. Gunter TE, Buntinas L, Sparagna GC, Gunter KK. The Ca^{2+} transport mechanisms of mitochondria and Ca^{2+} uptake from physiological type calcium transients. *Biochim Biophys Acta* 1998; **1366**: 5–15.
37. Matlib MA, Zhou Z, Knight S et al. Oxygen-bridged dinuclear ruthenium amine complex specifically inhibits Ca^{2+} uptake into mitochondria in vitro and in situ in single cardiac myocytes. *J Biol Chem* 1998; **273**: 10223–10231.
38. Crompton M, Andreeva L. On the interactions of Ca^{2+} and cyclosporin A with a mitochondrial inner membrane pore: a study using cobaltammine complex inhibitors of the Ca^{2+} uniporter. *Biochem J* 1994; **302**: 181–185.
39. Griffiths EJ. Reversal of mitochondrial NaCa exchange during metabolic inhibition in rat cardiomyocytes. *FEBS Lett* 1999; **453**: 400–404.
40. Gunter TE, Gunter KK, Sheu S-S, Gavin CE. Mitochondrial calcium transport: physiological and pathological relevance. *Am J Physiol Cell Physiol* 1994; **267**: C313–C339.
41. Fiskum G, Cockrell RS. Uncoupler-stimulated release of Ca^{2+} from Ehrlich ascites tumor cell mitochondria. *Arch Biochem Biophys* 1985; **240**: 723–733.
42. Zoratti M, Szabo I. The mitochondrial permeability transition. *Biochim Biophys Acta* 1995; **1241**: 139–176.
43. White RJ, Reynolds IJ. Mitochondria accumulate Ca^{2+} following intense glutamate stimulation of cultured rat forebrain neurones. *J Physiol (Lond)* 1997; **498**: 31–47.
44. Hoyt KR, Stout AK, Cardman JM, Reynolds IJ. An evaluation of intracellular sodium and mitochondria in the buffering of kainate-induced intracellular free calcium changes in rat forebrain neurons. *J Physiol (Lond)* 1998; **509**: 103–116.
45. Baron KT, Thayer SA. CGP 37157 modulates mitochondrial Ca^{2+} homeostasis in cultured rat dorsal root ganglion neurons. *Eur J Pharmacol* 1997; **340**: 295–300.
46. White RJ, Reynolds IJ. Mitochondria and Na^{+}/Ca^{2+} exchange buffer glutamate-induced calcium loads in cultured cortical neurons. *J Neurosci* 1995; **15**: 1318–1328.
47. Scanlon JM, Reynolds IJ. Effects of oxidants and glutamate receptor activation on mitochondrial membrane potential in rat forebrain neurons. *J Neurochem* 1998; **71**: 2392–2401.
48. McCormack JG, Halestrap AP, Denton RM. Role of calcium ions in regulation of mammalian intramitochondrial metabolism. *Physiol Rev* 1990; **70**: 391–425.
49. Brocard JB, Tassetto M, Reynolds IJ. Quantitative evaluation of mitochondrial calcium content following glutamate receptor stimulation in rat cortical neurones. *J Physiol (Lond)* 2000; (in press).
50. Budd SL, Castilho RF, Nicholls DG. Mitochondrial membrane potential and hydroethidine-monitored superoxide generation in cultured cerebellar granule cells. *FEBS Lett* 1997; **415**: 21–24.
51. Hartley Z, Dubinsky JM. Changes in intracellular pH associated with glutamate excitotoxicity. *J Neurosci* 1993; **13**: 4690–4699.
52. Irwin RP, Lin S-Z, Long RT, Paul SM. N-methyl-D-aspartate induces a rapid, reversible and calcium dependent intracellular acidosis in cultured fetal rat hippocampal neurons. *J Neurosci* 1994; **14**: 1352-1357.
53. Wang GJ, Randall RD, Thayer SA. Glutamate-induced intracellular acidification of cultured hippocampal neurons demonstrates altered energy metabolism resulting from Ca^{2+} loads. *J Neurophysiol* 1994; **72**: 2563–2569.
54. Di Lisa F, Blank PS, Colonna R et al. Mitochondrial membrane potential in single living adult rat cardiac myocytes exposed to anoxia or metabolic inhibition. *J Physiol (Lond)* 1995; **486**: 1–13.
55. Burnier M, Centeno G, Burki E, Brunner HR. Confocal microscopy to analyze cytosolic and nuclear calcium in cultured vascular cells. *Am J Physiol* 1994; **266**: C1118–C1127.
56. Simpson PB, Russell JT. Mitochondria support inositol 1,4,5-trisphosphate-mediated Ca^{2+} waves in cultured oligodendrocytes. *J Biol Chem* 1996; **271**: 33493–33501.
57. Babcock DF, Herrington J, Goodwin PC, Park YB, Hille B. Mitochondrial participation in the intracellular Ca^{2+} network. *J Cell Biol* 1997; **136**: 833–844.
58. Trollinger DR, Cascio WE, Lemasters JJ. Selective loading of Rhod 2 into mitochondria shows mitochondrial Ca^{2+} transients during the contractile cycle in adult rabbit cardiac myocytes. *Biochem Biophys Res Commun* 1997; **236**: 738–742.
59. David G, Barrett JN, Barrett EF. Evidence that mitochondria buffer physiological Ca^{2+} loads in lizard motor nerve terminals. *J Physiol (Lond)* 1998; **509**: 59–65.
60. Peng TI, Jou MJ, Sheu S-S, Greenamyre JT. Vizualization of NMDA receptor-induced mitochondrial calcium accumulation in striatal neurons. *Exp Neurol* 1998; **149**: 1–12.
61. Peng TI, Greenamyre JT. Privileged access to mitochondria of calcium influx through N-methyl-D-aspartate receptors. *Mol Pharmacol* 1998; **53**: 974–980.
62. Zhang YL, Lipton P. Cytosolic Ca^{2+} changes during in vitro ischemia in rat hippocampal slices: major roles for glutamate and Na^{+}-dependent Ca^{2+} release from mitochondria. *J Neurosci* 1999; **19**: 3307–3315.
63. Tretter L, Chinopoulos C, Adam-Vizi V. Plasma membrane depolarization and disturbed Na^{+} homeostasis induced by the protonophore carbonyl cyanide-p-trifluoromethoxyphenyl-hydrazone in isolated nerve terminals. *Mol Pharmacol* 1998; **53**: 734–741.

Journal of Neurochemistry, 2001, **79**, 266–277

$\Delta\Psi_m$-Dependent and -independent production of reactive oxygen species by rat brain mitochondria

Tatyana V. Votyakova and Ian J. Reynolds

Department of Pharmacology, University of Pittsburgh, Pittsburgh, Pennsylvania, USA

Abstract

Mitochondria are widely believed to be the source of reactive oxygen species (ROS) in a number of neurodegenerative disease states. However, conditions associated with neuronal injury are accompanied by other alterations in mitochondrial physiology, including profound changes in the mitochondrial membrane potential $\Delta\Psi_m$. In this study we have investigated the effects of $\Delta\Psi_m$ on ROS production by rat brain mitochondria using the fluorescent peroxidase substrates scopoletin and Amplex red. The highest rates of mitochondrial ROS generation were observed while mitochondria were respiring on the complex II substrate succinate. Under this condition, the majority of the ROS signal was derived from reverse electron transport to complex I, because it was inhibited by rotenone. This mode of ROS generation is very sensitive to depolarization of $\Delta\Psi_m$, and even the depolarization associated with ATP generation was sufficient to inhibit ROS production. Mitochondria respiring on the complex I substrates, glutamate and malate, produce very little ROS until complex I is inhibited with rotenone, which is also consistent with complex I being the major site of ROS generation. This mode of oxidant production is insensitive to changes in $\Delta\Psi_m$. With both substrates, ubiquinone-derived ROS can be detected, but they represent a more minor component of the overall oxidant signal. These studies demonstrate that rat brain mitochondria can be effective producers of ROS. However, the optimal conditions for ROS generation require either a hyperpolarized membrane potential or a substantial level of complex I inhibition.

Keywords: Amplex red, free radicals, mitochondrial membrane potential, rotenone, scopoletin.

J. Neurochem. (2001) **79**, 266–277.

In addition to their critical role in ATP synthesis, mitochondria are also the major source of reactive oxygen species (ROS) in most cell types. Generated by the incomplete reduction of molecular oxygen during the process of oxidative phosphorylation, superoxide is the main form of ROS produced by mitochondria (Sorgato *et al.* 1974; Boveris and Cadenas 1975). It has been suggested that 2% of the oxygen consumed by mitochondria is converted to superoxide (Boveris and Chance 1973). In turn, superoxide is converted by manganese superoxide dismutase to H_2O_2, which is more stable and more lipid soluble, and thus can be more readily released by mitochondria. Although it is possible that mitochondrially derived ROS serve a signaling function in cells, it is more widely believed that ROS are harmful as the result of the oxidative modification of proteins, nucleic acids and lipid membranes.

The mechanisms responsible for the generation of ROS by the electron transport chain have been extensively investigated, primarily in mitochondria derived from heart muscle (Loschen *et al.* 1971; Boveris and Chance 1973; Cadenas and Boveris 1980; Turrens *et al.* 1985; Korshunov *et al.* 1997). The principal source appears to be the redox cycling ubiquinone in complex III (Boveris *et al.* 1976; Cadenas *et al.* 1977). An additional source of superoxide is complex I, which is also endowed with a number of redox centers (Cadenas *et al.* 1977; Takeshige and Minakami 1979; Turrens and Boveris 1980). In isolated mitochondrial preparations it is possible to demonstrate ROS generation from these two major sites when mitochondria respire on substrates that drive either complex I (glutamate and malate) or complex II (succinate). It is interesting to note that the relative magnitude of the ROS signal deriving from either substrate varies quite considerably between tissues. For example, in heart mitochondria complex I substrates

Received June 7, 2001; revised manuscript received July 19, 2001; accepted July 19, 2001.

Address correspondence and reprint requests to Ian J. Reynolds, Department of Pharmacology, University of Pittsburgh, W1351 Biomedical Science Tower, Pittsburgh PA 15261, USA.
E-mail: iannmda@pitt.edu

Abbreviations used: $\Delta\Psi_m$, mitochondrial transmembrane potential; 2,4-DNP, 2,4-dinitrophenol; FCCP, carbonyl cyanide *p*-(trifluoromethoxy) phenyl hydrazone; HRP, horseradish peroxidase; ROS, reactive oxygen species.

generate the largest ROS signal (in the presence of appropriate inhibitors) (Boveris and Chance 1973), while in brain mitochondria complex II substrates appear to be quantitatively more important (Cino and Del Maestro 1989). However, the specific, endogenous mechanisms responsible for altering ROS production by mitochondria are poorly understood.

It is widely believed that ROS contribute to the pathogenesis of a number of neurodegenerative diseases (Halliwell 1992; Beal *et al.* 1997), and given the high rate of oxygen consumption by the brain, it may be reasonable to assume that mitochondria are responsible for the majority of the ROS burden under both normal and pathophysiological situations. However, the mechanisms by which brain mitochondria produce ROS have been investigated less than in other tissues. Indeed, the earliest investigation of this topic concluded that brain mitochondria do not produce ROS (Sorgato *et al.* 1974). More recent studies have conclude that peroxide production can be detected from brain mitochondria from several species, and that the ROS derive from both complex I and ubiquinone (Patole *et al.* 1986; Zoccarato *et al.* 1988; Cino and Del Maestro 1989). Several studies in intact neurons have used oxidation-sensitive fluorescent dyes to detect ROS generation following glutamate receptor activation, and have concluded that mitochondria are the likely source of the ROS signal (Reynolds and Hastings 1995; Dugan *et al.* 1995; Bindokas *et al.* 1996). This suggests that glutamate- and calcium-mediated alterations in mitochondrial function might contribute to the acute injury of neurons, as well as to chronic neurodegenerative states. However, there is a major gap in the understanding of the mechanisms that link glutamate receptor activation to the alteration of mitochondrial ROS production.

We undertook the present study to characterize the mechanisms responsible for ROS production by brain mitochondria using the peroxidase substrates scopoletin and Amplex red to detect peroxide production by mitochondria. In particular, we have investigated the influence of the mitochondrial membrane potential on ROS production because this has been reported to modify certain forms of ROS production by mitochondria in some tissues (Loschen *et al.* 1971; Korshunov *et al.* 1997), and may also be a key variable in the injury of neurons by glutamate (Nieminen *et al.* 1996; Schinder *et al.* 1996; White and Reynolds 1996; Vergun *et al.* 1999). We report here that there are mitochondrial membrane potential dependent and independent mechanisms for the generation of ROS by isolated rat brain mitochondria.

Materials and methods

Isolation of rat brain mitochondria

All procedures using rats were approved by the Institutional Animal Care and Use Committee of the University of Pittsburgh, and are consistent with guidelines provided by the National Institutes of Health. Rat brain mitochondria were isolated from the cortex of adult Sprague–Dawley strain rats by conventional differential centrifugation as described by Rosenthal *et al.* (1987) with minor modifications. After removal, brains were placed in isolation media which contained: 225 mM mannitol, 75 mM sucrose, 5 mM HEPES buffer (pH adjusted to 7.3 with KOH), 1 mg/mL BSA and 0.5 mM tetrapotassium EDTA. After centrifugation at 10 500 *g*, the first mitochondrial pellet was treated with digitonin (40 : 1 of 10% w/v digitonin solution per brain) with a final concentration of 0.013%. Mitochondria were then resuspended and centrifuged in isolation medium without digitonin. All the isolation procedures were carried out at 0 ± 2°C. Prior to experimentation, mitochondria were stored on ice at final concentration of 20–30 mg protein/mL in isolation medium. The protein concentration was determined by the Bradford method (Bradford 1976). Mitochondria prepared in this way were active for 5–6 h, as determined by their ability to maintain a transmembrane potential in the presence of oxidizable substrates.

Fluorescence measurements of H_2O_2 production and mitochondrial transmembrane potential $\Delta\Psi_m$

Fluorescence measurements were performed in a Shimadzu RF5301 spectrofluorimeter in a stirred cuvette maintained at 37°C. Mitochondria were added to a standard incubation buffer that contained: 125 mM KCl; 2 mM K_2HPO_4; 5 mM $MgCl_2$; 10 mM HEPES (pH adjusted to 7.0 with KOH); 10:M EGTA; and 0.2 mg/mL mitochondrial protein. Substrates (5 mM of succinate or 5 mM of glutamate plus 5 mM malate) and adenine nucleotides were added separately as indicated on figures. Hydrogen peroxide was measured using either scopoletin or Amplex red in the presence of 1 U/mL of horseradish peroxidase (HRP). The concentration of both dyes was 2 μM. Measurements were carried out at excitation/emission wavelengths of 365 nm (slit 3 nm)/460 nm (slit 5 nm) for scopoletin and 560 (slit 1.5 nm)/590 (slit 3 nm) for Amplex red, respectively. Since hydrogen peroxide was measured by a decrease of fluorescence in the case of scopoletin, this method is less sensitive to low concentrations of H_2O_2 and may underestimate slow rates of release by mitochondria. On the other hand, the advantage of this method is the opportunity to follow long-lasting reactions by addition of a second aliquot of dye upon the complete oxidation of the initial dye addition. In the case of Amplex red, fluorescence is increased with the generation of H_2O_2. This method is more sensitive to low concentrations of H_2O_2 (Mohanty *et al.* 1997; Zhou and Panchuk-Voloshina 1997). We tested both Amplex red and its oxidation product, resorufin, on mitochondrial function using polarography and found that neither agent at 4 μM had any effect on the respiratory control ratio with either glutamate and malate or succinate as substrate. Note also that the addition of superoxide dismutase to the assay medium did not further increase the signal with either scopoletin or Amplex red (data not shown) suggesting that the endogenous dismutase capacity was sufficient to metabolize all of the superoxide produced in this system. The signals detected by both scopoletin and Amplex red were decreased by 85% by the inclusion of 800 U/mL catalase in the reaction mixture. $\Delta\Psi_m$ was estimated using fluorescence quenching of the cationic dye safranine O which is accumulated and quenched inside energized mitochondria (Akerman and Wikstrom 1976). The excitation wavelength was 495 nm (slit

3 nm) and emission 586 nm (slit 5 nm), and the dye concentration used was 2.5 μM. We attempted to calibrate the safranine O signal using media with different KCl concentrations and valinomycin. Using rat liver mitochondria we obtained a good linear correlation between values calculated from the Nernst equation and measured changes in dye fluorescence within the range of 48–150 mV (data not shown). However, using similar conditions with rat brain mitochondria we were not able to record significant changes in safranine O fluorescence in the calibration buffer because the mitochondria appeared to spontaneously depolarize. This could be due to depletion of potassium from the matrix during the tissue isolation process (in potassium free buffer), or it is also possible that brain mitochondria could be more sensitive to valinomycin-induced swelling. However, this limitation prevented precise calibration of the safranine O signal, and instead the results for this dye are reported in fluorescence units or as a percent of maximal values.

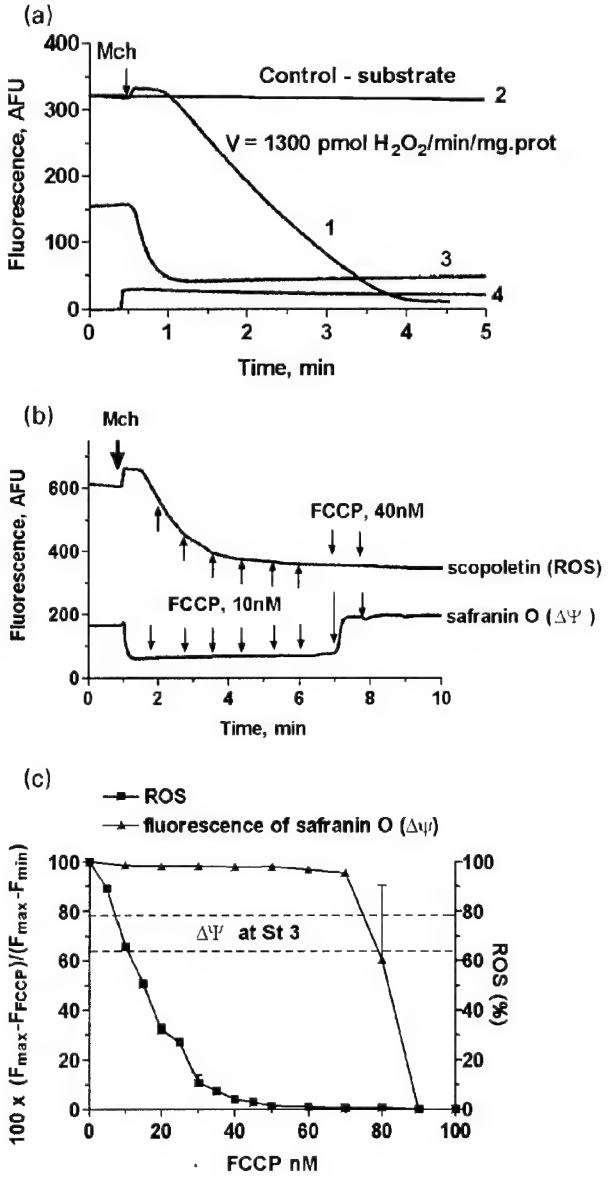

Fig. 1 Hydrogen peroxide production by rat brain mitochondria respiring in the presence of succinate. Hydrogen peroxide release was measured by the scopoletin method. The traces represent independent measurements of the different parameters that were then aligned by the start positions. (a) Typical traces of hydrogen peroxide release (traces 1 and 2), membrane potential (trace 3) and NADH fluorescence (trace 4). Substrate was absent in trace 2. (b) The effect of uncoupler FCCP on hydrogen peroxide release and membrane $\Delta\Psi_m$. FCCP was added to increment the final concentration by 10 or 40 nM with each addition as indicated. (c) The dependence of the rate of hydrogen peroxide release and membrane potential value on FCCP concentration. The plot presents calculations of the data similar to that from panel (b) with the following designations: F_{max}, fluorescence with saturated concentration of uncoupler; F_{min}, fluorescence at maximal energized state; F_{FCCP}, fluorescence with a given concentration of FCCP. The values of rate of ROS production are the means of three or four experiments. The interval in between two dotted lines indicates margins of mitochondrial membrane potential in state 3 respiration.

Data analysis

H_2O_2 generation was calibrated by constructing standard curves using known H_2O_2 concentrations in the presence of the standard incubation buffer, the appropriate dye and horseradish peroxidase but without mitochondria. In this study we show either traces reflecting the fluorescence values measured during the experiment or rates determined from the slope of the fluorescence change and converted to H_2O_2/min/mg protein. Statistical analysis was performed using PRISM (GraphPad Software, San Diego, CA, USA). Typically data were subjected to an ANOVA followed by an appropriate *post hoc* test. Differences were considered significant when $p < 0.05$.

Materials

Amplex red was obtained from Molecular Probes (Eugene, OR, USA). Scopoletin, safranine O, and HRP were obtained from Sigma (St Louis, MO, USA). Myxothiazol was purchased from Fluka (Buchs, Switzerland). All other reagents and inhibitors were purchased from Sigma.

Results

ROS production by mitochondria metabolizing succinate

We first investigated the characteristics of mitochondrial ROS production in rat brain mitochondria incubated with the complex II substrate succinate (Fig. 1). In the absence of succinate the rate of oxidation of scopoletin was very low. However, mitochondria aerobically incubated in media with succinate begin to release hydrogen peroxide after a short lag period of some 30 s. This lag period coincides with the time necessary for mitochondria to gain their maximal value of $\Delta\Psi_m$ (Fig. 1a). Interestingly, the ROS generation supported by succinate is highly sensitive to small changes in $\Delta\Psi_m$ (Fig. 1b). To determine the threshold of $\Delta\Psi_m$ loss necessary to block ROS production, mitochondria were titrated with uncoupler in small increments. Figure 1(b)

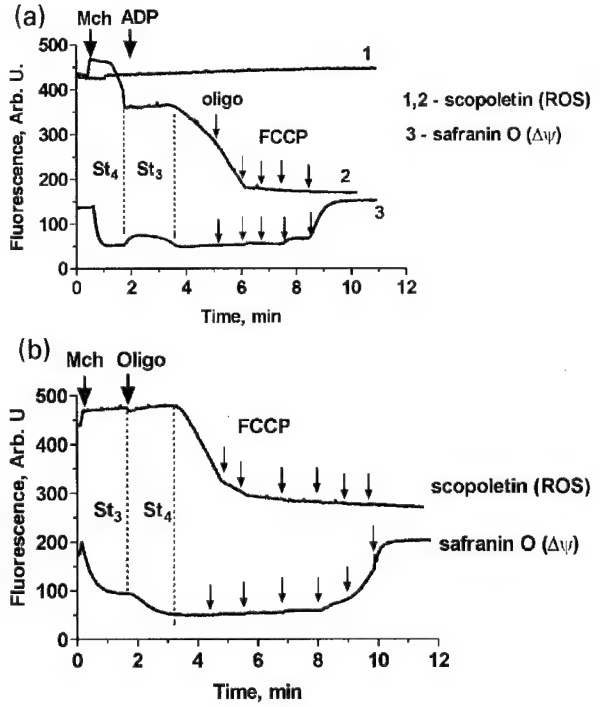

Fig. 2 Activation of ATP synthesis strongly inhibits generation of hydrogen peroxide. Hydrogen peroxide was measured with scopoletin in these experiments. (a) Rat brain mitochondria were incubated in standard media with succinate (traces 2 and 3) or in the same media supplemented with 3 mM ADP (trace 1). Additions: 40 μM ADP; 100 μM oligomycin; FCCP in 30 nM increments. (b) The mitochondria were incubated in standard media with succinate and 3 mM ADP. Additions: 100 nM oligomycin; FCCP in 20 nM increments. Dotted vertical lines on both graphs indicate time points when mitochondria switched phosphorylation on and off, as determined from the $\Delta\Psi_m$ recordings.

shows that 15 nM of carbonyl cyanide *p*-(trifluoromethoxy) phenyl hydrazone (FCCP) caused 50% inhibition of ROS production while producing very small changes in $\Delta\Psi_m$. The minimum concentration of uncoupler that fully blocks the ROS generation was found to be 40–50 nM, which caused decreased the safranine O signal by only 2–3%, while a complete depolarization was observed at 80–100 nM depending on mitochondrial preparation (Fig. 1c). A similar result was obtained with the uncoupler 2,4-dinitrophenol (2,4-DNP) which is known to have a different uncoupling mechanism (Skulachev 1998). The ROS generation was inhibited by 95% at 4 μM of 2,4-DNP while the corresponding decrease of $\Delta\Psi_m$ was as little as 5% (data not shown). It is important to note that the measurements of membrane potential with safranine O may underestimate hyperpolarized values of $\Delta\Psi_m$ which, in turn, might underestimate the magnitude of the depolarization in the presence of low uncoupler concentrations (Akerman and Wikstrom 1976). The concentration of uncoupler that abruptly and completely depolarizes mitochondria varies for different mitochondria preparations, and this is reflected at greater standard error at the end of the graph for membrane potential (Fig. 1c). Nevertheless, these data clearly indicate that succinate driven ROS production is very sensitive to changes in $\Delta\Psi_m$.

The physiological relevance of small depolarizations of $\Delta\Psi_m$ are illustrated in Fig. 2. Providing ADP together with succinate results in phosphorylating, or state 3 respiration. The synthesis of ATP depletes $\Delta\Psi_m$, and this depletion is sufficient to decrease $\Delta\Psi_m$ to the point that ROS generation is fully inhibited. The subsequent addition of oligomycin to prevent oxidative phosphorylation results in hyperpolarization of $\Delta\Psi_m$ and the resumption of ROS production. This principle can also be illustrated by the addition of a limited concentration of ADP (40 μM). This completely stopped ROS generation concurrently with a depolarization of mitochondria by some 30–40% of the safranine O signal (Fig. 2b). After the ADP was fully consumed and $\Delta\Psi_m$ recovered to a maximum value, the ROS production resumes. When ADP was present in excess and mitochondria are permanently in state 3, no ROS production was observed up to 30 min of incubation (Fig. 2a and data not shown). A low concentration of oligomycin (100 nM) inhibited the ATPase and restored $\Delta\Psi_m$ and then re-initiated ROS generation when the membrane potential reached its maximal value. These data show the reversibility of the process of free radical generation supported by succinate. It is worth noting that the changes of $\Delta\Psi_m$ at the transition from state 4 to state 3 (ATP synthesis switched off and switched on, respectively) measured by safranine O are greater than the depolarization necessary for complete inhibition of ROS production by an uncoupler. This suggests that brain mitochondria with an uninhibited respiratory chain engaged in ATP synthesis are protected from ROS generation mediated by complex II substrates.

Mechanism of ROS generation mediated by succinate

Previous studies have shown that in mitochondria derived mainly from tissues other than brain, ROS originate in two sites of the respiratory chain. Superoxide can be generated from complex I as a result of reverse electron transfer at high membrane potential values (Hinkle *et al.* 1967) (Croteau *et al.* 1997) (Korshunov *et al.* 1998), and also from the Q-cycle of complex III (see Turrens 1997). We used a series of selective inhibitors to evaluate the site(s) of the respiratory chain of rat brain mitochondria responsible for succinate supported ROS production.

Addition of the complex I inhibitor rotenone to mitochondria oxidizing succinate decreased ROS production (Fig. 3, Table 1). $\Delta\Psi_m$ remains high in this case, because proton pumping can still occur at complexes III and IV (data not shown). This suggests that the principle effect of rotenone is to block reverse electron transfer from complex II to complex I, and that this pathway is the major route of succinate-driven ROS generation. The complex III

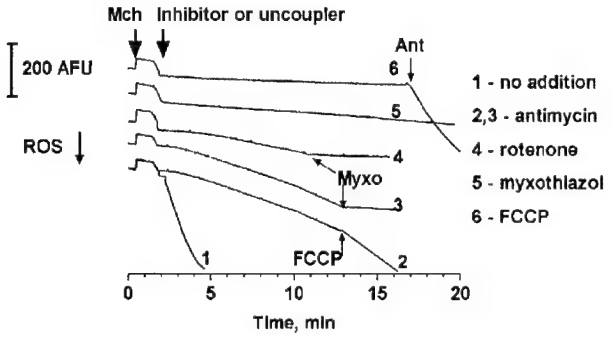

Fig. 3 The effect of respiratory chain inhibitors or uncoupler on hydrogen peroxide release by rat brain mitochondria oxidizing succinate. Hydrogen peroxide was measured with scopoletin in these experiments. Mitochondria were incubated in standard media. 1.5 min after addition of mitochondria to the incubation media an inhibitor or uncoupler was added. Additions: trace 2, 150 nM FCCP; traces 2,3, 1 μM myxothiazol; trace 6, 1 μM antimycin. These traces have been offset for clarity.

inhibitor antimycin also substantially inhibited ROS generation (Fig. 3), and also rapidly decreased $\Delta\Psi_m$. However, it is evident from Fig. 3 that there is a smaller and delayed oxidation of scopoletin that occurs following the addition of rotenone or antimycin. This remaining ROS production is likely to be due to free radical formation in the Q-cycle. Myxothiazol was reported to inhibit ROS generation in Q-cycle of bovine heart submitochondrial particles (Turrens *et al.* 1985). In our experiments, the addition of myxothiazol alone inhibited ROS generation by 97–98%. Application of myxothiazol after rotenone or antimycin results in the same rate of ROS generation, supporting, supporting the suggestion of Q-cycle as a source of the residual ROS signal when reverse electron transport to complex I is blocked.

Interestingly, when mitochondria are uncoupled with FCCP, antimycin stimulates Q-cycle ROS generation to an even greater extent. The rate of H_2O_2 generation is dependent on the ratio of [fumarate]/[succinate] in the mitochondrial matrix with maximum at 10 : 1 (Ksenzenko *et al.* 1984). Thus, building up fumarate as a result of succinate oxidation favors H_2O_2 production. For this reason, both the order and timing of additions of inhibitor and uncoupler is important. When inhibitor comes first the amount of fumarate accumulated is less compared to the case when mitochondria were first uncoupled. In our conditions, when succinate is present in excess, the later antimycin was added the higher rate of H_2O_2 was observed (not shown). This process was also substantially inhibited by myxothiazol (Fig. 3, Table 1).

ROS production supported by NADH-linked substrates

We next examined the characteristics of ROS generation by mitochondria utilizing glutamate and malate to drive NADH-linked respiration at complex I. The rate of endogenous hydrogen peroxide release was much lower when rat brain mitochondria oxidize NADH-linked substrates glutamate and malate and was undetectable using the scopoletin method (Fig. 4a, Table 1). However, the addition of rotenone, antimycin and even myxothiazol increased the rate of scopoletin oxidation (Fig. 4a, Fig. 5, Table 1).

The mechanism(s) of NADH-supported ROS generation

We further investigated the properties of ROS production triggered by the addition of inhibitors to mitochondria utilizing glutamate and malate. However, the short lag period observed between the addition of the inhibitor and the initiation of scopoletin oxidation added an ambiguity to these experiments, because this might reflect either a delay in ROS production or else a threshold below which scopoletin was unable to detect a ROS signal. To avoid this problem we detected ROS with the Amplex red method instead. We first investigated the concentration dependence of ROS generation triggered by rotenone. The aim of these experiments was to find out minimal degree of complex I inhibition which causes ROS generation in the respiratory chain and whether any correlation between ROS generation

Table 1 Effect of electron transport inhibitors and uncoupler on ROS generation by isolated mitochondria

	Rate of peroxide production (pmol/min/mg protein)	
	Succinate	Glutamate + malate
Control	1388 ± 59 (25)	Not detected
Antimycin	275 ± 18 (11)	228 ± 6 (20)
+ Myxothiazole	46 ± 2 (3)	59 ± 7 (4)
+ Rotenone	–	1266 ± 98 (3)
Rotenone	174 ± 18 (8)	434 ± 9 (19)
+ Myxothiazole	56 ± 18 (3)	–
Myxothiazole	40 ± 2 (6)	82 ± 11 (4)
+ Rotenone	–	450 ± 20 (5)
+ Antimycin	–	67 ± 7 (3)
FCCP then antimycin	1105 ± 130 (3)	254 ± 39 (3)
+ Myxothiazole	53 ± 12 (3)	85 ± 9 (3)
Antimycin then FCCP	463 ± 29 (6)	283 ± 8 (6)
+ Myxothiazole	–	79 ± 11 (3)
FCCP then rotenone	–	148 ± 7 (3)
Rotenone then FCCP	–	155 ± 15 (8)

Values are the mean ± SEM (*N* in parentheses) of determinations from different mitochondrial preparations. Peroxide production was determined using the scopoletin/horseradish peroxidase technique. Concentrations of drugs: antimycin 1 μM; rotenone 1 μM; myxothiazol 1 μM; FCCP 150 nM. Drugs were added together when indicated by +, and sequentially when indicated by 'then'. –, condition not tested.

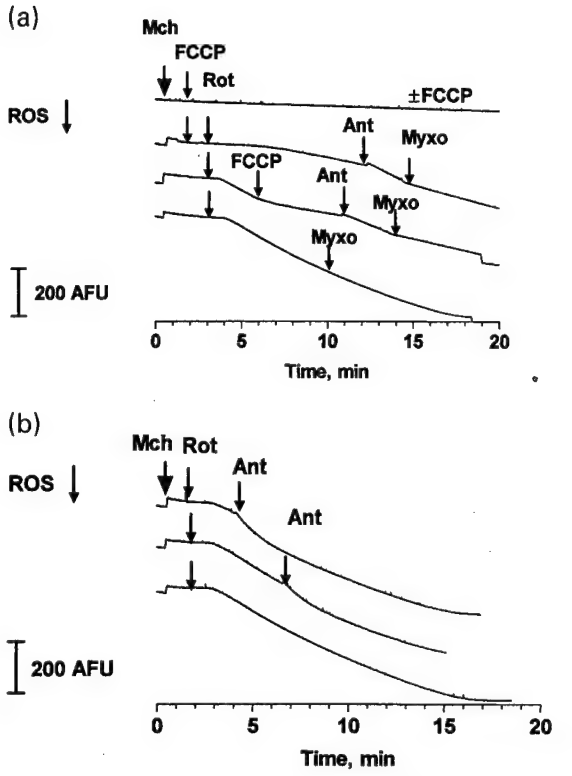

Fig. 4 The effect of respiratory chain inhibitors or uncoupler on the rotenone-induced hydrogen peroxide release by rat brain mitochondria oxidizing glutamate and malate as substrates. (a) Effect of uncoupler and myxothiazole. (b) Effect of antimycin. Mitochondria were incubated in standard media. Drugs were added in the following concentrations: 150 nM FCCP; 1 μM rotenone; 1 μM antimycin; 1 μM myxothiazol. Hydrogen peroxide was measured by the scopoletin method. These traces have been offset for clarity.

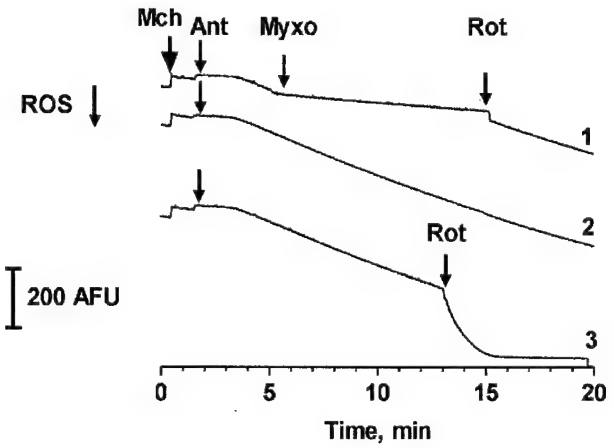

Fig. 5 The effect of respiratory chain inhibitors on antimycin-induced hydrogen peroxide release by rat brain mitochondria with glutamate and malate as substrates. Mitochondria were incubated in standard media. Drugs were added in the following concentrations: 1 μM antimycin; 1 μM rotenone; 1 μM myxothiazol. Hydrogen peroxide was measured by the scopoletin method.

and membrane potential value existed (Fig. 6). Treatment of mitochondria with increasing rotenone concentrations resulted in a gradual increase in the rate of ROS generation (Fig. 6a). The minimal rotenone concentration causing noticeable hydrogen peroxide release was 20 nM (equal to 100 pmol rotenone per mg mitochondrial protein). ROS generation by rotenone-inhibited mitochondria was not linear and typically increased during the experiment. The initial rate of ROS production (V_i) gradually rose with increasing inhibitor concentration and showed saturation at 500 nM, while the maximal rate (V_m) reached a plateau at a lower concentration (200 nM) (Figs 6a and c). Complex I contains several types of redox centers including eight or nine Fe–S clusters, flavin mononucleotide (FMN) and the tightly bound ubiquinone pool (Onishi 1998). The accelerated rate of peroxide production may be due to the progressive reduction of the upstream redox groups upon complete block of electron flow at rotenone binding site. Alternatively, increase in rate may reflect the point at which the endogenous antioxidant systems become depleted.

The kinetics of depolarization upon administration of different rotenone concentrations (Fig. 6b) are biphasic. These two components are likely to be attributable to a combination of the removal of the proton-motive force upon inhibition by rotenone, and the non-ohmic inherent proton leak of the inner membrane because the remaining respiratory chain activity is no longer able to compensate this passive leak. These experiments do not allow us to determine which component is attributable to which phase of the response. The apparent similarity between the kinetics of ROS production and loss of membrane potential can be explained by the fact that both processes are dependent on the degree of inhibition at complex I. However, in this case, membrane potential does not control the process of free radical production (see below).

To determine the extent of respiratory chain inhibition necessary to start free radical generation we performed polarographic measurements of oxygen consumption (Fig. 6c). There is an interesting discrepancy between the concentration dependence of the inhibition of respiration compared to ROS generation. Twenty nanomolar rotenone inhibits respiration by some 50%, while minimally altering H_2O_2 release. In the presence of 50 nM of rotenone 90% of respiration is inhibited, whereas V_m of ROS generation is only half maximal. Likewise, rotenone at 200 nM inhibited respiration by 98%, and V_m also reached a maximum, although the initial rate of ROS generation, V_i, is still submaximal at this concentration.

The addition of rotenone to mitochondria clearly decreases $\Delta\Psi_m$ in addition to increasing ROS generation. To determine whether ROS production was driven by the loss of $\Delta\Psi_m$ we performed experiments with FCCP. Depolarization of

mitochondria itself with FCCP does not cause ROS production (Fig. 4a, Table 1). Indeed, uncoupler FCCP partially inhibited ROS generation induced by rotenone. Similarly, addition of rotenone to mitochondria previously exposed to FCCP results in ROS generation at a rate comparable to the experiment with the reversed order of drug addition. These data show that dissipation of $\Delta\Psi_m$ alone is insufficient to trigger ROS production. Additionally, in rotenone-induced ROS production with glutamate and malate as substrate there is an uncoupler sensitive component. The latter is consistent with previous reports using mitochondria derived from tissues other than brain (Vinogradov *et al.* 1995).

To further probe the source of ROS in rotenone-inhibited mitochondria we tested the effects of antimycin and myxothiazol. Addition of antimycin to rotenone-poisoned mitochondria (Fig. 4b) accelerates H_2O_2 release. However, this enhancement is quite transient, because within 1–2 min the rate returns to the same level as observed with rotenone alone. In addition, myxothiazol has minimal effects on ROS generation in rotenone-inhibited mitochondria (Fig. 4a). The transient effect of antimycin may be due to small amounts of succinate present in the system from the transamination of glutamate and oxaloacetate, giving α-ketoglutarate. As this source of succinate donating electrons to Q-cycle is limited (analogous to the succinate experiments shown in Fig. 3) the addition of antimycin causes only transient acceleration of ROS production before the succinate is consumed. The limited effects of myxothiazol in this case indicates that upon glutamate-malate oxidation ROS generation does not involve the ubiquinone pool from complex III.

We also examined the effects of antimycin alone on ROS generation supported by glutamate and malate. For these studies we used Amplex red to ensure that we detected the full range of the ROS signal. Where rotenone provided a clear concentration dependence for ROS generation and mitochondrial depolarization, antimycin essentially produced an all-or-none effect with the critical concentration being between 40 and 50 nM (Fig. 7). Like rotenone, the effects of antimycin on both ROS production and $\Delta\Psi_m$ were only apparent when respiration had been almost completely inhibited (Fig. 7c). Increasing the antimycin concentration from 50 nM up to 1 μM did not further increases in the rate of ROS generation, though mitochondria lost membrane potential faster (Figs 7a and b). Similar data were obtained with scopoletin (not shown). The antimycin-induced ROS generation by mitochondria was almost completely inhibited by myxothiazol, and resumed after the subsequent addition

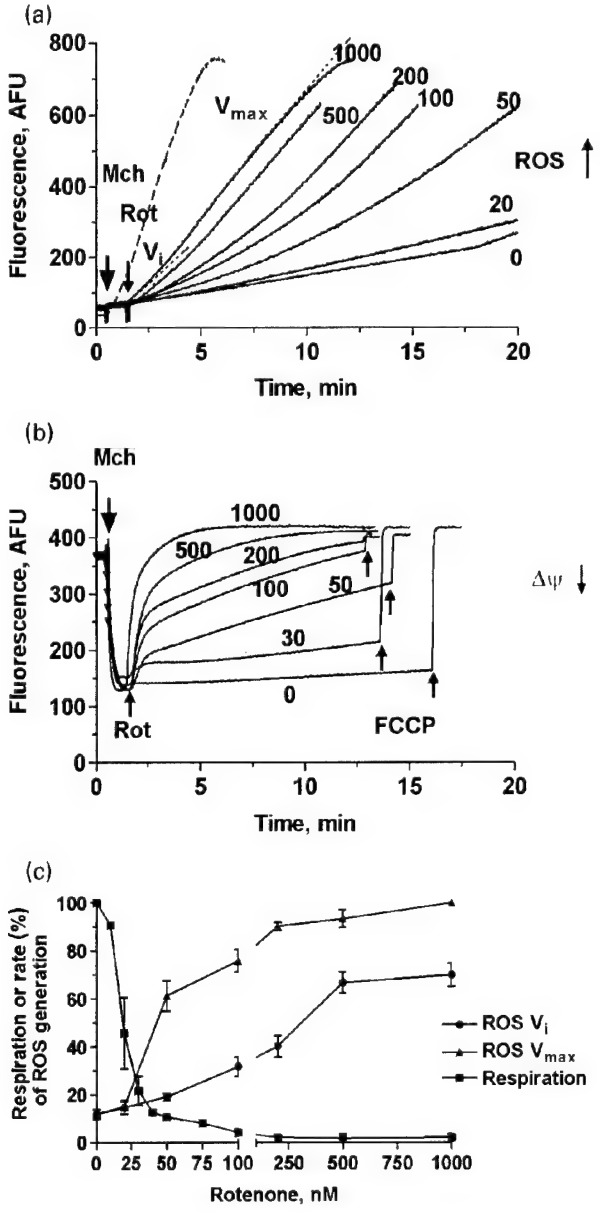

Fig. 6 Rotenone-induced hydrogen peroxide release (a and c), changes in membrane potential (b), and inhibition of respiration (c) of rat brain mitochondria oxidizing glutamate and malate. Hydrogen peroxide was measured with Amplex red in these experiments. (a and b) Various concentrations of rotenone were added to the mitochondria incubated in the standard media after maximal membrane potential had been established. Figures by each trace indicate rotenone concentration in nM. V_i and V_{max} indicate the initial and the maximal rate of H_2O_2 generation, respectively, as illustrated by the lines superimposed on the fluorescence traces. The dashed line shows succinate supported ROS generation for comparison. The concentration of FCCP in (b) was 150 nM. (c) The degree of inhibition of respiratory chain activity by different concentrations of rotenone was accessed in the media supplemented with 3 mM ATP and 1 μM oligomycin. The reaction was started by addition of 150 nM FCCP followed by addition of rotenone. A separate trace was made for each rotenone concentration. The ratio of the respiration rate in the presence of given rotenone concentration to uncoupled, maximal respiration in percent was plotted as curve 1. Calculation of the rates of hydrogen peroxide generation were normalized to the rate at 1000 nM rotenone.

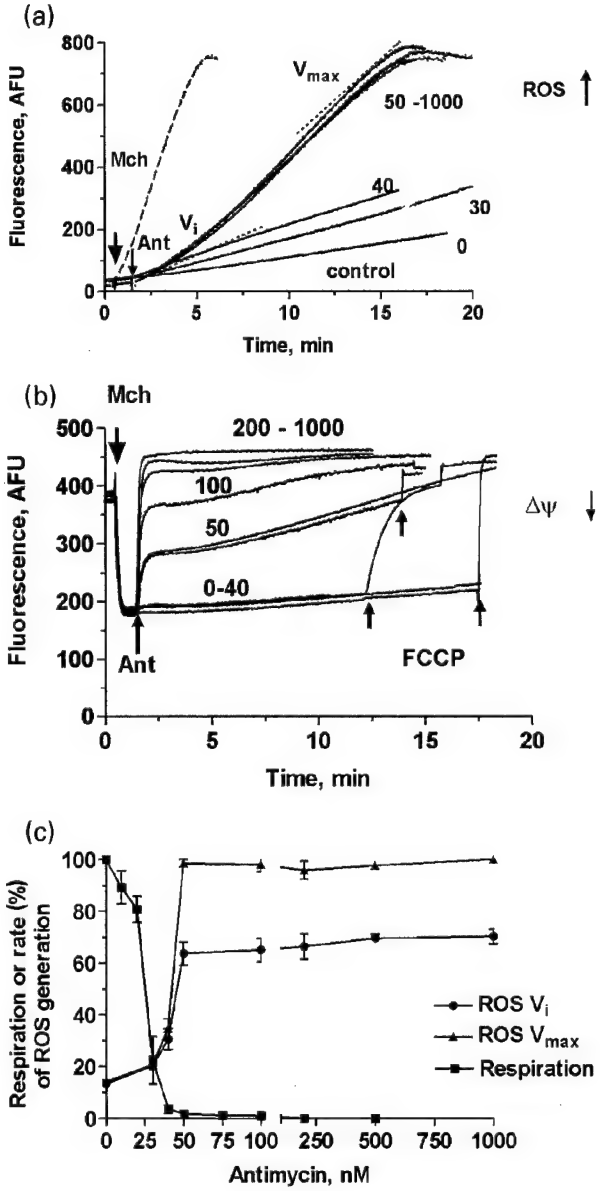

Fig. 7 The effect of antimycin on hydrogen peroxide release (a and c), membrane potential (b) and inhibition of respiration (c) of rat brain mitochondria oxidizing glutamate and malate. Conditions and experimental design are similar that of Fig. 6, except that antimycin was added as indicated when $\Delta\Psi_m$ was maximal. The dashed line on (a) shows succinate supported ROS generation for comparison.

of rotenone (Fig. 5, Table 1). The fact that myxothiazol suppressed the ROS production supported by glutamate and malate substrates in the presence of antimycin suggests that the hydrogen peroxide derives from Q-cycle under these conditions. However, in the presence of rotenone ROS production is likely to originate from complex I. Consistent with the involvement of the Q-cycle in antimycin-induced ROS production is the slight stimulatory effect of FCCP (Table 1).

Administration of myxothiazol to mitochondria oxidizing glutamate and malate caused a slow ROS production (Table 1). This is an interesting observation because myxothiazol is known to inhibit free radical production in Q-cycle (Turrens *et al.* 1985) and can be used to identify the Q-cycle as the source of ROS. A recent study also reported a slow ROS production in the presence of myxothiazol (Starkov and Fiskum 2001). Using another inhibitor of complex III, stigmatellin, the authors concluded that myxothiazol induces ROS in complex III, but at a site different from that of antimycin A action. In our experiments addition of rotenone to myxothiazol-poisoned mitochondria increased ROS production, though antimycin had no effect in this condition. The rates of ROS generation induced by rotenone alone and rotenone added to myxothiazol-poisoned mitochondria were the same indicating that myxothiazol block does not affect the ability of complex I to generate radicals.

Discussion

In this study we have investigated the regulation of mitochondrial ROS generation by $\Delta\Psi_m$ in a brain mitochondria preparation. There is clear evidence for ROS production originating from at least two different sites in the electron transport chain. In addition, mitochondria clearly produce ROS using both $\Delta\Psi_m$-dependent and -independent mechanisms.

Detailed information on the mechanism of ROS generation by respiratory chain in mitochondria and submitochondrial particles has been accumulated for tissues other than brain. In the majority of studies investigating intact mitochondria, it has been shown that oxidation of succinate gives the most effective production of ROS (Loschen *et al.* 1971; Boveris *et al.* 1972; Boveris and Chance 1973; Croteau *et al.* 1997; Korshunov *et al.* 1998; Kwong and Sohal 1998). Data on brain mitochondria are rather less, and have been summarized in Table 2. Our data along with data of Cino and Del Maestro (1989) and Kwong and Sohal (1998) clearly indicate succinate as the most effective ROS generating substrate for intact mitochondria, while others (Herero and Barja 1997; Barja and Herero 1998) failed to measure significant ROS production by rat mitochondria in the presence of this substrate. Arnaiz (Arnaiz *et al.* 1999) found that for mice brain mitochondria succinate was almost as effective as NADH-linked substrates. There are clearly several critical variables in these studies; the choice of incubation media is important, as well as the method of ROS detection. However, perhaps the most important factor is the ability of the mitochondria to maintain a sufficiently hyperpolarized membrane potential to support reversed electron transport. Some of the studies summarized in Table 2 used uncouplers or antimycin in their experiments,

Table 2 Prior studies on ROS generation by brain mitochondria

Study	Species	Incubation media	Detection method	Substrates tested	Key conclusions on source of ROS
Sorgato *et al.* (1974)	Rat	Sucrose	Scopoletin/HRP	Succinate	None
Patole *et al.* (1986)	Rat	KCl	Scopoletin/HRP	Succinate, _-glycerol phosphate, glutamate, malate, pyruvate	Q cycle > Complex I
Cino and Del Maestro (1989)	Rat	KCl	Compound II/HRP	Succinate, glutamate, malate	Complex I > Q cycle
Zoccarato *et al.* (1988)	Guinea pig	KCl	Cytochrome c/HRP	Succinate, α-glycerol phosphate, malate, pyruvate	Q cycle in uncoupled mitochondria
Dykens (1994)	Rat	KCl	Electron paramagnetic resonance	Succinate	Succinate signal stimulated by calcium
Herero and Barja (1997)	Rat, Pigeon	KCl	Homovanillic acid/HRP	Succinate, pyruvate, malate	No effect of $\Delta\Psi_m$ on Complex I
Barja and Herero (1998)	Rat, Pigeon	KCl	Homovanillic acid/HRP	Succinate, pyruvate, malate	Q cycle > complex I
Kwong and Sohal (1998)	Mouse	KCl	p-hydroxyphenylacetate /HRP	Succinate, α-glycerol phosphate, malate, pyruvate, β-hydroxybutyrate	Complex I > Q cycle
Arnaiz *et al.* (1999)	Mouse	Mannitol/ sucrose	Scopoletin/HRP	Succinate, glutamate, malate	Q cycle > complex I
Starkov and Fiskum (2001)	Rat	KCl	Scopoletin/HRP	Succinate, α-glycerol phosphate, malate	Myxothiazole induces Q cycle ROS signal

which would result in different results than those reported here.

The substantial succinate driven ROS production observed in previous studies and in our experiments is likely to be the result of reversed electron transport from complex II to complex I. Reversed electron transport has been shown to be very sensitive to $\Delta\Psi_m$ (Korshunov *et al.* 1998), and the present studies show that a very small degree of depolarization are sufficient to completely inhibit ROS generation by this pathway. Thus, low concentrations of the uncouplers FCCP and dinitrophenol, active oxidative phosphorylation, and the complex III inhibitors are each sufficient to depolarize $\Delta\Psi_m$ to the extent that ROS production is greatly reduced in succinate-oxidizing mitochondria. The finding that rotenone blocks this ROS signal, even though it does not depolarize $\Delta\Psi_m$ is also consistent with this conclusion, because it prevents electrons from reaching the redox centers associated with complex I responsible for superoxide generation. This means that the redox center(s) responsible for ROS production during reverse electron transport are located upstream of rotenone block. According to Hansford and colleagues (Croteau *et al.* 1997) all free radicals generated upon succinate oxidation originate in complex I.

Our data, along with experiments on rat heart mitochondria (Korshunov *et al.* 1998), clearly indicate that there is a secondary source of ROS in mitochondria respiring on succinate. This signal is likely to be derived from the ubiquinone cycle, because it is enhanced by antimycin and blocked by myxothiazol, and in the presence of antimycin is stimulated by the addition of uncouplers. This is consistent with the model of superoxide generation proposed in previous studies (Boveris *et al.* 1976; Cadenas *et al.* 1977; Cadenas and Boveris 1980; Turrens and Boveris 1980; Turrens *et al.* 1985). Notably, this pathway appears to be insensitive to changes in $\Delta\Psi_m$. Reverse electron transfer is a function that requires tightly coupled mitochondrial membranes capable of maintaining hyperpolarized potentials.

The contribution of complex III in overall ROS signal may depend on the concentration of CoQ in mitochondrial membrane, which is type and tissue specific. As Turrens has shown (Turrens *et al.* 1982), there is strong correlation between rates of H_2O_2 release and ubiquinone content in mitochondria of different sources. In addition, the impact of complex III and complex I in the overall ROS signal associated with succinate respiration depends on other factors, such as functional integrity of mitochondrial membrane and the potential, the redox state of the electron transport complexes under the appropriate experimental conditions, relative activity of the complexes themselves, and also the activity of ROS scavenging systems.

Rat brain mitochondria respiring on NADH-linked substrates produce a very small ROS signal in the absence of electron transport chain inhibitors. This is distinct from mitochondria derived from other species and tissues [mouse heart, kidney, brain (Kwong and Sohal 1998); pigeon heart (Boveris and Chance 1973); rat liver (Boveris *et al.* 1972);

porcine lung (Turrens *et al.* 1982); and mouse brain (Arnaiz *et al.* 1999)], where the uninhibited, complex I-derived signal is some 50–70% of that obtained with succinate. The basis for these intertissue differences remains unclear.

Significant ROS generation is triggered by the addition of rotenone which promotes superoxide generation by the redox center(s) of complex I. Our data are in agreement with those of Takeshige and Minakami (1979) who concluded that rotenone induces ROS only from complex I in NADH oxidizing bovine heart submitochondrial particles. It has subsequently been demonstrated that there are redox centers in complex I that are capable of generating superoxide though the precise location of the site(s) has not been identified (Kang *et al.* 1983; Krishnamoorthy and Hinkle 1988; Onishi 1998; Vinogradov 1998). These centers are apparently upstream of the site of rotenone blockade, and ROS production at this site(s) would account for the lack of sensitivity of this signal to myxothiazol or antimycin beyond that which can be accounted for by succinate generation (Fig. 3).

When either antimycin or rotenone were present with complex I substrates, the ROS production appears to be largely independent of $\Delta\Psi_m$. Although the addition of these inhibitors substantially alters $\Delta\Psi_m$, the changes in membrane potential occur independently of ROS generation, as indicated by the failure of FCCP to trigger a ROS signal in mitochondria respiring on glutamate and malate (Fig. 6). Interestingly, in the presence of rotenone and FCCP, antimycin does have a more substantial accelerating effect on ROS generation (Fig. 6a) than the transient effect of antimycin in the presence of rotenone alone (Fig. 6b), although the mechanism underlying this effect is not clear. Free radical production supported by succinate in the presence of antimycin block has previously been shown to be dependent on the redox potential of the fumarate/succinate pair (Loschen *et al.* 1973; Ksenzenko *et al.* 1984). The dependence had a bell shape with maximum at about 40 mV which is close to E_m of ubiquinones. These experiments were carried out on submitochondrial particles since fumarate poorly penetrates into mitochondria. Similar results were obtained for brain mitochondria, where dependence of ROS production in the presence of antimycin on the concentration of succinate had the same bell-shaped form (Patole *et al.* 1986; Zoccarato *et al.* 1988). Another confirmation of this notion was recently reported, where the problem of poor delivery of fumarate was overcome by using alamethicin-permeabilized mitochondria (Starkov and Fiskum 2001).

It is important to notice that both types of substrates we used in this work, succinate and glutamate with malate, cannot be considered 'pure' substrates of a particular complex. The oxidation of succinate in the Krebs cycle results in the production of fumarate and then malate, which can fuel complex I. In turn, some quantity of succinate is built up in the process of malate oxidation as well as from the transamination of glutamate. The transient effect of antimycin on rotenone treated mitochondria may be due to the to oxidation of succinate formed in this way.

It is widely believed that oxidative stress contributes to the demise of neurons in a number of neurodegenerative diseases, and it is likely that mitochondria are quantitatively the most important source of ROS in the brain. There have been numerous reports of impairment of the function of electron transport complexes in association with disorders like Parkinson's disease and Alzheimer's disease, conditions that are also associated with increases in markers of oxidative stress (Halliwell 1992; Beal *et al.* 1997). It is tempting to speculate that the partial inhibition of the electron transport chain reported in these diseases results in a feed forward effect, such that mitochondrial ROS generation is enhanced by the mechanisms evident when mitochondria respire on glutamate and malate. There are several potential limitations to this speculation, including the finding that very substantial inhibition of respiration is required prior to observing increased ROS generation, in other words the mitochondrial machinery may have a broad margin of safety. There is little evidence that the inhibition of respiration reaches this extent in any chronic neurological disorder. Perhaps a more reasonable speculation is that there may be conditions whereby mitochondria are excessively hyperpolarized under certain conditions, so that succinate-driven ROS generation occurs. This would not require extensive impairment of electron transport, but would imply that endogenous mechanisms that limit membrane potential [such as uncoupling proteins or endogeneous fatty acids, for example, Korshunov *et al.* (1998); Ricquier and Bouillaud (2000)] are dysfunctional. It is also possible that inhibition of ATP synthesis could generate a sufficiently hyperpolarized state to support succinate-driven ROS generation in intact tissues. Given the magnitude of the ROS signal from this mechanism and the liability this oxidant burden would impose on neurons, these are clearly issues which require further investigation.

One circumstance of mitochondrial involvement in neuronal injury that has received particular attention is excitotoxicity, where neurons die as the result of excessive activation of NMDA receptors and substantial cellular calcium accumulation. This process is associated with mitochondrial depolarization (Nieminen *et al.* 1996; Schinder *et al.* 1996; White and Reynolds 1996; Vergun *et al.* 1999), mitochondrial calcium accumulation (Kiedrowski and Costa 1995; White and Reynolds 1995; White and Reynolds 1997) and ROS generation (Lafon-Cazal *et al.* 1993; Dugan *et al.* 1995; Reynolds and Hastings 1995; Bindokas *et al.* 1996). Moreover, preventing mitochondrial calcium accumulation protects neurons from injury (Budd and Nicholls 1996; Stout *et al.* 1998). The mechanisms linking glutamate-induced mitochondria calcium accumulation to neuronal death

remain unclear. One candidate mechanism is the generation of ROS. Previously, it has been suggested that mitochondrial calcium and sodium accumulation could promote ROS generation by isolated mitochondria (Dykens 1994). However, this paper reported a lack of ROS production in mitochondria respiring on succinate, and an increase in ROS generation under conditions where mitochondria would be depolarized following the addition of calcium. These claims are in direct contrast to the present findings, as well as those of Cino and Del Maestro (1989). The basis for this substantial discrepancy remains unclear. Indeed, it is not easy to account for the effects of glutamate or calcium on the basis of the results presented here. The depolarization of $\Delta\Psi_m$ that is associated with mitochondria calcium cycling (Nicholls and Akerman 1982) is sufficient to completely inhibit succinate-driven ROS generation. In addition, the experiments reporting glutamate-induced ROS generation in intact neurons is obviously performed without the addition of complex I or complex III inhibitors. In fact, Dugan *et al.* (1995) reported that glutamate-induced oxidation of dihydrorhodamine was prevented by rotenone. There are rather few reports of mitochondrial ROS generation in intact neurons that can be compared to the present study, although Budd *et al.* (1997) did find that antimycin increased the oxidation of dihydroethidium in cerebellar granule cells. Perhaps the most reasonable way to account for the consequences of NMDA receptor activation in intact neurons is to propose a calcium-mediated inhibition of complex I or complex III. This might be accomplished by the production of nitric oxide, which is an effective inhibitor of complex III (Brown 1999; Stewart *et al.* 2000), although NOS inhibitors did not prevent the oxidation of either dichlorofluorescin or dihydroethidium (Reynolds and Hastings 1995; Bindokas *et al.* 1996). The actual mechanism of calcium-mediated mitochondrial ROS generation in neurons awaits further investigation.

Acknowledgements

This work was supported by USAMRMC Neurotoxin Initiative (grant number DAMD17–98–1-8627). We would like to thank Lauren Richards for help in some experiments, Dr Teresa Hastings for access to an oxygen electrode, Kirk Dineley for reading the manuscript and Dr Alexei Permin for helpful discussion of these findings.

References

Akerman K. E. O. and Wikstrom M. K. F. (1976) Safranine as a probe of the mitochondrial membrane potential. *FEBS Lett.* **68**, 191–197.

Arnaiz S. L., Coronel M. F. and Boveris A. (1999) Nitric Oxide, superoxide, and hydrogen peroxide production in brain mitochondria after haloperidol treatment. *Nitric Oxide: Biol. Chem.* **3**, 235–243.

Barja G. and Herero A. (1998) Localization at complex I and mechanism of higher free radical production of brain nonsynaptic mitochondria in the short-lived rat than in the longevous pigeon. *J. Bioenerg. Biomemb.* **30**, 235–243.

Beal M. F., Howell N. and Bodis-Wollner I. (1997). *Mitochondria and Free Radicals in Neurodegenerative Disease*. Wiley-Liss, New York.

Bindokas V. P., Jordan J., Lee C. C. and Miller R. J. (1996) Superoxide production in rat hippocampal neurons: selective imaging with hydroethidine. *J. Neurosci* **16**, 1324–1336.

Boveris A. and Chance B. (1973) The mitochondrial generation of hydrogen peroxide: general properties and effect of hyperbaric oxygen. *Biochem. J.* **134**, 707–716.

Boveris A. and Cadenas E. (1975) Mitochondrial production of superoxide anions and its relationship to the antimycin insensitive respiration. *FEBS Lett.* **54**, 311–314.

Boveris A., Oshino N. and Chance B. (1972) The cellular production of hydrogen peroxide. *Biochem. J.* **128**, 617–630.

Boveris A., Cadenas E. and Stoppani A. O. M. (1976) Role of ubiquinone in the mitochondrial generation of hydrogen peroxide. *Biochem. J.* **156**, 435–444.

Bradford M. M. (1976) A rapid and sensitive method for the quantitation of microgram quantities of protein utlizing the principle of protein-dye binding. *Anal. Biochem.* **72**, 248–254.

Brown G. C. (1999) Nitric oxide and mitochondrial respiration. *Biochim. Biophys. Acta Bio-Energetics* **1411**, 351–369.

Budd S. L. and Nicholls D. G. (1996) Mitochondria, calcium regulation and acute glutamate excitotoxicity in cultured cerebellar granule cells. *J. Neurochem.* **67**, 2282–2291.

Budd S. L., Castilho R. F. and Nicholls D. G. (1997) Mitochondrial membrane potential and hydroethidine-monitored superoxide generation in cultured cerebellar granule cells. *FEBS Lett.* **415**, 21–24.

Cadenas E. and Boveris A. (1980) Enhancement of hydrogen peroxide formation by protonophores and ionophores in antimycin supplemented mitochondria. *Biochem. J.* **188**, 31–37.

Cadenas E., Boveris A., Ragan C. I. and Stoppani A. O. M. (1977) Production of superoxide radicals and hydrogen peroxide by NADH-ubiquinone reductase and ubiquinol-cytochrome c reductase from beef heart mitochondria. *Arch. Biochem. Biophys.* **180**, 248–257.

Cino M. and Del Maestro R. F. (1989) Generation of hydrogen peroxide by brain mitochondria: the effect of reoxygenation following postdecapitative ischemia. *Arch. Biochem. Biophys.* **269**, 623–638.

Croteau D. L., Ap R., Hudson E. K., Dianov G. L., Hansford R. G. and Bohr V. A. (1997) An oxidative damage-specific endonuclease from rat liver mitochondria. *J. Biol. Chem.* **272**, 27338–27344.

Dugan L. L., Sensi S. L., Canzoniero L. M. T., Handran S. D., Rothman S. M., Lin T.-S., Goldberg M. P. and Choi D. W. (1995) Mitochondrial production of reactive oxygen species in cortical neurons following exposure to N-methyl-D-aspartate. *J. Neurosci* **15**, 6377–6388.

Dykens J. A. (1994) Isolated cerebral and cerebellar mitochondria produce free radicals when exposed to elevated Ca^{2+} and Na^{+}: implications for neurodegeneration. *J. Neurochem.* **63**, 584–591.

Halliwell B. (1992) Reactive oxygen species in the central nervous system. *J. Neurochem.* **59**, 1609–1623.

Herero A. and Barja G. (1997) ADP-regulation of mitochondrial free radical production is different with complex I- or complex II-linked substrates: implications for the exercise paradox and brain hypermetabolism. *J. Bioenerg. Biomemb.* **29**, 241–249.

Hinkle P. C., Butow R. A. and Racker E. (1967) Partial resolution of the enzymes catalyzing oxidative phosphorylation. *J. Biol. Chem.* **242**, 5169–5173.

Kang D., Narabayashi H., Sata T. and Takeshige K. (1983) Kinetics of superoxide formation by respiratory chain NADH dehydrogenase of bovein heart mitochondria. *J. Biochem. (Tokyo)* **64**, 1301–1306.

Kiedrowski L. and Costa E. (1995) Glutamate-induced destabilization of intracellular calcium concentration homeostasis in cultured cerebellar granule cells: role of mitochondria in calcium buffering. *Mol. Pharmacol.* **47**, 140–147.

Korshunov S. S., Skulachev V. P. and Starkov A. A. (1997) High protonic potential actuates a mechanism of production of reactive oxygen species in mitochondria. *FEBS Lett.* **416**, 15–18.

Korshunov S. S., Korkina O. V., Ruuge E. K., Skulachev V. P. and Starkov A. A. (1998) Fatty acids as natural uncouplers preventing generation of O_2^- and H_2O_2 by mitochondria in the resting state. *FEBS Lett.* **435**, 215–218.

Krishnamoorthy G. and Hinkle P. C. (1988) Studies on the electron transfer pathway, topography of iron sulfur centers, and site of coupling in NADH-Q oxidoreductase. *J. Biol. Chem.* **263**, 17566–17575.

Ksenzenko M., Konstantinov A. A., Khomutov G. B., Tikhonov A. N. and Ruuge E. K. (1984) Relationships between the effects of redox potential, α-thenoyltrifluoroacetone and malonate on O_2^- and H_2O_2 generation by submitochondrial particles in the presence of succinate and antimycin. *FEBS Lett.* **175**, 105–108.

Kwong L. K. and Sohal R. S. (1998) Substrate and site specificity of hydrogen peroxide generation in mouse mitochondria. *Arch. Biochem. Biophys.* **350**, 118–126.

Lafon-Cazal M., Pietri S., Culcasi M. and Bockaert J. (1993) NMDA-dependent superoxide production and neurotoxicity. *Nature* **364**, 535–537.

Loschen G., Flohe L. and Chance B. (1971) Respiratory chain linked H_2O_2 production in pigeon heart mitochondria. *FEBS Lett.* **18**, 261–264.

Loschen G., Azzi A. and Flohe L. (1973) Mitochondrial H_2O_2 formation: relationship with energy conservation. *FEBS Lett.* **33**, 84–88.

Mohanty J. G., Jaffe J. S., Schulman E. S. and Raible D. G. (1997) A highly sensitive fluorescent micro-assay of H_2O_2 release from activated human leukocytes using a dihydroxyphenoxazine derivative. *J. Immunol. Methods* **202**, 133–141.

Nicholls D. G. and Akerman K. E. O. (1982) Mitochondrial calcium transport. *Biochim. Biophys. Acta* **683**, 57–88.

Nieminen A.-L., Petrie T. G., Lemasters J. J. and Selman W. R. (1996) Cyclosporin A delays mitochondrial depolarization induced by *N*-methyl-D-aspartate in cortical neurons: evidence of the mitochodrial permeability transition. *Neuroscience* **75**, 993–997.

Onishi T. (1998) Iron-sulfur clusters/semiquinones in complex I. *Biochim. Biophys. Acta* **1364**, 186–206.

Patole M. S., Swaroop A. and Ramarsarma T. (1986) Generation of H_2O_2 in brain mitochondria. *J. Neurochem.* **47**, 1–8.

Reynolds I. J. and Hastings T. G. (1995) Glutamate induces the production of reactive oxygen species in cultured forebrain neurons following NMDA receptor activation. *J. Neurosci.* **15**, 3318–3327.

Ricquier D. and Bouillaud F. (2000) The uncoupling protein homologues: UCP1, UCP2, UCP3, StUCP and AtUCP. *Biochem. J.* **345**, 161–179.

Rosenthal R. E., Hamud F., Fiskum G., Varghese P. J. and Sharpe S. (1987) Cerebral ischemia and reperfusion: prevention of brain mitochondrial injury by lidoflazine. *J. Cereb. Blood Flow Metab.* **7**, 752–758.

Schinder A. F., Olson E. C., Spitzer N. C. and Montal M. (1996) Mitochondrial dysfunction is a primary event in glutamate neurotoxicity. *J. Neurosci.* **16**, 6125–6133.

Skulachev V. P. (1998) Uncoupling: new approaches to an old problem of bioenergetics. *Biochim. Biophys. Acta* **1363**, 100–124.

Sorgato M. C., Sartorelli L., Loschen G. and Azzi A. (1974) Oxygen radicals and hydrogen peroxide in rat brain mitochondria. *FEBS Lett.* **45**, 92.

Starkov A. A. and Fiskum G. (2001) Myxothiazol induces H2O2 production from mitochondrial respiratory chain. *Biochem. Biophys. Res. Comm* **281**, 645–650.

Stewart V. C., Sharpe M. A., Clark J. B. and Heales S. J. (2000) Astrocyte derived nitric oxide causes both reversible and irreversible damage to the neuronal mitochondria respiratory chain. *J. Neurochem.* **75**, 649–700.

Stout A. K., Raphael H. M., Kanterewicz B. I., Klann E. and Reynolds I. J. (1998) Glutamate-induced neuron death requires mitochondrial calcium uptake. *Nat. Neurosci.* **1**, 366–373.

Takeshige K. and Minakami S. (1979) NADH- and NADPH-dependent formation of superoxide anions by bovine heart submitochondrial particles and NADH-ubiquinone reductase preparation. *Biochem. J.* **180**, 129–135.

Turrens J. F. (1997) Superoxide production by the mitochondrial respiratory chain. *Biosci. Rep.* **17**, 3–8.

Turrens J. F. and Boveris A. (1980) Generation of superoxide anion by the NADH dehydrogenase of bovine heart mitochondria. *Biochem. J.* **191**, 421–427.

Turrens J. F., Freeman B. A. and Crapo J. D. (1982) Hyperoxia increases H_2O_2 release by lung mitochondria and microsomes. *Arch. Biochem. Biophys.* **217**, 411–421.

Turrens J. F., Alexandre A. and Lehninger A. L. (1985) Ubisemiquinone is the electron donor for superoxide formation by complex III of heart mitochondria. *Arch. Biochem. Biophys.* **237**, 408–414.

Vergun O., Keelan J., Khodorov B. I. and Duchen M. R. (1999) Glutamate-induced mitochondrial depolarisation and pertubation of calcium homeostasis in cultured rat hippocampal neurons. *J. Physiol. (Lond.)* **519**, 451–466.

Vinogradov A. D. (1998) Catalytic properties of the mitochondrial NADH-ubiquinone oxidoreductase (complex I) and the pseudo-reversible active/inactive enzyme transition. *Biochim. Biophys. Acta* **1364**, 169–185.

Vinogradov A. D., Sled V. D., Burbaev D. S., Drivennikova V. G., Moroz I. A. and Onishi T. (1995) Energy-dependent complex I-associated ubisemiquinones in submitochondrial particles. *FEBS Lett.* **370**, 83–87.

White R. J. and Reynolds I. J. (1995) Mitochondria and Na^+/Ca^{2+} exchange buffer glutamate-induced calcium loads in cultured cortical neurons. *J. Neurosci.* **15**, 1318–1328.

White R. J. and Reynolds I. J. (1996) Mitochondrial depolarization in glutamate-stimulated neurons: an early signal specific to excitotoxin exposure. *J. Neurosci.* **16**, 5688–5697.

White R. J. and Reynolds I. J. (1997) Mitochondria accumulate Ca^{2+} following intense glutamate stimulation of cultured rat forebrain neurones. *J. Physiol. (Lond.)* **498**, 31–47.

Zhou M. and Panchuk-Voloshina N. (1997) A one-step fluorometric method for the continuous measurement of monoamine oxidize activity. *Anal. Biochem.* **253**, 169–174.

Zoccarato F., Cavallini L., Deana R. and Alexandre A. (1988) Pathways of hydrogen peroxide generation in guinea pig cerebral cortex mitochondria. *Biochem. Biophys. Res. Commun.* **154**, 727–734.

ELSEVIER

Journal of Neuroscience Methods 104 (2001) 165–176

JOURNAL OF NEUROSCIENCE METHODS

www.elsevier.com/locate/jneumeth

MitoTracker labeling in primary neuronal and astrocytic cultures: influence of mitochondrial membrane potential and oxidants

Jennifer F. Buckman, Hélène Hernández, Geraldine J. Kress, Tatyana V. Votyakova, Sumon Pal, Ian J. Reynolds *

Department of Pharmacology, University of Pittsburgh, E1351 Biomedical Science Tower, Pittsburgh, PA 15261, USA

Received 31 July 2000; received in revised form 3 October 2000; accepted 3 October 2000

Abstract

MitoTracker dyes are fluorescent mitochondrial markers that covalently bind free sulfhydryls. The impact of alterations in mitochondrial membrane potential ($\Delta\Psi_m$) and oxidant stress on MitoTracker staining in mitochondria in cultured neurons and astrocytes has been investigated. *p*-(Trifluoromethoxy) phenyl-hydrazone (FCCP) significantly decreased MitoTracker loading, except with MitoTracker Green in neurons and MitoTracker Red in astrocytes. Treatment with FCCP after loading increased fluorescence intensity and caused a relocalization of the dyes. The magnitude of these effects was contingent on which MitoTracker, cell type and dye concentration were used. H_2O_2 pretreatment led to a consistent increase in neuronal MitoTracker Orange and Red and astrocytic MitoTracker Green and Orange fluorescence intensity. H_2O_2 exposure following loading increased MitoTracker Red fluorescence in astrocytes. In rat brain mitochondria, high concentrations of MitoTracker dyes uncoupled respiration in state 4 and inhibited maximal respiration. Thus, loading and mitochondrial localization of the MitoTracker dyes can be influenced by loss of $\Delta\Psi_m$ and increased oxidant burden. These dyes can also directly inhibit respiration. Care must be taken in interpreting data collected using MitoTrackers dyes as these dyes have several potential limitations. Although MitoTrackers may have some value in identifying the location of mitochondria within cultured neurons and astrocytes, their sensitivity to $\Delta\Psi_m$ and oxidation negates their use as markers of mitochondrial dynamics in healthy cultures.

Keywords: Fluorescence imaging; Mitochondria; Oxidative stress

1. Introduction

There is an emerging appreciation for a role of mitochondria in excitotoxic injury pathways as well as injury mechanisms manifested as apoptotic or necrotic death processes. The development of novel mitochondrion-specific fluorescent dyes is necessary to explore the significance of mitochondria in these cell death pathways. Although some mitochondrial fluorescent probes are available that allow the assessment of mitochondrial membrane potential ($\Delta\Psi_m$), most fluorescent dyes that measure ions, such as calcium, magnesium and zinc, or reactive oxygen species (ROS) generation and pH are not specific to mitochondria. Moreover, dyes that can detect activity at the elusive permeability transition pore (PTP) in cultured neurons are currently unavailable.

The MitoTracker dyes, developed commercially by Molecular Probes (Eugene, OR), are structurally novel fluorescent probes that have been used to measure $\Delta\Psi_m$ (Macho et al., 1996), $\Delta\Psi_m$-independent mitochondrial mass (Krohn et al., 1999) and photosensitization (Minamikawa et al., 1999). The MitoTracker dyes (MitoTracker Green FM, MitoTracker Orange CMTMRos, MitoTracker Red CMXRos) contain chloromethyl moieties that are thought to react with free sulfhydryls within the cell. MitoTracker Green has been suggested to be $\Delta\Psi_m$-insensitive and capable of loading and remaining within depolarized mitochondria, which implies that it would be an exceptional tool for assessing mitochondrial mass (Poot et al., 1996). MitoTrackers Orange and Red are positively charged rosamine

* Corresponding author. Tel.: +1-412-6482134; fax: +1-412-6240794.

E-mail address: iannmda+@pitt.edu (I.J. Reynolds).

0165-0270/01/$ - see front matter
PII: S0165-0270(00)00340-X

derivatives that are rapidly taken up into the negatively charged mitochondria, suggesting that their loading would be dependent on $\Delta\Psi_m$, but their localization should be mitochondrial specific. However, MitoTracker Orange and Red, at least in their reduced state, may be strongly influenced by the presence of ROS (Poot and Pierce, 1999a,b) and MitoTracker Orange may directly inhibit the respiratory chain at complex I and induce permeability transition (PT) (Scorrano et al., 1999). All three MitoTracker probes are believed to be retained following fixation due to the membrane-impermeant dye complex that is created when the dyes enters the mitochondria. However, the sensitivity of these dyes to $\Delta\Psi_m$ and oxidant status and their permeability through the mitochondrial membrane has not been fully explored in unfixed cultured neurons and astrocytes.

This laboratory is interested in identifying fluorescent dyes that can specifically label mitochondria in the central nervous system under a variety of conditions. The aim of the present study was to characterize the MitoTracker dyes in primary forebrain neurons and astrocytes to determine their dependency on $\Delta\Psi_m$ and oxidant status, especially given the widespread interest in using these dyes as fixable markers of $\Delta\Psi_m$. In addition, one addressed whether the MitoTrackers altered respiratory chain activity in isolated brain mitochondria to determine whether these dyes altered mitochondrial physiology.

2. Materials and methods

2.1. Cell culture

All procedures were in strict accordance with the NIH Guide for the Care and Use of Laboratory Animals and were approved by the University of Pittsburgh's Institutional Animal Care and Use Committee. Primary forebrain neurons were prepared as previously described (White and Reynolds, 1995). Briefly, forebrains from embryonic day-17 Sprague Dawley rats were removed and dissociated. Cells were plated on poly-D-lysine coated 31 mm glass coverslips at a density of 450 000/ml (1.5 ml/coverslip) and inverted after 24 h to decrease glial growth. Experiments were performed when cells were 14–17 days in culture.

Primary forebrain astrocytes were prepared as described by McCarthy and de Vellis (1980) with minor modifications. Briefly, forebrains from postnatal day-1 Sprague Dawley rats were dissociated and plated in 75 cm^2 plastic flasks at a density of 860 000 cells/ml (10 ml/flask). Media was changed every other day. Cells were grown to the point of confluency, at which point the flasks were orbitally shaken for 15–18 h at 37°C. Adherent cells were then plated onto poly-D-lysine coated 31 mm glass coverslips and fed every other day and used for up to 5 days in culture.

2.2. Solutions

Coverslips were perfused with a HEPES-buffered salt solution (HBSS) with (in mM): NaCl (137), KCl (5), $NaHCO_3$ (10), HEPES (20), glucose (5.5), KH_2PO_4 (0.6), Na_2HPO_4 (0.6), $CaCl_2$ (1.4), $MgSO_4$ (0.9), pH adjusted to 7.4 with NaOH. The protonophore and mitochondrial uncoupler carbonyl cyanide *p*-(trifluoromethoxy) phenyl-hydrazone (FCCP) was used at a concentration of 750 nM (diluted in HBSS from a 750 μM stock in methanol). Hydrogen peroxide (H_2O_2) was diluted in HBSS to concentrations ranging from 10 μM to 3 mM (from a 30% w/w stock solution). Oligomycin was used at a 2 μM concentration (diluted from a 10 mM stock in methanol).

2.3. Fluorescence imaging

For all experiments, individual coverslips were rinsed twice in HBSS and loaded with 10–500 nM concentrations of MitoTracker Green FM, MitoTracker Orange (CMTMRos) or MitoTracker Red (CMXRos) (Molecular Probes, Eugene, OR) for 15 min at 37°C. Dyes were diluted in HBSS from a 1 mM stock in anhydrous dimethyl sulfoxide. Coverslips were rinsed for 15 min in HBSS at room temperature. Loading parameters were tested and optimized for assessing fluorescence intensity and localization.

Experiments were performed at room temperature on two light microscope-based imaging systems with 40 × quartz objectives. Cells were illuminated using a Xenon lamp-based monochromator (TILL, Photonics, Germany) and light detected using a CCD camera. Data acquisition was controlled using Simple PCI software (Compix, Cranberry, PA). Cells were illuminated with a 490, 550 or 575 nm light depending on the dye and incidence light was attenuated with neutral density filters (Omega Optical, Brattleboro, VT). Emitted fluorescence from MitoTracker Green was passed through a 500 or 515 long pass (LP) dichroic mirror and a 535, 25 band pass (BP) or 535, 40BP emission filter (depending on the imaging system used). For MitoTracker Orange, a 570 or 575LP dichroic and a 590, 35BP or 605, 35BP emission filter was used. For MitoTracker Red, a 590LP dichroic with a 600LP emission filter was used. Coverslips were placed on the microscope stage, a field of cells (with at least ten viable neurons or five viable astrocytes in the field) was chosen and a bright field image was captured. From this image, cell bodies were circled and used as regions of interest from which cellular fluorescence intensity was measured. Three small cell-free regions on the coverslip were also chosen to assess background fluorescence

intensity. Images were collected once every 15 s for baseline and once every 5 s for the remainder of the experiment. Data were collected as background subtracted fluorescence intensity. All experiments were performed on at least three different culture dates. For most experiments, data were converted to percent baseline or percent of untreated control. The number of cells analyzed are presented with each graph, however in order to insure stringency in the statistical analyses, all cells from a single coverslip were combined and statistics were performed with the more conservative '*n*' of the number of coverslips. Where pertinent, data were statistically analyzed using a two-tailed *t*-test or a one-way ANOVA and a Dunnett post-hoc test (when $P < 0.05$).

2.4. FCCP experiments

To determine the effect of $\Delta\Psi_m$ depolarization on MitoTracker-loaded cells, individual coverslips were loaded with 10–500 nM concentrations of MitoTracker dye (Green, Orange or Red) and imaged to observe changes in the intensity and/or pattern of fluorescence. Coverslips were perfused with HBSS for 5 min, with FCCP (750 nM) for 5 min, and then with HBSS again for 5 min. The effect of $\Delta\Psi_m$ on loading was assessed by comparing fluorescence intensity (over 5 min, 1 frame/15 s) from coverslips incubated with 50 nM MitoTracker alone to coverslips incubated in 750 nM FCCP + 50 nM MitoTracker.

2.5. H_2O_2 experiments

As with the FCCP experiments, the effect of an oxidant burden on pre-loaded cells was tested by loading coverslips with 50 nM MitoTracker dye and imaging. Coverslips were perfused with HBSS, H_2O_2 (500 μM in neurons, 3 mM in astrocytes) and HBSS again. The effect of an oxidant burden on loading was assessed by incubating coverslips in H_2O_2 (10–500 μM in neurons, 500 μM–3 mM in astrocytes) for 15 min, then immediately loading 50 nM MitoTracker dye (Green, Orange or Red) and imaging for 5 min.

2.6. Isolated brain mitochondria preparation

Rat brain mitochondria were isolated according to Rosenthal et al. (1987). Briefly, a rat forebrain was removed, homogenized and suspended in 10 ml of isolation buffer (pH 7.4, containing 225 mM mannitol, 75 mM sucrose, 1 mg/ml BSA, 1 mM EDTA, 5 mM HEPES-KOH). The brain homogenates were subjected to differential centrifugation and the final suspensions contained a heterogeneous population of synaptosomal and non-synaptosomal mitochondria. Protein concentration in the mitochondrial suspensions was determined according to Bradford (1976). Only mitochondria that had a respiration ratio of 6 or higher (phosphorylating state 3 to resting state 4 with glutamate and malate as substrates) were used.

2.7. Respiratory experiments

Mitochondrial respiration rates were measured polarographically at 37°C with a Clark oxygen electrode (Yellow Springs Instrument, Yellow Springs, OH) in a buffer containing 125 mM KCl, 2 mM K_2HPO_4, 4 mM $MgCl_2$, 3 mM ATP, 5 mM glutamate, 5 mM malate, 5 mM HEPES-KOH (pH 7.0). This buffer exhibits similarities to the intracellular environment and is believed to decrease the probability of PT (Andreyev et al., 1998; Andreyev and Fiskum, 1999). Energized brain mitochondria (0.25 mg protein/ml), oligomycin (2 μM) and the MitoTracker dyes (at concentrations of 50 nM (low) or 3.12 μM (high) concentrations) were incubated in a 1.6 ml water-jacketed glass chamber (Gilson, Middletown, WI). The experiment was initiated in an open chamber (to maintain oxygen concentration close to saturation) and mitochondrial suspension was stirred at 37°C for 10 min. The chamber was then sealed, state 4 (resting) respiration was measured and 1 min later the uncoupling agent, FCCP (200 nM) was added and the rate of uncoupled (maximal) respiration was determined.

Data were collected as nanograms of oxygen atoms consumed per minute per milligram of protein. Data were then transformed into percent of control respiration (in the absence of MitoTracker dye) and three separate one-way ANOVAs (for each MitoTracker dye), comparing respiration in control mitochondria to that in mitochondria incubated with the low and high concentration of dye. A Bonferroni post-hoc test was performed when $P < 0.05$.

3. Results

3.1. FCCP-induced changes in dye labeling

All three MitoTrackers labeled neurons and astrocytes in a punctate fashion anticipated for a mitochondrion-specific dye. Staining was typically observed in perinuclear regions and processes, while the nucleus was typically devoid of staining (Fig. 1A,B, top panels). The fluorescence intensity of the MitoTrackers was concentration dependent with maximal staining seen with 200–500 nM (data not shown). To determine the effect of $\Delta\Psi_m$ on fluorescence intensity, cells were loaded with different dye concentrations and then exposed the cells to FCCP. At high concentrations, the MitoTracker dyes showed an increase in fluorescence intensity upon loss of $\Delta\Psi_m$, suggesting that they be-

come so tightly packed within mitochondria at these concentrations that fluorescence intensity is underestimated due to the phenomenon of quenching (see Section 4). MitoTracker Green showed the smallest increase in fluorescence intensity during treatment with FCCP, however, in both neurons and astrocytes, no return to baseline was observed during a 5-min wash period (Fig. 2A,D). MitoTracker Orange showed the most robust increase in fluorescence intensity in neurons and this was observed at concentrations of 50–500 nM. A slow, delayed decrease in fluorescence was observed during the wash period, indicating either re-sequestration as mitochondria repolarize or a leakage of the dye from the cell (Fig. 2B,E). MitoTracker Red showed variability in the time course of the FCCP-induced fluorescence increases, however, every concentration of MitoTracker Red tested was influenced by mitochondrial depolarization. In addition, a rapid return to basal fluorescence was observed during the recovery period (Fig. 2C,F). All three MitoTrackers showed a diffusion of fluorescence upon mitochondrial depolarization (Fig. 1A,B, bottom panels). Interestingly, the redistribution of dye was apparent even when there was no overall change in fluorescence intensity. Taken together these data suggest that MitoTrackers are membrane-permeable and diffuse out of mitochondria during a depolarizing stimulus. It also appears that MitoTrackers, at concentrations as low as 25 nM (in MitoTracker Red), are quenched in mitochondria as evidenced by the increase in fluorescence signal seen when the dyes are released from mitochondria.

3.2. FCCP-induced changes in dye loading

A concentration of 50 nM, the lowest concentration that reliably gave a good signal:noise ratio, was used

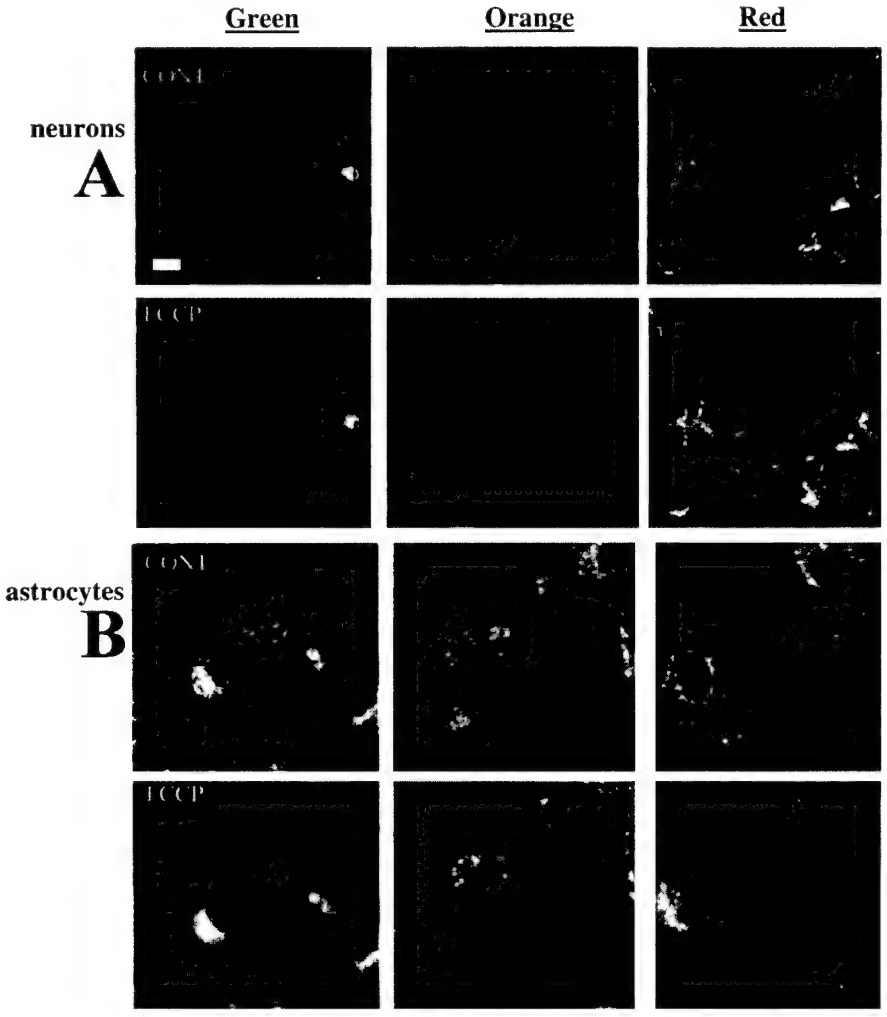

Fig. 1. Representative micrographs of fluorescence intensity and distribution of the MitoTracker dyes prior to and during treatment with *p*-(trifluoromethoxy) phenyl-hydrazone (FCCP) in (A) primary neurons and (B) astrocytes. In both (A) and (B), the upper row of images shows baseline fluorescence in cells loaded with 50 nM MitoTracker Green, Orange and Red (from left to right). The lower row of images shows fluorescence in cells treated with a mitochondrial depolarizing stimulus (images collected after approximately 3 min of FCCP treatment). Bar, 25 μM.

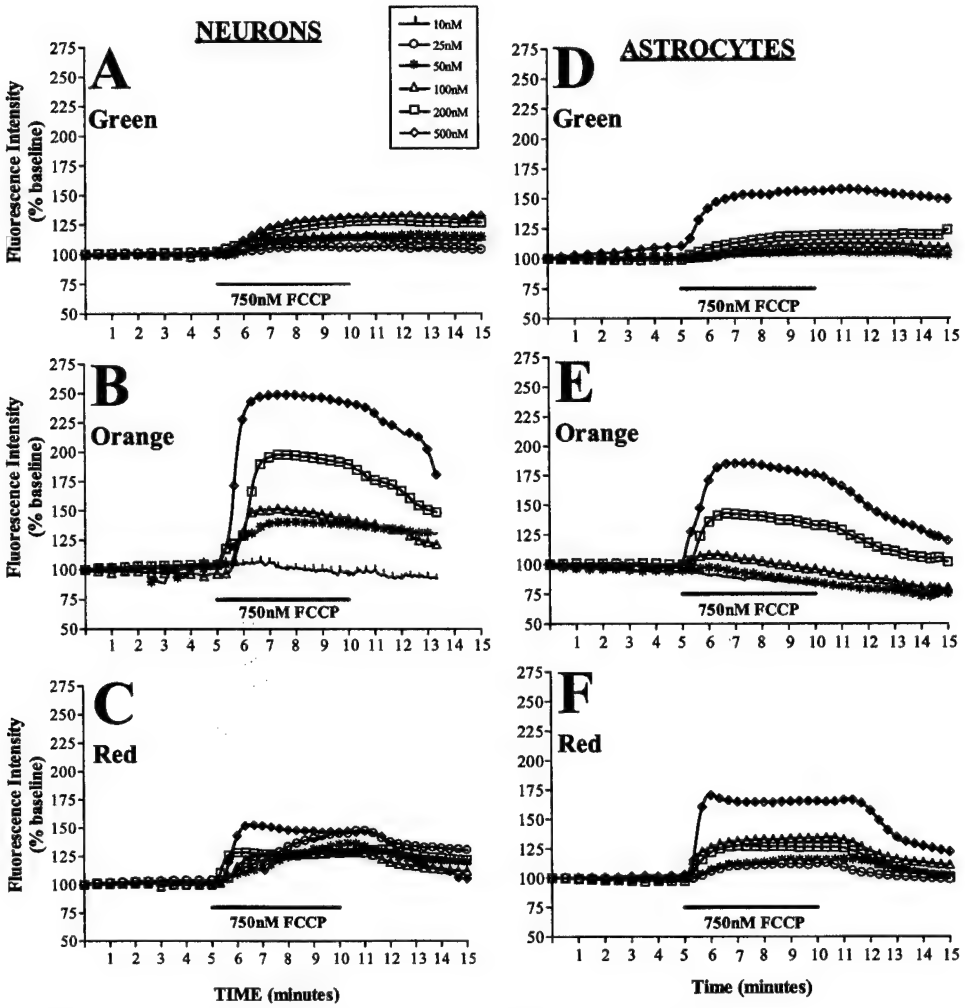

Fig. 2. Intensity of MitoTracker fluorescence during mitochondrial depolarization. (A–C) Primary neurons and (D–F) astrocytes were loaded with varying concentrations of MitoTracker (A,D) Green, (B,E) Orange or (C,F) Red and the fluorescence intensity was measured. Baseline fluorescent images were recorded for 5 min, then the MitoTracker response to a depolarizing concentration (750 nM) of the uncoupling agent, *p*-(trifluoromethoxy) phenyl-hydrazone (FCCP) was measured for 5 min. Following treatment, cells were allowed to recover for 5 min. Data are presented as percent of baseline fluorescence intensity.

for all MitoTrackers in this experiment. Neurons or astrocytes were loaded with MitoTracker dyes alone or in the presence of 750 nM FCCP. This concentration of FCCP has been shown to result in a profound, but reversible depolarization of the $\Delta\Psi_m$ (White and Reynolds, 1996). In neurons, MitoTracker Green appeared to load equally well into polarized or depolarized mitochondria, however MitoTracker Orange and Red showed considerably lower fluorescence intensity when loaded into neurons treated with FCCP (Fig. 3A). In astrocytes, MitoTracker Green loading appeared to depend on the $\Delta\Psi_m$, with lower fluorescence intensity observed in the presence of FCCP. Similarly, MitoTracker Orange loading into astrocytes was compromised when mitochondria were depolarized. In contrast, MitoTracker Red appeared to load into astrocytic mitochondria regardless of $\Delta\Psi_m$ (Fig. 3B). A less punctate label (vs. Fig. 1A,B, upper panels) was observed under these loading conditions, except with MitoTracker Red in astrocytes (Fig. 4). These data reflect the different loading behaviors of the MitoTrackers and point to the significance of cell model for the appropriate use of these dyes.

3.3. H_2O_2-induced changes in dye loading

Cells were incubated with H_2O_2 for 15 min prior to loading with 50 nM MitoTracker in order to induce an oxidant stress. H_2O_2-induced oxidative stress was seen in neurons at concentrations as low as 10 μM and at concentrations greater than 500 μM considerable cell death was evident. Astrocytes were more resistant to oxidant stress and thus higher concentrations of H_2O_2 were utilized. The chloromethyl moieties of the MitoTracker dyes have been suggested to react with free sulfhydryls (Haugland, 1996). Thus, an oxidative stress

was expected to change the loading and stability of the MitoTrackers labeling. Comparison of the mean fluorescence intensity following pretreatment, using unpaired t tests, showed that some concentrations of H_2O_2 increased neuronal MitoTracker Green fluorescence (Fig. 5A) and astrocytic MitoTracker Red fluorescence (Fig. 5F); however, with MitoTracker Orange and Red in neurons (Fig. 5B,C) and MitoTracker Green and Orange in astrocytes (Fig. 5D,E) statistically significant increases in fluorescence were more broadly seen and appeared, in some cases, to correspond to an H_2O_2 concentration-dependence. The changes in fluorescence intensity did not correlate with a relocalization of the dyes (Fig. 6), in that H_2O_2 increased fluorescence intensity without the migration of the dye into parts of the cell not normally labeled. This may be consistent with an alteration of the interaction of the dyes with cellular sulfhydryl moieties.

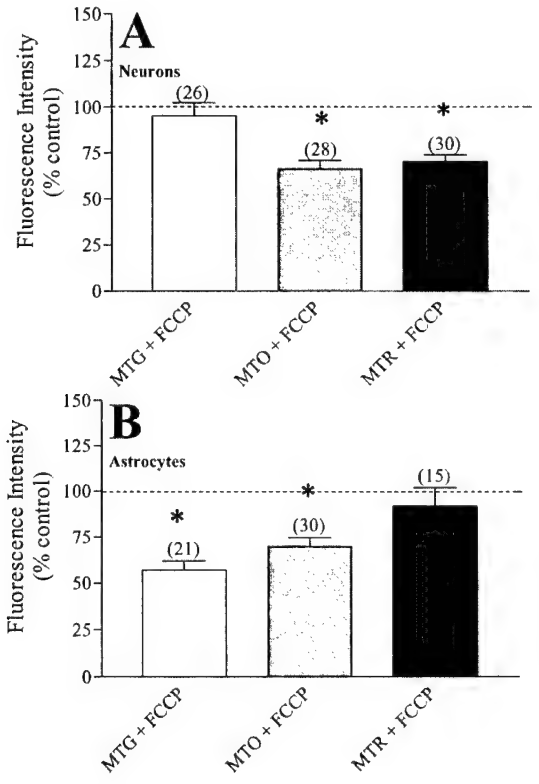

Fig. 3. Effect of mitochondrial depolarization on MitoTracker loading. (A) Neurons and (B) astrocytes were loaded with 50 nM MitoTracker dye in the presence of 750 nM p-(trifluoromethoxy) phenyl-hydrazone (FCCP) and the fluorescence intensity (averaged over 5 min) was compared to cells loaded without FCCP. The loading of MitoTracker Green (MTG) in astrocytes [$t = 2.6$, df = 5, $P < 0.05$], MitoTracker Orange (MTO) in neurons [$t = 3.7$, df = 4, $P < 0.05$] and astrocytes [$t = 2.8$, df = 6, $P < 0.05$] and Red (MTR) in neurons [$t = 3.6$, df = 4, $P < 0.05$] was sensitive to $\Delta\psi_m$, as evidenced by the significant decrease in fluorescence intensity when FCCP was present. The number of cells analyzed (n) is presented above each bar. Average fluorescence from each coverslip was then computed and used as degrees of freedom in unpaired t tests (see Section 2). [* $P < 0.05$].

3.4. H_2O_2-induced changes in dye labeling

Neurons and astrocytes were loaded with 50 nM MitoTracker dye and imaged for 5 min to achieve stable baseline fluorescence. Neurons were then treated with 500 μM H_2O_2 for 5 min and the intensity of fluorescence was measured. MitoTracker Green was unaffected by treatment with H_2O_2 and MitoTracker Orange and Red fluorescence were only very modestly increased by this short-term oxidative stress, with no return to baseline observed. In astrocytes treated with 3 mM H_2O_2, only MitoTracker Red fluorescence was increased (Fig. 7). No apparent relocalization of the dyes was observed (data not shown). These data suggest that once MitoTrackers, especially MitoTracker Green, are loaded into primary neuronal or astrocytic cultures, they are only mildly influenced by a change in the production of ROS and/or oxidation of sulfhydryl groups. However, the effect of a longer exposure to H_2O_2 (i.e. 15 min) may be necessary to see the more profound effect seen during pretreatment with H_2O_2.

3.5. Respiration in isolated brain mitochondria

Isolated rat brain mitochondria were incubated in the presence of 50 nM or 3.12 μM MitoTracker Green, Orange or Red and state 4 (resting) and uncoupled (maximal) respiration were recorded. Since dye distribution between the aqueous phase and the mitochondrial membranes is not homogeneous, MitoTracker concentrations are also denoted as nmoles of dye per mg of mitochondrial protein (50 nM corresponds to 0.2 nmol/mg protein and 3.12 μM corresponds to 12.5 nmol/mg protein). Initially mitochondria and the fluorescent dyes were incubated for 2–4 min prior to uncoupling, however, there was no inhibition seen at either concentration tested (data not shown). Because the MitoTrackers contain sulfhydryl-reactive moieties they may bind more slowly, therefore the incubation time was extended to 10 min. Under these conditions, high concentrations of MitoTracker Green (3.12 μM) significantly increased resting respiration, suggesting its ability to uncouple respiratory chain activity from ATP synthesis, and decreased maximal respiration rates, suggesting its ability to inhibit respiration (Fig. 8). MitoTracker Orange did not significantly impact respiration rate, however it exhibited trends towards increased state 4 respiration rate ($P = 0.07$) and decreased maximal respiration rate ($P = 0.13$) (Fig. 8). MitoTracker Red exhibited a trend towards increased resting respiration rate ($P = 0.09$) and significantly decreased the rate of maximal respiration rate (at 3.12 μM, but not at 50 nM). Taken together, these data suggest that all of the MitoTracker dyes are capable of inhibiting normal mitochondrial respiration at μM concentrations.

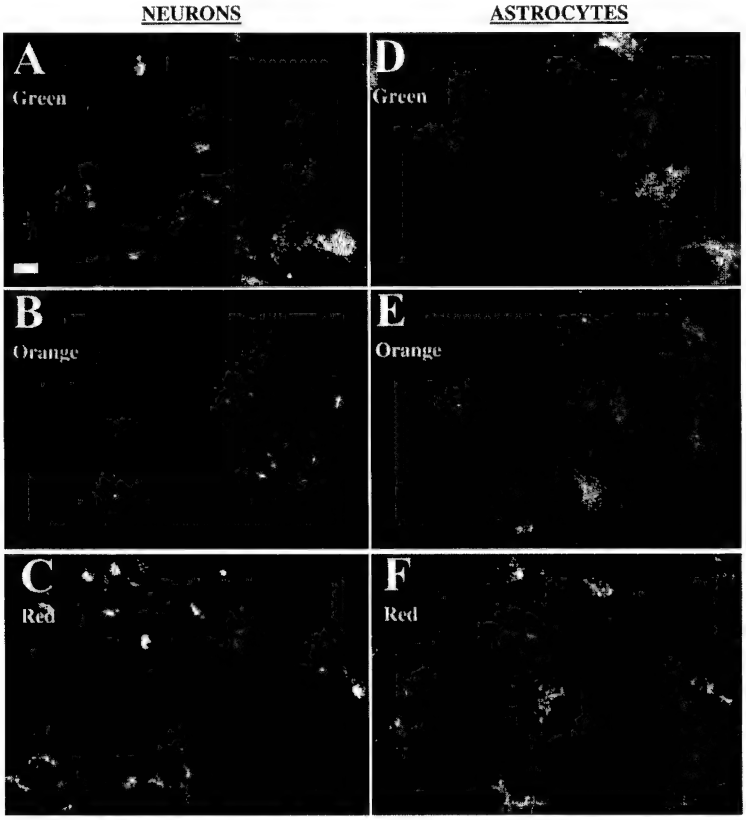

Fig. 4. Representative micrographs of distribution of the MitoTracker fluorescence when loaded in the presence of a mitochondrial depolarizing stimulus. (A–C) Primary neurons and (D–F) astrocytes were loaded with 50 nM MitoTracker (A,D) Green, (B,E) Orange or (C,F) Red in the presence of 750 nM *p*-(trifluoromethoxy) phenyl-hydrazone (FCCP). Bar, 25 μM.

4. Discussion

The MitoTracker dyes are being used with increasing frequency for morphological and functional measurements of mitochondria. While the pattern of their fluorescence strongly suggests mitochondrial specificity, parameters that influence their loading and/or labeling are still controversial and have not been fully explored in neural cells. For example, reports that during apoptosis the release of cytochrome c can occur independent of changes in mitochondrial membrane potential have been partially based on the lack of change in MitoTracker Orange fluorescence (which was being used as a $\Delta\Psi_m$ sensor) during cytochrome c release (Bossy-Wetzel et al., 1998; Li et al., 1998; Finucane et al., 1999). However, the present experiments suggest that there are numerous factors to consider prior to using the MitoTracker dyes and, in agreement with Scorrano et al. (1999) and Keij et al. (2000), that these aforementioned data must be interpreted with caution. It has been noted that not only are MitoTracker Green, Orange and Red different from one another, but also that each MitoTracker behaves differently in neurons and astrocytes.

For all three MitoTrackers, in both neurons and astrocytes, a concentration of 50 nM was sufficient to produce a bright, punctate label that appears to be associated with mitochondria. However, at this concentration, neurons and astrocytes treated with FCCP during or after loading showed a diffusion of the dye into the cytoplasm, nucleus and/or other organelles. In human osteosarcoma cells, a redistribution of MitoTracker Green was observed following a 30-min treatment with another uncoupler, CCCP (Minamikawa et al., 1999). However, these authors used high-resolution confocal microscopy and the observed redistribution appeared to coincide with mitochondrial swelling, not diffusion into cytoplasm (Minamikawa et al., 1999). Whether this observation is associated with confocal versus light microscopy or osteosarcomas versus primary neurons and astrocytes is unclear.

In addition to a relocalization of fluorescence observed in association with mitochondrial depolarization, an increase in fluorescence intensity was frequently seen, especially at higher concentrations and most intensely with MitoTracker Orange (Fig. 2). This increased fluorescence has been interpreted as an unquenching of dye. Quenching occurs as the result of

molecular interactions that inhibit the ability of a fluorophore to emit a photon. For example, rhodamine dyes aggregate based on $\Delta\Psi_m$ but these aggregates are non-fluorescent due to quenching. Quenching becomes most apparent with these rhodamine dyes when the mitochondria are depolarized and the intensity of fluorescence dramatically increases (Chen and Smiley, 1993). It is possible that MitoTrackers aggregate within mitochondria without truly quenching, however, due to the similarities of the current observations with those seen with rhodamine derivatives this phenomen will be tentatively referred to as quenching.

The use of quenching concentrations of MitoTracker dyes impacts a number of possible interpretations of the data. During washout after FCCP treatment, a slow decrease in fluorescence is observed (Fig. 2). This may be due to the movement of the dye back into the mitochondria as they repolarize (requenching) or due to slow leakage of the dye through the plasma membrane. As quenching interferes with linear measurements of fluorescence, it is not possible to determine whether one or both of these phenomena have occurred. However at the beginning and end of this experiment, small punctate spots of labeling can be observed within the cells. This suggests that some of the dye remains within the mitochondria, but quenching prohibits direct quantitation of a $\Delta\Psi_m$-insensitive pool, an irreversibly bound pool or re-sequestered pool of dye.

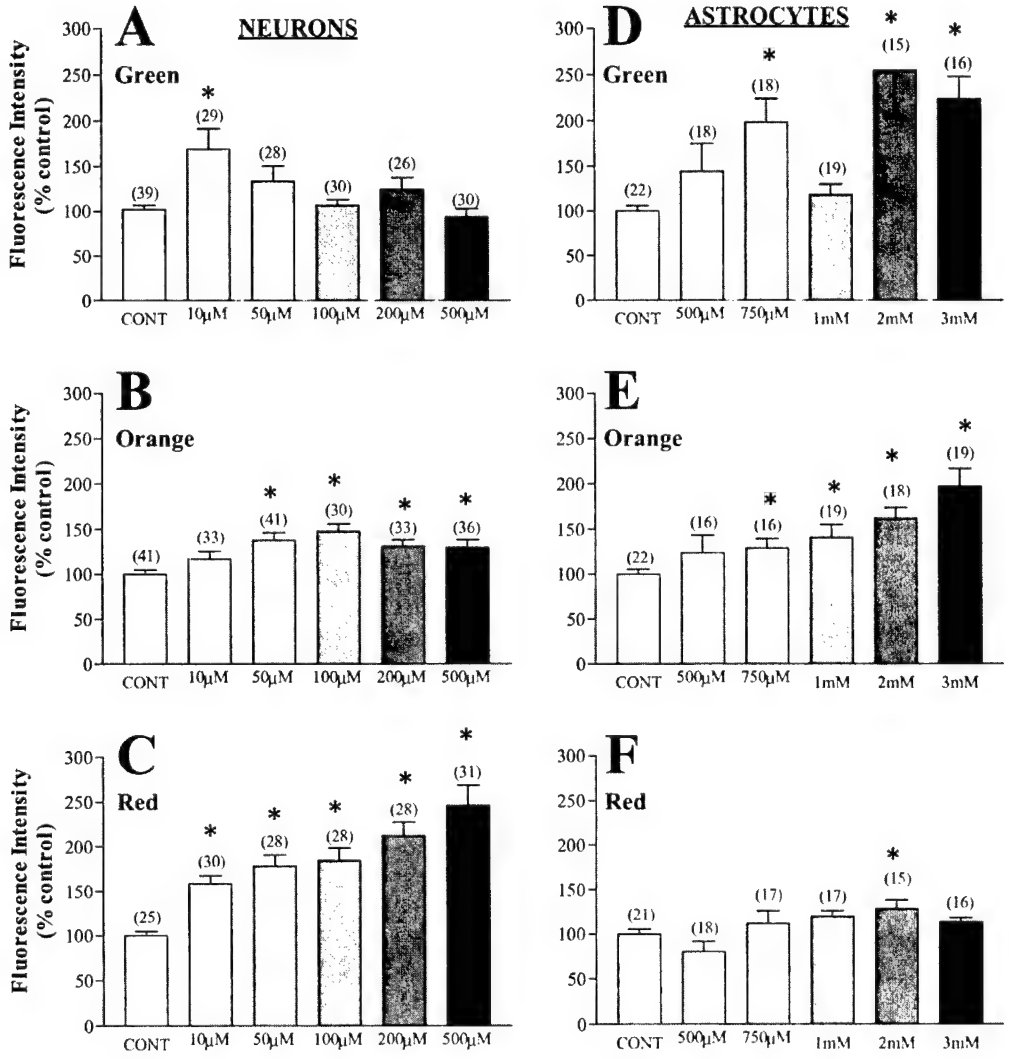

Fig. 5. Effect of H_2O_2 pretreatment on MitoTracker loading. (A–C) Neurons and (D–F) astrocytes were incubated with 10 μM–3 mM of H_2O_2 for 15 min, then loaded with 50 nM MitoTracker (A,D) Green, (B,E) Orange or (C,F) Red. The intensity of fluorescence was measured (over 5 min) and the mean ± S.E.M. was calculated. Data are expressed as percent of untreated control and the number of cells analyzed is presented above each bar. Unpaired *t* tests were performed to determine whether H_2O_2 pretreatment led to significant changes in fluorescence intensity. All points were individually compared to the untreated control. MitoTracker Orange and Red in neurons and MitoTracker Green and Orange in astrocytes exhibited H_2O_2 concentration-dependent changes in fluorescence [* $P < 0.05$].

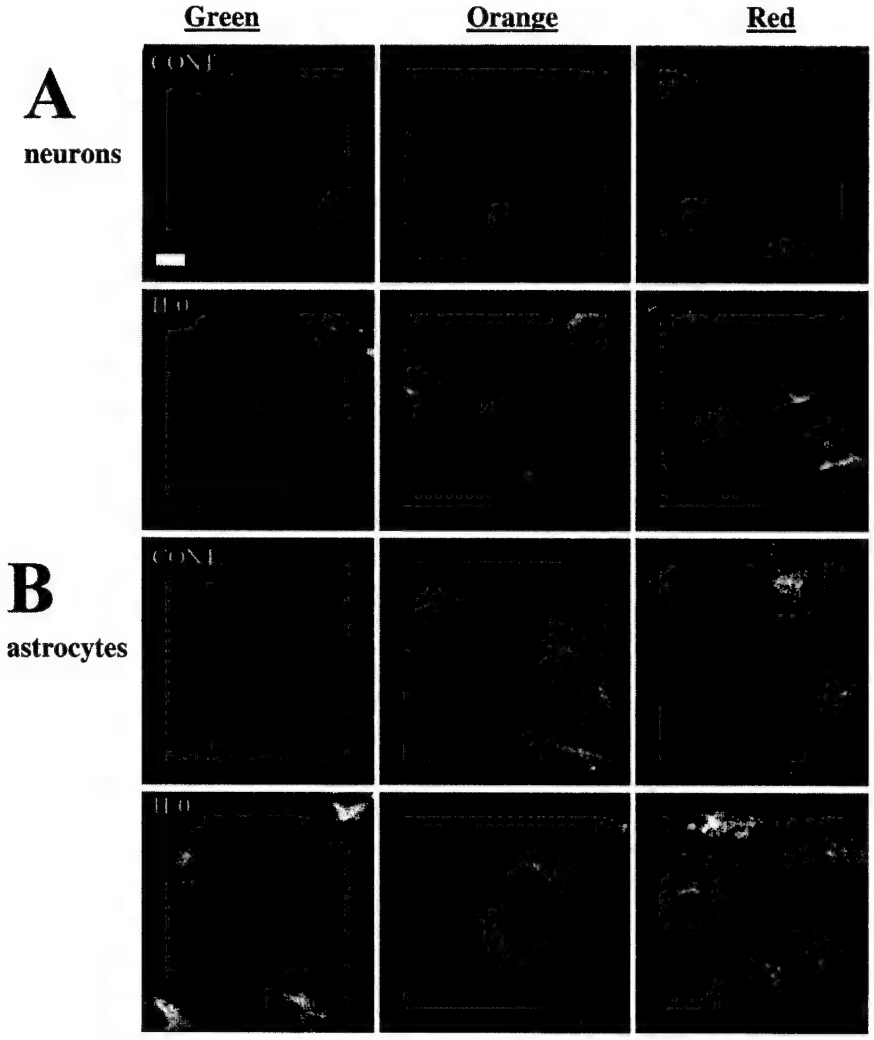

Fig. 6. Representative micrographs of distribution of the MitoTracker loading in cells pretreated with H_2O_2. (A,B) The upper rows of images show neurons loaded with 50 nM MitoTracker Green, Orange and Red (from left to right) without any pretreatment. In the lower rows, (A) neurons were preincubated with 500 μM H_2O_2 and then loaded with 50 nM MitoTracker (B) astrocytes were preincubated with 3 mM H_2O_2 and then loaded with 50 nM MitoTracker. Bar, 25 μM.

4.1.1. MitoTracker Green

MitoTracker Green is now commonly being used for measurement of mitochondrial shape changes, mass or swelling (Bowser et al., 1998; Funk et al., 1999; Krohn et al., 1999; Minamikawa et al., 1999; Monteith and Blaustein, 1999). At low concentrations (≤ 50 nM), MitoTracker Green may be useful for these measures, however several features of this dye must be acknowledged prior to use. There are cell type- and concentration-specific differences in MitoTracker Green labeling. At 50 nM, MitoTracker Green loading appeared $\Delta\Psi_m$- and oxidation-sensitive in astrocytes, but not neurons. At concentrations greater than 50 nM, MitoTracker Green exhibits a tendency to quench and, upon depolarization, exhibits an irreversible increase in fluorescence. Moreover, in isolated brain mitochondria, μM concentrations of MitoTracker Green appeared capable of acting as an uncoupler and inhibiting respiration. Taken together, the present data support the use of MitoTracker Green at low concentrations for assessing mitochondrial size, localization and structure. However, determination of the appropriate concentration of MitoTracker in individual cell models will be necessary for interpretable results.

4.1.2. MitoTracker Orange

MitoTracker Orange has been used as a marker for $\Delta\Psi_m$ (Matylevitch et al., 1998) and, in its reduced form, as a marker for ROS generation (Karbowski et al., 1999). Scorrano et al. (1999) characterized this dye in MH1C1 rat hepatoma cells and in agreement with the present findings, found that the fluorescence was punctate and stable. However, in their cell model, a redistribution of the dye was observed following pretreatment with agents that decrease free sulfhydryls, but not with FCCP. In the present paper, pretreatment with FCCP,

but not H_2O_2, caused a redistribution of MitoTracker Orange into neuronal and astrocytic cultures. H_2O_2 pretreatment, however, did appear to increase MitoTracker Orange fluorescence in neurons and astrocytes. Moreover, Scorrano et al. (1999) did not observe quenching or relocalization of MitoTracker Orange when cells were treated with FCCP following loading. In the present experiments, neurons and astrocytes treated with FCCP following loading showed increased fluorescence intensity (suggestive of quenching) as well as a relocalization of fluorescence. In isolated rat liver mitochondria, MitoTracker Orange inhibited complex I of the respiratory chain, induced PT and caused depolarization, swelling and the release of cytochrome c in liver mitochondria (Scorrano et al., 1999). However, in isolated brain mitochondria, no inhibition of complex I by MitoTracker Orange was observed, even at concentrations exceeding 3 μM. Again, these observed differences suggest that care must be taken in extrapolating MitoTracker data obtained in different cell models. In addition, MitoTracker Orange should be used with caution and that the interpretation of data with MitoTracker Orange must consider their effects on mitochondrial function and their sensitivity to $\Delta\Psi_m$ and free sulfhydryls.

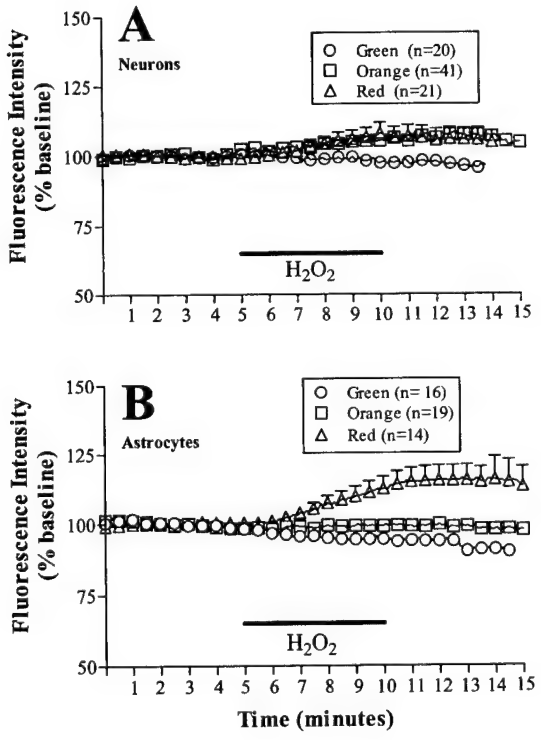

Fig. 7. Intensity of MitoTracker fluorescence in response to H_2O_2. (A) Neurons and (B) astrocytes were loaded with 50 nM MitoTracker and their response to 500 μM (neurons) or 3 mM (astrocytes) H_2O_2 was measured. Baseline fluorescent images were recorded for 5 min, followed by a 5-min H_2O_2 treatment and a 5-min recovery period. Data are expressed as percent of basal fluorescence (±S.E.M.). The number of cells analyzed in presented in the figure legend.

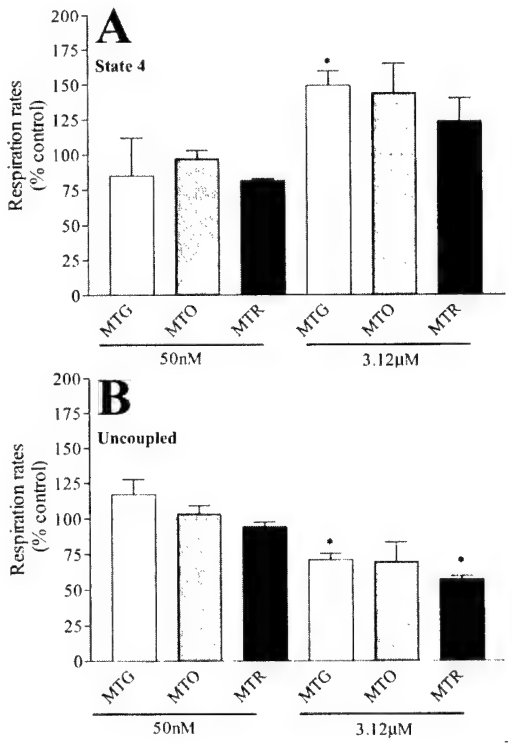

Fig. 8. Respiration of isolated rat brain mitochondria. (A) State 4 (resting) respiration rate was determined following a 10 min preincubation of isolated mitochondria with 2 μM oligomycin and 50 nM or 3.12 μM MitoTracker Green (MTG), Orange (MTO) or Red (MTR). The mean (±S.E.M.) respiration rates were computed and data were transformed into percent of respiration rate of control (without MitoTracker dyes). Statistical analysis using a one-way ANOVA and a Bonferroni's post-hoc test showed the following: MTG: $F_{(2, 10)} = 7.5$, $P < 0.05$ with the high concentration being significantly different from both the control and 50 nM group ($P < 0.05$). MTO: $F_{(2, 8)} = 3.7$, $P > 0.05$. MTR: $F_{(2, 8)} = 3.3$, $P > 0.05$. (B) Following assessment of resting respiration, 200 nM *p*-(trifluoromethoxy) phenyl-hydrazone (FCCP) was added and the maximal respiration rate was determine in the same isolated mitochondria. The mean (±S.E.M.) respiration rate was computed and data were transformed into percent of respiration rate of control (without MitoTracker dyes). Statistical analysis showed the following: MTG: $F_{(2, 8)} = 16.2$, $P < 0.05$ with the high concentration being significantly different from both the control and 50 nM group ($P < 0.05$). MTO: $F_{(2, 6)} = 2.9$, $P > 0.05$. MTR: $F_{(2, 6)} = 130.1$, $P < 0.05$ with the high concentration being significantly different from both the control and 50 nM group ($P < 0.05$).

4.1.3. *MitoTracker Red*

MitoTracker Red has been utilized as a $\Delta\Psi_m$-sensitive dye, since being reported as one by Macho et al. (1996). The linearity between $\Delta\Psi_m$ and MitoTracker Red fluorescence has been brought into question due to thiol binding of MitoTracker Red (Ferlini et al., 1998; Poot and Pierce, 1999a). It seems unlikely that this dye would offer advantages over JC-1, TMRE or rhodamine 123 for assessing $\Delta\Psi_m$. However, MitoTracker Red can be fixed and maintain a mitochondrial-specific localization, as observed in double labeling experiments with cytochrome c oxidase (Poot et al., 1996). Gilmore and Wilson (1999) used flow cytometry to show that

MitoTracker Red was $\Delta\Psi_m$-sensitive because it decreased with depolarizing stimuli, but it could not reliably indicate $\Delta\Psi_m$ at the time of fixation. Moreover, MitoTracker Red has been implicated as a mitochondrial-specific photosensitiser, due to the laser-induced mitochondrial damage observed in osteosarcomas (Minamikawa et al., 1999). In light of these observations, clear understanding of how MitoTracker Red influences neuronal and astrocytic mitochondria is necessary. In the present experiments, the loading of MitoTracker Red appeared $\Delta\Psi_m$- and oxidant-dependent in neurons, but not astrocytes. Following loading, MitoTracker Red fluorescence relocalized during mitochondrial depolarization and increased following treatment with FCCP and H_2O_2 in astrocytes, and to a lesser degree, neurons. It also appears to inhibit normal respiratory activity through complex I. These data illustrate that MitoTracker Red loading, stability and mitochondrial localization is contingent on cell type, $\Delta\Psi_m$, ROS and/or free sulfhydryl groups. Therefore, in addition to being less than ideal as a $\Delta\Psi_m$ marker, MitoTracker Red seems incapable of functionally characterizing mitochondria in intact cells and should be used only as a marker for the localization of normal, energized mitochondria.

To determine whether MitoTracker dyes directly influenced bioenergetics, isolated rat brain mitochondria were examined for resting and uncoupled (maximal) respiration rates through complex I in the presence of the different MitoTrackers. It was observed that MitoTracker Green acted as both a weak uncoupler and inhibitor of respiration and MitoTracker Red significantly decreased the rate of maximal respiration. MitoTracker Orange showed similar trends. These data suggest that the MitoTracker dyes are capable of inhibiting normal mitochondrial respiration at μM concentrations. Previously, MitoTracker Orange was found to inhibit complex I in isolated liver mitochondria and was observed to induce PT and swelling and release cytochrome c (Scorrano et al., 1999). In the present experiments, the respiration buffer contained physiological concentrations of Mg^{2+} and ATP and had a pH of 7.0 to minimize the likelihood of PT. The opening of the PTP can lead to the loss of respiratory substrates, such as NADH, as well as cytochrome c, thereby confounding the assessment of the MitoTracker dyes on respiratory chain activity. Moreover, since the MitoTracker dyes are sulfhydryl agents, they may increase the probability of opening the PTP (Zoratti and Szabo, 1995). The respiration experiments were therefore designed to enhance a straightforward assessment of respiratory chain activity through complex I and did not test the MitoTracker dyes' ability to induce transition. In keeping with Scorrano et al. (1999), however, preliminary experiments were performed in isolated liver mitochondria and observed inhibition of respiration with MitoTracker Red, and to a lesser extent with MitoTracker Orange (data not shown).

Potential problems associated with the use of the MitoTracker dyes, including their sensitivity to changes in $\Delta\Psi_m$, oxidant status and quenching have been addressed in these experiments. Although these features of the MitoTracker dyes makes data interpretation difficult, it should be noted that numerous other mitochondrial-specific dyes (e.g. $\Delta\Psi_m$-sensitive JC-1 and TMRM) also suffer from several of the same caveats in interpretation. For example, both JC-1 and TMRM can respond to changes in the plasma membrane potential, although fluorescence changes caused by mitochondrial versus plasma membrane depolarizations appear differently (Nicholls and Ward, 2000). Similar plasma membrane potential contributions cannot be ruled out with MitoTracker fluorescence. TMRM, being a rhodamine-based dye, is capable of quenching, in a similar fashion to the MitoTrackers, and may be sensitive to photo-oxidation (Nicholls and Ward, 2000). JC-1, however, is a dual emission dye that exhibits fluorescent monomers and aggregates. Although quenching per se may not occur, JC-1 aggregates localized specifically in mitochondria can disband during depolarization and cause a transient increase in monomer signal. It is also interesting to note that using JC-1, Chinopoulos et al. (1999) have reported a slight mitochondrial depolarization resulting from H_2O_2 treatment. However, Scanlon and Reynolds (1998) noted that H_2O_2 alters JC-1 fluorescence in a manner distinct from other known depolarizing agents. Typical depolarizing agents, such as FCCP, lead to increases in JC-1 monomer signal, whereas H_2O_2 leads to a decrease in the aggregate signal. Thus, although it seems that most mitochondrial dyes must be used with caution, a direct relationship between $\Delta\Psi_m$ and fluorescence intensity has been demonstrated with JC-1 and TMRM (Ward et al., 2000). This direct relationship does not appear to be as clear with the MitoTracker dyes.

There are clearly some potential limitations to the present studies. The resolution obtainable with wide-field microscopy precludes the ready assessment of the fluorescence signal at the single mitochondrion level, so that relocalization of dye is difficult to quantitatively measure. Indeed, it is even difficult to conclusively establish that the punctate staining that has been observed is associated with mitochondria, because any correlative co-staining approach would also require assumptions about the localization of the co-stain. The impact of permeability transition on the localization of the dyes was not monitored because of the lack of an unequivocal method for inducing robust and measurable transition in intact neurons or astrocytes. Nevertheless, the characterization provided by this study will help to establish suitable methods for the use of these dyes, and suggests caution when using the MitoTrackers for even a semi-quantitative determination of $\Delta\Psi_m$.

Acknowledgements

The authors gratefully acknowledge Teresa Hastings for her collaboration with the respiration experiments. This work was supported by USAMRMC grant DAMD-17-98-1-8627 (IJR), the Scaife Family Foundation (IJR) and an NIH grant T32NS07391 (JFB).

References

Andreyev A, Fiskum G. Calcium induced release of mitochondrial cytochrome c by different mechanisms selective for brain versus liver. Cell Death Differ 1999;6:825–32.

Andreyev AY, Fahy B, Fiskum G. Cytochrome c release from brain mitochondria is independent of the mitochondrial permeability transition. FEBS Lett 1998;439:373–6.

Bossy-Wetzel E, Newmeyer DD, Green DR. Mitochondrial cytochrome c release in apoptosis occurs upstream of DEVD-specific caspase activation and independently of mitochondrial transmembrane depolarization. EMBO J 1998;17:37–49.

Bowser DN, Minamikawa T, Nagley P, Williams DA. Role of mitochondria in calcium regulation of spontaneously contracting cardiac muscle cells. Biophys J 1998;75:2004–14.

Bradford MM. A rapid and sensitive method for the quantitation of microgram quantities of protein utilizing the principle of protein-dye binding. Anal Biochem 1976;72:248–54.

Chen LB, Smiley ST. Probing mitochondrial membrane potential in living cells by a J-aggregate-forming dye. In: Fluorescent and Luminescent Probes for Biological Activity. London: Academic Press, 1993:124–31.

Chinopoulos C, Tretter L, Adam-Vizi V. Depolarization of in situ mitochondria due to hydrogen peroxide-induced oxidative stress in nerve terminals: inhibition of alpha-ketoglutarate dehydrogenase. J Neurochem 1999;73:220–8.

Ferlini C, Scambia G, Fattorossi A. Is chloromethyl-X-rosamine useful in measuring mitochondrial transmembrane potential? Cytometry 1998;31:74–5.

Finucane DM, Bossy-Wetzel E, Waterhouse NJ, Cotter TG, Green DR. Bax-induced caspase activation and apoptosis via cytochrome c release from mitochondria is inhibitable by Bcl-xL. J Biol Chem 1999;274:2225–33.

Funk RH, Nagel F, Wonka F, Krinke HE, Golfert F, Hofer A. Effects of heat shock on the functional morphology of cell organelles observed by video-enhanced microscopy. Anat Rec 1999;255:458–64.

Gilmore K, Wilson M. The use of chloromethyl-X-rosamine (Mitotracker red) to measure loss of mitochondrial membrane potential in apoptotic cells is incompatible with cell fixation. Cytometry 1999;36:355–8.

Haugland RP. Handbook of Fluorescent Probes and Research Chemicals. Eugene, OR: Molec. Probes, 1996.

Karbowski M, Kurono C, Wozniak M, Ostrowski M, Teranishi M, Soji T, Wakabayashi T. Cycloheximide and 4-OH-TEMPO suppress chloramphenicol-induced apoptosis in RL-34 cells via the suppression of the formation of megamitochondria. Biochim Biophys Acta 1999;1449:25–40.

Keij JF, Bell-Prince C, Steinkamp JA. Staining of mitochondrial membranes with 10-nonyl acridine orange, MitoFluor Green, and MitoTracker Green is affected by mitochondrial membrane potential altering drugs. Cytometry 2000;39:203–10.

Krohn AJ, Wahlbrink T, Prehn JH. Mitochondrial depolarization is not required for neuronal apoptosis. J Neurosci 1999;19:7394–404.

Li N, Oberley TD, Oberley LW, Zhong W. Inhibition of cell growth in NIH/3T3 fibroblasts by overexpression of manganese superoxide dismutase: mechanistic studies. J Cell Physiol 1998;175:359–69.

Macho A, Decaudin D, Castedo M, Hirsch T, Susin SA, Zamzami N, Kroemer G. Chloromethyl-X-Rosamine is an aldehyde-fixable potential-sensitive fluorochrome for the detection of early apoptosis. Cytometry 1996;25:333–40.

Matylevitch NP, Schuschereba ST, Mata JR, Gilligan GR, Lawlor DF, Goodwin CW, Bowman PD. Apoptosis and accidental cell death in cultured human keratinocytes after thermal injury. Am J Pathol 1998;153:567–77.

McCarthy KD, de Vellis J. Preparation of separate astroglial and oligodendroglial cell cultures from rat cerebral tissue. J Cell Biol 1980;85:890–902.

Minamikawa T, Williams DA, Bowser DN, Nagley P. Mitochondrial permeability transition and swelling can occur reversibly without inducing cell death in intact human cells. Exp Cell Res 1999;246:26–37.

Monteith GR, Blaustein MP. Heterogeneity of mitochondrial matrix free Ca2+: resolution of Ca2+ dynamics in individual mitochondria in situ. Am J Physiol 1999;276:C1193–204.

Nicholls DG, Ward MW. Mitochondrial membrane potential and neuronal glutamate excitotoxicity: mortality and millivolts. Trends Neurosci 2000;23:166–74.

Poot M, Pierce RC. Detection of apoptosis and changes in mitochondrial membrane potential with chloromethyl-X-rosamine. Cytometry 1999a;36:359–60.

Poot M, Pierce RH. Detection of changes in mitochondrial function during apoptosis by simultaneous staining with multiple fluorescent dyes and correlated multiparameter flow cytometry. Cytometry 1999b;35:311–7.

Poot M, Zhang YZ, Kramer JA, Wells KS, Jones LJ, Hanzel DK, Lugade AG, Singer VL, Haugland RP. Analysis of mitochondrial morphology and function with novel fixable fluorescent stains. J Histochem Cytochem 1996;44:1363–72.

Rosenthal RE, Hamud F, Fiskum G, Varghese PJ, Sharpe S. Cerebral ischemia and reperfusion: prevention of brain mitochondrial injury by lidoflazine. J Cereb Blood Flow Metab 1987;7:752–8.

Scanlon JM, Reynolds IJ. Effects of oxidants and glutamate receptor activation on mitochondrial membrane potential in rat forebrain neurons. J Neurochem 1998;71:2392–400.

Scorrano L, Petronilli V, Colonna R, Di Lisa F, Bernardi P. Chloromethyltetramethylrosamine (Mitotracker Orange) induces the mitochondrial permeability transition and inhibits respiratory complex I. Implications for the mechanism of cytochrome c release. J Biol Chem 1999;274:24657–63.

Ward MW, Rego AC, Frenguelli BG, Nicholls DG. Mitochondrial membrane potential and glutamate excitotoxicity in cultured cerebellar granule cells. J Neurosci 2000;20:7208–19.

White RJ, Reynolds IJ. Mitochondria and Na+/Ca2+ exchange buffer glutamate-induced calcium loads in cultured cortical neurons. J Neurosci 1995;15:1318–28.

White RJ, Reynolds IJ. Mitochondrial depolarization in glutamate-stimulated neurons: an early signal specific to excitotoxin exposure. J Neurosci 1996;16:5688–97.

Zoratti M, Szabo I. The mitochondrial permeability transition. Biochim Biophys Acta 1995;1241:139–76.

Quantitative evaluation of mitochondrial calcium content in rat cortical neurones following a glutamate stimulus

Jacques B. Brocard, Michel Tassetto* and Ian J. Reynolds

*Department of Pharmacology, University of Pittsburgh, School of Medicine, Pittsburgh, PA 15261, USA and *Ecole Normale Supérieure, Département de Neurobiologie, 46 rue d'Ulm, 75005 Paris, France*

(Received 29 June 2000; accepted after revision 12 November 2000)

1. Recent observations showed that a mitochondrial Ca^{2+} increase is necessary for an NMDA receptor stimulus to be toxic to cortical neurones. In an attempt to determine the magnitude of the Ca^{2+} fluxes involved in this phenomenon, we used carbonylcyanide-*p*-(trifluoromethoxy)-phenylhydrazone (FCCP), a mitochondrial proton gradient uncoupler, to release mitochondrial free calcium ($[Ca^{2+}]_m$) during and following a glutamate stimulus, and magfura-2 to monitor cytoplasmic free calcium ($[Ca^{2+}]_c$).

2. FCCP treatment of previously unstimulated neurones barely changed $[Ca^{2+}]_c$ whereas when added after a glutamate stimulus it elevated $[Ca^{2+}]_c$ to a much greater extent than did exposure to glutamate, suggesting a very large accumulation of Ca^{2+} in the mitochondria.

3. Mitochondrial Ca^{2+} uptake was dependent on glutamate concentration, whereas the changes in the overall quantity of Ca^{2+} entering the cell, obtained by simultaneously treating neurones with glutamate and FCCP, showed a response that was essentially all-or-none.

4. Mitochondrial Ca^{2+} uptake was also dependent on the nature and duration of a given stimulus as shown by comparing $[Ca^{2+}]_m$ associated with depolarization and treatment with kainate, NMDA or glutamate. Large mitochondrial Ca^{2+} accumulation only occurred after a glutamate or NMDA stimulus.

5. These studies provide a method of estimating the accumulation of Ca^{2+} in the mitochondria of neurones, and suggest that millimolar concentrations of Ca^{2+} may be reached following intense glutamate stimulation. It was shown that substantially more Ca^{2+} enters neurones following glutamate receptor activation than is reflected by $[Ca^{2+}]_c$ increases.

Glutamate is the predominant excitatory neurotransmitter in mammalian brain (Headley & Grillner, 1990). However, an excess of glutamate can be toxic to various populations of neuronal cells (Rothman & Olney, 1986; Choi *et al.* 1987; Manev *et al.* 1989). Delayed glutamatergic excitotoxicity has been identified as a consequence of NMDA receptor activation which requires an intracellular calcium ($[Ca^{2+}]_i$) increase (Choi, 1987; Randall & Thayer, 1992; Hartley *et al.* 1993). Although mitochondria are known to accumulate Ca^{2+} following cytosolic free calcium ($[Ca^{2+}]_c$) increases in neurones (Nicholls & Åkerman, 1982; White & Reynolds, 1995), it was thought for a long time that this process was not involved in cell death but in preventing toxicity associated with elevated $[Ca^{2+}]_i$. However, recent studies showed that when mitochondrial Ca^{2+} uptake is prevented during glutamate stimulation, neuronal cells survive toxic doses (Dessi *et al.* 1995; Budd & Nicholls, 1996*b*; Stout *et al.* 1998).

Ca^{2+} entry in mitochondria may be linked to cell death in many ways. These include changes in the polarization state of the mitochondria which jeopardize the energy balance maintained by the metabolic functions of the mitochondria and also lead to the production of reactive oxygen species (for reviews see Duchen, 1999; Nicholls & Budd, 2000). Several studies have monitored alterations in mitochondrial free calcium ($[Ca^{2+}]_m$) using fluorescent indicators such as rhod-2 (Peng & Greenamyre, 1998; Peng *et al.* 1998). However, rhod-2 has a relatively high affinity for Ca^{2+} and it is not clear that it can accurately report $[Ca^{2+}]_m$ under conditions involving large fluxes of Ca^{2+} which may lead to the saturation of the dye.

We used the protonophore carbonylcyanide-*p*-(trifluoromethoxy)phenylhydrazone (FCCP) to release mitochondrial Ca^{2+} into the cytoplasm (Duchen, 1990; Thayer & Miller, 1990; Kiedrowski & Costa, 1995), where it is measured with the low affinity Ca^{2+}-sensitive fluorescent dye magfura-2 (Raju *et al.* 1989; Stout & Reynolds, 1999). We were able to demonstrate that mitochondrial Ca^{2+} accumulation is large compared to that seen in the cytoplasm during a given stimulus and to establish the

kinetics of Ca^{2+} fluxes during and after different stimuli.

METHODS

Cell culture

Pregnant Sprague-Dawley female rats were anaesthetized with diethyl ether inhalation until complete loss of responsiveness to tail and foot pinch was achieved. Embryonic day 17 fetuses were released from the uterus and decapitated. The mothers were then humanely killed without being allowed to regain consciousness. The forebrains were then removed from the fetuses and dissected as follows. The lobes were incubated in 0.005–0.01% trypsin in 2 ml of Ca^{2+}, Mg^{2+}-free medium (mM: 115 NaCl, 5.4 KCl, 26.2 $NaHCO_3$, 9.9 NaH_2PO_4, 5.5 glucose; 0.001% phenol red, and minimum essential medium amino acids; pH was adjusted to 7.4 with NaOH) for 30 min at 37 °C. The tissue was triturated an average of 12 times before the volume was brought to 10 ml and viability determinations were made with trypan blue (0.08%) exclusion. The plating suspension was diluted to 450 000 cells ml^{-1} using plating medium (v/v solution of 90% Dulbecco's modified Eagle's medium, 10% heat-inactivated fetal bovine serum, 24 u ml^{-1} penicillin, 24 μg ml^{-1} streptomycin; final glutamine concentration, 3.9 mM). Cells were plated onto poly-D-lysine-coated (M_r = 120 400; 40 mg ml^{-1}) 31 mm glass coverslips that were inverted 1 day later into maintenance medium (horse serum substituted for fetal bovine serum, all other constituents identical). Neurones were used after 13–16 days in culture, with no further medium changes. These culture conditions provide the sparse, glia-poor neuronal cultures that are optimal for fluorescence microscopy measurements. Each experiment described was performed on 8–25 neurones per coverslip and 5–15 coverslips from two or more different culture dates. All procedures using animals were in accordance with the National Institutes of Health Guide for the Care and Use of Laboratory Animals and were approved by the University of Pittsburgh's Institutional Animal Care and Use Committee.

Solutions and drugs

For perfusion of coverslips in the fluorescence microscopy experiments, we used a Hepes-buffered salt solution (HBSS, adjusted to pH 7.4 with NaOH) of the following composition (mM): NaCl 137, KCl 5, $NaHCO_3$ 10, Hepes 20, glucose 5.5, KH_2PO_4 0.6, Na_2HPO_4 0.6, $CaCl_2$ 1.4 and $MgSO_4$ 0.9. Ca^{2+} was omitted in the Ca^{2+}-free HBSS buffer; high KCl buffer contained 50 mM KCl and 92 mM NaCl. The drugs used in the present experiments were purchased from Sigma (USA) and prepared from the following stock solutions: 1–100 μM glutamate from 10 mM in water, 1 μM glycine from 10 mM in water, 750 nM FCCP from 750 μM in methanol, 100 μM kainate from 10 mM in water and 300 μM *N*-methyl-D-aspartic acid (NMDA) from 10 mM in water. One micromolar glycine was always added to the glutamate- and NMDA-containing solutions. For treatments with FCCP alone, the drug was diluted in Ca^{2+}-free buffer to avoid external Ca^{2+} entry in the cells.

$[Ca^{2+}]_c$ measurements

A 1 mM stock solution for the acetoxymethyl ester form of magfura-2 (magfura-2 AM; Molecular Probes) was prepared in anhydrous DMSO. Coverslips were incubated in HBSS containing 5 μM of magfura-2, 0.5% DMSO and 5 mg ml^{-1} bovine serum albumin for 10–15 min at 37 °C. Cells were then rinsed with HBSS, mounted on a record chamber and perfused with HBSS at a rate of 20 ml min^{-1}. All recordings were made at room temperature (20–25 °C). The imaging system used in this study consisted of a Nikon Diaphot 300 inverted microscope fitted with a × 40 objective, a digital camera (Hamamatsu Corporation, NJ, USA) and a 75 W xenon lamp-based monochromator light source (Applied Scientific Instrumentation Inc., OR, USA) as specified (Stout *et al.* 1998). Cells were alternately illuminated with 335 nm and 375 nm wavelengths. Incident light was attenuated with neutral density filters (ND 0.5 and 0.3 for 16% transmittance; Omega Optical, VT, USA) and emitted fluorescence passed through a 515 nm dichroic mirror and a 535 nm/525 nm band pass filter (Omega Optical). Background fluorescence, determined from three cell-free regions of the coverslips, was subtracted from all the signals prior to calculating the ratios. The baseline ratio corresponded to the last ratio before the first stimulus (usually glutamate; see the arrows in Fig. 1*A–D*). The areas under curve (AUCs) were calculated from baseline-subtracted magfura-2 ratios during the first 5 min of a given stimulus as described (see Fig. 1*F* and *G*).

Statistics

Student's unpaired *t* test and one-way analysis of variance (ANOVA) coupled with Bonferroni's multicomparison *post hoc* test were performed using Prism 3.0 software (GraphPad Software Inc., San Diego, CA, USA).

RESULTS

Ca^{2+} uptake and Ca^{2+} release in neuronal cells

We have previously shown that the Ca^{2+} that enters cells during glutamate application is largely due to NMDA receptor activation, and that a substantial fraction of the Ca^{2+} load is buffered by mitochondria (White & Reynolds, 1997). In this study, we used the low affinity Ca^{2+} indicator magfura-2 to estimate $[Ca^{2+}]_c$ (Raju *et al.* 1989; Stout & Reynolds, 1999). We ruled out the possibility that magfura-2 was measuring large cytoplasmic $[Mg^{2+}]$ changes, because Calcium Green-5N, a low affinity Ca^{2+} dye that is insensitive to Mg^{2+} (Rajdev & Reynolds, 1993) produced qualitatively similar results in the protocol described below (J. B. Brocard & I. J. Reynolds, unpublished observations). Magfura-2 is almost exclusively found in the cytoplasm of neurones under the loading conditions used here because all of the dye could be released (as indicated by a decrease of cell-associated fluorescence) by a low concentration of digitonin ($\leqslant$ 5 μM) that selectively removed the plasma membrane (Ishijima *et al.* 1991). Magfura-2 loaded into the cells could be quenched by the addition of Mn^{2+}, in a depolarizing solution to the outside of the cell; dye released from neurones by 5 μM digitonin displayed a peak excitation wavelength of 340 nm when incubated with saturating Ca^{2+} concentrations and could also be completely quenched by Mn^{2+}, which does not bind to the uncleaved magfura-2 AM (Brocard *et al.* 1993). To evaluate $[Ca^{2+}]_m$ following glutamate stimulation we used the protonophore FCCP, which rapidly and reversibly causes the mitochondrial membrane potential to collapse. This results in the release of Ca^{2+} from the mitochondria, probably by the reversed operation of the Ca^{2+} uniporter (Budd & Nicholls, 1996*a*). Thus, assessing $[Ca^{2+}]_c$ during an FCCP application in the absence of Ca^{2+} in the external buffer corresponds to measuring $[Ca^{2+}]_m$.

Concentration-dependent increase of $[Ca^{2+}]_m$

Representative curves of magfura-2 ratios (background subtracted) obtained for 1, 3, 10 and 30 μM glutamate are shown in Fig. 1*A–D*. The arrows indicate the ratio taken as the baseline for further studies. They show a

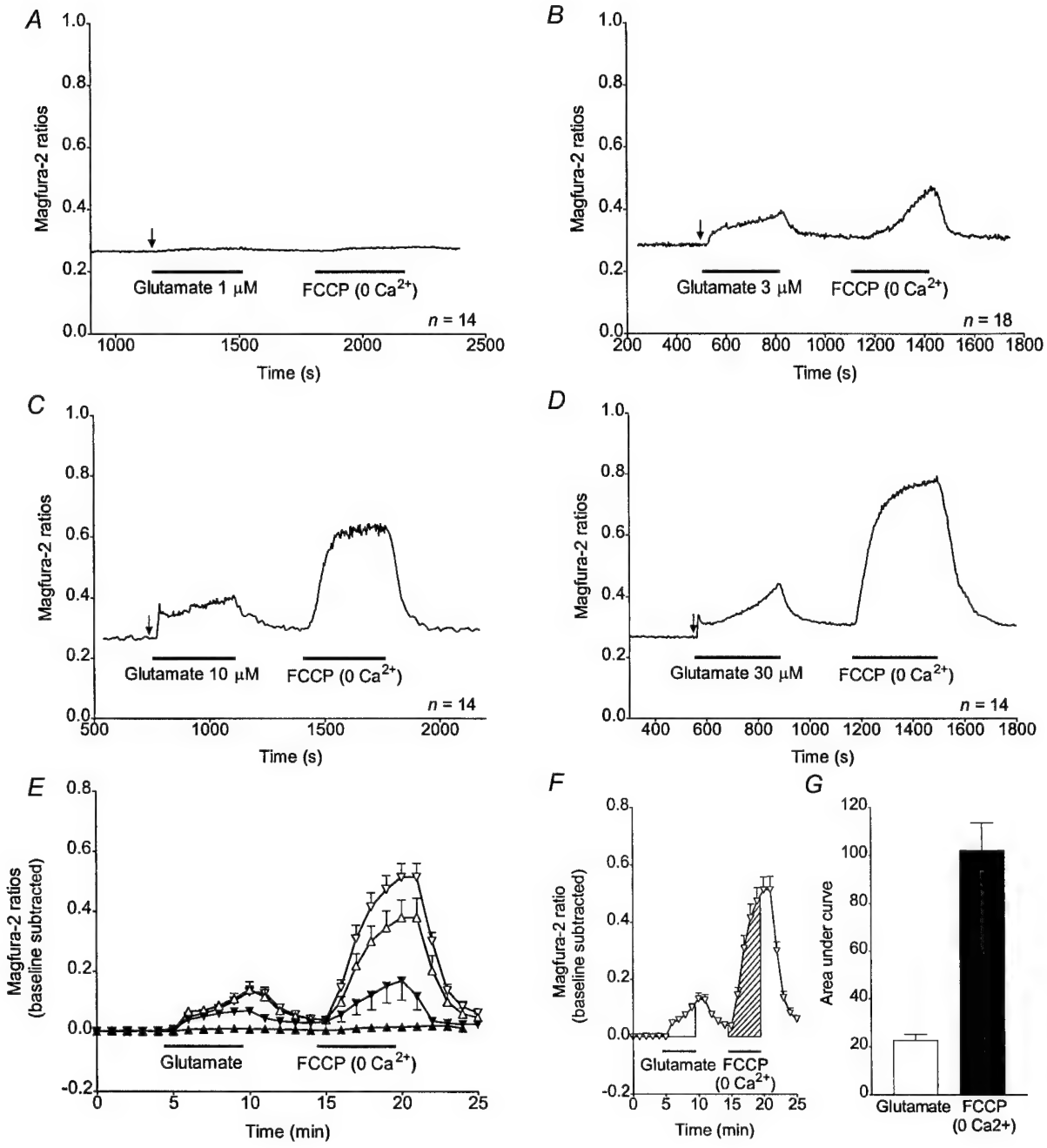

Figure 1. Evaluation of $[Ca^{2+}]_c$ and mitochondrial Ca^{2+} accumulation during and following a glutamate stimulus

A–D, representative traces obtained from *n* neurones treated with 1 (*A*), 3 (*B*), 10 (*C*) or 30 μM (*D*) glutamate and with FCCP as indicated. The arrows point to the ratio taken as the baseline. The FCCP applications were performed in the absence of Ca^{2+} in the buffer. *E*, means ± S.E.M. of the magfura-2 ratios (baseline subtracted) obtained from *n* coverslips for each glutamate treatment: 1 μM glutamate (▲; $n = 5$), 3 μM glutamate (▼; $n = 10$), 10 μM glutamate (△; $n = 10$), 30 μM glutamate (▽; $n = 15$). *F*, mean ± S.E.M. of the magfura-2 ratios (baseline subtracted) obtained from 15 coverslips with 30 μM glutamate (▽; $n = 15$) and areas under the curve (AUCs) used as a measure of the $[Ca^{2+}]_i$ changes after the glutamate stimulation (open area) and the FCCP application (hatched area). *G*, means ± S.E.M. for AUCs as described in *F*, for the 30 μM glutamate stimulus (□) and the FCCP treatment (■).

concentration-dependent increase of $[Ca^{2+}]_i$ with both glutamate and FCCP. These curves represent the means from 8–25 neurones on a single coverslip, and the mean response is considered to be a single experiment. The mean magfura-2 ratios obtained from 5–15 experiments with each concentration of glutamate were baseline subtracted and plotted in Fig. 1*E*. Due to the variability in the characteristics of the Ca^{2+} responses in single cells (as exemplified in Fig. 2*A* and *B*), we calculated the area under the curve (AUC), defined as the sum of the baseline-subtracted ratios for the duration of the treatment (Fig. 1*F*), as a measure of the overall $[Ca^{2+}]_i$ changes occurring during a specific treatment (Fig. 1*G*). Mean AUCs ± S.E.M. for glutamate-induced and FCCP-induced Ca^{2+} responses are shown in Fig. 3*A*. At all concentrations, the FCCP-induced Ca^{2+} release is greater than that observed during the glutamate treatment. Thus, most of the Ca^{2+} entering the neurones is not measured by the fluorescent dye during the glutamate treatment (Thayer & Miller, 1990). The ratio of the FCCP-induced to the glutamate-induced $[Ca^{2+}]_c$ changes (F/G ratio) is also concentration dependent and increases with the concentration of glutamate used during the stimulus (Fig. 3*B*). However, the increase in the rate of Ca^{2+} uptake seems to reach a maximum at high concentrations of glutamate. Taken together, these data indicate that the higher the glutamate concentration, the more Ca^{2+} is taken up by the mitochondria until the limit of their capacity is reached.

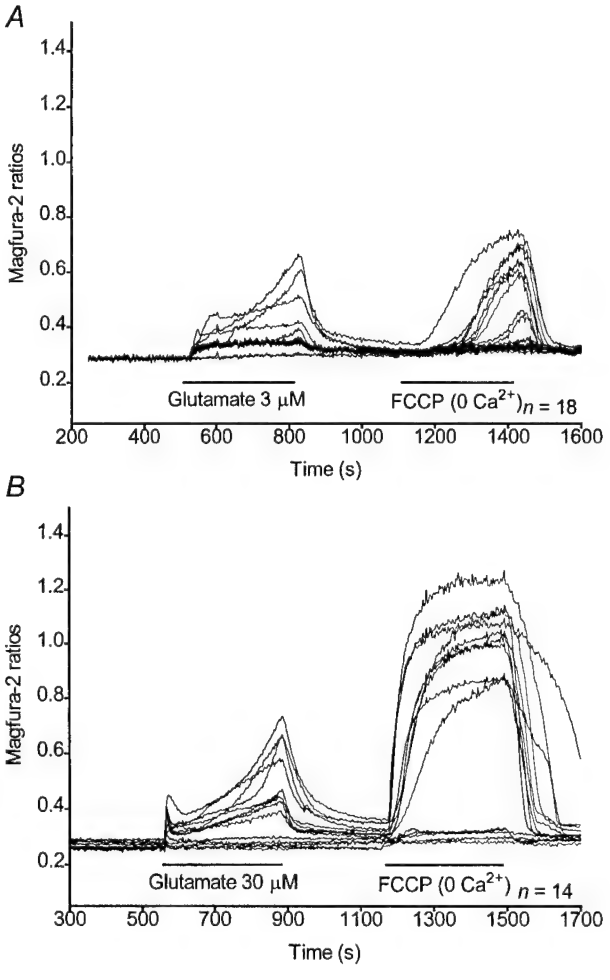

Figure 2. Variability in single-cell responses during and following a glutamate stimulus

Traces for single cells treated with 3 μM (*A*) or 30 μM (*B*) glutamate corresponding to Fig. 1*B* and *D*, respectively.

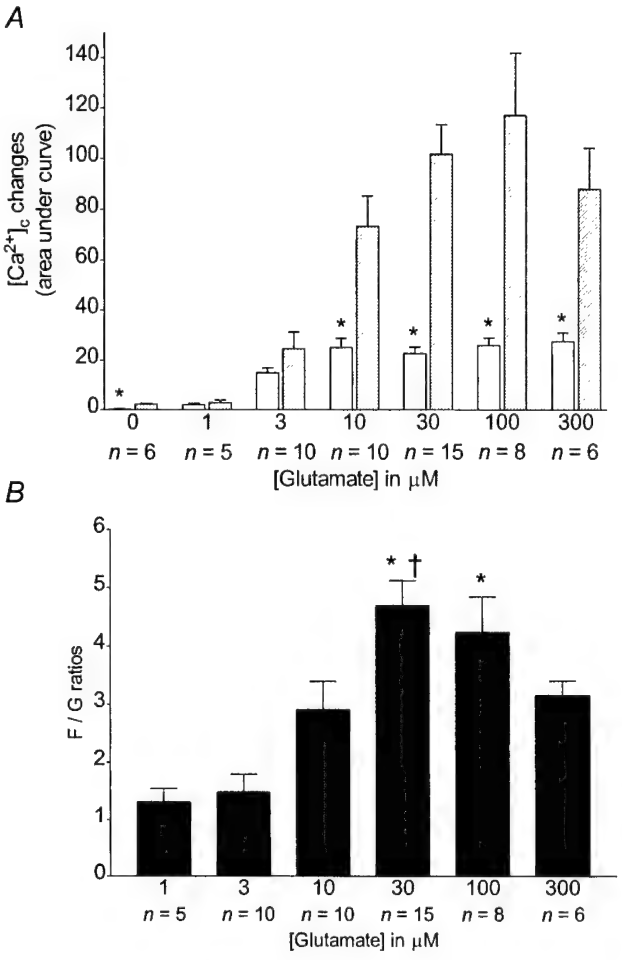

Figure 3. Dose-dependent increase of $[Ca^{2+}]_c$ and $[Ca^{2+}]_m$ during and following a glutamate stimulus

A, *n* coverslips were treated as indicated in Fig. 1 and means ± S.E.M. for AUCs after the glutamate (open bars) and FCCP treatments (hatched bars) were plotted. * Significant differences from the corresponding FCCP treatment, Student's unpaired *t* test; $P < 0.05$. *B*, means ± S.E.M. of normalized ratios of FCCP-induced to glutamate-induced $[Ca^{2+}]_c$ changes. * Significant difference from the 1 μM and 3 μM glutamate treatments, ANOVA followed by Bonferroni's test; $P < 0.05$. † Significant differences from the 10 μM glutamate treatment, ANOVA followed by Bonferroni's test; $P < 0.05$.

Overall cellular Ca^{2+} uptake during a glutamate stimulus

By inactivating the predominant Ca^{2+} buffering mechanism with FCCP during glutamate stimulations, it is possible to evaluate the overall quantity of Ca^{2+} being taken up by the neurones (Stout *et al.* 1998). Representative curves of magfura-2 ratios (background subtracted) obtained for glutamate (0, 1, 3, 30 and 300 μM) + FCCP are shown in Fig. 4*A*–*E*. AUCs obtained for those treatments are shown in Fig. 4*F*. Although the concentration at which glutamate started to produce a sizeable response was similar in the absence or presence of FCCP, there appeared to be an all-or-none characteristic

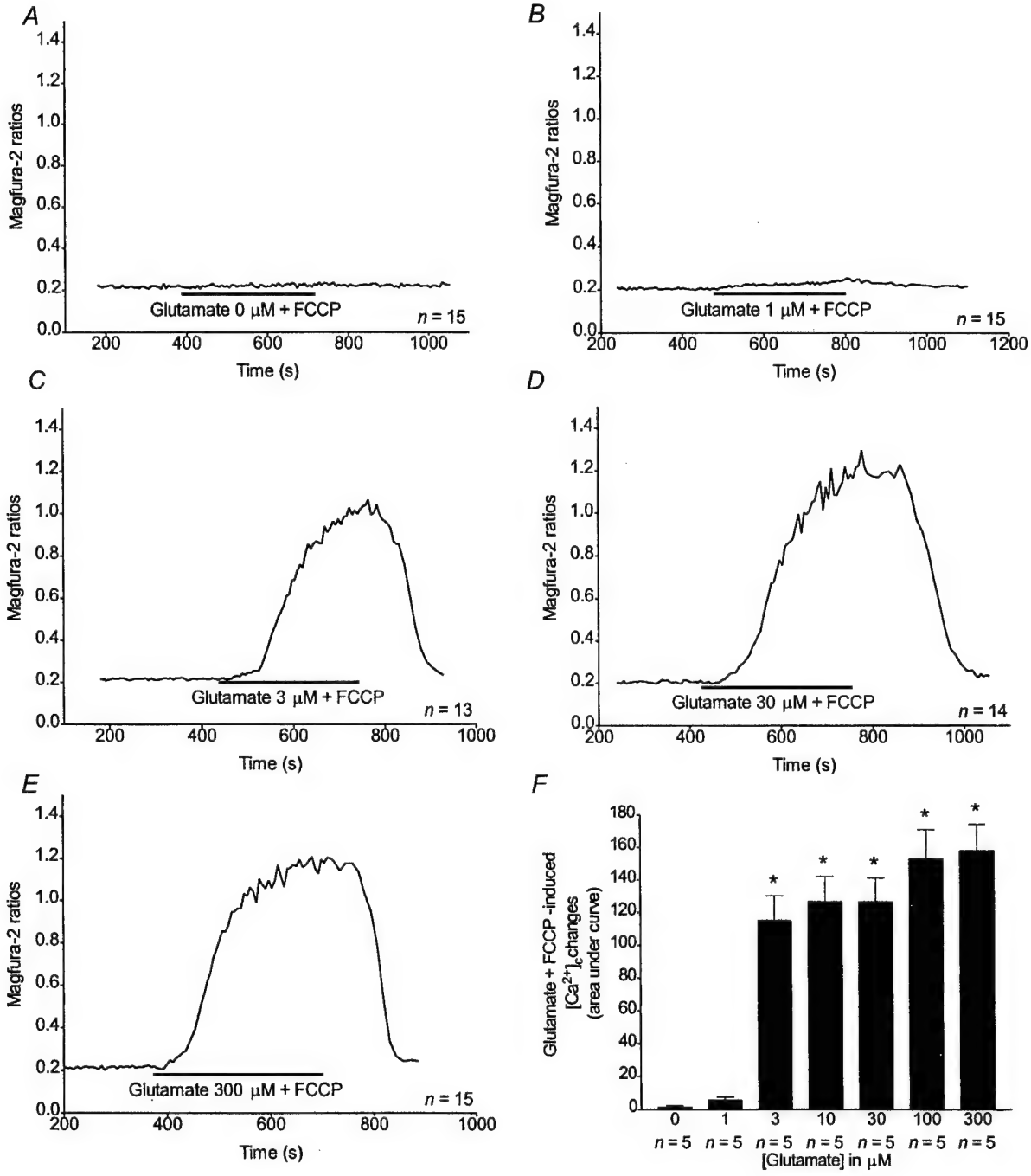

Figure 4. Evaluation of $[Ca^{2+}]_c$ and $[Ca^{2+}]_m$ during a simultaneous glutamate + FCCP stimulus

A–*E*, representative traces obtained from n neurones treated with 0 (*A*), 1 (*B*), 3 (*C*), 30 (*D*) or 300 μM glutamate (*E*) + FCCP as indicated. *F*, n coverslips were treated as indicated above and means ± S.E.M. for AUCs after the glutamate + FCCP treatments were plotted. * Significant differences from 0 and 1 μM glutamate treatments, ANOVA followed by Bonferroni's test; $P < 0.05$.

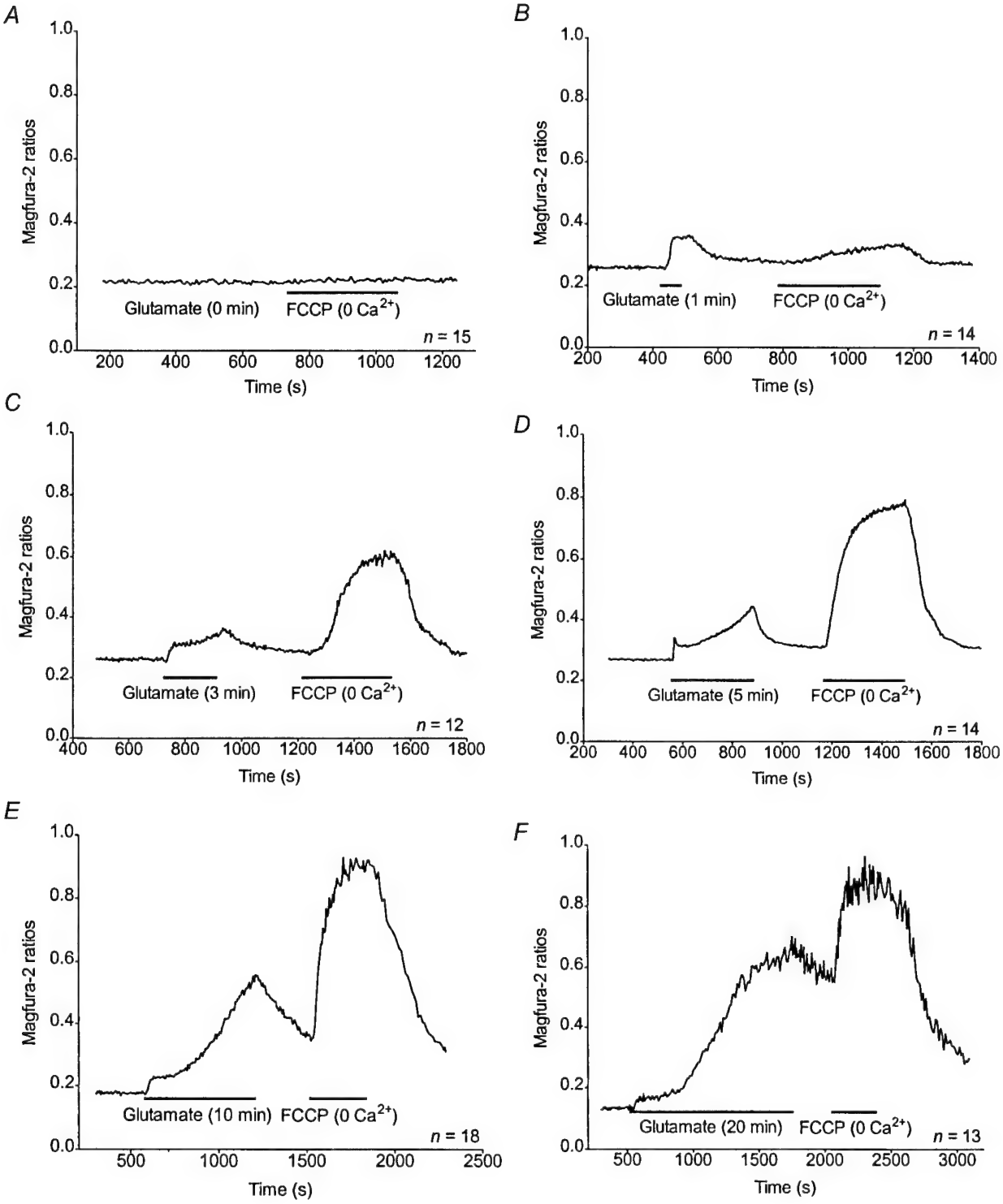

Figure 5. Evaluation of $[Ca^{2+}]_c$ and mitochondrial Ca^{2+} accumulation during and following a glutamate stimulus

A–F, representative traces obtained from *n* neurones treated with 30 μM glutamate for 0 (*A*), 1 (*B*), 3 (*C*), 5 (*D*), 10 (*E*) or 20 min (*F*) and FCCP as indicated. The FCCP applications were performed in the absence of Ca^{2+} in the buffer. Neurones treated for 0 min were subjected to the same experimental procedure but not to the glutamate stimulus.

to the concentration–response relationship for glutamate in the presence of FCCP. However, at most concentrations, the AUCs shown in Fig. 4*F* appear to reflect the sum of the glutamate-induced transient and the subsequent FCCP-induced release (with the notable exception of the measurements made with 3 μM glutamate) suggesting that this approach does provide a reasonable estimate of the total Ca^{2+} load during glutamate exposure.

Duration-dependent increase of $[Ca^{2+}]_m$ after a glutamate stimulus

We next sought to determine the time dependence of the mitochondrial Ca^{2+} accumulation in the neurones. Representative curves of magfura-2 ratios (background subtracted) obtained for 0, 1, 3, 5, 10 and 20 min of 30 μM glutamate stimulation are shown in Fig. 5*A–F*. AUCs obtained for the FCCP treatment correspond to significantly bigger $[Ca^{2+}]_i$ changes than that measured in the cytoplasm during any glutamate stimulus shorter than 10 min (Fig. 6*A*). However, after 20 min of 30 μM glutamate activation, the AUC obtained after the FCCP treatment is significantly smaller than the $[Ca^{2+}]_i$ change measured during the stimulus (Fig. 6*A*). Thus, the F/G ratio is stable for 1–5 min of glutamate treatment, then drops for 10 and 20 min to a value significantly smaller than that observed for 1, 3 or 5 min (Fig. 6*B*).

Recovery-dependent decrease of $[Ca^{2+}]_m$

We also estimated the rate of Ca^{2+} extrusion from the mitochondria by varying the duration of the washout following a 30 μM glutamate stimulus. Representative curves of magfura-2 ratios (background subtracted) obtained for 0, 5, 10 and 20 min after exposure to glutamate when the cells were washed in the absence of external Ca^{2+} are shown in Fig. 7*A–D*. As a comparison, the response obtained when using FCCP in previously unstimulated cells is shown in Fig. 7*E*. AUCs obtained for the FCCP treatment 0–5 min after glutamate correspond to higher $[Ca^{2+}]_m$ than 10 or 20 min after the stimulus or in previously unstimulated cells (Fig. 7*F*). The absence of Ca^{2+} in the medium during glutamate washout did not significantly alter Ca^{2+} extrusion from the neurones. However, after a $[Ca^{2+}]_m$ decrease of threefold within the first 10 min of Ca^{2+}-free buffer washout, it stays stable over the next 10 min period. Thus, $[Ca^{2+}]_m$ is still higher after 20 min of washout compared to previously unstimulated cells (Fig. 7*F*).

Stimulus-dependent increase of $[Ca^{2+}]_m$

Previous studies have suggested that the magnitude of $[Ca^{2+}]_m$ increase depends on the route of Ca^{2+} entry *per se* (Sattler *et al.* 1998), whereas others showed that only NMDA receptor activation would lead to large $[Ca^{2+}]_c$ followed by high $[Ca^{2+}]_m$ increases (Hyrc *et al.* 1997; Stout & Reynolds, 1999; Keelan *et al.* 1999). Moreover, as magfura-2 is sensitive to physiological $[Mg^{2+}]_i$ (Raju *et al.* 1989), it was important to determine whether there were dye changes in the absence of Ca^{2+} in the buffer. We investigated these principles further by exposing neurones to other stimuli that elevate Ca^{2+} to a varying extent (Stout & Reynolds, 1999). Representative curves of magfura-2 ratios (background subtracted) obtained for 30 μM glutamate in Ca^{2+}-free buffer, high KCl buffer, 100 μM kainate and 300 μM NMDA are shown in Fig. 8. AUCs obtained using glutamate in Ca^{2+}-free buffer, high KCl or kainate correspond to significantly smaller Ca^{2+} fluxes than the $[Ca^{2+}]_c$ change obtained with 30 μM glutamate (Fig. 9*A*). Similarly, Ca^{2+} responses with FCCP following those stimuli are significantly smaller than the response obtained with FCCP after a 30 μM glutamate

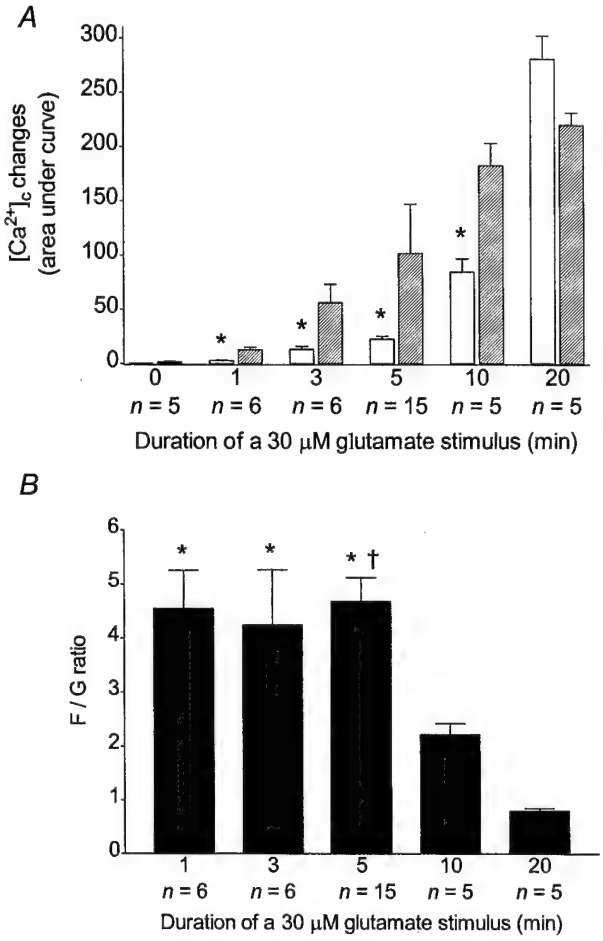

Figure 6. Duration-dependent increase of $[Ca^{2+}]_c$ and $[Ca^{2+}]_m$ during and following a glutamate stimulus

A, *n* coverslips were treated as indicated in Fig. 5 and means ± S.E.M. for AUCs after the glutamate (open bars) and the FCCP treatments (hatched bars) were plotted. * Significant differences from the corresponding FCCP treatment, Student's unpaired *t* tests; $P < 0.05$. *B*, means ± S.E.M of normalized ratios of FCCP-induced to glutamate-induced cytoplasmic Ca^{2+} changes. * Significant differences from the 20 min glutamate treatment, ANOVA followed by Bonferroni's test; $P < 0.05$. † Significant differences from the 10 min glutamate treatment, ANOVA followed by Bonferroni's test; $P < 0.05$.

stimulation (Fig. 9*B*). Interestingly, though, the magnitude of the $[Ca^{2+}]_c$ changes following glutamate stimulation in Ca^{2+}-free buffer and kainate is significantly higher than the $[Ca^{2+}]_c$ change observed in previously unstimulated cells (see Fig. 7*F*, and J. B. Brocard & I. J. Reynolds, unpublished observations).

DISCUSSION

The goal of these experiments was to develop a method of measuring the mitochondrial Ca^{2+} accumulation during and after glutamate stimulation in cortical neurones. The protonophore FCCP was used to release Ca^{2+} from mitochondria, and the Ca^{2+} elevation was detected in the

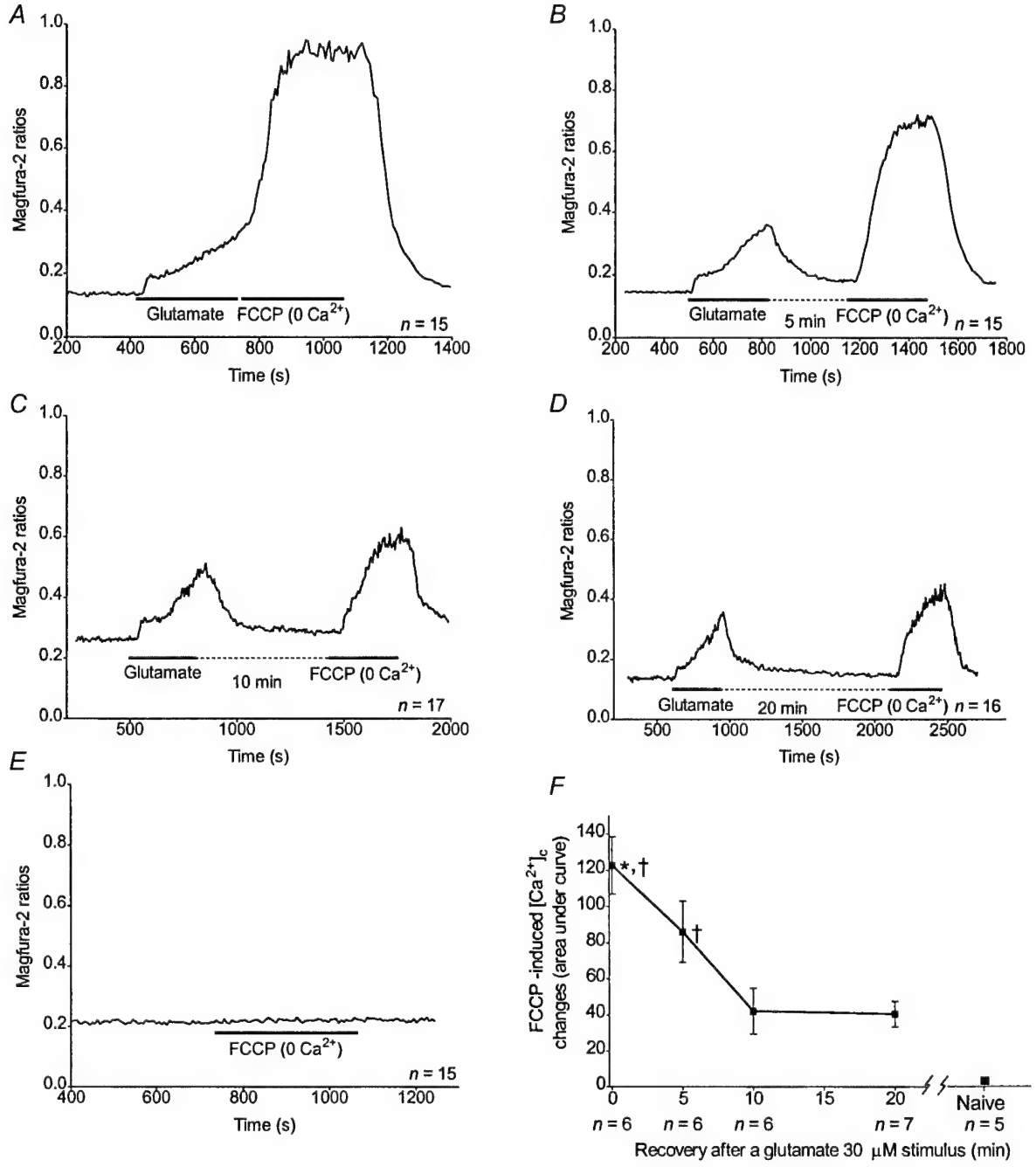

Figure 7. Recovery-dependent decrease of $[Ca^{2+}]_m$ following a glutamate stimulus

A–D, representative traces obtained from *n* neurones treated with 30 μM glutamate, rinsed for 0 (*A*), 5 (*B*), 10 (*C*) or 20 min (*D*) in Ca^{2+}-free buffer and treated with FCCP as indicated. *E*, *n* previously unstimulated cells were treated with FCCP only, as indicated. The FCCP applications were performed in the absence of Ca^{2+} in the buffer. *F*, *n* coverslips were treated as indicated above and means ± S.E.M for AUCs obtained after the glutamate and FCCP treatments were plotted. * Significant differences from 10 and 20 min recovery, ANOVA followed by Bonferroni's test; $P < 0.05$. † Significant differences from previously unstimulated cells, ANOVA followed by Bonferroni's test; $P < 0.05$.

cytoplasm using the low affinity Ca^{2+} indicator magfura-2. Our results demonstrate the value of this approach, as we show that mitochondrial Ca^{2+} accumulation is dependent on the glutamate concentration, the time of exposure to glutamate and the duration of the washout following the glutamate stimulus. The only exception seems to be the Ca^{2+} increases measured during combined FCCP and glutamate applications (Fig. 4). This result may be explained by the inhibition of the NMDA receptor through high $[Ca^{2+}]_c$, thereby underestimating the overall Ca^{2+} entry at high glutamate concentrations (Rosenmund *et al.* 1995). However, the most notable observation is the size of the $[Ca^{2+}]_m$ pool. The Ca^{2+} changes detected by magfura-2 approached the maximal ratios we have obtained with this dye, suggesting that the dye is close to being saturated with Ca^{2+}. Given that the K_d of the dye for Ca^{2+} is ~10–20 μM (Raju *et al.* 1989; Stout & Reynolds, 1999), this suggests that $[Ca^{2+}]_c$ following FCCP-induced release may significantly exceed 100 μM. When one considers that the usual estimate of the fractional volume of the cytoplasm occupied by mitochondria is < 5 % (Scott & Nicholls, 1980) this implies that $[Ca^{2+}]_m$ following exposure to glutamate approaches several millimolar.

This study reveals some interesting characteristics of the relationship between $[Ca^{2+}]_c$ and $[Ca^{2+}]_m$ after NMDA receptor activation. The threshold glutamate concentration for producing $[Ca^{2+}]_m$ increase in this study was approximately 1 μM, and this led to similar small increases in magfura-2 fluorescence during the stimulus and FCCP application. Higher glutamate concentrations produced an elevation in $[Ca^{2+}]_c$ that exceeds the set point with the result that there is a progressive accumulation of Ca^{2+} in the matrix (Nicholls, 1978). There was a clear relationship between the magnitude of the $[Ca^{2+}]_c$ response to glutamate (between 1 and 100 μM) and the subsequent FCCP-induced Ca^{2+} release from the mitochondrial Ca^{2+} stores following a 5 min glutamate exposure. This suggests that the approach provides a reasonable, semi-quantitative estimate of $[Ca^{2+}]_m$ under these conditions. A similar relationship was observed when the time of glutamate exposure was varied between 1 and 5 min, again suggesting that the method can report

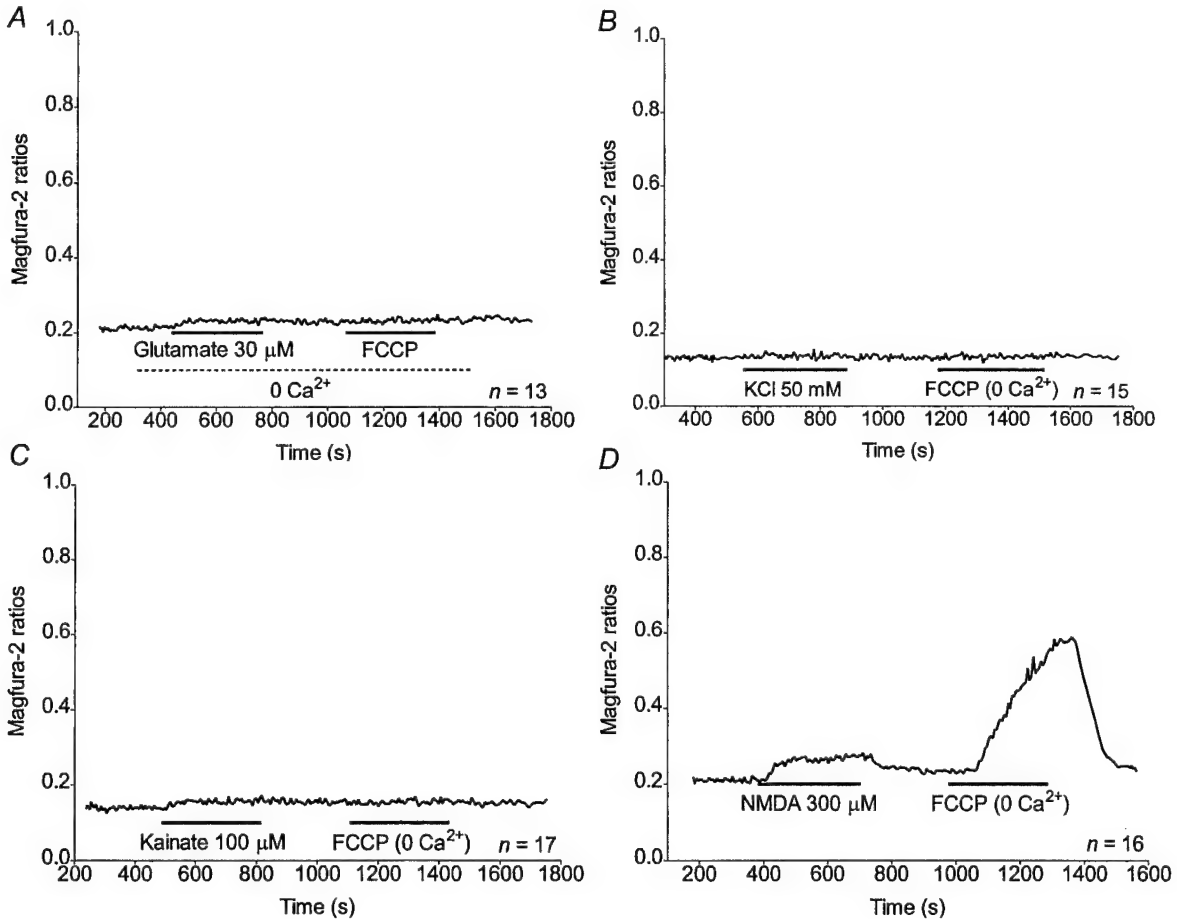

Figure 8. Evaluation of $[Ca^{2+}]_c$ and mitochondrial Ca^{2+} accumulation during and following various stimuli

A–D, representative traces obtained from *n* neurones treated with 30 μM glutamate in Ca^{2+}-free buffer (*A*), 50 mM KCl (*B*), 100 μM kainate (*C*) or 300 μM NMDA (*D*) and FCCP as indicated. The FCCP applications were performed in the absence of Ca^{2+} in the buffer.

mitochondrial Ca^{2+} accumulation under the conditions of these experiments. It is worth noting, though, that the relationship between $[Ca^{2+}]_m$ and $[Ca^{2+}]_c$ is not linear under these circumstances, as revealed by the variation in the F/G ratio obtained with increasing concentrations of glutamate (Fig. 3*B*). This non-linear relationship could be due to the inherent properties of the low-affinity dye magfura-2 itself, as described elsewhere (Hyrc *et al.* 2000), or alternatively it could be a consequence of the activation of the mitochondrial Ca^{2+} uniporter by high $[Ca^{2+}]_c$, as reported previously (Colegrove *et al.* 2000). Furthermore, mitochondrial Ca^{2+} buffering capacity is limited as becomes evident when stimulating cells with concentrations of glutamate greater than 100 μM or for periods of time beyond 5 min. With these more extreme stimulation protocols we observed that the F/G ratio decreased, reflecting a limitation in the accumulation of Ca^{2+} by mitochondria. This could reflect a saturation phenomenon, where the limit of the ability of mitochondria to accumulate Ca^{2+} is reached. Alternatively, the limitation could reflect the dissipation of the gradient that drives Ca^{2+} into the mitochondria ($\Delta\Psi_m$; Zoccarato & Nicholls, 1982), the glutamate-induced Ca^{2+}-dependent decrease of $\Delta\Psi_m$ being a well-characterized property of neuronal mitochondria (Khodorov *et al.* 1996; Schinder *et al.* 1996; White & Reynolds, 1996; Vergun *et al.* 1999). It is also possible that the later failure of Ca^{2+} accumulation and/or release of matrix Ca^{2+} in these long exposures reflects activation of permeability transition (Hunter & Haworth, 1979; Al Nasser & Crompton, 1986). However, recent studies argued against the induction of transition in a similar experiment (Castilho *et al.* 1998; Hüser *et al.* 1998). Interestingly, $[Ca^{2+}]_c$ always stayed high for the whole duration of the FCCP treatment, probably reflecting a continuous release of Ca^{2+} from the mitochondria and/or a slow rate of Ca^{2+} extrusion from the cytoplasm. Given that the subsequent decline in $[Ca^{2+}]_c$ appeared to be the consequence of FCCP removal, this observation suggests that the FCCP treatment was not of sufficient duration to empty the mitochondria of calcium. It is not clear whether this is due to the relatively slow mobilization of intramitochondrial calcium, or whether the efflux pathway is rate limiting in this process.

For smaller concentrations of glutamate (1 μM) and non-NMDA stimulation, the stimulus- and FCCP-induced increases in magfura-2 fluorescence are not necessarily related to mitochondrial Ca^{2+} accumulation. We first confirmed that the initial $[Ca^{2+}]_m$ in previously unstimulated cells is very small by monitoring magfura-2 fluoresence increase during an FCCP application to untreated cells (see Fig. 7*E*). This content was estimated to be $\ll$ 1 μM (J. B. Brocard & I. J. Reynolds, unpublished observations) when using fura-2, a fluorescent dye more sensitive to Ca^{2+} (Grynkiewicz *et al.* 1985; Stout & Reynolds, 1999). The magfura-2 fluorescence increases obtained when using 0 μM glutamate (+1 μM glycine; see Methods) followed by FCCP were identical to those observed in previously unstimulated cells, thus confirming the absence of any intrinsic ability of glycine to activate the NMDA receptor (Johnson & Ascher, 1987).

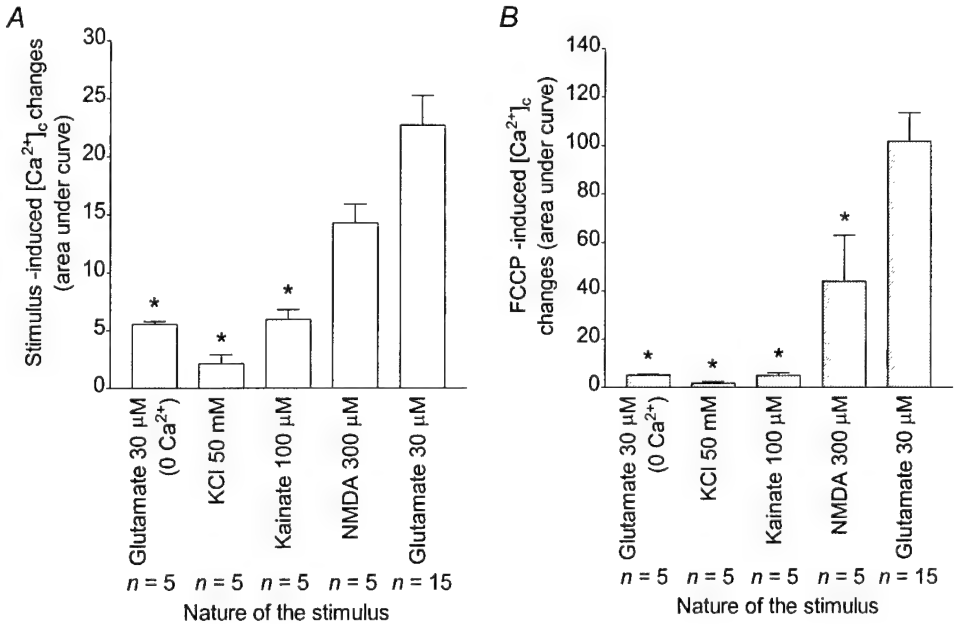

Figure 9. Stimulus-dependent increase of $[Ca^{2+}]_c$ and $[Ca^{2+}]_m$

n coverslips were treated as indicated in Fig. 8 and means ± S.E.M. for AUCs obtained after the stimuli (*A*) and the FCCP (*B*) treatments were plotted. * Significant differences from the 30 μM glutamate treatment, ANOVA followed by Bonferroni's test; $P < 0.05$.

The use of 1 μM glutamate led to similar small increases in magfura-2 fluorescence during the stimulus and FCCP application. If there is any Ca^{2+} entry, it does not lead to $[Ca^{2+}]_c$ changes large enough to trigger the process of mitochondrial buffering (Nicholls, 1978; see above). Identical results were obtained when using depolarization as a stimulus. In contrast, increases in magfura-2 fluorescence observed during a 30 μM glutamate stimulus followed by an FCCP application, all in Ca^{2+}-free buffer, are unlikely to be due to Ca^{2+} variations. However, we previously demonstrated that glutamate can stimulate the influx of Mg^{2+} in Ca^{2+}-free buffer, and this may be the source of magfura-2 fluorescence changes in the absence of Ca^{2+} (Brocard *et al.* 1993; Stout *et al.* 1996). Interestingly, the AUC obtained during FCCP application in this experiment is higher than that obtained when the drug was applied to previously unstimulated cells. Therefore, this signal could be due to either Mg^{2+} initially taken up, then extruded by the mitochondria, or Mg^{2+} released from ATP during the FCCP application (Leyssens *et al.* 1996). Interestingly, similar observations were made with kainate stimuli (in the presence of Ca^{2+} in the buffer); in this case, it is difficult to decide between a Ca^{2+}- or a Mg^{2+}-specific increase or both.

Several previous studies have described the determination of $[Ca^{2+}]_m$ in neurones. Perhaps the most direct approach involves electron microprobe X-ray analysis to determine the mitochondrial ion content (Pivovarova *et al.* 1999; Taylor *et al.* 1999). However, as of yet it has not proved possible to apply this method to monolayer cultures of neurones, and it is also rather more difficult to establish time courses with this technique. Others have reported the use of fluorescent indicators that report Ca^{2+} and preferentially accumulate in mitochondria. The major limitation in this approach would appear to be the problem of dye saturation. For example, rhod-2 has an affinity for Ca^{2+} of $\sim$0.5 μM, and can selectively accumulate in mitochondria because the acetoxymethyl ester is a partially charged cation (Peng & Greenamyre, 1998; Peng *et al.* 1998). However, as noted above, the estimate of $[Ca^{2+}]_m$ suggests that millimolar concentrations might be expected, which is far beyond the levels that these dyes can measure accurately. Alternatively, it is also possible that a substantial majority of the Ca^{2+} that enters mitochondria is not actually free in solution, and is instead precipitated as calcium phosphate or sequestered in some other form in the matrix (Lehninger, 1974; Zoccarato & Nicholls, 1982). Thus, the actual $[Ca^{2+}]_m$ may still be in the low micromolar range.

We have not directly investigated the efflux mechanisms triggered by FCCP. It has previously been reported that the dissipation of $\Delta\Psi_m$ results in the reverse operation of the Ca^{2+} uniporter in isolated mitochondria (Budd & Nicholls, 1996*a*). Other potential efflux mechanisms are the mitochondrial Na^+–Ca^{2+} exchanger (White & Reynolds, 1995 and references therein) and the activation of permeability transition (for review see Duchen, 1999; Nicholls & Budd, 2000). As already noted, it is likely that some fraction of the Ca^{2+} that accumulates in mitochondria is taken out of solution in the form of calcium phosphate or some other insoluble form in the matrix (Lehninger, 1974; Zoccarato & Nicholls, 1982). It is difficult to establish the extent to which this alters the characteristics of the efflux that we observed. We might tentatively infer, based on the experiments shown in Fig. 7, that there are two pools of releasable Ca^{2+}. The first and larger pool leaves the mitochondria within 10 min, while the second pool remains stable prior to the addition of FCCP. One might speculate that these pools represent soluble and insoluble forms of Ca^{2+} in the mitochondrion, recognizing that there is as yet, little direct evidence to support this supposition. Alternatively, the activation of the Ca^{2+} efflux routes may be less sensitive to $[Ca^{2+}]_m$ than entry routes are to $[Ca^{2+}]_c$. In any case, whatever the form of Ca^{2+} that these pools represent, both must be mobilized by the effects of FCCP, either as the result of the alteration of membrane potential or by the change in the matrix pH.

Al Nasser, I. & Crompton, M. (1986). The reversible Ca^{2+}-induced permeabilization of rat liver mitochondria. *Biochemical Journal* **239**, 19–29.

Brocard, J. B., Rajdev, S. & Reynolds, I. J. (1993). Glutamate-induced increases in intracellular free Mg^{2+} in cultured cortical neurons. *Neuron* **11**, 751–757.

Budd, S. L. & Nicholls, D. G. (1996*a*). A reevaluation of the role of mitochondria in neuronal Ca^{2+} homeostasis. *Journal of Neurochemistry* **66**, 403–411.

Budd, S. L. & Nicholls, D. G. (1996*b*). Mitochondria, calcium regulation, and acute glutamate excitotoxicity in cultured cerebellar granule cells. *Journal of Neurochemistry* **67**, 2282–2291.

Castilho, R. F., Hansson, O., Ward, W. M., Budd, S. L. & Nicholls, D. G. (1998). Mitochondrial control of acute glutamate excitotoxicity in cultured cerebellar granule cells. *Journal of Neuroscience* **18**, 10277–10286.

Choi, D. W. (1987). Ionic dependence of glutamate neurotoxicity. *Journal of Neuroscience* **7**, 369–379.

Choi, D. W., Maulucci-Gede, M. & Kriegstein, A. R. (1987). Glutamate neurotoxicity in cortical cell culture. *Journal of Neuroscience* **7**, 357–368.

Colegrove, S. L., Albrecht, M. A. & Friel, D. D. (2000). Dissection of mitochondrial Ca^{2+} uptake and release fluxes in situ after depolarization-evoked $[Ca^{2+}]_i$ elevations in sympathetic neurons. *Journal of General Physiology* **115**, 351–370.

Dessi, F., Ben-Ari, Y. & Charriaut-Marlangue, C. (1995). Ruthenium red protects against glutamate-induced neuronal death in cerebellar culture. *Neuroscience Letters* **201**, 53–56.

Duchen, M. R. (1990). Effects of metabolic inhibition on the membrane properties of isolated mouse primary sensory neurones. *Journal of Physiology* **424**, 387–409.

Duchen, M. R. (1999). Contributions of mitochondria to animal physiology: from homeostatic sensor to calcium signalling and cell death. *Journal of Physiology* **516**, 1–17.

Grynkiewicz, G., Poenie, M. & Tsien, R. Y. (1985). A new generation of Ca^{2+} indicators with greatly improved fluorescence properties. *Journal of Biological Chemistry* **260**, 3440–3450.

Hartley, D. M., Kurth, M. C., Bjerkness, L., Weiss, J. H. & Choi, D. W. (1993). Glutamate receptor-induced $^{45}Ca^{2+}$ accumulation in cortical cell culture correlated with subsequent neuronal degeneration. *Journal of Neuroscience* **13**, 1993–2000.

Headley, P. M. & Grillner, S. (1990). Excitatory amino acids and synaptic transmission: evidence for a physiological function. *Trends in Pharmacological Sciences–A special report* **1991**, 30–36.

Hunter, D. R. & Haworth, R. A. (1979). The Ca^{2+}-induced membrane transition in mitochondria. I. The protective mechanisms. *Archives in Biochemistry and Biophysics* **195**, 453–459.

Hüser, J., Rechenmacher, C. E. & Blatter, L. A. (1998). Imaging the permeability pore transition in single mitochondria. *Biophysical Journal* **74**, 2129–2137.

Hyrc, K., Handran, S. D., Rothman, S. M. & Goldberg, M. P. (1997). Ionized intracellular calcium concentration predicts excitotoxic neuronal death: observations with low-affinity fluorescent calcium indicators. *Journal of Neuroscience* **17**, 6669–6677.

Hyrc, K. L., Bownik, J. M. & Goldberg, M. P. (2000). Ionic selectivity of low-affinity ratiometric calcium indicators: mag-Fura-2, Fura-2FF and BTC. *Cell Calcium* **27**, 75–86.

Ishijima, S., Sonoda, T. & Tatibana, M. (1991). Mitogen-induced early increase in cytosolic free Mg^{2+} concentrations in single Swiss 3T3 fibroblasts. *American Journal of Physiology* **261**, C1074–1080.

Johnson, J. W. & Ascher, P. (1987). Glycine potentiates the NMDA response in cultured mouse brain neurons. *Nature* **325**, 529–531.

Keelan, J., Vergun, O. & Duchen, M. R. (1999). Excitotoxic mitochondrial depolarisation requires both calcium and nitric oxide in rat hippocampal neurons. *Journal of Physiology* **520**, 797–813.

Khodorov, B., Pinelis, V., Vergun, O., Storozhevykh, T. & Vinskaya, N. (1996). Mitochondrial deenergization underlies neuronal calcium overload following a prolonged glutamate challenge. *FEBS Letters* **397**, 230–234.

Kiedrowski, L. & Costa, E. (1995). Glutamate-induced destabilization of intracellular calcium concentration homeostasis in cultured cerebellar granule cells: role of mitochondria in calcium buffering. *Molecular Pharmacology* **47**, 140–147.

Lehninger, A. L. (1974). Role of phosphate and other proton-donating anions in respiration-coupled transport of Ca^{2+} by mitochondria. *Proceedings of the National Academy of Sciences of the USA* **71**, 1520–1524.

Leyssens, A., Nowicky, A. V., Patterson, L., Crompton, M. & Duchen, M. R. (1996). The relationship between mitochondrial state, ATP hydrolysis, $[Mg^{2+}]_i$ and $[Ca^{2+}]_i$ studied in isolated rat cardiomyocytes. *Journal of Physiology* **496**, 111–128.

Manev, H., Favaron, M., Guidotti, A. & Costa, E. (1989). Delayed increase of Ca^{2+} influx elicited by glutamate: role in neuronal death. *Molecular Pharmacology* **36**, 106–112.

Nicholls, D. G. (1978). The regulation of extra-mitochondrial free Ca^{2+} by rat liver mitochondria. *Biochemical Journal* **176**, 463–474.

Nicholls, D. G. & Åkerman, K. E. O. (1982). Mitochondrial calcium transport. *Biochimica et Biophysica Acta* **683**, 57–88.

Nicholls, D. G. & Budd, S. L. (2000). Mitochondria and neuronal survival. *Physiological Reviews* **80**, 315–360.

Peng, T. I. & Greenamyre, J. T. (1998). Privileged access to mitochondria of calcium influx through *N*-methyl-D-aspartate receptors. *Molecular Pharmacology* **53**, 974–980.

Peng, T. I., Jou, M. J., Sheu, S. S. & Greenamyre, J. T. (1998). Visualization of NMDA receptor-induced mitochondrial calcium accumulation in striatal neurons. *Experimental Neurology* **149**, 1–12.

Pivovarova, N. B., Hongpaisan, J., Andrews, S. B. & Friel, D. D. (1999). Depolarization-induced mitochondrial Ca^{2+} accumulation in sympathetic neurons: spatial and temporal characteristics. *Journal of Neuroscience* **19**, 6372–6384.

Rajdev, S. & Reynolds, I. J. (1993). Calcium green-5N, a novel fluorescent probe for monitoring high intracellular free Ca^{2+} concentrations associated with glutamate excitotoxicity in cultured rat brain neurons. *Neuroscience Letters* **162**, 149–152.

Raju, B., Murphy, E., Levy, L. A., Hall, R. D. & London, R. E. (1989). A fluorescent indicator for measuring cytosolic free magnesium. *American Journal of Physiology* **256**, C540–548.

Randall, R. D. & Thayer, S. A. (1992). Glutamate-induced calcium transient triggers delayed calcium overload and neurotoxicity in rat hippocampal neurons. *Journal of Neuroscience* **12**, 1882–1895.

Rosenmund, C., Feltz, A. & Westbrook, G. L. (1995). Calcium-dependent inactivation of synaptic NMDA receptors in hippocampal neurons. *Journal of Neurophysiology* **73**, 427–430.

Rothman, S. M. & Olney, J. W. (1986). Glutamate and the pathophysiology of hypoxic-ischaemic brain damage. *Annals of Neurology* **19**, 105–111.

Sattler, R., Charlton, M. P., Hafner, M. & Tymianski, M. (1998). Distinct influx pathways, not calcium load, determine neuronal vulnerability to calcium neurotoxicity. *Journal of Neurochemistry* **71**, 2349–2364.

Schinder, A. F., Olson, E. C., Spitzer, N. C. & Montal, M. (1996). Mitochondrial dysfunction is a primary event in glutamate excitotoxicity. *Journal of Neuroscience* **16**, 6125–6133.

Scott, I. D. & Nicholls, D. G. (1980). Energy transduction in intact synaptosomes. Influence of plasma-membrane depolarization on the respiration and membrane potential of internal mitochondria determined in situ. *Biochemical Journal* **186**, 21–33.

Stout, A. K., Li-Smerin, Y., Johnson, J. W. & Reynolds, I. J. (1996). Mechanisms of glutamate-stimulated Mg^{2+} influx and subsequent Mg^{2+} efflux in rat forebrain neurones in culture. *Journal of Physiology* **492**, 641–657.

Stout, A. K., Raphael, H. M., Kanterewicz, B. I., Klann, E. & Reynolds, I. J. (1998). Glutamate-induced neuron death requires mitochondrial calcium uptake. *Nature Neuroscience* **1**, 366–373.

Stout, A. K. & Reynolds, I. J. (1999). High-affinity calcium indicators underestimate increases in intracellular calcium concentrations associated with excitotoxic glutamate stimulations. *Neuroscience* **89**, 91–100.

Taylor, C. P., Weber, M. L., Gaughan, C. L., Lehning, E. J. & Lopachin, R. M. (1999). Oxygen/glucose deprivation in hippocampal slices: altered intraneuronal elemental composition predicts structural and functional damage. *Journal of Neuroscience* **19**, 619–629.

Thayer, S. A. & Miller, R. J. (1990). Regulation of the intracellular free calcium concentration in single rat dorsal root ganglion neurones *in vitro*. *Journal of Physiology* **425**, 85–115.

Vergun, O., Keelan, J., Khodorov, B. I. & Duchen, M. R. (1999). Glutamate-induced mitochondrial depolarisation and perturbation of calcium homeostasis in cultured rat hippocampal neurones. *Journal of Physiology* **519**, 451–466.

WHITE, R. J. & REYNOLDS, I. J. (1995). Mitochondria and Na^+/Ca^{2+} exchange buffer glutamate-induced calcium loads in cultured cortical neurons. *Journal of Neuroscience* **15**, 1318–1328.

WHITE, R. J. & REYNOLDS, I. J. (1996). Mitochondrial depolarization in glutamate-stimulated neurons: an early signal specific to excitotoxin exposure. *Journal of Neuroscience* **16**, 5688–5697.

WHITE, R. J. & REYNOLDS, I. J. (1997). Mitochondria accumulate Ca^{2+} following intense glutamate stimulation of cultured rat forebrain neurones. *Journal of Physiology* **498**, 31–47.

ZOCCARATO, F. & NICHOLLS, D. G. (1982). The role of phosphate in the regulation of the Ca^{2+} efflux pathway of liver mitochondria. *European Journal of Biochemistry* **127**, 333–338.

Acknowledgements

We gratefully thank G. J. Kress for excellent technical help and Dr J. F. Buckman for critically reading this manuscript. J.B.B. was supported by a long term fellowship from the European Molecular Biology Organization (ALTF-743-1998). This study was also supported by NIH grant NS34138.

Corresponding author

I. J. Reynolds: Department of Pharmacology, W1351 Biomedical Science Tower, Pittsburgh, PA 15261, USA.

Email: iannmda@pop.pitt.edu

Author's present address

M. Tassetto: Ecole Normale Supérieure, ACI Biologie Cellulaire des Homéoprotéines (UMR 8542), 46, rue d'Ulm, 75005 Paris, France.

The Journal of Neuroscience, July 15, 2001, 21(14):5054–5065

Spontaneous Changes in Mitochondrial Membrane Potential in Cultured Neurons

Jennifer F. Buckman and Ian J. Reynolds

Department of Pharmacology, University of Pittsburgh, Pittsburgh, Pennsylvania 15261

Using the mitochondrial membrane potential ($\Delta\Psi_m$)-sensitive fluorescent dyes 5,5′,6,6′-tetrachloro-1,1′,3,3′-tetraethylbenzimidazolocarbocyanine iodide (JC-1) and tetramethylrhodamine methyl ester (TMRM), we have observed spontaneous changes in the $\Delta\Psi_m$ of cultured forebrain neurons. These fluctuations in $\Delta\Psi_m$ appear to represent partial, transient depolarizations of individual mitochondria. The frequency of these $\Delta\Psi_m$ fluctuations can be significantly lowered by exposure to a photo-induced oxidant burden, an ATP synthase inhibitor, or a glutamate-induced sodium load, without changing overall JC-1 fluorescence intensity. These spontaneous fluctuations in JC-1 signal were not inhibited by altering plasma membrane activity with tetrodotoxin or MK-801 or by blocking the mitochondrial permeability transition pore (PTP) with cyclosporin A. Neurons loaded with TMRM showed similar, low-amplitude, spontaneous fluctuations in $\Delta\Psi_m$. We hypothesize that these $\Delta\Psi_m$ fluctuations are dependent on the proper functioning of the mitochondria and reflect mitochondria alternating between the active and inactive states of oxidative phosphorylation.

Key words: mitochondria; membrane potential; ATP; JC-1; TMRM; F_1F_O ATPase

Mitochondria have been implicated in excitotoxic injury pathways, as well as injury mechanisms manifested as apoptotic or necrotic death processes. The mitochondrial membrane potential ($\Delta\Psi_m$) has often been used as a marker for mitochondrial activity and neuronal viability during the various cell death cascades (for review, see Kroemer et al., 1998; Nicholls and Ward, 2000). Injurious stimuli, leading to either excitotoxicity or apoptosis, can lead to profound depolarization of $\Delta\Psi_m$ resulting from abnormalities in neuronal processes, including alterations in intracellular calcium dynamics and the opening of the mitochondrial permeability transition pore (PTP) (Ankarcrona et al., 1995; Nieminen et al., 1996; Schinder et al., 1996; White and Reynolds, 1996; Vergun et al., 1999; Budd et al., 2000). Although a loss of $\Delta\Psi_m$ may be linked to various inducers of cell death, these are observed as large and possibly catastrophic changes in mitochondrial function.

Mitochondria under physiological conditions also play active roles in the maintenance of normal cellular functioning. A key feature of mitochondria that allows them to participate in cell survival is proton pumping across the impermeable inner membrane. This generates an electrochemical gradient, composed of $\Delta\Psi_m$ and ΔpH, which is used for ATP synthesis, ADP–ATP exchange, uptake of respiratory substrates and inorganic phosphate, transport of K^+, Na^+, and anions to regulate volume, and regulation of protons to control heat production (for review, see Bernardi, 1999). Mitochondria also play protective roles by buffering cells against high concentrations of calcium (Budd and Nicholls, 1996; White and Reynolds, 1997; Stout et al., 1998) and sequestering proapoptotic agents, such as cytochrome c (for review, see Green and Reed, 1998; Desagher and Martinou, 2000). Compared with the catastrophic changes in acute injury states, healthy mitochondria may exhibit smaller functional changes in ion transport, ATP production or consumption, volume, and permeability, all of which may impact $\Delta\Psi_m$, to optimize the balance between the need for respiration and ATP synthesis and the production of free radicals (Nicholls and Budd, 2000). In the present experiments, the physiological activity of mitochondria has been assessed using $\Delta\Psi_m$-sensitive fluorescent dyes. These dyes exhibit exceptional sensitivity to small changes in $\Delta\Psi_m$ (Ward et al., 2000) and offer the opportunity to study subtle activities inherent in mitochondria.

Several laboratories have reported fluctuations in $\Delta\Psi_m$ in isolated mitochondria (Ichas et al., 1997; Huser and Blatter, 1999), cardiomyocytes (Duchen et al., 1998), neuroblastoma (Loew et al., 1994; Fall and Bennett, 1999), vascular endothelial (Huser and Blatter, 1999), and pancreatic B-cells (Krippeit-Drews et al., 2000). We report here that spontaneous, low-amplitude changes in the $\Delta\Psi_m$ occur in neuronal mitochondria. The widespread occurrence of these spontaneous fluctuations have prompted us to hypothesize that mitochondria exhibit partial, transient depolarizations that represent an inherent physiological function of mitochondria thus far undescribed in neurons. A significant role for the functional state of mitochondria in these fluctuations in $\Delta\Psi_m$ is discussed.

MATERIALS AND METHODS

Cell culture

All procedures were in strict accordance with the *NIH Guide for the Care and Use of Laboratory Animals* and were approved by the Institutional Animal Care and Use Committee of the University of Pittsburgh. Primary forebrain neurons were prepared as described previously (White and Reynolds, 1995). Briefly, forebrains from embryonic day 17 Sprague Dawley rats were removed and dissociated. Cells were plated on poly-D-lysine-coated 31 mm glass coverslips at a density of 450,000 per

Received March 8, 2001; revised April 25, 2001; accepted April 30, 2001.

This work was supported by United States Army Medical Research and Materiel Command Grant DAMD-17–98-1–8627 (I.J.R.), the Scaife Family Foundation (I.J.R.), and National Institutes of Health Grants T32NS07391 (J.F.B.) and F32NS11147 (J.F.B.). We thank Jacques Brocard, Gareth Dewalt, Kirk Dineley, and Yong Yun Han for their assistance in data collection and analysis.

Correspondence should be addressed to Dr. Ian J. Reynolds, Department of Pharmacology, University of Pittsburgh, W1351 Biomedical Sciences Tower, Pittsburgh, PA 15261. E-mail: iannmda+@pitt.edu.

 0270-6474/01/215054-12$15.00/0

milliliter (1.5 ml/coverslip) and inverted after 24 hr to decrease glial growth. Experiments were performed when cells were 12–14 d in culture.

Solutions

Coverslips were perfused with HBSS containing (in mM): 137 NaCl, 5 KCl, 10 $NaHCO_3$, 20 HEPES, 5.5 glucose, 0.6 KH_2PO_4, 0.6 Na_2HPO_4, 1.4 $CaCl_2$, and 0.9 $MgSO_4$, pH adjusted to 7.4 with NaOH. (+)-5-Methyl-10,11-dihydro-5H-dibenzo [a,d] cyclohepten-5,10-imine maleate (MK-801) (10 mM stock in dH_2O) was purchased from Research Biochemicals (Natick, MA), cyclosporin A (20 mM stock in methanol) from Calbiochem (San Diego, CA), kainic acid (10 mM stock in dH_2O), oligomycin (10 mM stock in ethanol), and *p*-(trifluoromethoxy)phenylhydrazone (FCCP) (750 μM in methanol) from Sigma (St. Louis, MO), and tetrodotoxin (TTX) (200 mM stock in dH_2O) from Alomone Labs (Jerusalem, Israel). Tetramethylrhodamine methyl ester (TMRM) and 5,5′,6,6′-tetrachloro-1,1′,3,3′-tetraethylbenzimidazolocarbocyanine iodide (JC-1) were purchased from Molecular Probes (Eugene, OR).

Fluorescence imaging

Coverslips were mounted on a BX50WI Olympus Optical (Tokyo, Japan) light microscope fitted with an Olympus Optical LUMPlanFI 60× water immersion quartz objective. All recordings were made at room temperature while cells were perfused with 10 ml/min HBSS (alone or containing various drugs, as described below). Imaging was performed using a 75 W xenon lamp-based monochromator light source (T.I.L.L. Photonics GmbH, Martinsried, Germany), and light was detected using a CCD camera (Orca; Hamamatsu, Shizouka, Japan). Data acquisition was controlled using Simple PCI software (Compix, Cranberry, PA). For JC-1 (see below), cells were illuminated with a 485 ± 12 nm light (incident light is attenuated with neutral density filters; Omega Optical, Brattleboro, VT), and emitted fluorescence was passed through 500 nm long-pass dichroic mirror. The aggregate signal was obtained using a 605/55 nm filter, and the monomer signal was collected using a 535/25 nm filter. For TMRM (see below), cells were illuminated with a 550 ± 12 nm light, emitted fluorescence was passed through a 570 nm long-pass dichroic mirror, and the single emission signal was obtained using a 605/55 nm filter. An image was collected every 5 sec for the duration of the 10 min experiment.

JC-1. Coverslips were incubated for 20 min at 37°C with a 3 μM JC-1 and then rinsed in HBSS for 15 min at room temperature. Coverslips were mounted on the microscope and perfused with HBSS. A region of cell processes (adjacent to healthy cell bodies) was chosen, and a differential interference contrast image of this field was digitally captured. Mitochondria within neuronal processes, but not cell bodies, were used in these analyses because the dimensions of these processes are such that the movement of mitochondria is constrained to the *x–y* plane (no *z*-plane depth) and mitochondrial movement is readily observable.

The length of time cells were illuminated was minimized and kept constant across coverslips. The coverslip was briefly illuminated with 485 nm light, an image of the aggregate signal was captured, and the monomer signal was focused. The coverslip was then left unilluminated for 3 min while the dye reequilibrated (after light exposure). For post-treated coverslips, basal fluorescence was recorded for 4 min, followed by a 5 min drug exposure and a 1 min recovery. Data were collected from neurons from at least four separate culture dates (except for BAPTA experiments, in which two culture dates were tested).

TMRM. Optimal conditions for TMRM were observed when cells were loaded for 30 min with 200 nM TMRM in HBSS and perfused with 20 nM TMRM during the experiment. At this concentration of TMRM, the dye that accumulates in the mitochondria becomes quenched and a depolarization leads to an increase in fluorescence (Ward et al., 2000). The TMRM experiments were identical to those with JC-1, except that cells were not exposed to light before the initiation of the experiment because TMRM does not appear to reequilibrate after light exposure as JC-1 does.

Data analysis

A 640 × 512 pixel field of neuronal processes was imaged, and a "mask" that identified regions of interest (ROIs) that correlated with the expected number, appearance, and distribution of mitochondria within these neuronal processes was generated. The mask was made using a single JC-1 aggregate image taken before the initiation of the monomer imaging or from a stacking of TMRM images. The mask isolated individual spots of fluorescence that had a fluorescence intensity indicative of physiological $\Delta\Psi_m$ and were more than eight contiguous pixels. Cell bodies present in the imaged field were excluded from the mask to prevent analysis of mitochondrial clusters often observed within these regions. Using the fluorescence images from these dyes, ~1000 ROIs per field were detected. The ROIs generated from the punctate JC-1 aggregate signal were transferred onto the diffuse JC-1 monomer signal, and the fluorescence intensity within each individual ROI was analyzed over time. TMRM, unlike JC-1, is a single wavelength dye that has nonfluorescent, quenching aggregates. Thus, to locate mitochondria, fluorescent images collected during the 10 min experiment were stacked, and a mask was generated based on the brightest spots of fluorescence. ROIs were further qualified based on size, as they were with JC-1 (more than eight pixels, not within cell bodies).

The differences in the techniques used to identify mitochondria with JC-1 and TMRM were useful in determining whether mitochondrial motility was a significant factor in the assessment of $\Delta\Psi_m$ fluctuations. With JC-1, mitochondrial location was identified only at the onset of the experiment, a percentage of mitochondria moved during the experiment (for review, see Overly et al., 1996), and a decrease in the number of $\Delta\Psi_m$ fluctuations was observed. This decrease was at least partially attributable to mitochondria moving out of the defined ROI. Using an image-stacking procedure to identify mitochondria in TMRM-loaded cells, the number of mitochondria was overestimated because the same mitochondrion could be identified at more than one location. With TMRM, we corrected for mitochondrial motility (there was no decrease in the number of fluctuations) but, in turn, underestimated the number of fluctuations occurring per 1000 ROIs. By using both dyes, we were thus able to determine the overall pattern of spontaneous $\Delta\Psi_m$ fluctuations.

The fluorescence intensity data from each ROI were analyzed separately, allowing us to determine $\Delta\Psi_m$ in individual mitochondria within cultured neuronal processes and measure changes in that $\Delta\Psi_m$ over the course of 10 min. Several mathematical criteria were set to detect the spontaneous fluctuations in mitochondrial fluorescence intensity. The first criterion was set to determine whether the changes in the raw fluorescence values exceeded basal fluctuations. Preliminary data suggested that inherent variability within the system accounted for fluorescent fluctuations of 4 units or less. Therefore, the first criterion was that changes in raw fluorescence between two sequential images (taken 5 sec apart) were >4 fluorescent units. The second criterion for detection of a spontaneous $\Delta\Psi_m$ fluctuation was that the slope of the fluorescence change had to be >0.3 fluorescent units per second for both the rise and fall of the fluctuation. The slope was determined using a moving average of three sequential images. This criterion was set to distinguish fluctuations from changes in basal fluorescence attributable to photo-oxidation, focus drifts, debris in the field temporarily impeding fluorescence detection, or other spurious changes in signal. Using these two criteria, preliminary analysis showed substantial correspondence between the observation of changes in fluorescence (on the computer screen) and the statistical detection of a spontaneous $\Delta\Psi_m$ fluctuation.

The number of a spontaneous $\Delta\Psi_m$ fluctuation detected in a field of neuronal processes was determined and normalized as the number of spontaneous $\Delta\Psi_m$ fluctuations occurring per minute per 1000 ROIs. Data were graphed as either the percentage of fluctuations in a drug-treated field versus an untreated control field (for pretreatment experiments) or as a ratio of the number of spontaneous $\Delta\Psi_m$ fluctuations per minute per 1000 ROIs before versus after drug treatment (for post-treatment experiments). Presentation of a ratio was chosen because, as a result of mitochondrial motility, all JC-1-loaded neuronal fields analyzed showed a decreasing number of fluctuations with time. For the post-treatment experiments, the number of fluctuations occurring per minute per 1000 ROIs was counted, and the average of minutes 2–4 (baseline) and minutes 6–8 (treatment) were calculated. This corrected for any instability in the baseline at the onset of the experiment and allowed treatment effects to stabilize for 2 min before analysis. Data from controls and individual drug treatments were averaged across coverslip and culture date and statistically compared using a *t* test or ANOVA.

To distinguish between long-term, global mitochondrial depolarizations and the spontaneous, small-amplitude fluctuations in $\Delta\Psi_m$, the average fluorescence intensity in all mitochondria in a field of neurons was calculated. This enabled us to determine whether there was an association between average $\Delta\Psi_m$ and the occurrence of spontaneous fluctuations. Average fluorescence intensity (in arbitrary units) is presented for all pharmacological experiments.

RESULTS

Under physiological conditions, mitochondria located within cultured neuronal processes exhibit a great deal of spontaneous activity, including repetitive, small-amplitude depolarizations. Our previous measurements of $\Delta\Psi_m$ were limited in both spatial and temporal resolution (White and Reynolds, 1996; Scanlon and Reynolds, 1998), and thus these phenomena were undetected. Using the wide-field imaging system described here, we captured images at 0.2 Hz with resolution adequate to monitor signals from neuronal processes. Replaying these images at a rate of 6 Hz revealed some unappreciated dynamics in the dye signal. Mitochondria traverse several tens of micrometers and, more surprisingly, exhibit extensive spontaneous alterations in dye signal consistent with depolarization of $\Delta\Psi_m$ over the period of the experiment. With real-time imaging (0.2 Hz), fluctuations in $\Delta\Psi_m$ could occasionally be observed; however, on playback (6 Hz), this phenomenon was observed throughout the field of neurons during the entirety of the experiment.

Figure 1 illustrates the spontaneous $\Delta\Psi_m$ fluctuations in JC-1-loaded (Fig. 1*A*) and TMRM-loaded (Fig. 1*B*) neurons. This figure shows small regions of fluorescence (*arrowheads*) within untreated neuronal processes that appear to be spontaneously increasing and decreasing in intensity. We were unable to determine whether there was a propagation of this signal down a process, although this did not appear to be the case. The fluctuations in fluorescence within individual mitochondria appear independent, and no wave-like activity was noted. Movies of JC-1- and TMRM-loaded neurons illustrating this phenomenon are included in the supplemental data section located in the on-line version of this article. For details of these movies, see the legend for Figure 1.

Measurement of spontaneous $\Delta\Psi_m$ fluctuations

To provide a quantitative analysis of this phenomenon, we developed a technique for identifying individual mitochondria within a field of neuronal cell bodies and processes (Fig. 2). The majority of the data presented were collected using the potentiometric dye JC-1, although qualitatively similar results were obtained with TMRM. JC-1 was preferred for these experiments because its aggregates accumulate within the mitochondria based on $\Delta\Psi_m$ and are fluorescent. This allowed us to use the aggregate fluorescent signal to locate individual mitochondria and the monomer signal to detect changes in $\Delta\Psi_m$. A loss of $\Delta\Psi_m$ results in an increase in JC-1 monomer fluorescence in the regions in and around the mitochondria.

A differential interference contrast image was taken (Fig. 2*A*), followed by a single fluorescent image of the JC-1 aggregate signal (Fig. 2*B*). We then isolated each individual fluorescent area and identified it as an ROI depicting what is likely to be a single mitochondrion (Fig. 2*C*). Because of the thickness of the cell bodies and the wide-field microscopy used, it was difficult to distinguish individual mitochondria within the soma. This is evidenced by the large regions of aggregate fluorescence present in the cell body (*arrowhead*), most likely resulting from numerous mitochondria overlapping in the *z*-axis. These large regions of fluorescence, most typically seen in cell bodies, were excluded from analysis based on size. The mask containing the ROIs (Fig. 2*C*) was overlaid onto the JC-1 monomer signal (Fig. 2*D*), and the fluorescence intensity from each individual ROI was recorded (Fig. 2*E*). This technique allowed us to measure the fluorescence intensity of ~1000 ROIs per field from images collected every 5 sec for 10 min.

A graphical illustration of the spontaneous $\Delta\Psi_m$ fluctuations is presented in Figure 3, *A* and *B*. There appears to be no regularity in amplitude or frequency of the spontaneous depolarizations. Note that the individual mitochondria in each of these graphs (*traces A–D*) exhibit numerous spontaneous depolarizations and repolarizations over the course of the experiments, with the overall basal fluorescence intensity remaining relatively stable. However, not all mitochondria exhibit spontaneous fluctuations (*trace E* on both graphs). Over 35,000 mitochondria from untreated cells were assessed for spontaneous $\Delta\Psi_m$ fluctuations in these experiments. The percentage of mitochondria that exhibit at least one $\Delta\Psi_m$ fluctuation was calculated from ~15,600 mitochondria in JC-1-loaded control fields, and 55% of these mitochondria were inherently active.

From Figure 3, it is evident that the fluctuations appear different in JC-1- and TMRM-loaded mitochondria. The $\Delta\Psi_m$ fluctuations appear slower in JC-1-loaded neurons, probably because of the differences in the properties of the dyes. TMRM equilibrates faster across membranes, and thus the fluctuations appear more rapid. This difference in the rate of reequilibration of these dyes thus results in the same phenomenon having a somewhat different appearance, depending on the dye used (Nicholls and Ward, 2000).

JC-1- and TMRM-loaded mitochondria can also be distinguished by the fluctuation frequency, which appears to decrease over time with JC-1 but remain stable or increase with TMRM (Fig. 3*C*). This may be explained by the rapid distribution of TMRM across membranes, which necessitated the addition of TMRM into the perfusate to maintain the level of fluorescence within the neurons (Fig. 3*B*, note the stability of the basal fluorescence within the ROIs). In contrast, JC-1 was not included in the perfusate, making it likely that there is only a partial reaggregation of the dye during repolarization, with some dye diffusing out of the cell. This could lead to a decrease in JC-1 aggregate fluorescence, which could imply less monomer release until eventually the magnitude of the increase in monomer fluorescence would fall below the criterion needed to indicate a fluctuation. This explanation however seems unlikely because, when JC-1 aggregate fluorescence in neurons was decreased by high-light exposure, depolarization could still be observed as a rise in monomer fluorescence (data not shown).

Another factor that may impact the number of fluctuations is that a percentage of mitochondria are known to be motile within neurons (Overly et al., 1996). In fact, we note that a fraction of the mitochondria move throughout the processes of our cultured neurons, regardless of which dye we used. With JC-1, mitochondria were located and ROIs identified only at the onset of the experiment, using the JC-1 aggregate signal. Thus, over time, the regions being analyzed may no longer correlate with the regions exhibiting the changes in fluorescence (i.e., a mitochondrion may move out of the defined ROI). TMRM-loaded mitochondria were located using image stacking; thus, when a mitochondrion moves, each location may be associated with an independent ROI. This would suggest that TMRM overestimates the number of ROIs and thus underestimates the number of fluctuations per 1000 ROIs. These technical differences can explain why TMRM-loaded mitochondria appear more active than JC-1-loaded mitochondria, a fact that is not reflected in the average number of fluctuations reported in Figure 3*C*. In addition, they suggest that the percentage of mitochondria that move is stable because the decrease in fluctuations observed with JC-1 is very consistent. It is important to note, however, that regardless of the cause, we have corrected for this loss of fluctuation detection in subsequent

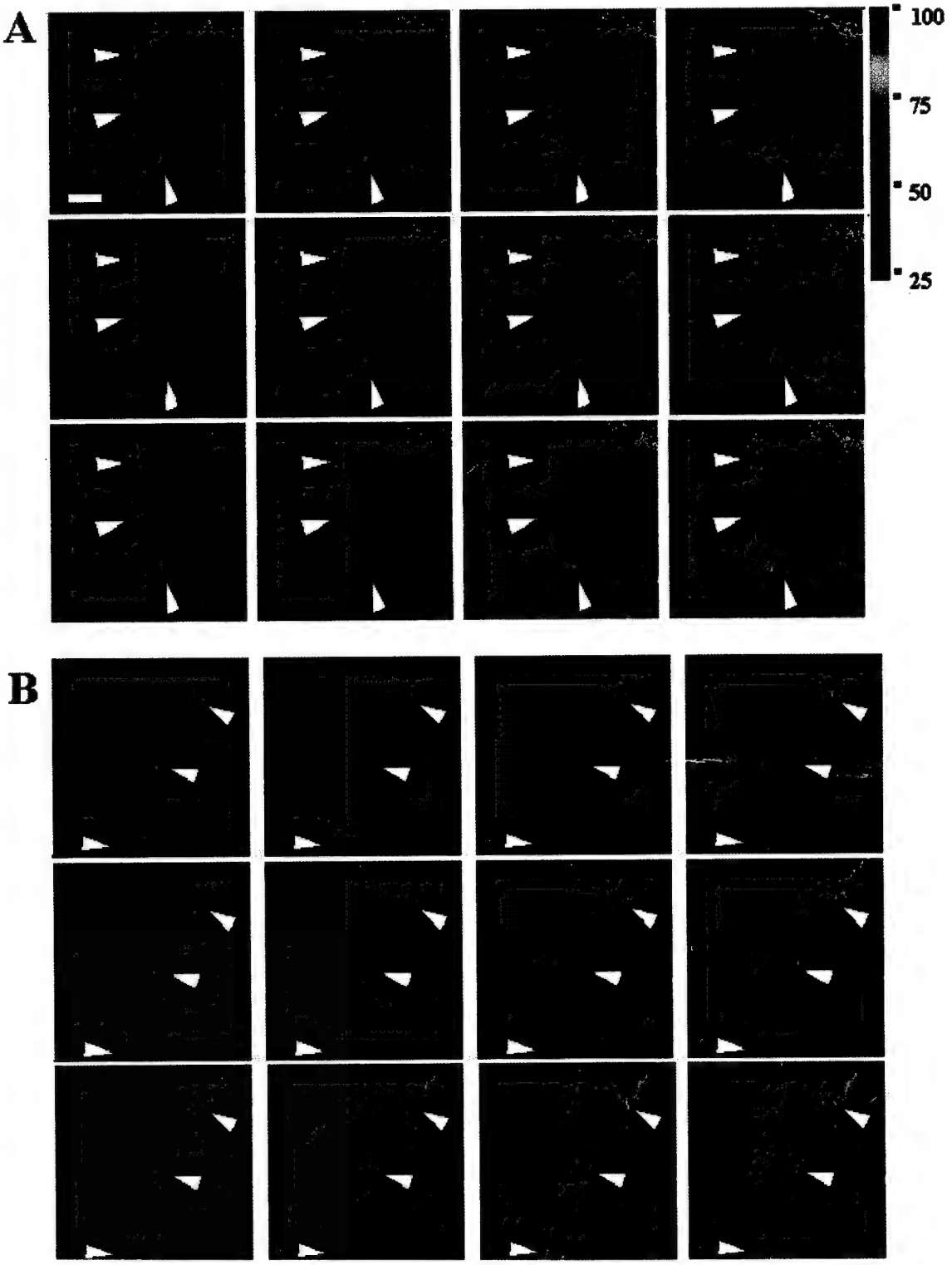

Figure 1. Representative fluorescent images of $\Delta\Psi_m$ fluctuations. *A*, JC-1-loaded neuronal processes. *B*, TMRM-loaded processes. These *panels* show spontaneous changes in fluorescent intensity occurring in small regions of neuronal processes. Images show a 200 × 200 pixel field. Images were taken 30 sec apart. *Arrowheads* identify examples of regions of fluorescence that correspond to the expected size and shape of neuronal mitochondria and show readily observed fluctuations in intensity. Increases in fluorescence imply depolarization. TMRM-loaded cells have lower basal fluorescence because light levels were kept low to avoid light-induced increase in fluorescence. Scale bar, 10 μM. Movie files corresponding to JC-1-loaded (*A*) and TMRM-loaded (*B*) neurons have been included in the supplemental data section located in the on-line version of this article. Movie images were taken 5 sec apart, and time is shown in minutes and seconds. Both spontaneous fluctuations and dye intensity and mitochondrial motility are evident.

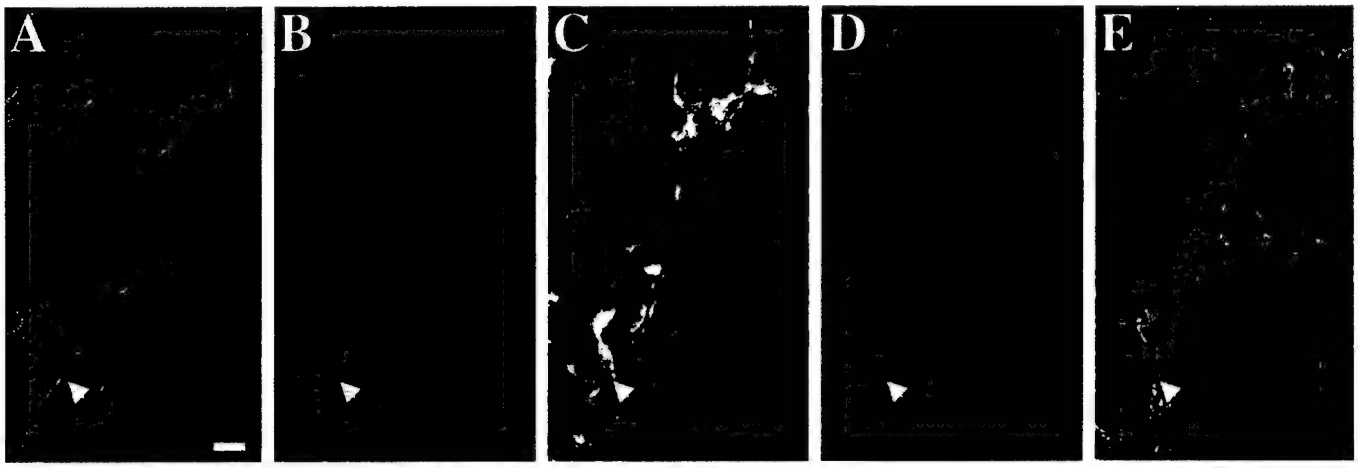

Figure 2. Imaging technique used to measure spontaneous changes in mitochondrial membrane potential using JC-1. *A*, Bright-field image, using differential interference contrast. The *arrow* shows a healthy neuronal cell body with processes within a field of neurites. *B–E* represent fluorescent images from this same field. *B*, The JC-1 aggregate image. Note the punctate nature of the label within the processes. *C*, The mask (*red*) created to discern ROIs thought to correspond to mitochondria. The bright fluorescent spots observed with the JC-1 aggregate image (same as *B*, now *white*) are detected using image analysis software based on size criteria. Regions uniformly labeled (e.g., cell bodies) are excluded from the mask based on size. *D*, The JC-1 monomer image. Note the diffuse nature of the label within the processes. *E*, The "overlay." The mask generated in *C* (*red*) is overlaid onto the JC-1 monomer image from *D* (*green*). Scale bar, 20 μM.

pharmacological experiments by analyzing only the ratio of spontaneous $\Delta\Psi_m$ fluctuations at the beginning versus end of the experiment.

It was important to rule out nonphysiological influences on the fluctuations in $\Delta\Psi_m$. Fluorescence imaging of organelles as small as mitochondria requires careful maintenance of the correct focal plane. Drifts in focus could lead to the appearance and/or disappearance of $\Delta\Psi_m$ fluctuations. To minimize inclusion of focus changes in our quantitation of $\Delta\Psi_m$ fluctuations, we used a moving average paradigm to smooth out brief irregularities in whole-field fluorescence (see Materials and Methods). However, because the cells were also being perfused throughout the experiment, it was possible that smaller regions of the field were drifting in and out of focus, thus leading to the graphical appearance of fluctuations. To show that the $\Delta\Psi_m$ fluctuations were not attributable to focus drift, we identified three adjacent mitochondria located within a single neuronal process and analyzed them for spontaneous $\Delta\Psi_m$ fluctuations (Fig. 4). If the $\Delta\Psi_m$ fluctuations were the result of drifts in focus, then mitochondria in close proximity to one another should all exhibit simultaneous fluctuations. This was not observed. Three neighboring ROIs were identified using the JC-1 aggregate signal (Fig. 4*A*, *red*), and the fluorescence intensity of JC-1 monomer signal (Fig. 4*A*, *green*) within each ROI was determined. As the monomer signal increases (indicating depolarization), the ROIs appear increasingly *yellow* (Fig. 4*A*) and an increase in fluorescence intensity is observed graphically (Fig. 4*B*). The fluctuations in fluorescence intensity observed qualitatively and quantitatively appear to correspond, with no evidence of changes in focus in any of the ROIs. Moreover, two mitochondria demonstrate fluctuations (ROIs 1 and 3), whereas the ROI in the middle does not (ROI 2). This strongly argues against a drift in focus or movement of the process as the underlying mechanism of this phenomenon.

Illumination of mitochondria loaded with cationic fluorescence dyes has been reported to lead to the generation of reactive oxygen species (ROS) and thus mitochondrial damage (Bunting, 1992). Photo damage to the mitochondria could therefore be a potential cause of the observed fluctuations in $\Delta\Psi_m$. Typically, during imaging, neurons were exposed to attenuated fluorescent light (5% transmitted light) for ~0.1 sec every 5 sec over the course of a 10 min experiment. To determine the relative contribution of light, we took JC-1-loaded neurons and exposed a portion of the field to a brief, intense light. For our high-light conditions, we maintained the exposure time of 0.1 sec (per 5 sec) but increased transmitted light to 100%. In these experiments, JC-1-loaded neuronal processes were imaged under standard conditions for 50 frames (one frame per 5 sec). The microscope aperture size was then decreased so that light exposure was limited to the center of the neuronal field and the processes in this central region were illuminated, for 20 frames (one frame per 5 sec), with a 20-fold higher light intensity. Light conditions were then returned to normal. We separated the imaged field into the exposed center region (illuminated under high-light conditions) and the peripheral, control region (unilluminated for the same 20 frames). The ratio of fluctuations occurring before versus after intense light exposure were compared across the control and exposed regions. The region exposed to high-light conditions showed significantly fewer spontaneous $\Delta\Psi_m$ fluctuations (Fig. 5*A*), without a concurrent change in average fluorescence intensity (Fig. 5*B*). Thus, photo damage cannot account for the observation of these phenomena; in fact, these data suggest that light exposure can lead to the loss of $\Delta\Psi_m$ fluctuations, potentially through a photo-induced oxidant burden.

Pharmacological analysis of spontaneous $\Delta\Psi_m$ fluctuations

Having established methods to measure spontaneous fluctuations in fluorescence intensity in JC-1-loaded mitochondria in untreated neurons, we explored mechanisms underlying this phenomenon. We first tested the possibility that the $\Delta\Psi_m$ fluctuations were the result of synaptic activity and thus were reflecting plasma membrane potential changes or calcium influx. Neurons were treated with TTX (200 nM), a sodium channel blocker, to inhibit spontaneous synaptic activity. We also tested an NMDA receptor antagonist, MK-801 (10 μM), to block a major route of calcium entry. JC-1-loaded neurons were perfused with HBSS for

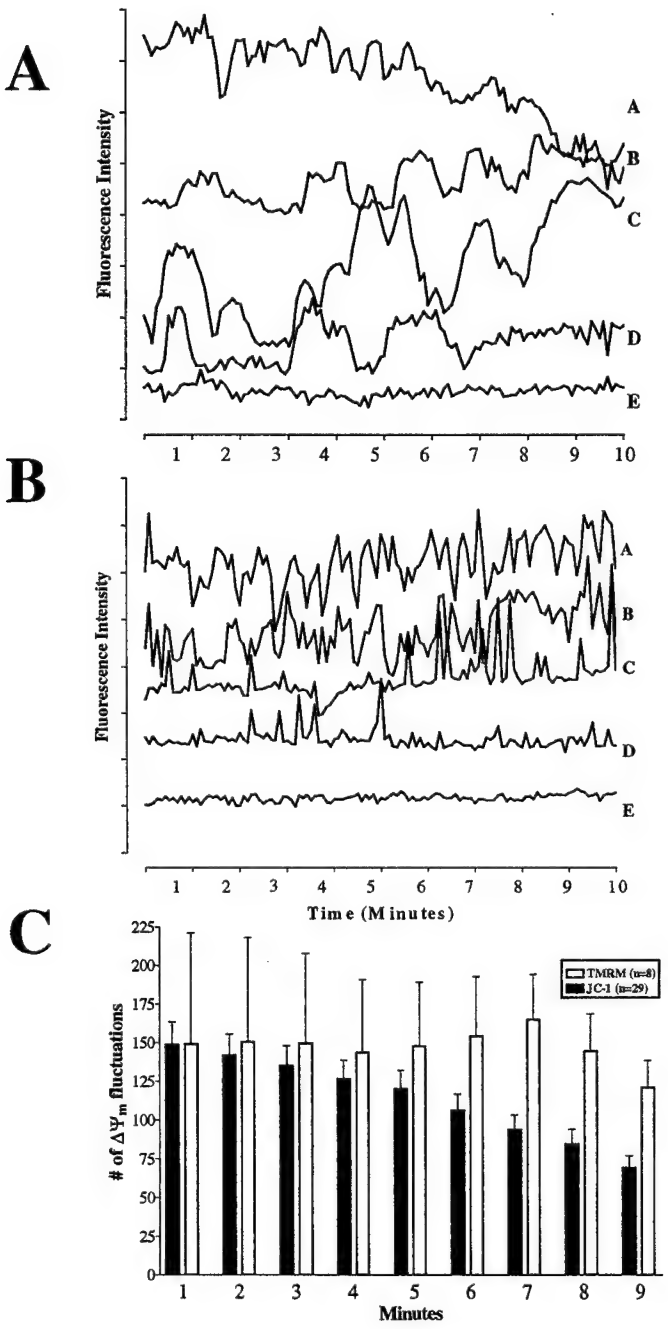

Figure 3. Quantification of $\Delta\Psi_m$ fluctuations within individual mitochondria. *A*, JC-1 monomer traces. *B*, TMRM fluorescence traces. Each *trace* represents in a single ROI corresponding to an individual mitochondrion. An increase in fluorescence is associated with depolarization. Note that the basal fluorescence in both graphs remains stable and that fluctuations are not all of the same magnitude or of regular frequency. Approximately 1000 such traces were collected per field. The *y*-axis represents arbitrary fluorescence units, with each *tick mark* equaling 10 units. *Traces* have been offset from one another for display purposes. *A*, *Trace* A shows a mitochondrion that fluctuates repeatedly followed by a loss of fluorescence, most likely indicating the movement of the mitochondrion out of the ROI. *Trace* B shows a mitochondrion that fluctuates especially as the experiment continues. *Trace* C shows large fluctuations and then a slow increase in fluorescence suggesting a gradual depolarization. *Trace* D initially exhibits fluctuations, but by 7 min activity ceases. *B*, *Traces* A and B show mitochondria that fluctuate repeatedly throughout the experiment. *Trace* C shows a mitochondrion that fluctuates especially as the experiment continues. *Trace* D initially has fluctuations, but by 5 min activity ceases. *Trace* E from both figures shows background noise in the system and reflects mitochondria that do not exhibit spontaneous fluctuations. *C*, Average number of spontaneous $\Delta\Psi_m$ fluctuations in JC-1- or TMRM-loaded neurons from *traces* such as those presented in *A* and *B*. Criteria for a spontaneous fluctuation in $\Delta\Psi_m$ were set a priori: fluorescence changes >4 fluorescent units and a slope >0.3 fluorescent units per second. The number of $\Delta\Psi_m$ fluctuations that occurred per minute per 1000 ROIs is presented. A decrease in the number of $\Delta\Psi_m$ fluctuations over time was observed in JC-1-loaded, but not in TMRM-loaded, neurons (see Results). Data are presented as means ± SEM. The number of fields (*n*) imaged (~1000 ROIs per field) is presented in the key.

4 min to establish basal activity. Neurons were then exposed to the inhibitors for 5 min. The ratio of fluctuations occurring before versus those occurring after drug treatment was graphed to correct for the decrease in the number of fluctuations that occurs even in untreated control mitochondria (Fig. 3*C*). There was no difference in the ratio of fluctuations between control mitochondria and those treated with TTX or MK-801 (Fig. 6*A*). These treatments did not alter the average fluorescence intensity of the JC-1 monomer signal within the mitochondria (Fig. 6*B*). This suggests that drugs that inhibit plasma membrane activities do not inhibit spontaneous fluctuations or change the resting level of $\Delta\Psi_m$.

There are several additional routes of calcium entry beyond NMDA receptor activation. Mitochondria are intricately involved in shaping calcium dynamics (Duchen, 1999), and calcium has also been suggested to regulate $\Delta\Psi_m$ fluctuation in other cells (Loew et al., 1994; Ichas et al., 1997; Duchen, 1999; Krippeit-Drews et al., 2000). BAPTA, an intracellular calcium chelator, interrupts calcium-mediated events that result from calcium influx and release from intracellular stores. Because of the close apposition of mitochondria to endoplasmic reticulum, release of calcium from the reticular stores can alter mitochondrial function by creating microdomains of high calcium (Rizzuto et al., 1993, 1998; Hajnoczky et al., 1995). Thus, any involvement of calcium-mediated activity in the observed spontaneous mitochondrial depolarizations should become evident with BAPTA treatment. Neurons were preincubated with BAPTA-AM (50 μM) showed a dramatic decrease in the number of spontaneous fluctuations compared with controls (Fig. 7*A*). However, this BAPTA-induced inhibition was associated with a dramatic rise in fluorescence intensity (Fig. 7*B*). This implies that BAPTA-AM, at this concentration, leads to mitochondrial depolarization. The mechanism by which this occurs is unclear and cannot necessarily be attributed to calcium chelation. Respiratory complex inhibitors and the uncoupler FCCP depolarized $\Delta\Psi_m$ and decreased the number of spontaneous fluctuations (data not shown). This raises the possibility that the effects of BAPTA are attributable to general mitochondrial depolarization, which occludes the smaller fluctuations rather than a result of modifying intrinsic calcium changes.

Activity of the respiratory chain complexes leads to the extrusion of protons from the mitochondrial matrix, whereas synthesis of ATP through the F_1F_O ATPase (ATP synthase) is driven by proton reentry. Thus, whereas inhibition at the respiratory chain complexes may lead to a slow loss of $\Delta\Psi_m$, inhibition at the ATP synthase should lead to a subtle hyperpolarization in healthy, ATP-generating mitochondria and a depolarization in damaged, ATP-consuming mitochondria (Scott and Nicholls, 1980; Nicholls and Ward, 2000). Neurons pretreated with oligomycin (15 min) showed a significant decrease in the number of spontaneous $\Delta\Psi_m$ fluctuations compared with untreated control mitochondria (Fig. 8*A*) but no significant change in initial basal fluorescence (Fig. 8*B*). Because it is unlikely that all mitochondria within a field of

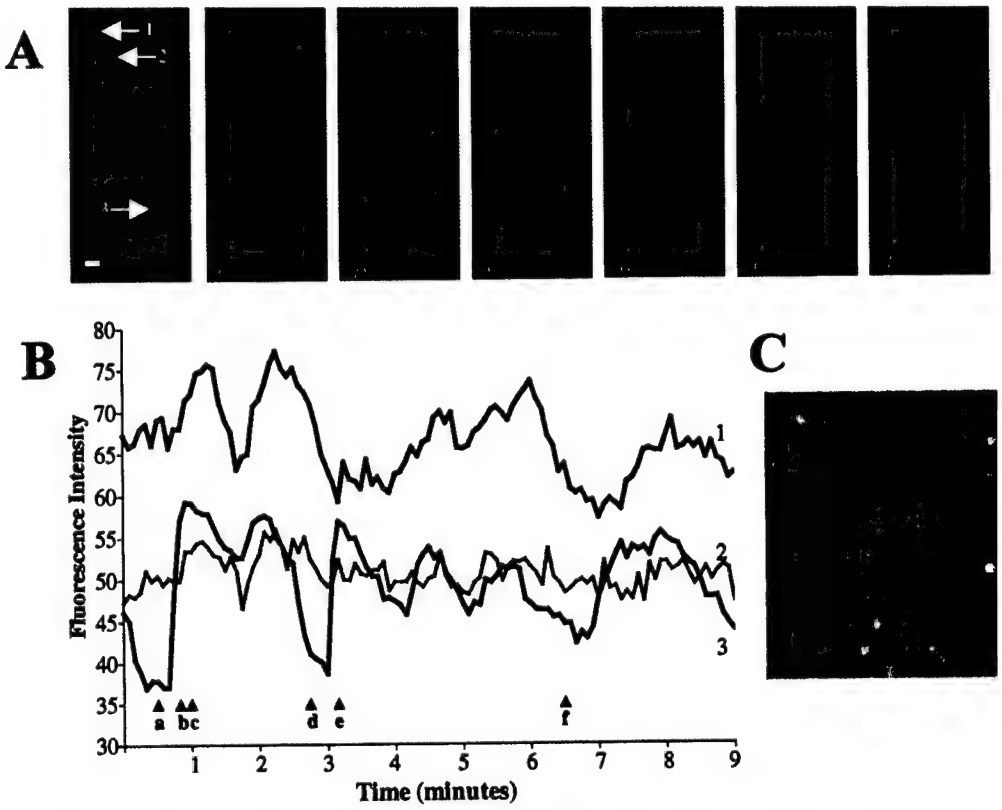

Figure 4. $\Delta\Psi_m$ fluctuations are not attributable to focus drift. Three individual ROIs located within a single neuronal process analyzed for spontaneous $\Delta\Psi_m$ fluctuations. *A*, In this series of images, the JC-1 aggregate signal (*red*, depicting individual ROIs) has been overlaid on the corresponding JC-1 monomer (*green*) images (as shown in Fig. 2*E*). The first image in this series identifies three mitochondria at the onset of imaging (*arrows*). The *numbers* associated with each mitochondrion correspond to the *traces* in *B*. In images *a–f*, a static aggregate (*red*) image has been used; thus, changes in the ratio of *green* to *red* represent changes in JC-1 monomer fluorescence. (i.e., when mitochondria appear *yellow*, monomer signal has increased, suggesting depolarization). Note that fluctuations in JC-1 monomer fluorescence intensity can be observed qualitatively over time. *B*, Fluorescence intensity of the JC-1 monomer signal within each of the three ROIs identified in *A* was quantified (*arrowheads a–f* show the time points when the images in *A* were taken). Note that *traces 1* and *3* show significant fluctuations in fluorescence intensity, but *trace 2* does not. This illustrates that changes in fluorescence intensity are not simply attributable to a drift in focus or movement of the process. If this were the case, then all three mitochondria within this process should exhibit similar $\Delta\Psi_m$ fluctuations. *C*, A differential interference contrast image showing the neuronal process from which the fluorescent images were taken. The *arrows* correspond to the ROIs analyzed. Scale bar, 5 μM.

neurons are of equivalent membrane potential and ATP synthase activity and ~1000 mitochondria were averaged per field, small changes in overall fluorescence intensity were not detected.

The PTP is thought to regulate matrix Ca^{2+}, pH, $\Delta\Psi_m$, and volume (Susin et al., 1998). Its opening is triggered by a wide variety of treatments, including increased Ca^{2+} (Zoratti and Szabo, 1995), and is inhibited by cyclosporin A (Crompton et al., 1988). Two open states for this pore have been proposed, with the low-conductance state causing transient openings that aid in stabilizing $\Delta\Psi_m$ and volume (Ichas et al., 1997) and the high-conductance state involved in irreversible openings, complete dissipation of the $\Delta\Psi_m$, extensive swelling, and cell death (Petit et al., 1996; Susin et al., 1997). Transient depolarizations in $\Delta\Psi_m$ have been reported to coincide with activation of the low-conductance state of the PTP in isolated mitochondria, which could represent a physiological process necessary for regulating $\Delta\Psi_m$ (Ichas et al., 1997) and limiting the generation of ROS in hyperpolarized mitochondria (Skulachev, 1996). We tested whether cyclosporin A influenced the frequency of the $\Delta\Psi_m$ fluctuations in our cultured neurons. No effect was observed at any concentration tested (Fig. 9*A*); however, cyclosporin A caused a modest decrease in fluorescence intensity at lower concentrations (Fig. 9*B*).

Taxing neurons by increasing synaptic activity may lead to an increase in mitochondrial activity. Stimulation of neurons by high concentrations of glutamate causes large calcium fluxes that directly influence mitochondrial function (White and Reynolds, 1995) and have been proposed to increase ATP demand by the plasma membrane ATPases. Although inhibition of basal synaptic activity with a sodium channel blocker or a glutamate receptor antagonist did not alter the frequency of $\Delta\Psi_m$ fluctuations (Fig. 6*A*), we tested whether increasing synaptic activity, and presumably increasing the demand placed on the mitochondria, would alter the frequency of fluctuations. Treatment with glutamate in the presence of extracellular calcium leads to an increase in fluorescence intensity in a similar manner to that observed with BAPTA-AM. In fact, stimulation with glutamate is known to cause mitochondrial calcium influx and depolarization (Ankarcrona et al., 1995; White and Reynolds, 1996). We attempted to circumvent the problem of the superimposition of the catastrophic depolarization on the smaller spontaneous changes using two approaches. First, we treated neurons with kainic acid, an agonist of the AMPA–kainate subtype of glutamate receptors. Activation of glutamate receptors with kainic acid results in increased intracellular sodium and calcium but does not lead to mitochondrial depolarization (Courtney et al., 1995, Hoyt et al., 1998). Accumulation of calcium within mitochondria is also significantly lower using kainic acid than it is with NMDA (Budd and Nicholls, 1996; Stout et al., 1998). Therefore, neurons were treated with 100 μM kainic acid for 5 min, in either the presence or absence of calcium, but no evidence of altered $\Delta\Psi_m$ fluctuation frequency (Fig. 10*A*) or overall fluorescence intensity (Fig. 10*B*) was observed.

We then attempted to increase synaptic activity and mitochondrial demand without flooding mitochondria with calcium and depolarizing them by treating neurons with glutamate (in the presence of its coagonist glycine) in buffer that is nominally calcium free. This should lead to the activation of the glutamate receptors without the concurrent increase in intracellular and intramitochondrial calcium concentrations. Receptor activation should, however, lead to an influx of sodium and thus manipulate mitochondrial ion concentrations through sodium-related path-

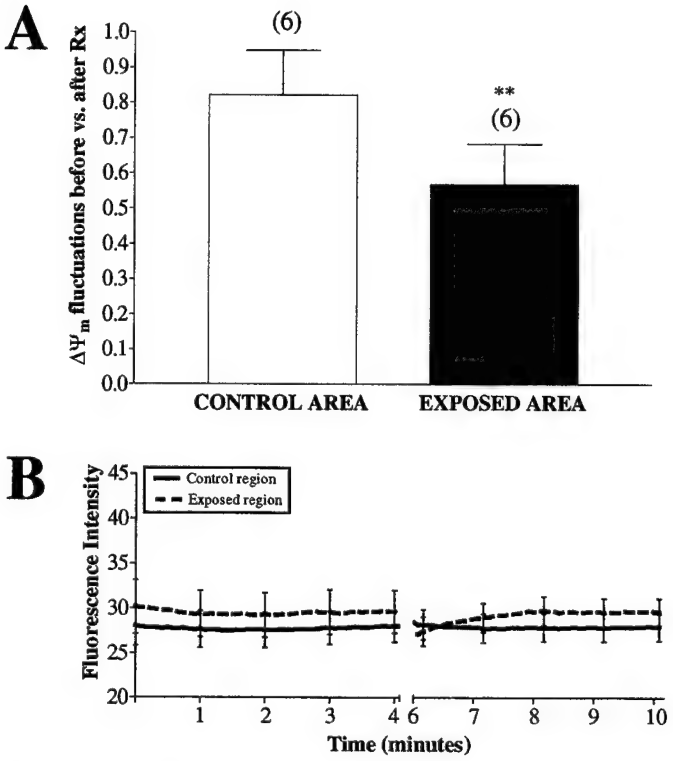

Figure 5. $\Delta\Psi_m$ fluctuations in JC-1-loaded neurons are not caused by light. Untreated neurons were loaded with JC-1 and imaged under our standard light conditions for 50 frames (neutral density attenuating transmitted light to 5%). The aperture on the microscope was then closed to allow light to hit only the center portion of the field, and the cells were imaged for 20 frames. Under this condition, the middle portion of the coverslip was exposed to intense light (100% transmitted light; *EXPOSED AREA*), whereas the periphery of the coverslip was left unexposed (*CONTROL AREA*). The imaging conditions were then returned to the standard conditions from the beginning of the experiment for 50 more frames. *A*, The number of fluctuations in $\Delta\Psi_m$ per minute per 1000 ROIs was determined in the control and exposed regions, and the ratio of fluctuations occurring before versus after intense light exposure are presented (note that the control area received no light during this period). Data are presented as means ± SEM, and the *numbers* above each *bar* equal the number of fields imaged. The region exposed to high-light conditions showed significantly fewer spontaneous $\Delta\Psi_m$ fluctuations (paired t test; $t = 3.77$; df = 5; $p < 0.05$). *B*, Average fluorescence intensity of all mitochondria imaged, with representative error bars indicating SEM. Basal fluorescence did not change after light exposure.

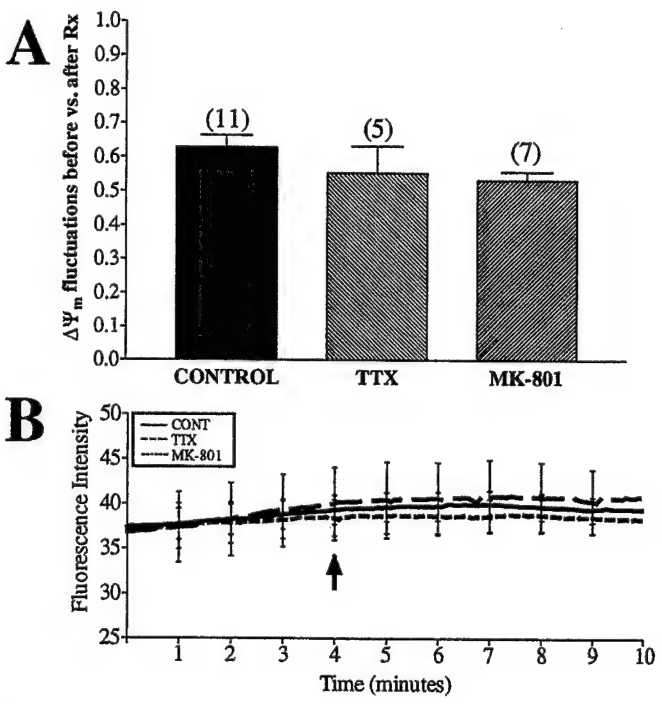

Figure 6. $\Delta\Psi_m$ fluctuations are not attributable to synaptic activity. Untreated neurons were loaded with JC-1 and imaged for 4 min before the addition of drugs (*arrow*). TTX (200 nM) (a Na^+ channel blocker) or 10 μM MK-801 (NMDA antagonist) were perfused over the cells for 5 min, and fluorescence intensity and number of fluctuations per minute per 1000 ROIs were calculated. *A*, The ratio of fluctuations occurring during the baseline to those occurring after drug treatment. This corrected for the consistent decrease in fluctuations observed in untreated mitochondria (see Fig. 3). Data are presented as means ± SEM, and the *numbers* above each *bar* equal the number of fields imaged (~1000 ROIs per field). Neither treatment had a significant impact on $\Delta\Psi_m$ fluctuations (TTX, $t = 1.03$, df = 14, $p > 0.05$; MK-801, $t = 1.98$, df = 16, $p > 0.05$). *B*, Average fluorescence intensity of all mitochondria imaged, with representative error bars indicating SEM. Neither treatment altered basal fluorescence.

ways. JC-1-loaded neurons were treated with 100 μM glutamate and 10 μM glycine in calcium-free buffer for 5 min. This treatment led to a significant decrease in $\Delta\Psi_m$ fluctuations (Fig. 11*A*) without a concomitant rise in fluorescence intensity (Fig. 11*B*). The differences between glutamate and kainate on $\Delta\Psi_m$ fluctuations are not surprising in light of the observation that their ability to activate glutamate receptors is not equivalent qualitatively or quantitatively (Hoyt et al., 1998; Sattler et al., 1998; Brocard et al., 2001).

DISCUSSION

In this study, we report that mitochondria in neuronal cultures display small, spontaneous fluctuations in $\Delta\Psi_m$ and that these fluctuations can be dramatically decreased, without a concurrent change in basal fluorescence, by treatments that alter mitochondrial activity. Although there has been a great deal of recent interest in large-scale changes in mitochondrial function associated with neuronal injury, the present findings reveal a previously unappreciated property of mitochondria in resting, uninjured neurons.

The $\Delta\Psi_m$ is a key marker of mitochondrial function, generated by the pumping of protons across the inner mitochondrial membrane in association with electron transport. In turn, $\Delta\Psi_m$ drives many key mitochondrial functions, including ATP synthesis, calcium accumulation, and maintenance of ion gradients that permit the influx of substrates and egress of metabolic products. Clearly, $\Delta\Psi_m$ has a number of important functions, and thus a variety of activities could account for the spontaneous changes in $\Delta\Psi_m$ reported here. Our observations of $\Delta\Psi_m$ fluctuations could reflect inherent changes in mitochondrial ion transport, ATP production–consumption, respiration, or volume, all of which are essential for proper mitochondrial function. We believe that spontaneous $\Delta\Psi_m$ fluctuations represent a normal physiological feature of neuronal mitochondria such that the presence or absence of these fluctuations may be useful as a novel marker for mitochondrial activity.

The pharmacological approach of using tetrodotoxin or MK-801 clearly excludes alterations in plasma membrane potential and ion fluxes as the basis for the change in the mitochondrial dye signal. However, the mitochondrial mechanism that causes the fluctuations is less clear. Attempts to regulate the permeability transition pore with cyclosporin A had no effect on either $\Delta\Psi_m$ fluctuations or fluorescence intensity, which ostensibly excludes

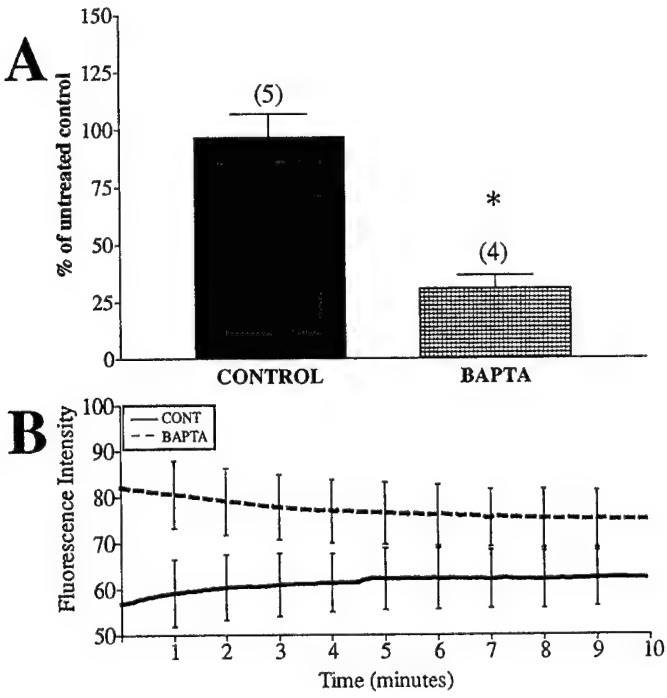

Figure 7. An intracellular calcium chelator alters $\Delta\Psi_m$ fluctuations and basal fluorescence. Neurons loaded with JC-1 were treated with 50 μM BAPTA-AM for 15 min before imaging. The fluorescence intensity and number of fluctuations per minute per 1000 ROIs were calculated. *A*, The percentage of fluctuations occurring in BAPTA-pretreated mitochondria to untreated mitochondria. Data are presented as means ± SEM. *Numbers* above each *bar* equal the number of fields imaged (~1000 ROIs per field). BAPTA decreased $\Delta\Psi_m$ fluctuations ($t = 5.17$; df = 7; $^*p < 0.05$; but see Discussion). *B*, Average fluorescence intensity of all mitochondria imaged, with representative error bars indicating SEM. BAPTA increased the average fluorescence intensity. (Note that the scale is twice that of Figs. 8–10).

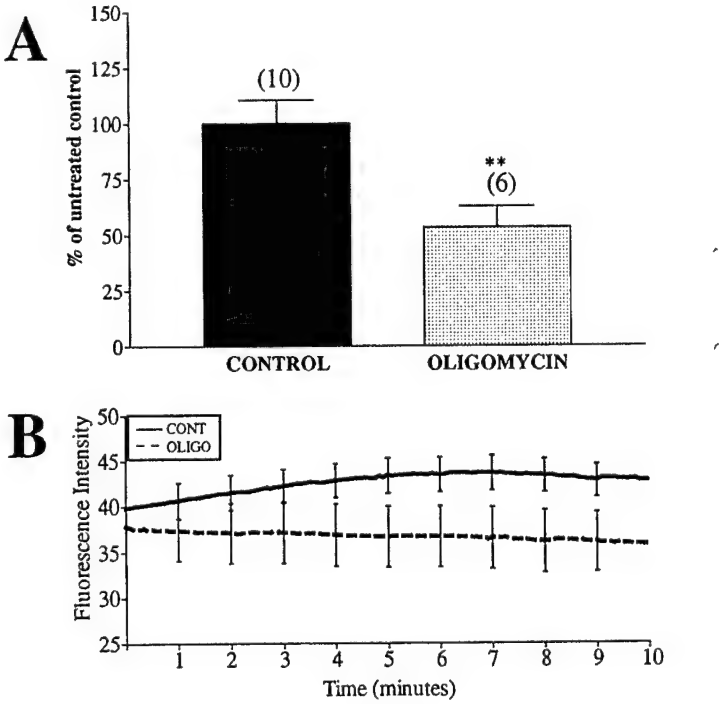

Figure 8. $\Delta\Psi_m$ fluctuations are decreased by pretreatment with an ATP synthase inhibitor. Neurons loaded with JC-1 were treated with 10 μM oligomycin (*OLIGO*) for 15 min before imaging to ensure substantial inhibition of the synthase. Fluorescence intensity and number of fluctuations per minute per 1000 ROIs were calculated. *A*, Percentage of fluctuations in oligomycin-pretreated to untreated mitochondria (means ± SEM). Oligomycin significantly decreased $\Delta\Psi_m$ fluctuations ($t = 3.03$; $df = 14$; $^{**}p < 0.01$). *Numbers* above *bars* equals the number of fields imaged (~1000 ROIs per field). *B*, Average fluorescence intensity of all mitochondria, with representative error bars indicating SEM. Oligomycin had no effect.

low-amplitude transition as a basis for these changes (Ichas et al., 1997). Oligomycin, however, significantly decreased the frequency of fluctuations, which argues that the fluctuations are associated with oxidative phosphorylation.

Oxidative phosphorylation may impact $\Delta\Psi_m$ fluctuations by one of two mechanisms. The first mechanism would suggest that, as mitochondria go from a resting state to active phosphorylation (state 4 to state 3), the fluctuations reflect the transient loss of $\Delta\Psi_m$ as proton flux increases (Nicholls and Ferguson, 1992). In this case, the increase in dye signal would be attributable to the disaggregation and subsequent dissipation of dye from mitochondria. Alternatively, because state 3 mitochondria adopt a condensed configuration whereas state 4 mitochondria adopt the larger orthodox configuration (Scalettar et al., 1991), the fluctuations would reflect changes in mitochondrial matrix volume. In this case, the increase in dye signal attributable to the increased volume would lead to a disaggregation of dye that is retained within the mitochondrial matrix. Although these mechanisms are contradictory in that the first proposes that a fluctuation is associated with the onset of phosphorylation whereas the second suggests that the signal should be associated with the termination of active phosphorylation, the key feature of both mechanisms is that the fluctuations represent an on–off transition. Thus, either mechanism could explain the decrease in fluctuations observed with a glutamate-induced sodium load. In this condition, an increase in ATP demand presumably occurs causing the mitochondria to spend a greater fraction of the time engaged in active phosphorylation rather than switching on and off. One could also argue that light-induced damage places greater demands on the mitochondria to be met by increasing ATP synthesis (or perhaps by decreasing synthetic capacity).

Predicting manipulations that increase the frequency of fluctuations is harder. We have observed differences in the number fluctuations on a culture-to-culture basis but have not yet established a mechanism for these differences. We are not aware of any previous studies that have suggested that individual mitochondria can be observed to change between states of resting and active phosphorylation. However, the architecture of neurons is uniquely suited to making such observations because optically isolating individual mitochondria in neuronal processes is straightforward (Figs. 1, 2).

Cationic dyes used to measure $\Delta\Psi_m$ (such as JC-1 and TMRM) can lead to toxicity resulting from light-induced singlet oxygen generation (Bunting, 1992) and inhibition of respiration. Although light exposure was carefully controlled and minimized to that necessary for adequate recordings, some effects of light exposure were observed even under these low-light conditions. With JC-1, exposure to light before recording stabilized the baseline, and with TMRM, increasing light exposure tended to increase the overall fluorescent signal. Both of these light-induced changes in dye signal could be indicative of a potential impact of phototoxicity in $\Delta\Psi_m$ measurements. A more immediate concern was that the spontaneous changes were triggered by light expo-

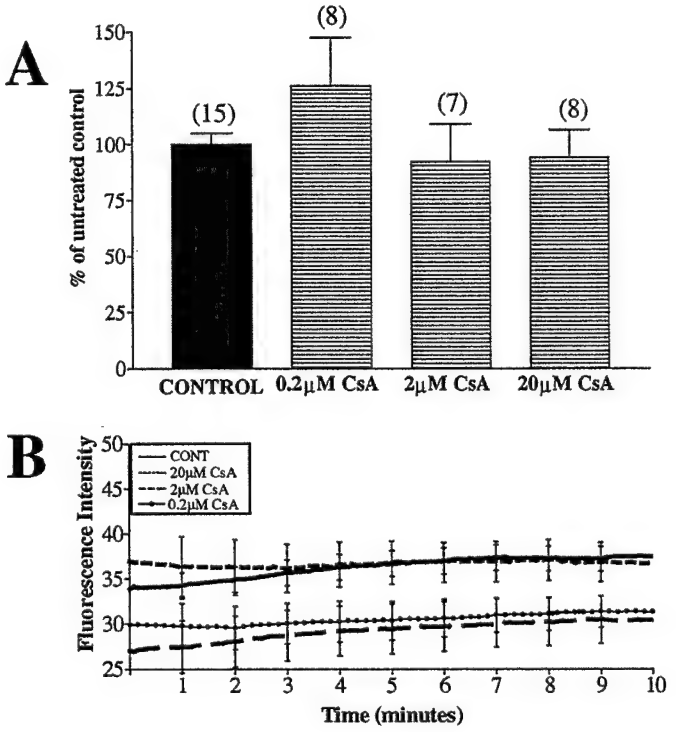

Figure 9. $\Delta\Psi_m$ fluctuations are not altered by treatment with cyclosporin A. Neurons loaded with JC-1 were treated with 0.2–20 μM cyclosporin A (*CsA*) for 15 min before imaging. Fluorescence intensity and number of fluctuations per minute per 1000 ROIs were calculated. *A*, Percentage of fluctuations in cyclosporin A-pretreated mitochondria to untreated mitochondria. Cyclosporin A did not significantly alter $\Delta\Psi_m$ fluctuations ($F_{(3,34)} = 1.27$; $p > 0.05$). Data are presented as means ± SEM, and the *numbers* above *bars* equal the number of fields imaged (~1000 ROIs per field). *B*, Average fluorescence intensity, with representative error bars indicating SEM. Cyclosporin A did not substantially alter the average fluorescence intensity.

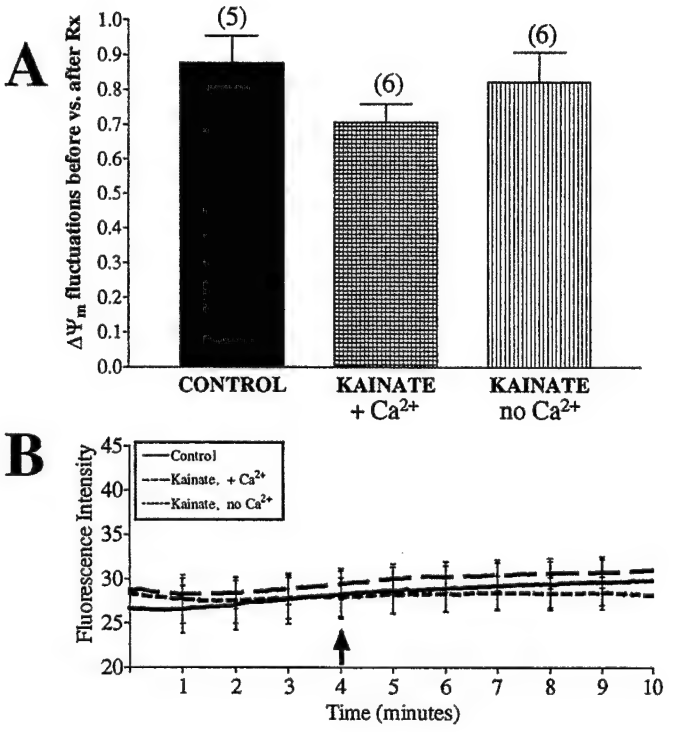

Figure 10. $\Delta\Psi_m$ fluctuations are not altered by treatment with kainic acid. Untreated neurons were loaded with JC-1 and imaged for 4 min before the addition of drug (*arrow*). Kainic acid (100 μM) was perfused over the cells in a buffer containing 1.4 mM (*+Ca²⁺*) or 0 mM (*no Ca²⁺*) calcium for 5 min, and fluorescence intensity and number of fluctuations per minute per 1000 ROIs were calculated. *A*, The ratio of fluctuations occurring during baseline to those occurring after drug treatment. Data are presented as means ± SEM, and the *numbers* above each *bar* equal the number of fields imaged (~1000 ROIs per field). Neither treatment had a significant impact on $\Delta\Psi_m$ fluctuations (with Ca^{2+}, $t = 1.90$, df = 9, $p > 0.05$; without Ca^{2+}, $t = 0.48$, df = 9, $p > 0.05$). *B*, Average fluorescence intensity of all mitochondria imaged, with representative error bars indicating SEM. Neither treatment altered basal fluorescence.

sure. Thus, if a brief, intense light augmented the frequency of $\Delta\Psi_m$ fluctuations, it would suggest that these fluctuations were merely reflecting photo damage. We saw, however, a decrease in the number of fluctuations under high-light conditions, suggesting that dye-loaded mitochondria exhibit spontaneous fluctuations in $\Delta\Psi_m$, which were not a consequence of illumination. These high-light conditions led to a decrease in the JC-1 aggregate signal without a concurrent change in the monomer signal (data not shown), similar to what is observed with oxidant treatments, such as hydrogen peroxide (Scanlon and Reynolds, 1998; Chinopoulos et al., 1999). However, treatment with the uncoupler FCCP at the end of the high-light experiments led to an increase in monomer fluorescence of the same magnitude in both the exposed and unexposed regions (data not shown). This supports the hypothesis that JC-1 aggregate fluorescence responds to more than just changes in $\Delta\Psi_m$ (Scanlon and Reynolds, 1998; Chinopoulos et al., 1999) but indicates that light-induced changes in aggregate fluorescence do not change the ability of the JC-1 monomer signal to respond to changes in $\Delta\Psi_m$.

Calcium may have a profound impact on mitochondrial function in general and on membrane potential in particular. Small transient changes in $\Delta\Psi_m$ observed in cardiomyocytes were reported to be the result of mitochondrial calcium transport (Duchen et al., 1998; Fall and Bennett, 1999). Furthermore, calcium can induce the generation of ROS, alter respiration (McCormack et al., 1990), and possibly open the large, nonselective PTP (Zoratti and Szabo, 1995). This suggests that calcium could be a key mediator of changes in $\Delta\Psi_m$. Inhibiting the NMDA receptor, thus decreasing the entry accumulation of calcium (Fig. 6*A*), chelating extracellular calcium with EGTA (data not shown), and inhibiting the PTP with cyclosporin A (Fig. 9) all failed to change $\Delta\Psi_m$ fluctuations, which argues against this possibility. Chelating intracellular calcium with BAPTA (Fig. 7*A*) did decrease fluctuations, but this occurred in conjunction with a considerable mitochondrial depolarization. The large rise in monomer fluorescence induced by BAPTA most likely occluded our ability to detect small fluctuations and was similar to the effects of the protonophore FCCP. However, it remains unclear how adding BAPTA influences the free calcium because, under resting conditions, the calcium concentration in both the cytoplasm and mitochondria of these neurons is low (Brocard et al., 2001).

We believe that these are the first experiments that illustrate spontaneous changes in $\Delta\Psi_m$ in neurons. Previous studies have suggested cyclosporin A-stimulated changes in whole-cell TMRM signal in neuroblastoma cells (Fall and Bennett, 1999), which are obviously distinct from the single organelle signals reported here. In cardiomyocytes, transient depolarizations in single mitochondria have been seen (Duchen et al., 1998), but these changes were the consequence of calcium movements.

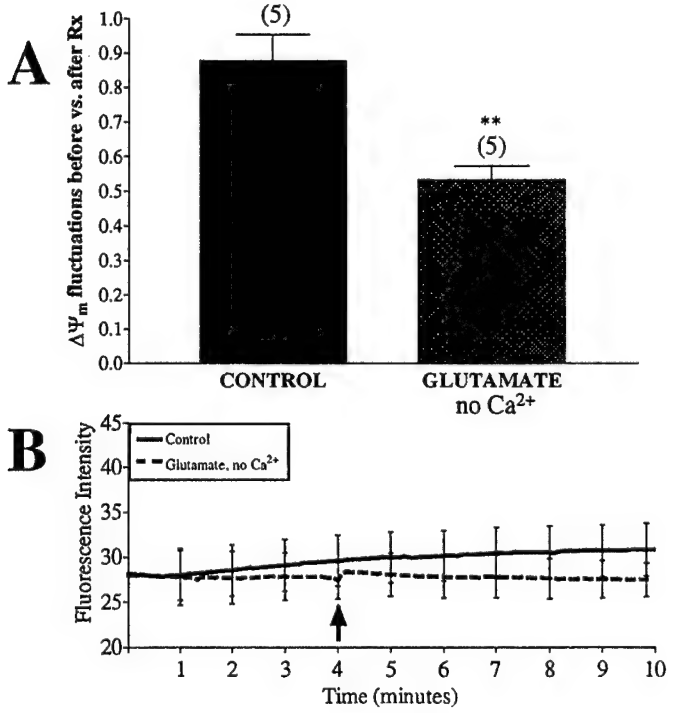

Figure 11. $\Delta\Psi_m$ fluctuations are decreased after treatment with glutamate in a calcium-free buffer. Untreated neurons were loaded with JC-1 and imaged for 4 min before the addition of drug (*arrow*). Glutamate (100 μM, with 10 μM glycine) was perfused over the cells in a Ca^{2+}-free buffer for 5 min. Fluorescence intensity and number of fluctuations per minute per 1000 ROIs were calculated. Glutamate in the presence of Ca^{2+} caused mitochondrial depolarization and thus was not tested. *A*, The ratio of fluctuations occurring during baseline to those occurring after drug treatment. Data are presented as means ± SEM, and the *numbers* above each *bar* equal the number of fields imaged (~1000 ROIs per field). Glutamate in Ca^{2+}-free buffer significantly decreased the number of spontaneous fluctuations ($t = 4.04$; df = 8; $^{**}p < 0.01$). *B*, Average fluorescence intensity of all mitochondria imaged, with representative error bars indicating SEM. Glutamate (*no* Ca^{2+}) treatment did not alter basal fluorescence.

Other studies have investigated single mitochondria but only after their isolation from cells (Ichas et al., 1997; Huser and Blatter, 1999). Apparently none of these studies have reported oligomycin sensitivity of the fluctuations.

Herein, we have documented a novel feature of mitochondrial physiology in neurons. Unlike previous studies that have reported large changes in $\Delta\Psi_m$ associated with neuronal injury, the spontaneous changes in $\Delta\Psi_m$ reported here appear to be a normal characteristic of mitochondrial function in neurons and may reflect alterations in the activity of individual mitochondria associated with the transition between rest and active oxidative phosphorylation. We suggest that this phenomenon that may prove to be a useful marker of mitochondrial function in neurons and hypothesize that these fluctuations in $\Delta\Psi_m$ reflect variations in the cellular environment associated with altered states of respiratory control or ion-induced matrix swelling.

REFERENCES

Ankarcrona M, Dypbukt JM, Bonfoco E, Zhivotovsky B, Orrenius S, Lipton SA, Nicotera P (1995) Glutamate-induced neuronal death: a succession of necrosis or apoptosis depending on mitochondrial function. Neuron 15:961–973.

Bernardi P (1999) Mitochondrial transport of cations: channels, exchangers, and permeability transition. Physiol Rev 79:1127–1155.

Brocard JB, Tassetto M, Reynolds IJ (2001) Quantitative evaluation of mitochondrial calcium content following a glutamate stimulation in rat cortical neurones. J Physiol (Lond) 531:793–805.

Budd SL, Nicholls DG (1996) Mitochondria, calcium regulation, and acute glutamate excitotoxicity in cultured cerebellar granule cells. J Neurochem 67:2282–2291.

Budd SL, Tenneti L, Lishnak T, Lipton SA (2000) Mitochondrial and extramitochondrial apoptotic signaling pathways in cerebrocortical neurons. Proc Natl Acad Sci USA 97:6161–6166.

Bunting JR (1992) A test of the singlet oxygen mechanism of cationic dye photosensitization of mitochondrial damage. Photochem Photobiol 55:81–87.

Chinopoulos C, Tretter L, Adam-Vizi V (1999) Depolarization of in situ mitochondria due to hydrogen peroxide-induced oxidative stress in nerve terminals: inhibition of alpha-ketoglutarate dehydrogenase. J Neurochem 73:220–228.

Courtney MJ, Enkvist MO, Akerman KE (1995) The calcium response to the excitotoxin kainate is amplified by subsequent reduction of extracellular sodium. Neuroscience 68:1051–1057.

Crompton M, Ellinger H, Costi A (1988) Inhibition by cyclosporin A of a Ca^{2+}-dependent pore in heart mitochondria activated by inorganic phosphate and oxidative stress. Biochem J 255:357–360.

Desagher S, Martinou JC (2000) Mitochondria as the central control point of apoptosis. Trends Cell Biol 10:369–377.

Duchen MR (1999) Contributions of mitochondria to animal physiology: from homeostatic sensor to calcium signalling and cell death. J Physiol (Lond) 516:1–17.

Duchen MR, Leyssens A, Crompton M (1998) Transient mitochondrial depolarizations reflect focal sarcoplasmic reticular calcium release in single rat cardiomyocytes. J Cell Biol 142:975–988.

Fall CP, Bennett Jr JP (1999) Visualization of cyclosporin A and Ca^{2+}-sensitive cyclical mitochondrial depolarizations in cell culture. Biochim Biophys Acta 1410:77–84.

Green DR, Reed JC (1998) Mitochondria and apoptosis. Science 281:1309–1312.

Hajnoczky G, Robb-Gaspers LD, Seitz MB, Thomas AP (1995) Decoding of cytosolic calcium oscillations in the mitochondria. Cell 82:415–424.

Hoyt KR, Stout AK, Cardman JM, Reynolds IJ (1998) The role of intracellular Na^+ and mitochondria in buffering of kainate-induced intracellular free Ca^{2+} changes in rat forebrain neurones. J Physiol (Lond) 509:103–116.

Huser J, Blatter LA (1999) Fluctuations in mitochondrial membrane potential caused by repetitive gating of the permeability transition pore. Biochem J 343:311–317.

Ichas F, Jouaville LS, Mazat JP (1997) Mitochondria are excitable organelles capable of generating and conveying electrical and calcium signals. Cell 89:1145–1153.

Krippeit-Drews P, Dufer M, Drews G (2000) Parallel oscillations of intracellular calcium activity and mitochondrial membrane potential in mouse pancreatic B-cells. Biochem Biophys Res Commun 267:179–183.

Kroemer G, Dallaporta B, Resche-Rigon M (1998) The mitochondrial death/life regulator in apoptosis and necrosis. Annu Rev Physiol 60:619–642.

Loew LM, Carrington W, Tuft RA, Fay FS (1994) Physiological cytosolic Ca^{2+} transients evoke concurrent mitochondrial depolarizations. Proc Natl Acad Sci USA 91:12579–12583.

McCormack JG, Halestrap AP, Denton RM (1990) Role of calcium ions in regulation of mammalian intramitochondrial metabolism. Physiol Rev 70:391–425.

Nicholls DG, Budd SL (2000) Mitochondria and neuronal survival. Physiol Rev 80:315–360.

Nicholls DG, Ferguson SJ (1992) Bioenergetics 2. San Diego: Academic.

Nicholls DG, Ward MW (2000) Mitochondrial membrane potential and neuronal glutamate excitotoxicity: mortality and millivolts. Trends Neurosci 23:166–174.

Nieminen AL, Petrie TG, Lemasters JJ, Selman WR (1996) Cyclosporin A delays mitochondrial depolarization induced by *N*-methyl-D-aspartate in cortical neurons: evidence of the mitochondrial permeability transition. Neuroscience 75:993–997.

Overly CC, Rieff HI, Hollenbeck PJ (1996) Organelle motility and metabolism in axons vs dendrites of cultured hippocampal neurons. J Cell Sci 109:971–980.

Petit PX, Susin SA, Zamzami N, Mignotte B, Kroemer G (1996) Mitochondria and programmed cell death: back to the future. FEBS Lett 396:7–13.

Rizzuto R, Brini M, Murgia M, Pozzan T (1993) Microdomains with high Ca^{2+} close to IP3-sensitive channels that are sensed by neighboring mitochondria. Science 262:744–747.

Rizzuto R, Pinton P, Carrington W, Fay FS, Fogarty KE, Lifshitz LM, Tuft RA, Pozzan T (1998) Close contacts with the endoplasmic reticulum as determinants of mitochondrial Ca^{2+} responses. Science 280:1763–1766.

Sattler R, Charlton MP, Hafner M, Tymianski M (1998) Distinct influx pathways, not calcium load, determine neuronal vulnerability to calcium neurotoxicity. J Neurochem 71:2349–2364.

Scalettar BA, Abney JR, Hackenbrock CR (1991) Dynamics, structure, and function are coupled in the mitochondrial matrix. Proc Natl Acad Sci USA 88:8057–8061.

Scanlon JM, Reynolds IJ (1998) Effects of oxidants and glutamate receptor activation on mitochondrial membrane potential in rat forebrain neurons. J Neurochem 71:2392–2400.

Schinder AF, Olson EC, Spitzer NC, Montal M (1996) Mitochondrial dysfunction is a primary event in glutamate neurotoxicity. J Neurosci 16:6125–6133.

Scott ID, Nicholls DG (1980) Energy transduction in intact synaptosomes. Influence of plasma-membrane depolarization on the respiration and membrane potential of internal mitochondria determined in situ. Biochem J 186:21–33.

Skulachev VP (1996) Role of uncoupled and non-coupled oxidations in maintenance of safely low levels of oxygen and its one-electron reductants. Q Rev Biophys 29:169–202.

Stout AK, Raphael HM, Kanterewicz BI, Klann E, Reynolds IJ (1998) Glutamate-induced neuron death requires mitochondrial calcium uptake. Nat Neurosci 1:366–373.

Susin SA, Zamzami N, Castedo M, Daugas E, Wang HG, Geley S, Fassy F, Reed JC, Kroemer G (1997) The central executioner of apoptosis: multiple connections between protease activation and mitochondria in Fas/APO-1/CD95- and ceramide-induced apoptosis. J Exp Med 186:25–37.

Susin SA, Zamzami N, Kroemer G (1998) Mitochondria as regulators of apoptosis: doubt no more. Biochim Biophys Acta 1366:151–165.

Vergun O, Keelan J, Khodorov BI, Duchen MR (1999) Glutamate-induced mitochondrial depolarisation and perturbation of calcium homeostasis in cultured rat hippocampal neurones. J Physiol (Lond) 519:451–466.

Ward MW, Rego AC, Frenguelli BG, Nicholls DG (2000) Mitochondrial membrane potential and glutamate excitotoxicity in cultured cerebellar granule cells. J Neurosci 20:7208–7219.

White RJ, Reynolds IJ (1995) Mitochondria and Na^+/Ca^{2+} exchange buffer glutamate-induced calcium loads in cultured cortical neurons. J Neurosci 15:1318–1328.

White RJ, Reynolds IJ (1996) Mitochondrial depolarization in glutamate-stimulated neurons: an early signal specific to excitotoxin exposure. J Neurosci 16:5688–5697.

White RJ, Reynolds IJ (1997) Mitochondria accumulate Ca^{2+} following intense glutamate stimulation of cultured rat forebrain neurones. J Physiol (Lond) 498:31–47.

Zoratti M, Szabo I (1995) The mitochondrial permeability transition. Biochim Biophys Acta 1241:139–176.

Program Number: 96.9 **Day / Time:** Sunday, Nov. 11, 8:00 AM - 9:00 AM

SPONTANEOUS MITOCHONDRIAL ACTIVITIES IN ASTROCYTES

J.F.Buckman*; I.J.Reynolds

Dept Pharmacol, Univ Pittsburgh, Pittsburgh, PA, USA

Mitochondria in healthy neuronal cultures display small, spontaneous fluctuations in mitochondrial membrane potential (delta psi-m), which are dependent upon the mitochondrial ATP synthase (Buckman & Reynolds, J Neurosci, in press). In this study we have investigated spontaneous mitochondrial activities in primary astrocyte cultures loaded with a quenching concentration of the delta psi-m indicator, TMRM. We have observed several, phenomenologically distinct events. The first activity we noted was small-amplitude fluctuations in TMRM signal similar to those observed in neurons. Here the mitochondria appear to get brighter, then dimmer over a 10-15 second interval. We also noted that some mitochondria within untreated astrocytes exhibit much larger fluctuations in delta psi-m, which appear as mitochondria that display complete dye loss, followed by re-sequestration occurring over the course of 20-30 seconds. This phenomenon was not observed in neuronal cultures, suggesting that these fluctuations are mechanistically different from those we previously reported. Over the course of these experiments, we observe a trend towards increased TMRM signal with light exposure indicating that these phenomena may be related to mitochondrial injury. Finally, we have begun to investigate the properties of large mitochondrial networks, which can be several hundred microns in length and extensively branched. These networks also display large, synchronous delta psi-m fluctuations. Although this electrical coupling has been previously reported, questions remain about the nature, mechanism and purpose of this phenomenon.
Supported by: USAMRMC, Scaife Family Foundation, NIH grants NS34138, T32NS07391 and F32NS11147

Program Number: 96.10 **Day / Time:** Sunday, Nov. 11, 9:00 AM - 10:00 AM

HYPOXIA AND HYPOGLYCEMIA PRODUCE A STABLE INCREASE IN SUSCEPTIBILITY TO GLUTAMATE IN CULTURED RAT CORTICAL NEURONS

O.V.Vergun *; J.Fuhr; I.J.Reynolds

Dept of Pharmacology, Univ of Pittsburgh, Pittsburgh, PA, USA

Changes in cytosolic Ca2+ concentration ([Ca2+]i) and mitochondrial potential in individual forebrain neurons coloaded with fura-2FF and Rh123 were monitored simultaneously using digital fluorescence imaging techniques. Exposure of the cells to 100 μ M of glutamate (GLU) produced complete mitochondrial depolarization (MD) with a concurrent high irreversible increase in [Ca2+]i. In contrast, low concentrations of GLU (5-10 μ M) induced only a relatively small and reversible MD and increase in [Ca2+]i. To suppress cellular metabolism the neurons were incubated in glucose-free, 2-deoxy-D-glucose-containing medium for 60 min or in 5 mM KCN-containing medium for 40 min followed by a 30-40 min washout. MD or increase in [Ca2+]i were not typically observed during and after the removal of glucose; expose of the cells to KCN produced full MD and very small increase in Fura-2FF ratio with following full recovery after washout of KCN. After KCN or glucose-free medium washout the low concentrations of GLU produced MD and increase in [Ca2+]i similar with those observed in the control neurons exposed to 100 μ M GLU. Blockade of glycolysis had an effect greater than inhibition of respiration by KCN. Exposure of the cells to nitrogen-mediated hypoxia (nitrogen-equilibrated medium with addition of Na2S2O4) for 40 min did not increase the susceptibility of the neurons to GLU. The data show that suppression of even one of the sources of ATP production by blockade of glycolysis or respiration produce sustained increase in sensitivity of cultured neurons to GLU, which may greatly increase the toxic action of GLU.
Supported by: USAMRMC grant DAMD 17-98-1-8628

Program Number: 96.11 **Day / Time:** Sunday, Nov. 11, 10:00 AM - 11:00 AM

EFFECTS OF MITOCHONDRIAL DEPOLARIZATION ON Ca2+ RELEASE FROM NEURONAL MITOCHONDRIA

J.B.Brocard *; M.S.Santos; T.V.Votyakova; I.J.Reynolds

Pharmacol, Univ Pittsburgh, Pittsburgh, PA, USA

Recent studies (Brocard et al., J. Physiol. 531:793, 2001) suggest that mitochondrial Ca2+ concentrations exceed 1mM following a 5min exposure to glutamate. Here we investigated the characteristics of Ca2+ release from mitochondria. We monitored intracellular Ca2+ in cultured forebrain neurons with magfura-2. Neurons exposed to 30uM glutamate for 5min accumulate a substantial mitochondrial Ca2+ load. This Ca2+ was rapidly released following the addition of 750nM FCCP. Antimycin A (AA, 1uM) or KCN (1mM) depolarized mitochondria to a similar extent and prevented mitochondrial Ca2+ accumulation when applied together with glutamate. However, AA and KCN were much less effective in releasing previously accumulated Ca2+ compared to FCCP. In addition, exposing neurons to glutamate in phosphate-free buffer resulted in smaller Ca2+ stores, as estimated from the amount of Ca2+ released by FCCP. Isolated brain mitochondria accumulate Ca2+ in a potential-dependent manner. Accumulation is mediated by the Ca2+ uniporter, because it is inhibited by ruthenium red (RR, IC50 = 7nM). Ca2+ loaded mitochondria release Ca2+ when depolarized with FCCP. Most Ca2+ release is blocked by RR together with the Na+ Ca2+ exchange inhibitor CGP 37157, although there is a residual Ca2+ efflux that appears to be independent of the uniport and NCE. AA was much less effective than FCCP in releasing Ca2+ from isolated mitochondria. These results suggest that factors other than simply membrane potential govern Ca2+ release from neuronal mitochondria, and may suggest that formation of less soluble Ca2+ phosphate complexes influence the dynamics of mitochondrial Ca2+ handling.

Supported by: DAMD 17-98-1-8628 and HFSP

An investigation of the properties of Ca2+ uniporter inhibitors in neuronal mitochondria

Tanya V. Votyakova, Jacques B. Brocard, Maria Santos, Ian J. Reynolds: University of Pittsburgh, Dept. Pharmacology

Glutamate-induced neuronal injury is associated with substantial Ca2+ accumulation by mitochondria. Moroever, preventing mitochondrial Ca2+ accumulation by collapsing the mitochondrial membrane potential protects neurons against excitotoxic injury. Thus, the prevention of mitochondrial Ca2+ uptake might be an effective strategy for neuroprotection. In this study we have evaluated the effects of ruthenium red (RR) and a derivative Ru360, that may inhibit the mitochondrial Ca2+ uniporter in isolated mitochondria and in intact cells.

In isolated brain mitochondria we monitored Ca2+ uptake using the fluorescent indicator Calcium Green 5N. Mitochondria effectively accumulate Ca2+ via the uniporter, and can also release Ca2+ if depolarized with the uncoupler FCCP. Both RR and Ru360 effectively inhibited Ca2+ accumulation in nanomolar concentrations. The inhibitors also decreased FCCP-induced Ca2+ release suggesting that the uniporter is the principle route of entry and depolarization-mediated Ca2+ release. A second slower mode of Ca2+ release is also seen in the presence of the inhibitors, possibly due to the mitochondrial Na+/Ca2+ exchange.

Primary cultures of forebrain neurons exposed to high concentrations of glutamate accumulate large quantities Ca2+ via activation of the NMDA receptor, and this Ca2+ is transported into mitochondria presumably by the uniporter. We can also demonstrate mitochondrial Ca2+ release triggered by FCCP, also likely to be mediated by the uniporter. We used high concentrations of Ru360 (10uM) and for long incubation periods (>30min). However, neither of these strategies altered either glutamate-induced cytosolic Ca2+ changes or FCCP-induced mitochondrial Ca2+ release.

These findings suggest that RR and Ru360 are effective inhibitors of the mitochondrial Ca2+ uniporter in neurons, but that Ru360 does not effectively penetrate cells.

Supported by USAMRMC grant DAMD 17-98-1-8627 and NIH grant NS34138